



PONTIFICIA UNIVERSIDAD CATÓLICA DE CHILE
FACULTAD DE CIENCIAS BIOLÓGICAS

“MECHANISMS INVOLVED IN THE LOSS OF BROWN ADIPOSE TISSUE IN THE AGPAT2 DEFICIENT MOUSE”

Thesis submitted to Pontificia Universidad Católica de Chile in partial fulfillment of the requirements for the degree of Doctor in Biological Sciences, Mention in Molecular Genetics and Microbiology.

By

PABLO JOSÉ TAPIA OSSA

Thesis advisor: Víctor A. Cortés Mora, M.D., Ph.D.

July 2019

Acknowledgements.

I sincerely thank to my tutor Víctor Cortés for the constant critical discussion of the results and experimental designs, being always an excellent guide and tutor. To Fermín Robledo, who with his skillful constructive criticism allowed this thesis to be carried out. To Kelly Cautivo for all her support, especially at the beginning of this thesis work. And to all the members of the laboratory who have supported me constantly.

In addition, I thank to my family, parents, brothers, nephews, wife and children, who with all their support and love allowed me to cheer my day to day during the development of this thesis.

Finally, I sincerely thank to all those that taught me to be the scientist that I am, but also to those that taught me not to be the scientist that I am not, and that I will never be.

Table of contents

Abbreviations.....	8
Resumen.....	11
Abstract.....	14
1. Introduction.....	17
1.1. Congenital generalized lipodystrophy and lipotoxicity as a possible mechanism for adipose tissue destruction in AGPAT2 deficient mice.	19
1.2. General concepts on adipose tissue biology.....	26
1.3. Regulation of brown adipogenesis.....	32
1.3.1. Brown adipose cell fate commitment.	33
1.3.2. Brown adipocyte differentiation: classical and novel regulators with potential importance for AGPAT2-dependent lipodystrophy.	36
Hypothesis and aims.....	43
3. Materials and methods.....	44
3.1. Materials.....	44
3.1.1. Genotyping reagents.....	44
3.1.2. Cell culture reagents.....	44
3.1.3. Reagents for cloning and generation of recombinant adenoviruses.....	44
3.1.4. Western blotting reagents.....	45
3.1.5. qRT-PCR reagents.....	45
3.1.6. Other reagents.....	45
3.1.7. Antibodies.....	45
3.2. Methods.....	46
3.2.1. Maintenance and genotyping of mice.....	46
3.2.2. Obtaining preadipocytes of interscapular brown adipose tissue (iBAT) and adipogenic differentiation.....	48
3.2.3. Immunofluorescence assays.....	49
3.2.4. Quantification of fluorescence microscopy images acquired by automated system.....	49
3.2.5. Oil-Red-O Stain.....	50
3.2.6. Western blotting.....	50
3.2.7. qRT-PCR and RNA Microarray.....	52
3.2.8. Electron microscopy.....	52
3.2.9. Histological sections and X-gal staining.....	53
3.2.10. Generation of recombinant adenoviruses.....	53

3.2.11. Fatty acid profile.....	54
3.2.12. Lipotoxicity assays and cell viability measurement.....	54
3.2.13. Statistics.....	55
3.2.14. Figures.....	55
4. Results.....	56
4.1. Differentiated brown adipocytes of <i>Agpat2</i> ^{-/-} mice have lower accumulation of lipid droplets.....	56
4.2. Expression levels of adipogenic transcriptional regulators PPAR γ , C/EBP α , PPAR α and PGC1 α but not PRDM16 and C/EBP β are decreased in differentiated brown adipocytes of <i>Agpat2</i> ^{-/-} mice.....	60
4.3. Preadipocyte abundance is normal in the interscapular brown adipose tissue of newborn <i>Agpat2</i> ^{-/-} mice and in their primary cultured stromal vascular fraction (SVF).....	68
4.4. <i>In vitro</i> differentiated brown adipocytes of <i>Agpat2</i> ^{-/-} mice have abnormal expression levels of genes related to type I interferon response and mitochondrial biogenesis/function.....	73
4.5. Mitochondrial morphology and distribution are altered at day 5 of differentiation in differentiated brown adipocytes of <i>Agpat2</i> ^{-/-} mice.....	81
4.6. Differentiated brown adipocytes of <i>Agpat2</i> ^{-/-} mice have similar STAT1/2 levels in comparison with wild type cells.....	85
4.2. Elovl3 and mitoNEET forced expression does not restore adipogenic differentiation in differentiated brown adipocytes of <i>Agpat2</i> ^{-/-} mice.....	92
4.2.1. Elovl3 and mitoNEET are induced in brown adipogenic differentiation of wild type adipocytes but their levels remain low in differentiated brown adipocytes of <i>Agpat2</i> ^{-/-} mice.....	92
4.2.2. Forced expression of Elovl3 and mitoNEET does not increase lipid droplets accumulation in differentiated brown adipocytes of <i>Agpat2</i> ^{-/-} mice.....	97
4.3. Palmitic acid overload determines excessive cell death in differentiated brown adipocytes of <i>Agpat2</i> ^{-/-} mice.....	103
5. Discussion.....	116
5.1. Considerations of the quantitative analysis of lipid-laden adipocytes and the evaluation of the adipogenic markers in the primary cultures of brown preadipocytes of <i>Agpat2</i> ^{+/+} and <i>Agpat2</i> ^{-/-} mice.....	116
5.2. Causes of impaired adipogenesis in <i>Agpat2</i> ^{-/-} cultures.....	118
5.3. Lipotoxicity.....	124
6. Conclusions.....	129
7. References.....	131

Index of Figures

FIGURE 1: Gene products implicated in lipodystrophy and lipid droplet formation in adipocytes	22
FIGURE 2: Brown, white and brite/beige adipocytes	27
FIGURE 3: β -adrenergic receptors coordinate triglyceride lipolysis, mitochondrial fatty acid oxidation and uncoupling protein 1 (UCP1) abundance and function in brown adipocytes. ...	31
FIGURE 4: Transcriptional regulation of brown adipogenesis	38
FIGURE 5: Activation of ISGs.....	40
FIGURE 6: Image analysis pipeline.	51
FIGURE 7: The accumulation of lipid droplets in differentiated brown adipocytes of <i>Agpat2</i> ^{-/-} mice is diminished	58
FIGURE 8: PPAR γ is located in the nucleus of cells that accumulate lipid droplets in differentiated brown adipocytes of wild type and <i>Agpat2</i> ^{-/-} mice.....	62
FIGURE 9: Protein and/or mRNA levels of PRDM16, C/EBP β , C/EBP α , PPAR α and PGC1 α in differentiated brown adipocytes of wild type and <i>Agpat2</i> ^{-/-} mice.....	64
FIGURE 10: Protein and mRNA levels UCP1 and adipocyte markers Plin1, Adiponectin and Cidea are strongly diminished in differentiated brown adipocytes of <i>Agpat2</i> ^{-/-} mice.	66
FIGURE 11: Preadipocyte abundance is normal in the iBAT of newborn <i>Agpat2</i> ^{-/-} mice.....	71
FIGURE 12: Preadipocyte abundance is normal in primary cultured stromal vascular fraction (SVF)	72
FIGURE 13: Global gene expression analysis of differentiated brown adipocytes of <i>Agpat2</i> ^{-/-} mice.....	74
FIGURE 14: Gene ontology (GO) analysis in differentiated brown adipocytes of <i>Agpat2</i> ^{-/-} mice.	77
FIGURE 15: qPCR quantification of differentially expressed genes in global gene expression analysis in differentiated brown adipocytes of <i>Agpat2</i> ^{-/-} mice.	79
FIGURE 16: Mitochondrial number and morphology is abnormal in differentiated brown adipocytes of <i>Agpat2</i> ^{-/-} mice	83
FIGURE 17: Differentiated brown adipocytes of <i>Agpat2</i> ^{-/-} mice have similar levels of nuclear STAT1 in comparison with wild type cells	89
FIGURE 18: Differentiated brown adipocytes of <i>Agpat2</i> ^{-/-} mice have higher levels of cytoplasmic STAT2 only at advanced stages of differentiation.....	91
FIGURE 19: Elov13 and mitoNEET levels are lower in differentiated brown adipocytes of <i>Agpat2</i> ^{-/-} mice in comparison with wild type cells	93
FIGURE 20: The forced overexpression of Elov13 does not restore lipid droplets accumulation in differentiated brown adipocytes of <i>Agpat2</i> ^{-/-} mice.	100
FIGURE 21: The forced overexpression of mitoNEET does not restore lipid droplets accumulation in differentiated brown adipocytes of <i>Agpat2</i> ^{-/-} mice.....	102
FIGURE 22: Levels of saturated, monounsaturated and polyunsaturated fatty acids are markedly increased in <i>Agpat2</i> ^{-/-} mice.....	104

FIGURE 23: Differentiated brown adipocytes of <i>Agpat2</i> ^{-/-} mice have increased susceptibility to palmitic acid-induced cell death at day 5 of differentiation.	108
FIGURE 24: Activated caspase 3 is not different between differentiated brown adipocytes of wild type and <i>Agpat2</i> ^{-/-} mice at day 0 differentiation but is higher in <i>Agpat2</i> ^{-/-} cells at day 5 after incubation with palmitic acid.....	109
FIGURE 25: Palmitic acid increases cytosolic cytochrome c in preadipocytes of both genotypes, but only in differentiated brown adipocytes of <i>Agpat2</i> ^{-/-} mice at day 5 of differentiation.....	112
FIGURE 26: Activated (cleaved) caspase 3 is increased in the iBAT of <i>Agpat2</i> ^{-/-} mice at the second post-natal day.....	114
FIGURE 27: Proposed model for impaired adipogenesis in differentiated brown adipocytes of <i>Agpat2</i> ^{-/-} mice.....	127
FIGURE 28: Model illustrating the potential causes of lipotoxicity in differentiated brown adipocytes of <i>Agpat2</i> ^{-/-} mice	128

Index of Tables

TABLE 1. Classification, clinical features, and molecular bases of congenital generalized lipodystrophy (CGL) syndromes	20
TABLE 2: Levels of saturated, monounsaturated, polyunsaturated fatty acids in plasma of wild type and <i>Agpat2</i> ^{-/-} mice at days 0, 2, and 4 after birth	105

Abbreviations.

2-5-oligoadenylate synthetase	:	OAS
¹⁸ F-fluorodeoxyglucose	:	18F-FDG
1-acylglycerol-3-phosphate O-acyltransferase-2	:	AGPAT2
3-isobutyl-1-methylxanthine	:	IBMX
4,4-difluoro-4-bora-3a, 4a-diaza-s-indacene	:	BODIPY
Absent in melanoma 2	:	AIM2
Activating transcription factor 2	:	ATF2
Adenosine triphosphate	:	ATP
Adenylate cyclase	:	AC
Adipose tissue	:	AT
Atypical protein kinase C	:	aPKC
B-cell factor 3	:	EBF3
Bone morphogenetic protein 7	:	BMP7
Bovine serum albumin	:	BSA
Brg1/Brm-associated factors	:	BAF
Brown adipose tissue	:	BAT
cAMP response element-binding	:	CREB
Carnitine palmitoyltransferase 1b	:	CPT1B
CCAAT/enhancer binding protein delta	:	C/EBP δ
CCAAT/enhancer-binding protein alpha	:	C/EBP α
CCAAT/enhancer-binding protein beta	:	C/EBP β
Cell death-inducing DNA fragmentation factor effector a	:	CIDEA
Chinese hamster ovary-K1	:	CHO
Computed tomography	:	CT
Congenital generalized lipodystrophy	:	CGL
Cyclic adenosine monophosphate	:	cAMP
Cytochrome c oxidase subunit 7A1	:	COX7A1
Cytochrome c oxidase subunit 8B	:	COX8B
DEAD (Asp-Glu-Ala-Asp) box polypeptide 58	:	DDX58
DEXH (Asp-Glu-X-His) box polypeptide 58	:	DHX58
Diacylglycerol acyltransferase	:	DGAT
Diacylglycerol	:	DAG
Double-stranded RNA-dependent protein kinase	:	PKR
Dulbecco's Modified Eagle Medium	:	DMEM
Early B cell factor 2	:	EBF2
Elongation of very-long-chain fatty acids 3	:	ELOVL3
Endoplasmic reticulum	:	ER
Engrailed-1	:	EN-1

Epithelial V-like antigen 1	:	EVA1
Estrogen-related receptors	:	ERR
Euchromatic histone methyltransferase 1	:	EHMT1
Ewing Sarcoma	:	EWS
Familial partial lipodystrophy	:	FPLD
Fatty acid binding protein 4	:	FABP4
Fatty acid methyl esters	:	FAME
Fatty acid synthase	:	FAS
Fatty acyl coenzyme A	:	FA-CoA
F-box only protein 31	:	FBXO31
Free fatty acids	:	FFA
Hormone-sensitive lipase	:	HSL
Horseradish peroxidase	:	HRP
Inner mitochondrial membrane	:	IMM
Interferon gamma inducible protein 16	:	IFI16
Interferon induced with helicase C domain 1	:	IFIH1
Interferon regulatory factor	:	IRF
Interferon	:	IFN
Interferon-activable protein 204	:	IFI204
Interferon-induced protein 44	:	IFI44
Interferon-induced protein with tetratricopeptide repeats 1	:	IFIT1
Interferon-stimulated genes	:	ISGs
Interscapular brown adipose tissue	:	iBAT
Iodothyronine deiodinase 2	:	DIO2
Lactate dehydrogenase	:	LDH
Lipid droplet	:	LD
Lysophosphatidic acid	:	LPA
Melanoma differentiation associated gene 5	:	MDA5
Mitochondrial antiviral-signaling protein	:	MAVS
Monoacylglycerol acyltransferase	:	MGAT
Monoacylglycerols	:	MAG
Mouse embryonic fibroblasts	:	MEFs
Muscle-derived multipotent cells	:	MDMCs
Myogenic factor 5	:	MYF5
Norepinephrine	:	NE
Nuclear respiratory factors	:	NRF
Optimal cutting temperature	:	OCT
p38 mitogen-activated protein kinases	:	p38 MAPK
Paired box 7	:	PAX7
Paraformaldehyde	:	PFA

Peroxisome proliferator-activated receptor alpha	:	PPAR α
Peroxisome proliferator-activated receptor gamma	:	PPAR γ
Phosphatidic acid phosphatase	:	PAP
Phosphatidic acid	:	PA
Placenta-specific gene 8 protein	:	PLAC8
Polymerase I and transcript release factor	:	PTRF
Positron emission tomography	:	PET
PRD1-BF1-RIZ1 homologous domain containing 16	:	PRDM16
Proliferator-activated receptor gamma coactivator 1-alpha	:	PGC1 α
Protein kinase A	:	PKA
Reactive oxygen species	:	ROS
Retinoic acid receptor	:	RAR
Retinoic acid-inducible gene I	:	RIG-1
Retinoid X receptor alpha	:	RXR α
Solute carrier family 2 member 4	:	SLC42A
Sterol regulatory element binding transcription factor 1	:	SREBP-1c
Stimulator of IFN genes	:	STING
Strictly standardized mean difference	:	SSMD
Stromal vascular fraction	:	SVF
Sympathetic nervous system	:	SNS
Thyroid receptor	:	TR
Thyroxine	:	T4
Triglycerides	:	TG
Triiodothyronine	:	T3
Ubl carboxyl-terminal hydrolase 18	:	USP18
Uncoupling protein 1	:	UCP1
White adipose tissue	:	WAT
Y-Box Binding Protein	:	YBX1
Zinc finger protein 516	:	ZFP516
β -galactosidase	:	β -Gal

Resumen

1-acilglicerol-3-fosfato O-aciltransferasa-2 (AGPAT2) es una enzima que participa en la síntesis de triacilgliceroles y glicerofosfolípidos. En la diferenciación de adipocitos (adipogénesis) el almacenamiento de lípidos en gotas lipídicas de los adipocitos tiene un rol fundamental. Mutaciones en el gen codificante para esta enzima generan lipodistrofia congénita generalizada, enfermedad caracterizada por la reducción severa de tejido adiposo blanco y pardo, así como también severas complicaciones metabólicas. Los ratones deficientes para AGPAT2 (*Agpat2*^{-/-}) nacen con tejido adiposo pardo de morfología y abundancia similar al de ratones normales, sin embargo, este tejido degenera completamente durante los primeros 6 días después de nacer. Las causas de este fenómeno son actualmente desconocidas. La hipótesis de esta tesis es que adipocitos pardos de ratones *Agpat2*^{-/-} tienen anomalías transcripcionales que determinan adipogénesis defectuosa y mayor susceptibilidad a muerte celular lipotóxica.

Para evaluar esta hipótesis, preadipocitos pardos del tejido adiposo interescapular de ratones *Agpat2*^{-/-} y tipo silvestre fueron diferenciados adipogénicamente en cultivo celular y comparados en diversos parámetros morfológicos y moleculares. Los cultivos de preadipocitos diferenciados *Agpat2*^{-/-} presentaron una menor proporción de células cargadas con gotas lipídicas a lo largo de la diferenciación y una expresión disminuida de los reguladores transcripcionales pro-adipogénicos PPAR γ , PPAR α , C/EBP α y PGC1 α . Importantly, los factores de transcripción PRDM16 y C/EBP β , previamente identificados como mediadores de la diferenciación adipogénica parda, tuvieron niveles normales en los adipocitos pardos *Agpat2*^{-/-} diferenciados *in vitro*. Concordantemente, la proteína UCP1, un marcador específico de adipocito pardo maduro, permaneció indetectable en los adipocitos *Agpat2*^{-/-} diferenciados. Por el contrario, sus niveles fueron fuertemente inducidos en los adipocitos pardos tipo silvestre

diferenciados *in vitro*. El análisis ultraestructural de los adipocitos diferenciados mostró que las mitocondrias de los adipocitos *Agpat2*^{-/-} diferenciados pardos tienen morfología notoriamente alterada, con crestas de geometría irregular, y una menor asociación física con gotas lipídicas, a diferencia de lo que ocurre en los adipocitos pardos normales diferenciados, que tienen mitocondrias con crestas plegadas en disposición paralela y que están íntimamente asociadas a gotas lipídicas con alta frecuencia. El análisis global del transcriptoma de los adipocitos diferenciados *in vitro* mostró divergencia significativa en la abundancia del mRNA codificado por varios grupos de genes. Entre estas destacaron, menor expresión de genes relacionados a la acumulación de lípidos y estructura y función mitocondrial, y mayor expresión de genes estimulados por interferón. Estos resultados fueron verificados independientemente por análisis de qRT-PCR.

Adicionalmente, los cultivos de adipocitos *Agpat2*^{-/-} diferenciados presentan menores niveles de Elovl3 y mitoNEET, ambos previamente identificados como reguladores de la diferenciación y función adiposa. Importantly, la sobreexpresión de estas proteínas por medio de vectores adenovirales, no normalizó la acumulación de gotas lipídicas en adipocitos *Agpat2*^{-/-} diferenciados, indicando que la diferenciación adipogénica defectuosa dependiente de la carencia de AGPAT2 no es revertida por estos productos génicos.

Finalmente, para evaluar la mayor susceptibilidad a muerte celular por lipotoxicidad en adipocitos pardos *Agpat2*^{-/-}, primero se cuantificó la concentración y composición de ácidos grasos en el plasma de ratones *Agpat2*^{-/-} recién nacidos en comparación con ratones tipo silvestre de la misma edad, mostrando una elevación marcada de todas las clases de ácidos grasos, en particular saturados y monoinsaturados, a partir del segundo día postnatal. Entre los primeros

destacó el ácido palmítico, cuya concentración fue ~5 veces mayor en los ratones *Agpat2*^{-/-} recién nacidos en comparación con el tipo silvestre.

La incubación de preadipocitos no diferenciados *Agpat2*^{-/-} y tipo silvestre con ácido palmítico, mostró similares niveles de muerte celular causada por lipotoxicidad. Sin embargo, cuando adipocitos pardos diferenciados *in vitro* fueron expuestos a ácido palmítico, los cultivos *Agpat2*^{-/-} presentaron niveles de muerte celular significativamente mayores, cuantificada por cuatro técnicas distintas y complementarias, en comparación con el tipo silvestre, indicado que la carencia de AGPAT2 determina mayor susceptibilidad de los adipocitos a muerte por lipotoxicidad.

Tomados en su conjunto, los resultados de esta tesis indican que AGPAT2 es esencial para la diferenciación adiposa parda, determinando perfiles transcripcionales anormales y que los adipocitos diferenciados carentes de esta enzima son más sensibles a altos niveles de ácidos grasos saturados presentes en los ratones *Agpat2*^{-/-} después de nacer.

Abstract

1-acylglycerol-3-phosphate O-acyltransferase-2 (AGPAT2) is an enzyme that participates in the synthesis of triacylglycerols and glycerophospholipids. In the differentiation of adipocytes (adipogenesis) the storage of lipids in lipid droplets of adipocytes plays a fundamental role. Mutations in the gene coding for this enzyme generate generalized congenital lipodystrophy, a disease characterized by severe reduction of white and brown adipose tissue, as well as severe metabolic complications. Mice deficient for AGPAT2 (*Agpat2*^{-/-}) are born with brown adipose tissue of morphology and abundance similar to that of normal mice, however, this tissue degenerates completely during the first 6 days after birth. The causes of this phenomenon are currently unknown. The hypothesis of this thesis is that brown adipocytes of *Agpat2*^{-/-} mice have transcriptional abnormalities that determine defective adipogenesis and greater susceptibility to lipotoxic cell death.

To evaluate this hypothesis, brown preadipocytes from the interscapular adipose tissue of *Agpat2*^{-/-} and wild type mice were differentiated adipogenically in cell culture and compared in various morphological and molecular parameters. Differentiated preadipocyte cultures *Agpat2*^{-/-} showed a lower proportion of lipid-laden cells throughout the differentiation and a decreased expression of the pro-adipogenic transcriptional regulators PPAR γ , PPAR α , C/EBP α and PGC1 α . Importantly, the transcription factors PRDM16 and C/EBP β , previously identified as mediators of brown adipogenic differentiation, had normal levels in the *Agpat2*^{-/-} brown adipocytes differentiated *in vitro*. Accordingly, the UCP1 protein, a specific marker of mature brown adipocyte, remained undetectable in the differentiated *Agpat2*^{-/-} adipocytes. On the contrary, their levels were strongly induced in *Agpat2*^{+/+} differentiated adipocytes *in vitro*. Ultrastructural analysis of the differentiated adipocytes showed that the mitochondria of the

differentiated *Agpat2*^{-/-} adipocytes have notoriously altered morphology and are not physically associated with lipid droplets, unlike what happens in differentiated *Agpat2*^{+/+} adipocytes. The overall transcriptome analysis of adipocytes differentiated *in vitro* showed significant divergence in the abundance of mRNA encoded by several groups of genes. These include, lower expression of genes related to the accumulation of lipids and mitochondrial structure and function, and greater expression of genes stimulated by interferon. These results were independently verified by qRT-PCR analysis.

Additionally, differentiated *Agpat2*^{-/-} adipocyte cultures have lower levels of Elovl3 and mitoNEET, both previously identified as regulators of differentiation and adipose function. Importantly, forced overexpression of these by means of adenoviral vectors did not normalize the accumulation of lipid droplets in differentiated *Agpat2*^{-/-} adipocytes.

Finally, to evaluate the increased susceptibility to cell death by lipotoxicity in differentiated *Agpat2*^{-/-} adipocytes, the concentration and composition of fatty acids in the plasma of newborn *Agpat2*^{-/-} mice were quantified in comparison with wild type mice of the same age, showing a marked increase of all classes of fatty acids, particularly saturated and monounsaturated, from the second postnatal day. Among the first ones, palmitic acid stood out, where concentration was ~5 times higher in the newborn *Agpat2*^{-/-} mice compared with the *Agpat2*^{+/+}.

The incubation of *Agpat2*^{-/-} and *Agpat2*^{+/+} preadipocytes with palmitic acid, showed similar levels of cell death caused by lipotoxicity. However, when adipocytes differentiated *in vitro* were exposed to palmitic acid, *Agpat2*^{-/-} cultures had significantly higher cell death levels compared to wild type.

Taken as a whole, the results of this thesis indicate that AGPAT2 is essential for brown adipose differentiation, determining abnormal transcriptional profiles and that differentiated adipocytes lacking this enzyme are more sensitive to high levels of saturated fatty acids present in *Agpat2*^{-/-} mice after birth.

1. Introduction.

Congenital generalized lipodystrophy (CGL) is a disease characterized by severe lipoatrophy, insulin resistance, diabetes and hepatic steatosis. The commonest cause of CGL are mutations in 1-acylglycerol-3-phosphate O-acyltransferase-2 (AGPAT2), which catalyzes the conversion of lysophosphatidic acid (LPA) into phosphatidic acid (PA) in the *de novo* synthesis of the glycerolipid pathway. People with mutations in *AGPAT2* have almost complete absence of functional adipose tissue and the mice lacking *Agpat2*, completely recapitulates this phenotype (Garg, 2004; Cortés *et al.*, 2009).

Interestingly, *Agpat2*^{-/-} mice have morphologically near-normal adipose tissue, including interscapular brown adipose tissue (iBAT), at the time of birth. Notably, whole body adipose tissue completely degenerates during the first 6 days after birth, as a result of adipocyte death and infiltration of inflammatory cells (Cautivo *et al.*, 2016). The causes and mechanisms of this severe and selective tissue destruction are currently unknown; however, lipotoxic cell death is a plausible mechanism.

In previous work of our laboratory, it was found that the absence of AGPAT2 in differentiated mouse embryonic fibroblasts (Cautivo *et al.*, 2016) and preadipocytes differentiated to white adipocytes (Fernández-Galilea *et al.*, 2015) results in failed adipogenesis. Therefore, impaired brown adipose adipogenesis might also be implicated in the loss of iBAT in *Agpat2*^{-/-} mice.

Adipogenesis proceeds by the coordinated action of multiple transcriptional regulators, some of them promoting the expression of genes important for lipid accretion, lipid droplet (LD) formation and function and secretion of key protein products (adipokines), whereas others

prevent the expression of genes implicated in the maintenance of stemness or the commitment into non-adipose phenotypes (Rauch *et al.*, 2019). In particular, brown adipogenesis involves the repression of genes implicated in both white adipocyte and skeletal muscle differentiation and the expression of genes implicated in mitochondrial biogenesis and function (Shapira *et al.*, 2019). In these latter group highlights uncoupling protein 1 (Ucp1), since its expression is a specific *bona fide* marker of brown adipocyte phenotype. Important for the interpretation of the findings of this thesis, it was recently described that genes involved in the innate immune response, specifically the Type I interferon (IFN) response genes (*Ifi44*, *Oas2*, *Oasl2*, *Rsad2*, among others) are implicated in adipogenesis regulation (Kissig *et al.*, 2017; Liu *et al.*, 2019).

In this thesis we aimed to progress in the understanding of the cellular and molecular causes of lipodystrophy in AGPAT2 (*Agpat2*^{-/-}) deficient mice. For this, we worked on a model of *in vitro* brown adipocyte differentiation starting from precursor cells harvested from the interscapular iBAT of these animals.

To contextualize the work developed in this thesis, in the following sections will be adressed general aspects of generalized congenital lipodystrophy caused by AGPAT2, the origin and function of brown adipose tissue and adipogenesis and its regulation.

1.1. Congenital generalized lipodystrophy and lipotoxicity as a possible mechanism for adipose tissue destruction in AGPAT2 deficient mice.

Lipodystrophies are heterogeneous disorders, inherited or acquired, characterized by the pathological loss of body adipose tissue (Agarwal *et al.*, 2003; Garg, 2004). Whereas some patients have fat loss restricted to specific anatomic areas (partial lipodystrophy), others have compromised whole body adiposity (generalized lipodystrophy). The extent of fat loss determines the severity of associated complications, that in cases of generalized lipodystrophies include metabolic abnormalities such as insulin resistance, diabetes mellitus, hypertriglyceridemia, hypercholesterolemia, hepatic steatosis, polycystic ovary, female infertility and acanthosis nigricans (Garg, 2011).

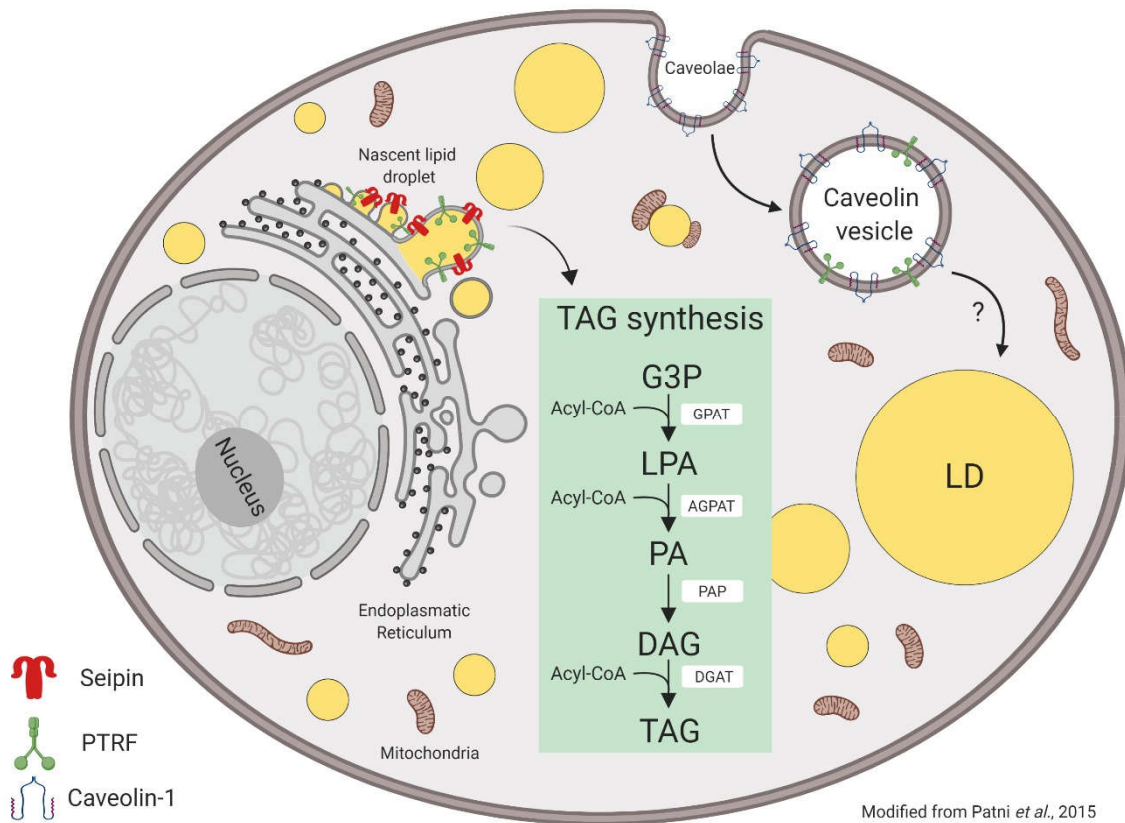
Genetic lipodystrophies can be classified as autosomal recessive or autosomal dominant based on inheritance patterns (Agarwal *et al.*, 2003). Congenital generalized lipodystrophy (CGL) was originally described by Berardinelli (Berardinelli, 1954) and Seip (Seip, 1959) and is a very infrequent autosomal recessive disease characterized by severe lipoatrophy in the whole body, insulin resistance and various endocrine abnormalities (Table 1). Characteristically, lipoatrophy is present since birth and dyslipidemia and diabetes are detectable at early childhood (Garg, 2004; Cortés *et al.*, 2015). The commonest cause of CGL are mutations in *AGPAT2* (CGL1) that encodes 1-acylglycerol-3-phosphate O-acyltransferase-2 (Agarwal *et al.*, 2002). Less frequent causes include mutations in *BSCL2* (CGL2), encoding SEIPIN, a large ER membrane protein important for lipid droplets maturation (Magré *et al.*, 2001), *CAVI* (CGL3), encoding Caveolin-1, a protein involved in caveolae formation and cholesterol and fatty acid cellular trafficking (Kim *et al.*, 2008), and *PTRF* (CGL4), encoding Cavin-1, also essential for caveolin formation (Hayashi *et al.*, 2009) (Figure 1).

Subtype (gene)	Key clinical features	Molecular basis/other comments CGL1
CGL1 (<i>AGPAT2</i>)	Lack of metabolically active adipose tissue since birth	AGPATs are key enzymes required for triglyceride and phospholipids biosynthesis. AGPATs acylate lysophosphatidic acid to form phosphatidic acid. AGPAT2 is highly expressed in adipose tissue.
CGL2 (<i>BSCL2</i>)	Lack of both metabolically active and mechanical adipose tissue since birth, mild mental retardation, cardiomyopathy	<i>BSCL2</i> encodes seipin, which may play a role in fusion of small lipid droplets and in adipocyte differentiation.
CGL3 (<i>CAVI</i>)	Single patient with extreme lack of body fat, short stature, and vitamin D resistance	Caveolin 1 is an integral component of caveolae, present in abundance on adipocyte membranes. Caveolin 1 binds fatty acids and translocates them to lipid droplets.
CGL4 (<i>PTRF</i>)	Extreme lack of body fat, congenital myopathy, pyloric stenosis, and cardiomyopathy	PTRF (also known as cavin) is involved in biogenesis of caveolae and regulates expression of caveolins 1 and 3.

TABLE 1. Classification, clinical features, and molecular bases of congenital generalized lipodystrophy (CGL) syndromes. Modified from Garg, 2011; Cortés *et al.*, 2015.

AGPAT2 is located on chromosome 9q34 (Garg *et al.*, 1999; Agarwal *et al.*, 2002) and encode a 278 amino acid enzyme that belongs to a family composed for another 10 acyl transferases. All isoforms are encoded by a different gene and have been detected in the ER membrane (Garg *et al.*, 2009; Agarwal *et al.*, 2010). All AGPATs catalyzes the second step in *de novo* glycerolipid synthesis pathway, acylating LPA (1-acylglycerol-3-phosphate) in the *sn*-2 position to form PA (1,2-diacylglycerol-3-phosphate) (Figure 1). All AGPATs belong to a larger family of acyltransferases that have four conserved motifs. Motif I has a catalytic role and the motifs II, III and IV are important for the binding of the substrate (Yamashita *et al.*, 2014). Different substrate preferences and tissue specific expression patterns have been described for the AGPAT isoforms; it is believed that these two facts explain the diverging functional and pathological consequences resulting from the lack of the different AGPATs (Agarwal, 2012). *AGPAT2* is highly expressed in adipocytes and is the only AGPAT isoform whose gene deletion results in generalized lipodystrophy in mouse models (Cortés *et al.*, 2009).

Knockdown of *AGPAT2* in Chinese hamster ovary-K1 (CHO) impairs adipogenic differentiation, resulting in lower triglycerides accumulation, decreased levels of CCAAT/enhancer-binding protein beta (C/EBP β) and peroxisome proliferator-activated receptor gamma (PPAR γ) and increased levels of PA (Gale *et al.*, 2006). Similar results were obtained in studies of adipogenic differentiation of muscle-derived multipotent cells of patients with *AGPAT2* mutations (Tsukahara *et al.*, 2010; Subauste *et al.*, 2012).



Modified from Patni *et al.*, 2015

FIGURE 1: Gene products implicated in lipodystrophy and lipid droplet formation in adipocytes. The biogenesis of lipid droplets (LD) is not completely understood but is believed that form as budding vesicles of endoplasmic reticulum membrane. Nascent LDs subsequently fused each other to form larger LDs in mature adipocytes. Many proteins, such as Seipin are present on the lipid droplet membrane. Caveolae are formed from lipid rafts on the cell surface, which include cholesterol, glycosphingolipids and Caveolin-1. Endocytosis of caveolae forms Caveolin vesicles that might directly merge with lipid droplets and translocate fatty acids to the lipid droplets. Acylation of glycerol-3-phosphate with fatty acyl coenzyme A (FA-CoA) at the *sn*-1 position is catalyzed by glycerol-3-phosphate acyltransferases (GPATs), resulting in the formation of 1-acylglycerol-3-phosphate or lysophosphatidic acid (LPA). LPA is then acylated at the *sn*-2 position by 1-acyl-*sn*-glycerol-3-phosphate acyltransferases (AGPATs) to yield phosphatidic acid (PA). Removal of a phosphate group from PA by PA phosphatases (PAPs) produces diacylglycerol (DAG). Further acylation of DAG at the *sn*-3 position by diacylglycerol acyltransferases (DGATs) finally produces triglyceride. Modified from Patni *et al.*, 2015.

Agpat2^{-/-} mice present a total deficiency of adipose tissue, including WAT and BAT, and severe insulin resistance, diabetes mellitus, dyslipidemia and hepatic steatosis (Cortés *et al.*, 2009). Importantly, in spite of the generalized lipodystrophy of *Agpat2*^{-/-} mice during adulthood, these animals are born with near normal WAT and BAT mass that is lost in the first week of life due to the massive adipocyte death and inflammatory infiltration (Cautivo *et al.*, 2016).

In previous work our laboratory showed that adipogenically differentiated mouse embryonic fibroblasts (MEFs) derived from *Agpat2*^{-/-} mice have decreased levels of PPAR γ and other mature adipocyte markers, in association with increased PA content (Cautivo *et al.*, 2016). Importantly, in this experimental model, forced expression of PPAR γ by recombinant adenovirus transduction only partially restored LD abundance in *Agpat2*^{-/-} cells (Cautivo *et al.*, 2016), indicating that the absence of AGPAT2 affects adipogenic differentiation on several levels, likely upstream to PPAR γ .

The causes of the adipose tissue destruction in the newborn *Agpat2*^{-/-} mice are unknown, however, increased circulating lipids generated by the inability to store lipids and the intake of milk after birth could promote adipocytes death by lipotoxic mechanisms (Liang *et al.*, 2016)

Excessive accumulation of lipids in non-adipose tissues such as liver, skeletal muscle, pancreas and arteries has been associated with cellular toxicity and insulin resistance in patients with obesity and diabetes (Brookheart *et al.*, 2009). Concordantly, experimental models of ectopic lipid build up develop insulin resistance and dyslipidemia (Shimabukuro *et al.*, 1998; Goh *et al.*, 2007; Zhou *et al.*, 2019). This pathophysiological mechanism is proposed underlying cause of insulin resistance in obesity as well as lipodystrophy (Unger, 1995; Krssak *et al.*, 1999; Perseghin *et al.*, 1999; Szczepaniak *et al.*, 1999; Simha *et al.*, 2003; Brookheart *et al.*, 2009).

In addition, the lack of adipose tissue in lipodystrophic patients and animal models determines leptin deficiency that, in turn, results in hyperphagia, insulin resistance and decreased fatty acid oxidation in skeletal muscle and liver. Combined, these abnormalities lead to a mismatch between lipid intake and the capacity deposit lipids in adipocytes (because of the intrinsic adipose tissue deficiency in lipodystrophy). At the end, this global mismatching between lipid intake and disposition-oxidation is thought to be the main driver of the ectopic accumulation of lipids in myocytes, hepatocytes and β -cells of the pancreatic islets in lipodystrophy (Unger, 2002, 2010).

Among the lipid species quantified in tissues of patients and animal models of lipotoxicity, highlight saturated fatty acids, particularly palmitic acid (C16:0) (Maedler *et al.*, 2001). Importantly, incubation of different cell types with high concentrations of C16:0 result in cell death (de Vries *et al.*, 1997; Paumen *et al.*, 1997). Interestingly, co-treatment with unsaturated fatty acids markedly reduces C16:0 lipotoxicity (Listenberger *et al.*, 2003; Maedler *et al.*, 2003).

The mechanisms of lipotoxic cell death are multiple and include oxidative stress, mitochondrial dysfunction (Yang *et al.*, 2014; Tsushima *et al.*, 2018) and excessive endoplasmic reticulum (ER) stress (Rius *et al.*, 2017; Zou *et al.*, 2017), all can ultimately lead to cell death, mostly by apoptotic mechanisms. Additionally, C16:0 is the biosynthetic precursor of ceramides and sphingolipids, including sphingomyelin and gangliosides. Ceramide levels are increased in cultured cells exposed to excessive palmitate (Shimabukuro *et al.*, 1998; Listenberger *et al.*, 2001) as well as in the liver and muscle of insulin resistant patients (Adams *et al.*, 2004) and obese (Sajan *et al.*, 2015) and lipodystrophic (Sankella *et al.*, 2017) mice.

Ceramides induces cell death due to mitochondrial dysfunction, oxidative stress and caspase activation (Law *et al.*, 2018; Walls *et al.*, 2018) and impairs insulin signaling by activating atypical protein kinase C (aPKC)-dependent (Chavez *et al.*, 2012; Sajan *et al.*, 2015) and double-stranded RNA-dependent kinase (PKR) (Ussher *et al.*, 2010) pathways. Importantly, experimental reduction of ceramide content improves insulin sensitivity in different animal models of obesity and diabetes (Ussher *et al.*, 2010; Holland *et al.*, 2011; Raichur *et al.*, 2019).

3T3-L1 cells differentiated to adipocytes and treated with C16:0 show increased autophagic flow, ER stress and decreased cell viability (Yin *et al.*, 2015). Similarly, exogenous administration of ceramides to this cell line decreases the abundance of adipogenic markers C/EBP β and PPAR γ and inhibits adipogenesis (Ordoñez *et al.*, 2017, 2018). In brown adipocytes, C16:0 decreases glucose transport (Teruel *et al.*, 2001), inhibits the induction of thermogenic genes by forskolin (Chaurasia *et al.*, 2016) and prevents browning of beige adipocytes (Jiang *et al.*, 2015).

1.2. General concepts on adipose tissue biology.

White adipose tissue (WAT) mainly stores large amount of lipids as a buffer for energy supply during fasting and secrete a vast number of protein products with hormone function (adipokines). By contrast, the main physiological function of brown adipose tissue (BAT) is the dissipation of energy in the form of heat, for thermoregulatory purposes. Brite/beige adipose tissue is an additional class that has been more recently characterized (Tapia *et al.*, 2018). Heat production by BAT results in non-shivering thermogenesis and requires the action of UCP1 in the inner mitochondrial membrane (IMM) of brown adipocytes. UCP1 (also referred as “thermogenin”) decouples the oxidation of metabolic substrates and proton electrochemical gradient across IMM from the synthesis of ATP, dissipating metabolic energy in the form of heat. The thermogenic capability of BAT is required for the adaptation to cold, particularly in small mammals including rodents and new born humans (Cannon *et al.*, 2004). By contrast, the physiological relevance of BAT in adult humans remain controversial, although it is thought to be a therapeutic target for obesity, by means of favoring a negative energy balance (Tapia *et al.*, 2018).

In mice and newborn humans, BAT is a well-defined anatomical structure, mostly located in the interscapular space and composed by cells laden with multiple middle-sized lipid droplets (multilocular adipocytes) and that have abundant UCP1-expressing mitochondria (Figure 2). iBAT has been known for a long time (Aherne *et al.*, 1966; Merklin, 1974) and is englobed by a layer of WAT. This tissue is fully developed and functional at the time of birth in mice and humans (Cannon *et al.*, 2004). By contrast, in mice WAT mass is minimal at birth

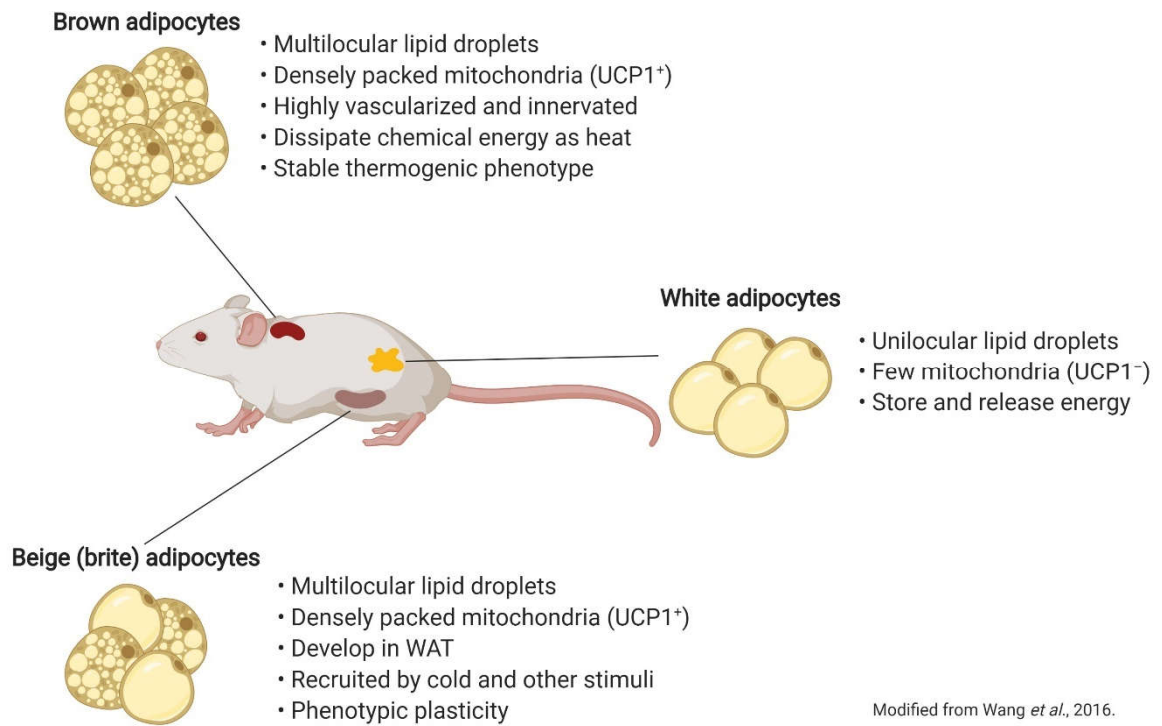


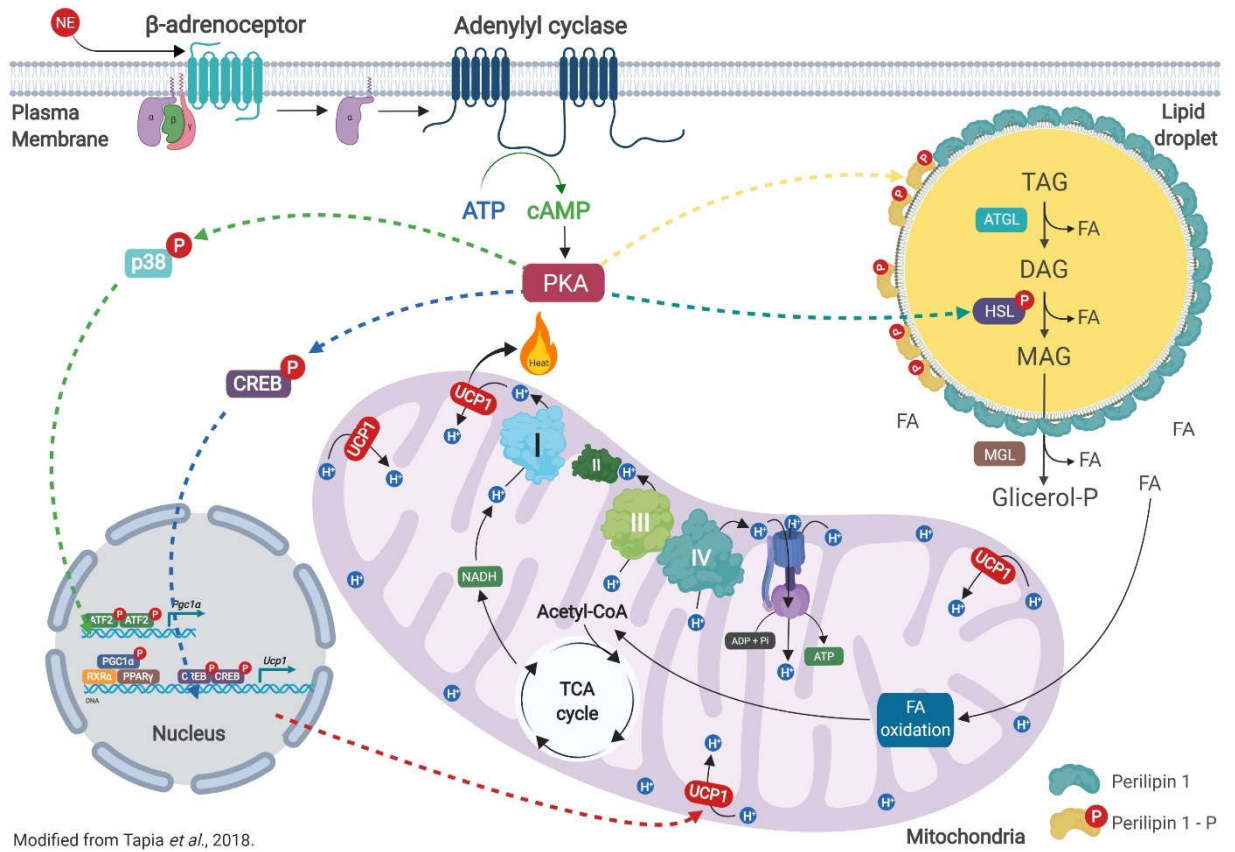
FIGURE 2: Brown, white and brite/beige adipocytes. There are three types of adipocyte: brown, white and beige. Brown adipocytes in brown adipose tissue (BAT) are characterized by the presence of multilocular lipid droplets and densely packed mitochondria containing uncoupling protein 1 (UCP1). White adipocytes in white adipose tissue (WAT) are characterized by the presence of unilocular lipid droplets and few mitochondria that are devoid of UCP1. Beige adipocytes are found in various WAT depots and are especially prominent in the subcutaneous inguinal WAT. Beige fat cells develop in response to cold and certain other stimuli. Like brown adipocytes, beige cells have multilocular lipid droplets and densely packed UCP1-positive mitochondria. Modified from Wang *et al.*, 2016.

but is substantially increased by both hypertrophic and hyperplastic mechanisms during the first days of postnatal life (Wang *et al.*, 2013). Importantly, iBAT persists as an anatomical entity in adult mice but disappears in humans as they age (Heaton, 1972). “Brite” (brown in white) adipose tissue refers to clusters of multilocular UCP1-expressing adipocytes included in a larger mass of otherwise classical WAT (Figure 2). Brite adipocytes have thermogenic capacity and are the exclusive form of BAT in adult humans (Shinoda *et al.*, 2015). Importantly, brite adipocytes are only apparent in studies using cold or β -adrenergic pharmacological stimulation, illustrating the sparse mass of this tissue *in vivo* (Cousin *et al.*, 1992). Subsequent characterizations have shown that brite adipocytes express specific molecular markers that are absent in classical iBAT and WAT (Petrovic *et al.*, 2010).

In mice, the main non-shivering thermogenic capacity roots in classical iBAT (Kalinovich *et al.*, 2017) although they also have metabolically active brite adipose tissue (Wu *et al.*, 2012). In adult humans, metabolically active deposits of BAT are present in the neck and supraclavicular areas, as indicated by 18F-fluorodeoxyglucose (18F-FDG) by positron emission tomography (PET)-based studies (Cypess *et al.*, 2009; van Marken *et al.*, 2009; Virtanen *et al.*, 2009). The thermogenic potential of BAT in adult humans is formally unknown but it is predicted to be small, given the small total mass of this tissue reported in most studies (~300 g) (Tapia *et al.*, 2018).

The main physiological thermogenic activator of BAT is cold. Low body temperature triggers sympathetic nervous system (SNS) activation and norepinephrine (NE) release (Cottle *et al.*, 1967). NE binds to β -adrenergic receptors – that in mice mostly correspond to β 3 but that in humans are both β 2 and β 3 receptors (Nahmias *et al.*, 1991; Krief *et al.*, 1993; Susulic *et al.*,

1995; Grujic *et al.*, 1997) –, increasing cyclic adenosine monophosphate (cAMP) levels via adenylate cyclase (AC) activation in brown adipocytes (Arch *et al.*, 1984; Granneman, 1988). This allows the activation of cAMP-dependent protein kinase (PKA) (Fredriksson *et al.*, 2001) that phosphorylates and activates cAMP response element-binding (CREB) (Chaudhry *et al.*, 1999). Along with CREB, the activation of p38 mitogen-activated protein kinases (p38 MAPK) has also been described, leading to phosphorylation of activating transcription factor 2 (ATF2) and peroxisome proliferative activated receptor, gamma, coactivator 1 alpha (PGC1 α), thus allowing its binding, together with PPAR γ and retinoid X receptor alpha (RXR α), to UCP1 promoter and thus increasing UCP1 protein levels. ATF2 also increases PGC1 α levels, further promoting adrenergic-mediated BAT thermogenesis (Cao *et al.*, 2001, 2004). In parallel, increased cAMP levels and activated PKA induces the lipolytic release of free fatty acids from lipid droplets triglycerides (Zechner *et al.*, 2009). These fatty acids are imported and oxidized in the mitochondria to generate reductive equivalents that ultimately fuel mitochondrial H⁺ electrochemical gradient that allows UCP1-dependent thermogenesis (Bertholet *et al.*, 2017) (Figure 3).



Modified from Tapia *et al.*, 2018.

FIGURE 3: β -adrenergic receptors coordinate triglyceride lipolysis, mitochondrial fatty acid oxidation and uncoupling protein 1 (UCP1) abundance and function in brown adipocytes. Sympathetic stimulation of interscapular brown adipose tissue (iBAT) is the main physiological mechanism for regulating non-shivering thermogenesis in response to cold exposure. After norepinephrine (NE) binding, β -adrenoceptor (BAR) activates adenylyl cyclase (AC) and increases cyclic AMP (cAMP) intracellular concentration through protein Gs-dependent mechanisms. cAMP binds to protein kinase A (PKA) and promotes the phosphorylation of direct PKA target proteins. These include perilipin 1, a structural protein present on the lipid droplet (LD) surface and hormone-sensitive lipase (HSL), a required enzyme for LD triglyceride (TAG) lipolysis. In its non-phosphorylated state, perilipin 1 prevents the interaction between HSL as well as other lipases adipose triglyceride lipase (ATGL) and monoacylglycerol lipase (MGL) with the LD. Phosphorylated perilipin1 allows the physical interaction between these lipolytic enzymes and the LD. In parallel, PKA-mediated phosphorylation of HSL triggers the translocation of this enzyme from the cytoplasm to the LD to mediate hydrolysis of sn-2,3 diacylglycerols (DAG). The resulting monoacylglycerols (MAG) are finally deacylated by MGL. The released fatty acids (FAs) are imported to the mitochondria where they are oxidized to acetyl-coenzyme A (acetyl Co-A) and ultimately fuel the oxidative phosphorylation of ADP to ATP. Adrenergic stimulation also increases the abundance of uncoupling protein 1 (UCP1) in the inner mitochondrial membrane (IMM) by transcriptional mechanisms that also depend on cAMP levels and PKA activation. PKA promotes the phosphorylation of cAMP response element-binding (CREB) allowing its binding to regions of the *Ucp1* promoter, and also phosphorylates p38 mitogen-activated protein kinases (p38 MAPK), leading to phosphorylation of activating transcription factor 2 (ATF2) allowing its binding to regions of the *Pgc1a* promoter. PGC1 α together with the peroxisome proliferator-activated receptor gamma (PPAR γ) and retinoid X receptor alpha (RXR α), to UCP1 promoter, thus increasing UCP1 protein levels. This results in the dissipation of the electrochemical H⁺ gradient across the inner mitochondrial membrane (IMM) and heat generation. Modified from Tapia *et al.*, 2018.

1.3. Regulation of brown adipogenesis.

Adipocyte development (adipogenesis) is currently understood as a two phases process. In the first step, pluripotential cells are committed to a lineage with differentiation potential mostly restricted to adipocytes, denominated “preadipocytes”. These cells have no lipid accumulation and preserve phenotypic features of mesenchymal stem cells, fusiform shape and elevated adherence to plastic dishes. Experimentally, preadipocytes can be recovered from the “stromal vascular fraction” (SVF) that is generated after the disaggregation and fractionation of adipose tissue.

In the following step, adipogenic differentiation results in the conversion of preadipocytes to mature adipocytes. This process has been extensively studied *in vitro*, and several pro- and anti-adipogenic regulators are currently identified (Inagaki *et al.*, 2016). The physiological relevance for the *in vivo* adipose tissue formation, growth and functioning has been confirmed for some of these factors, as explained in the following sections.

In the following sections, I detail the main processes and regulators of brown adipocytes differentiation that are relevant for the understanding of this thesis. Other aspects of BAT, such as its impact on human health, as well as its secretory activities, are not treated here but can be addressed in my review article "Biology and pathological implications of brown adipose tissue: promises and caveats for the control of obesity and its associated complications" (Tapia *et al.*, 2018).

1.3.1. Brown adipose cell fate commitment.

In mouse, iBAT develops from the central dermomyotome, a dorsal epithelial cell layer of the somite located immediately under the ectoderm, and that also give rise to the epaxial skeletal muscle (Tapia *et al.*, 2018). This was discovered after monitoring gene expression of transcription factor homeobox protein Engrailed-1 (EN1) in transgenic mice expressing beta galactosidase (β -Gal) upon the transcriptional control of *En1* promoter (Atit *et al.*, 2006). Dorsal dermomyotome En1-expressing cells are detectable at embryonic stages E8.5-E9.5 and give rise to iBAT brown adipocytes at day E10.5 as well as to muscle cells at stage E16.5 (Atit *et al.*, 2006). Also, gene fate mapping studies using β -Gal upon the transcriptional control of paired box 7 (PAX7) promoter, determined that *Pax7*-expressing cells in E9.5 give rise to iBAT as well as skeletal muscle myocytes and part of the dermis in the adult mice (Lepper *et al.*, 2010).

Although precursor cells that give rise to iBAT and muscle are different from those exclusively committed to muscle cells (*Pax7*-expressing cells at E12.5) (Lepper *et al.*, 2010), these two precursor cells share a large number of molecular markers. Importantly, these similarities are lost as myogenic and adipogenic programs progress (Timmons *et al.*, 2007). An exception is myogenic factor 5 (MYF5), that remains expressed in both skeletal muscle and iBAT until adulthood in mice (Seale *et al.*, 2008).

Based on the above findings, the current paradigm is that classical brown adipocytes and myocytes of epaxial skeletal muscle have a common cellular origin that is different from the one of white adipocytes. Importantly, in spite of the morphological, molecular and functional similitudes between beige/brite and classical brown adipocytes, the former lack *Myf5* expression, as well as other iBAT molecular markers, including early B-cell factor 3 (EBF3),

epithelial V-like antigen 1 (EVA1) and F-box only protein 31 (FBXO31), suggesting that classical brown adipocytes have a different cellular origin than beige/brite adipocytes (Wu *et al.*, 2012).

Several transcription factors have been described to positively or negatively regulate brown preadipocytes commitment to mature brown adipocytes (Figure 4).

PRD1-BF1-RIZ1 homologous domain containing 16 (PRDM16) is a “molecular switch” that facilitates the expression of genes required for brown adipocyte phenotype while blocks the expression of those that determine white adipocyte phenotype (Seale *et al.*, 2007). In fact, PRDM16 is highly enriched in brown adipose cells in comparison with white adipocytes, and its ectopic expression in cell lines, prior to adipogenic induction, leads to the expression of markers of mature brown adipocytes such as UCP1, as well as mitochondrial biogenesis and increased cellular respiration (Seale *et al.*, 2007). PRDM16 also suppresses myogenic program by a mechanism that requires euchromatic histone methyltransferase 1 (EHMT1) (Ohno *et al.*, 2013) and ZFP516 (Dempersmier *et al.*, 2015) *in vivo*.

B cell factor 2 (EBF2) is a highly expressed gene in BAT cells and its activation results in a brown adipocyte morphology and UCP1 gene expression (Rajakumari *et al.*, 2013). EBF2 is found in *Myf5*⁺ brown adipocytes, but not in muscle and dermal cells of the anterior dorsal region at E14.5 (Wang *et al.*, 2014). *Myf5*⁻ and *Ebf2*⁺ cells, isolated from the SVF of inguinal fat of mice and exposed to cold differentiate into cells expressing brown adipocyte markers and, concordantly, *Ebf2*^{-/-} mice fail to express UCP1 in inguinal white adipose tissue after cold exposure, indicating a possible participation of EBF2 in beige/brite adipocyte differentiation *in vivo* (Atit *et al.*, 2006; Wang *et al.*, 2014).

Additional proteins have also been described as participants in the adipose versus muscle differentiation, highlighting Ewing Sarcoma (EWS) that interacts with the transcription factor Y-Box Binding Protein (YBX1) and promotes the expression of bone morphogenetic protein 7 (BMP7) (Park *et al.*, 2013).

1.3.2. Brown adipocyte differentiation: classical and novel regulators with potential importance for AGPAT2-dependent lipodystrophy.

PPAR γ is a key transcriptional regulator of adipogenesis, is absolutely required for adipogenic differentiation *in vivo* and *in vitro* (Barak *et al.*, 1999; Rosen *et al.*, 1999). PPAR γ cooperates with CCAAT/enhancer binding protein alpha (C/EBP α) to regulate specific adipocyte genes (Madsen *et al.*, 2014). Importantly, PPAR γ and C/EBP α participate in later phases of adipogenesis. In the "first phase", pro-adipogenic factors CCAAT/enhancer binding protein delta (C/EBP δ) and C/EBP β are induced. This latter is expressed at higher levels in BAT than in WAT, and is strongly induced by cold in iBAT (Kajimura *et al.*, 2009). C/EBP β is the main target of many transcriptional and epigenetic regulators during brown adipocyte differentiation. One of these is placenta-specific gene 8 protein (PLAC8), which directly binds to C/EBP β regulatory region, activating its transcription and promoting brown adipogenesis (Jimenez-Preitner *et al.*, 2011).

PRDM16 forms a transcriptional complex with C/EBP β and PPAR γ to promotes brown adipogenesis (Seale *et al.*, 2007; Kajimura *et al.*, 2009). In addition, PRDM16 establishes enhancer-promoter contacts with genes such as peroxisome proliferator-activated receptor alpha (*Ppara*) and *Pgc1a* to activate mitochondrial biogenesis and UCP1 expression (Harms *et al.*, 2014; Iida *et al.*, 2015).

Members of the EBF family are also recognized regulators of brown adipogenesis. Ectopic expression of EBF1, EBF2 or EBF3 is sufficient to induce adipogenesis in fibroblasts (Akerblad *et al.*, 2002; Jimenez *et al.*, 2007) by recruiting PPAR γ to regulatory regions of selected brown adipocyte-specific genes (Rajakumari *et al.*, 2013).

PGC1 α was first discovered interacting with PPAR γ in brown adipocytes and its expression is highly induced by exposure to cold (Puigserver *et al.*, 1998). PGC1 α activates nuclear respiratory factors (NRF) 1 and 2 to activate a transcriptional program that drives mitochondria biogenesis. PGC1 α also co-activates nuclear hormone receptors PPAR α and estrogen-related receptors (ERR) $\alpha/\beta/\gamma$, to increase the transcription of brown adipocyte marker genes. PPAR α is a nuclear receptor that regulates lipid metabolism by promoting β -oxidation of fatty acids in mitochondria and peroxisomes (Figure 4).

Ppara gene expression is regulated by EBF2, PRDM16, PPAR γ and C/EBP β , and can directly activate *Ucp1* transcription (Hondares *et al.*, 2011). Interestingly, mice lacking PPAR α specifically in brown adipocytes have normal levels of UCP1 and survives to cold stress, indicating that this nuclear receptor is not absolutely required for *Ucp1* expression (Lasar *et al.*, 2018).

Several proteins have been identified as molecular markers of brown adipocyte cell identity, since are almost exclusively expressed in brown and beige adipocytes (Inagaki *et al.*, 2016). Besides UCP1, highlight cell death-inducing DNA fragmentation factor effector a (CIDEA), important for lipid drop remodeling, iodothyronine deiodinase 2 (DIO2), a deiodinase that converts thyroxine (T4) into the biologically active thyroid hormone triiodothyronine (T3) and elongation of very long chain fatty acids (ELOVL3), a fatty acid elongase that generates very long chain fatty acids (Shapira *et al.*, 2019).

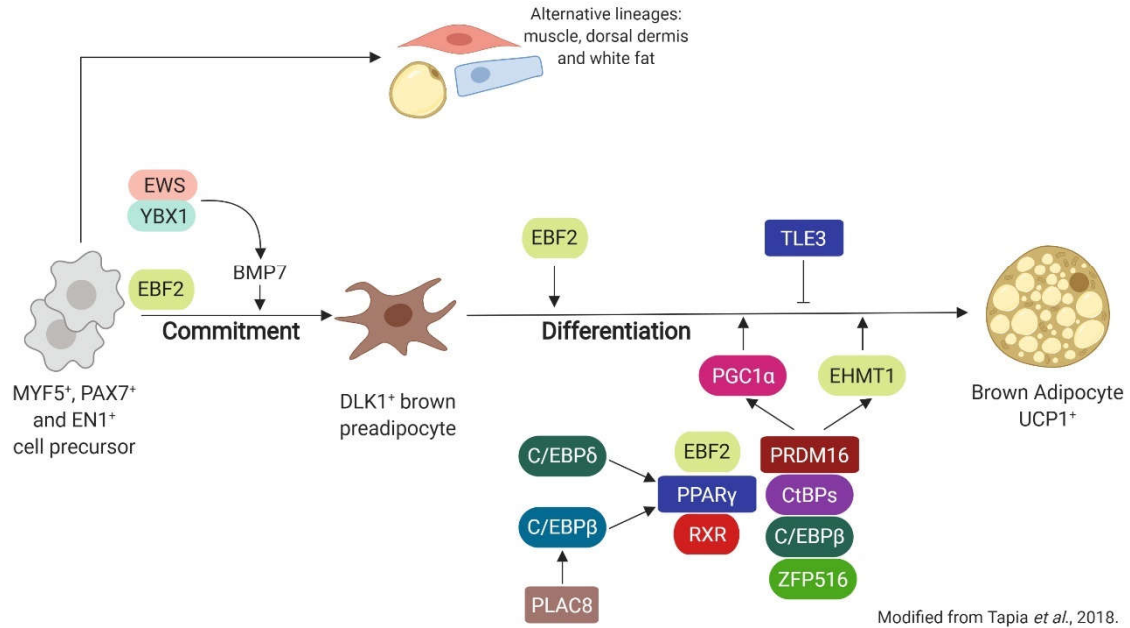


FIGURE 4: Transcriptional regulation of brown adipogenesis. Classical brown adipocytes reside in the interscapular adipose tissue of rodents and newborn humans. They derive from mesenchymal precursors that express myogenic factor 5 (MYF5) and that also generate skeletal muscle myocytes. Adipogenic stimuli favor the conversion of these undifferentiated precursors to committed preadipocytes that progressively transform into fully differentiated brown adipocytes upon the transcriptional control of several regulatory proteins and microRNAs (miRNAs) (not shown for simplicity). Peroxisome proliferator-activated receptor γ (PPAR γ) is necessary but not sufficient for brown adipogenesis. PRD1-BF-1RIZ1 homologous-containing protein 16 (PRDM16) is a co-regulatory factor that interacts with other proteins to assemble transcriptional complexes that coordinate to suppress WAT and activate BAT adipogenesis. BMP7: bone morphogenetic protein 7; C/EBP: CCAAT/enhancer binding protein; CtBPs: C-terminal binding proteins; EHMT1: euchromatic histone lysine methyltransferase 1; EN1: Engrailed homeobox 1; EWS: Ewing sarcoma; PAX7: Paired box 7; PGC1 α : PPARG coactivator 1 alpha; PLAC8: placenta-specific gene 8 protein; RXR: Retinoid X receptor; TLE3: Transducin like enhancer of split 3; YBX1: Y-Box binding protein 1; zinc finger protein 516: ZFP516. Modified from Tapia *et al.*, 2018.

UCP1, also known as SLC25A7, was discovered in 1976 (Nicholls, 1976). Mitochondria of brown adipocytes characteristically have large amounts of UCP1 in their IMM, where it dissipates the proton gradient generated by the electron transport chain system, releasing heat at the expense of decreasing ATP synthesis. *Ucp1* gene has regulatory regions with CREB-binding sites that mediates positive transcriptional response to cAMP and negative to c-Jun/c-Fos complexes (Kozak *et al.*, 1994; Yubero *et al.*, 1998). Recently, it was showed that transcription factor ZFP516 binds to a proximal region of the *Ucp1* gene, playing a key role in the response to cold (Dempersmier *et al.*, 2015). Also, the proximal region of *Ucp1* gene, has a strong enhancer region that contains a cluster of response elements for nuclear hormone receptors that bind PPAR α /RXR, PPAR γ /RXR, retinoic acid receptor (RAR)/RXR and thyroid receptor (TR)/RXR, providing response to PPAR α and PPAR γ activators (Villarroya *et al.*, 2017).

Elovl3 participates in the synthesis of saturated and monounsaturated fatty acids of up to 24 carbons. iBAT is the tissue with the highest Elovl3 abundance and its tissue levels are increased more than 200-fold in mice after cold exposure (Tvrđik *et al.*, 1997). *Elovl3* gene expression is under the control of glucocorticoids, norepinephrine, and the three isoforms of PPAR (α , β/δ and γ) (Guillou *et al.*, 2010). *Elovl3*^{-/-} mice have decreased adipose tissue mass and lower liver fat content, indicating that Elovl3 is necessary for tissue triglycerides build up (Zadravec *et al.*, 2010).

More recently it was shown that transcriptional regulation of adipogenesis is also regulated by innate immunity response genes, specifically type I interferon (IFN) pathways (Lee *et al.*, 2016; Kissig *et al.*, 2017; Liu *et al.*, 2019).

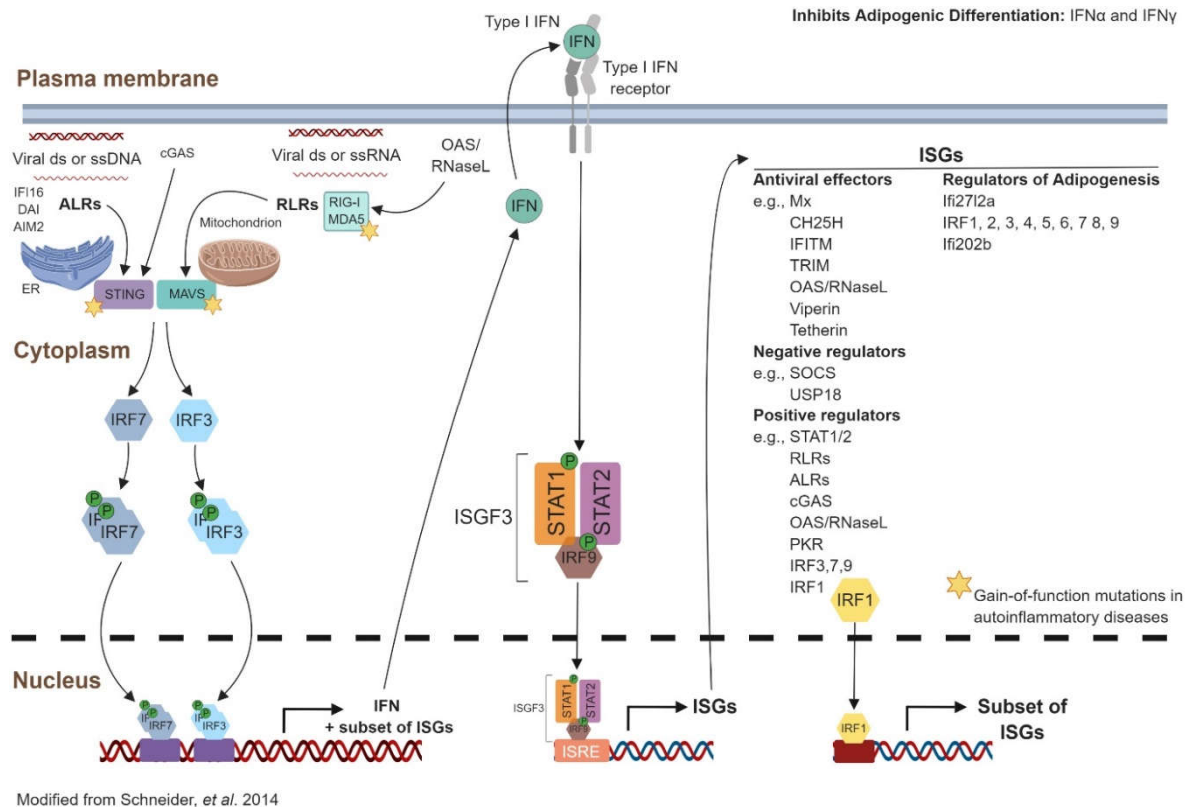


FIGURE 5: Activation of ISGs. Absent in melanoma 2 (AIM2)-like receptors (ALRs), such as interferon gamma inducible protein 16 (IFI16), DNA-dependent activator of interferon regulatory factors (IRFs) (DAI), or AIM2, specialize in DNA detection, while retinoic acid-inducible gene I (RIG-I) like receptors (RLR) -RIG-I and melanoma differentiation associated gene 5 (MDA5)- are specialized in the detection of RNA. Cyclic GMP-AMP synthase (cGAS) acts as an additional DNA sensor. 2-5-oligoadenylate synthetase (OAS) senses exogenous RNA and produces 2-5 adenylic acid that activates latent RNase (RNaseL). The degradation products produced by RNaseL stimulate RLRs. These signals activate factors activating the stimulator of IFN genes (STING) and the mitochondrial antiviral-signaling protein (MAVS) at the ER/mitochondrion-associated membrane, leading to the phosphorylation of interferon (IFN) response factors 3 or 7 (IRF3/7). Phosphorylated dimers of IRF3/7 trigger IFN expression as well as a subset of ISGs. IFN induces gene expression of the JAK-STAT pathway, resulting in the expression of a large number of interferon-stimulated genes (ISGs) (antiviral effectors and negative or positive regulators). IRF1 can also directly translocate to the nucleus and activate ISGs. Several ISGs have been described as modulators of adipogenic differentiation, as well as IFN α and IFN γ . In autoinflammatory diseases, mutated DNA or RNA recognition factors (STING, MAVS, RIG-1 and MDA5) cause a spontaneous increase in transcription of type I IFN-induced genes. Modified from Schneider *et al.*, 2014.

Type I interferons (IFNs) are encoded by a family of genes clustered in chromosome 9q in humans and chromosome 4 in mice. There are 14 subtypes of IFN α , one subtype of IFN β , and single IFN ϵ and an IFN ω (Hertzog *et al.*, 2013). All type I IFNs function to orchestrate the cellular response to acute viral, bacterial and parasite infections (Schneider *et al.*, 2014) (Figure 5). Exaggerated or dysregulated IFN responses, however, can lead to cell death and is the underlying cause of some genetic autoinflammatory syndromes (Manthiram *et al.*, 2017). IFNs bind to cell surface receptors and signal through common heterodimeric receiver of low- (IFNAR1) and high-affinity (IFNAR2) receiver components (de Weerd *et al.*, 2012), triggering a signaling cascade based on Janus kinase - signal transducer and activator of transcription (JAK-STAT) pathways, which in turn regulate the transcription of hundreds of genes. Many IFN-stimulated genes (ISGs), such as *Jak2*, *Stat1/2* and *Irf9*, are expressed at basal levels but their abundance is increased in response to IFNs (Ivashkiv *et al.*, 2014; Schneider *et al.*, 2014).

The role of type I IFNs was noted in 3T3-L1 cells treated with IFN- α and then subjected to adipogenic differentiation. These cells have lower accumulation of LDs and decreased levels of adipogenic regulators (C/EBP β , C/EBP α and PPAR γ) and mature adipocyte markers fatty acid binding protein 4 (FABP4), sterol regulatory element binding transcription factor 1 (SREBP-1c) and fatty acid synthase (FAS) (Lee *et al.*, 2016).

More recent works have shown that type I IFN-response impairs both mitochondrial biogenesis and thermogenesis during brown adipocyte differentiation by modulating PRDM16 transcriptional activity (Kissig *et al.*, 2017). In fact, PRDM16 and IFN-activated pathways antagonize each other to regulate ISGs *Irf7*, *Ifi44*, *Mx2*, *Cxcl9*, and *Oas2*, as well as brown

adipocyte markers *Ucp1*, *Cidea* and *Cox7a1*. Importantly, PRDM16 deficiency determines structural mitochondrial abnormalities in differentiated adipocytes (Kissig *et al.*, 2017).

Interestingly, patients with some autoinflammatory syndromes such as Otulipenia and proteasome-associated autoinflammatory syndromes (PRAAS)/Chronic Atypical Neutrophilic Dermatitis with Lipodystrophy and Elevated Temperature (CANDLE), develop severe forms of lipodystrophy, suggesting that dysregulated type I INFs pathways are implicated in human impaired adipogenesis (Manthiram *et al.*, 2017).

In summary, mutations in *AGPAT2* in humans cause congenital generalized lipodystrophy. The *Agpat2*^{-/-} mice also have the absence of adipose tissue during its adulthood, however, it is born with WAT and BAT, which are lost during the first week of life due to massive death of the adipocytes and inflammatory infiltration (Cautivo *et al.*, 2016).

The causes of the loss of BAT in the *Agpat2*^{-/-} mice is currently unknown, however, transcriptional problems caused by the absence of AGPAT2 in MEF differentiated to white adipocytes (Cautivo *et al.*, 2016) suggest that this phenomenon could be occurring in brown adipocytes, playing a role key in the loss of BAT. Together with the above, the high levels of circulating lipids in newborn animals could be contributing to tissue loss through lipotoxic-dependent adipocyte death.

Hypothesis and aims.**Hypothesis.**

“Brown adipocytes of *Agpat2*^{-/-} mice have transcriptional abnormalities that lead to impaired adipogenesis and increased susceptibility to cell death by lipotoxic mechanisms”

Aims.

1. To characterize the transcriptional program of *in vitro* differentiated brown adipocytes of *Agpat2*^{-/-} mice.
2. To evaluate the adipogenic effect of overexpressing specific genes decreased in differentiated brown adipocytes of *Agpat2*^{-/-} mice.
3. To determine the susceptibility of differentiated brown adipocytes of *Agpat2*^{-/-} mice to lipotoxic cell death.

3. Materials and methods.

3.1. Materials

3.1.1. Genotyping reagents.

Direct PCR Lysis Reagent (Viagen), Proteinase K (Merck Millipore), Phire Hot Start II DNA Polymerase (Thermo Scientific), dNTP Mix 10 mM (Thermo Scientific), GeneRuler 100 bp DNA Ladder DNA (Thermo Scientific), Gel Loading Dye 6X (Thermo Scientific), SeaKem LE Agarose (Lonza) and SYBR™ Safe DNA Gel Stain (Thermo Scientific).

3.1.2. Cell culture reagents.

DMEM/F-12 powder HEPES (Gibco), Antibiotic-Antimycotic (Thermo Scientific), Fetal Bovine Serum (Gibco), Fetal Bovine Serum (Biowest), Trypsin-EDTA 0,25% phenol red (Gibco), DMEM high glucose (Gibco), MEM Non-Essential Amino Acids Solution 100X (Gibco) and L-Glutamine 200 mM (Gibco).

3.1.3. Reagents for cloning and generation of recombinant adenoviruses.

PureLink™ Quick Gel Extraction Kit (Invitrogen), pENTR™/D-TOPO™ Cloning Kit with One Shot™ TOP10 Chemically Competent *E. coli* (Invitrogen), AxyPrep™ Plasmid Midiprep Kit (Axygen), Lipofectamine™ 2000 Transfection Reagent (Invitrogen), pAd/CMV/V5-DEST™ Gateway™ Vector Kit (Invitrogen), Gateway™ LR Clonase™ II Enzyme mix (Invitrogen), Pac I (New England Biolabs), Asc I (New England Biolabs), Not I HF (New England Biolabs), 293A Cell Line (Invitrogen), Cesium chloride (Merck) and Sephadex G-25 in PD-10 Desalting Columns (General Electric).

3.1.4. Western blotting reagents.

RIPA Lysis and Extraction Buffer (Thermo Scientific), Halt™ Protease Inhibitor Cocktail 100X (Thermo Scientific), Halt™ Phosphatase Inhibitor Cocktail 100X (Thermo Scientific), 40% Acrylamide/Bis Solution 37,5:1 (Biorad), Ammonium Persulfate (Biorad), Sodium Dodecyl Sulfate (Biorad), TEMED (Biorad), Lane Marker Reducing Sample Buffer (Thermo Scientific), AccuRuler RGB Plus Pre-stained Protein Ladder (Maestrogen), Immun-Blot® PVDF Membrane (Biorad), Westar Sun (Cyanagen) and Westar Supernova (Cyanagen).

3.1.5. qRT-PCR reagents.

UltraPure™ DNase/RNase-Free Distilled Water (Invitrogen), TURBO DNA-free™ Kit (Invitrogen), High-Capacity cDNA Reverse Transcription Kit (Applied Biosystems) and Fast SYBR™ Green Master Mix (Applied Biosystems).

3.1.6. Other reagents.

Glutaraldehyde 25% EM Grade Aqueous (Electron Microscopy Sciences), ONPG o-nitrophenyl-β-D-galactopyranoside (Thermo Scientific), Lactate dehydrogenase (LDH) Cytotoxicity Assay Kit (Cayman), Sodium palmitate (Sigma), Bovine Serum Albumin (BSA) Fraction V Fatty Acid-Free (Calbiochem), Gelatin from cold water fish skin (Sigma), Triton™ X-100 (Sigma), Paraformaldehyde (PFA) (Merck), Hoechst 33342 Trihydrochloride Trihydrate (Invitrogen), 4,4-difluoro-1,3,5,7,8-pentamethyl-4-bora-3a,4a-diaza-s-indacene (BODIPY) 493/503 (Invitrogen).

3.1.7. Antibodies.

Anti-GFP 1:1000 (Cell Signaling), Anti-PREF1 1:1000 (Cell Signaling), Anti-Tubulin 1:5000 (Abcam), Anti-PPARγ 1:1000 and 1:200 (Cell Signaling), Anti-PRDM16 1:400

(Abcam), Anti-C/EBP β 1:1000 (Cell Signaling), Anti-UCP1 1:400 (Abcam), Anti-PGC1 α 1:50 (Santa Cruz), Anti-STAT1 1:1000 and 1:400 (Cell Signaling), Anti-STAT2 1:1000 and 1:200 (Cell Signaling), Anti-FLAG 1:800 (Cell Signaling), Anti-mitoNEET 1:1000 (Cell Signaling), Anti-Cleaved Caspase 3 1:1000 and 1:200 (Cell Signaling), Anti-Caspase 3 1:1000 (Cell Signaling), Anti-Cytochrome c 1:200 (BD Biosciences), Donkey anti-Rabbit IgG (H+L) Highly Cross-Adsorbed Secondary Antibody Alexa Fluor 555 1:1000 (Invitrogen), Goat anti-Rabbit IgG (H+L) Highly Cross-Adsorbed Secondary Antibody Alexa Fluor 647 1:1000 (Invitrogen), Goat anti-Mouse IgG (H+L) Cross-Adsorbed Secondary Antibody Alexa Fluor 555 1:1000 (Invitrogen), Goat anti-Mouse IgG (H+L) Cross-Adsorbed Secondary Antibody Alexa Fluor 633 1:1000 (Invitrogen).

3.2. Methods

3.2.1. Maintenance and genotyping of mice.

The *Agpat2*^{+/+} and *Agpat2*^{-/-} mice were generated by crossing the *Agpat2*^{+/-} strain. These were developed at the University of Texas Southwestern Medical Center (UTSW) and transferred to the Pontificia Universidad Católica de Chile, through a material transfer agreement (MTA). Mice were maintained with 12 h light and dark cycles. All animal experiments were performed according to procedures approved by the Pontificia Universidad Católica de Chile committee for animal safety and bioethics (Protocol 13-029).

For genotyping, tissues from adult mice and neonates were digested with proteinase K 0,4 mg/mL in Lysis Reagent PCR for 12 h at 55°C and 2 h at 85°C. The product of the digestion was centrifuged for 5 minutes at 3000 x g, and the gDNA used as a template for genotyping PCR. This PCR uses the A8 starters (5'-AAA GCT GTG CCA GGG TGG GT-3'), A15 (5'-

CGG CTA GGT AAG CAG TTT GA-3') and SI75 (5'-GAT TGG GAA GAC AAT AGC AGG CAT GC-3'), and its program consists of: a) 30 seconds at 98°C initial denaturation, b) 7 cycles of 5 seconds at 98°C denaturation, 5 seconds at 70°C alignment, 10 seconds at 72°C extension and 24 cycles of 5 seconds at 98°C denaturation, 5 seconds at 62°C alignment, 10 seconds at 72°C extension, and c) 1 minute at 72°C final extension. The bands obtained were 782 bp for *Agpat2*^{+/+} and 614 bp for *Agpat2*^{-/-}.

The strain *Agpat2*^{+/-}/*Zfp423*^{GFP} was generated by successive crosses of *Agpat2*^{+/-} and *Zfp423*^{GFP} (B6; FVB-Tg (Zfp423-EGFP)7Brsp/J, 19381, Jackson Laboratory), which was used for the generation of *Agpat2*^{+/+}/*Zfp423*^{GFP} and *Agpat2*^{-/-}/*Zfp423*^{GFP}, as well as for the maintenance of the colony. The genotyping PCR of *Zfp423*^{GFP} uses the primers: 15020 (5'-CTG AAC TTG TGG CCG TTT AC-3'), 16612 (5'-AAG TTT CCG AGA GGC AGG AG-3'), 20286 (5'- TGT CTC TGA ACC CTG GGA AG-3') and 20287 (5'-GCA CCT TGA ACGA ACG ACA TC-3'). The expected bands are 250 bp for the transgene and 197 bp for the internal control. The PCR program consists: a) 30 seconds at 98°C initial denaturation, b) 25 cycles of 10 seconds at 98°C denaturation, 10 seconds at 61°C alignment, 20 seconds at 72°C extension and c) 1 minute at 72°C of final extension.

Agpat2^{+/+}/*Fabp4-Cre*⁺/*R26R*^{+/+} and *Agpat2*^{-/-}/*Fabp4-Cre*⁺/*R26R*^{+/+} mice were generated by the successive crossing of *Agpat2*^{+/-} mice, *Fabp4-Cre*⁺ (B6.Cg-Tg(Fabp4-cre)1Rev/J, 005069, Jackson Laboratory) and *R26R*^{+/+} (B6.129-*Gt(ROSA)26Sor*^{tm1Joc}/J, 8606, Jackson Laboratory). Genotyping PCR for *Fabp4-Cre*⁺ uses the primers oIMR1084 (5'-GCG GTC TGG CAG TAA AAA CTA TC-3'), oIMR1085 (5'- GTG AAA CAG CAT TGC TGT CAC TT-3'), oIMR7338 (5'- CTA GGC CAC AGA ATT GAA AGA TCT-3') and oIMR7339 (5'- GTA

GGT GGA AAT TCT AGC ATC ATC C-3'). PCR genotyping consists of the following steps: a) 30 seconds at 98°C initial denaturation, b) 35 cycles of 5 seconds at 98°C denaturation, 5 seconds at 51,7°C alignment, 10 seconds at 72°C extension and c) 1 minute at 72°C final extension. The expected bands are 100 bp for the transgene and 324 bp for the internal control.

The *R26R^{+/+}* PCR uses the primers oIMR8038 (5'- TAA GCC TGC CCA GAA GAC TC-3'), oIMR8545 (5'- AAA GTC GCT CTG AGT TGT TAT-3') and oIMR9539 (5'- TCC AGT TCA ACA TCA GCC GCT ACA-3'). The PCR program consists of the following steps: a) 30 seconds at 98°C initial denaturation, b) 35 cycles of 10 seconds at 98°C denaturation, 5 seconds at 64°C alignment, 10 seconds at 72°C extension and c) 1 minute at 72°C final extension. The expected bands are 575 bp for the mutant and 235 bp for the wild type mouse.

3.2.2. Obtaining preadipocytes of interscapular brown adipose tissue (iBAT) and adipogenic differentiation.

The newborn pups are euthanized by decapitation to obtain the iBAT by surgery. The tissue is washed in PBS and left in digestion buffer (0,2% type II collagenase in buffer [25 mM KHCO₃, 12 mM KH₂PO₄, 1,2 mM MgSO₄, 4,8 mM KCl, 120 mM NaCl, 1,2 mM CaCl₂, 5 mM glucose, 2,5% BSA and 1% penicillin/streptomycin, at pH 7,4]) for 45 min at 37°C at 800 rpm. The product of digestion was filtered through a 100 µm mesh and ACK were added for 4 min. Wash with culture medium (DMEM-F12 10% FBS, 1% Antibiotic Antimycotic, pH 7,2), centrifuging at 300 x g for 5 min. It is again filtered through a 40 µm mesh, washed with medium and seeded in 24-well plates. When they reach confluence, the cells were trypsinized and seeded six times the original surface area. This process is repeated and afterwards the cells are incubated with 500 nM dexamethasone, 125 nM indomethacin, 0,5 mM 3-isobutyl-1-methylxanthine

(IBMX), 5 μ M rosiglitazone, 1 nM T3 and 20 nM insulin. After 72 h of induction, the cells are maintained in culture medium supplemented with 20 nM insulin and 1 nM T3.

3.2.3. Immunofluorescence assays.

Primary cultures of brown preadipocytes from *Agpat2*^{-/-} and *Agpat2*^{+/+} mice were seeded and differentiated in 96 well plates with optical background or in sterile glass covers. They were fixed with 4% PFA for 20 min and washed 3 times with PBS, permeabilized with 0,1% Triton X-100 for 15 minutes and blocked with 3% fish gelatin by 1 h at room temperature. Was washed 3 times with PBS and incubated with primary antibody (1% BSA/PBS) overnight at 4°C in a humid chamber. After washing 3 times with PBS, it was incubated with fluorescent secondary antibodies 1:1000 (1% BSA/PBS) for 1 h at room temperature. The nuclei were stained with Hoechst 33342 1 μ g/mL and lipid drops with BODIPY 1 μ g/mL for 30 minutes at room temperature.

3.2.4. Quantification of fluorescence microscopy images acquired by automated system.

Brown iBAT preadipocytes from *Agpat2*^{-/-} and *Agpat2*^{+/+} mice were seeded in 96 well plates with optical-bottom. The differentiated and treated according to protocol. Later the fluorescence images were acquired in the Cytation 5 equipment and analyzed with the Gen 5 Image Prime software. 9 or 16 photos per well were acquired, with 2 to 3 channels, with a magnification of 20X. The cells were first segmented by the cell nucleus (primary mask). Next, a secondary mask was generated around the cell nucleus with a radial distance of 5 μ M. The intensity of green fluorescence in the secondary mask was measured to identify the cells with lipid droplets. In the red channel, the fluorescence intensity in the primary mask was measured for nuclear markers, and the fluorescence intensity in the secondary mask was measured in

cytoplasmic markers. The cells were considered as positive or negative for the markers, and the populations were validated by Strictly standardized mean difference (SSMD) (Figure 4).

3.2.5. Oil-Red-O Stain

To quantify neutral lipids, primary cultures of brown preadipocytes were stained with Oil Red O. Cells fixed with 4% PFA, were incubated with Oil Red O solution (six parts of 0,6% Oil network O dye in isopropyl alcohol and four parts water) for 30 minutes at room temperature. It was washed 3 times with 75% ethanol in PBS and incubated with isopropanol for 15 minutes. The isopropanol was transferred to a new 96-well plate and the absorbance at 570 nm was measured.

3.2.6. Western blotting

Extracts from differentiated preadipocyte cultures or iBAT were resuspended in RIPA buffer with protease and phosphatase inhibitors. The lysates were sonicated on ice and centrifuged at 14,000 x g for 15 min at 4°C. 25 µg of the supernatant proteins was incubated with Lane Marker Reducing Sample Buffer and resolved in polyacrylamide gel electrophoresis-SDS. Subsequently they were electrotransferred in PVDF membranes. Membranes were blocked with 3% BSA/0,1% Tween 20 in tris phosphate buffer (TBS-T) for 1 h and incubated with primary antibody 1% BSA overnight at 4°C. The membranes were washed with TBS-T and incubated with secondary antibody conjugated with horseradish peroxidase (HRP) for 2 h at room temperature. The membranes were visualized by chemiluminescence using C-DiGit Blot Scanner (Licor) or G:Box (Syngene).

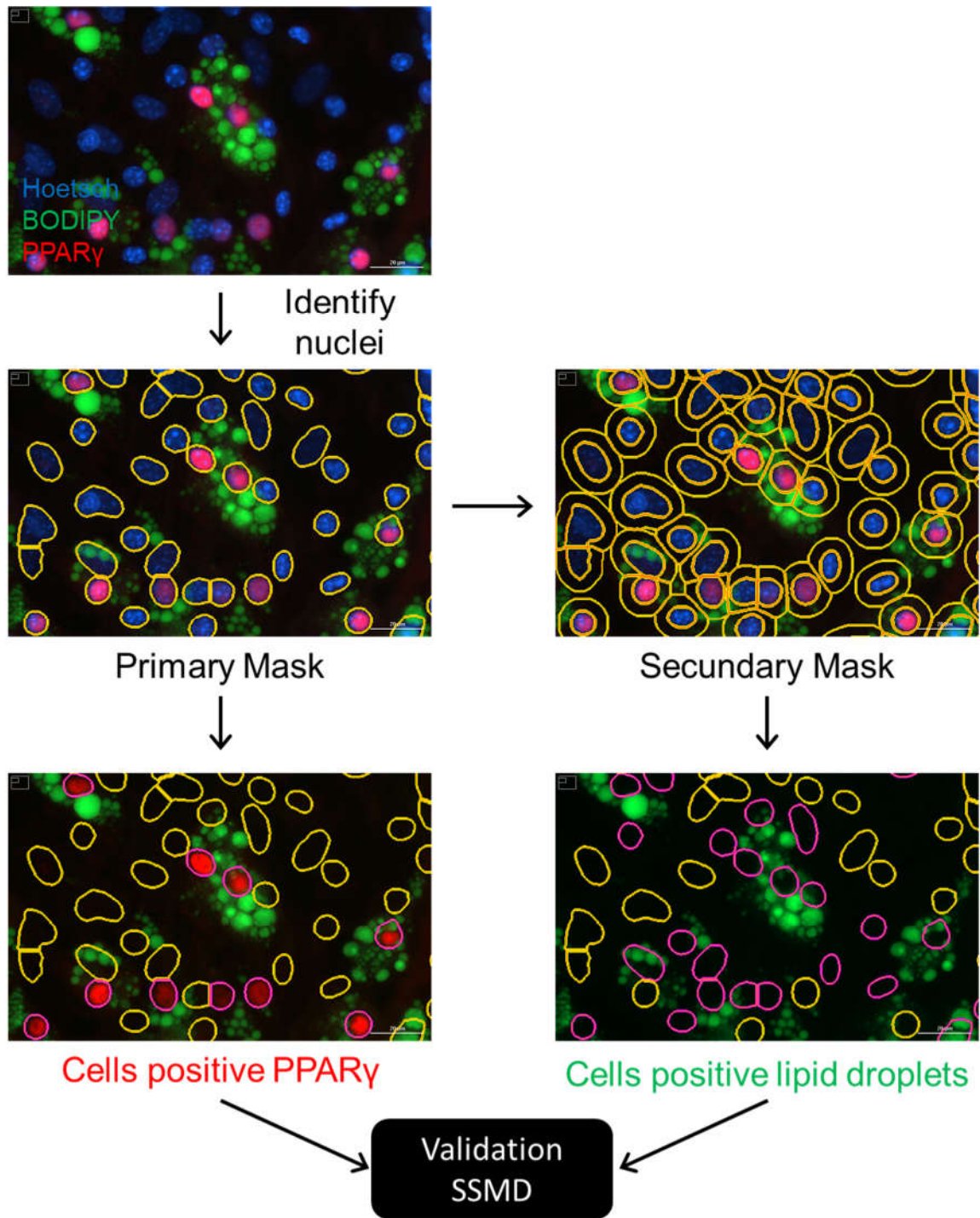


FIGURE 6: Image analysis pipeline. After the acquisition, the images were analyzed using the Gen 5 Image Prime software.

3.2.7. qRT-PCR and RNA Microarray.

The total RNA was obtained from samples of primary cultures of brown preadipocytes with Trizol according to the instructions of the manufacturer. 2 µg of RNA were treated with TURBO DNA-free™ Kit for the elimination of contaminating DNA. Subsequently, the cDNA was generated by the High-Capacity cDNA Reverse Transcription Kit. The relative expression levels of the mRNAs were calculated with the $\Delta\Delta C_t$ method using *36b4* as the reference gene.

For the microarray, the total RNA purity and integrity were evaluated by ND-1000 Spectrophotometer (NanoDrop, Wilmington, USA), Agilent 2100 Bioanalyzer (Agilent Technologies, Palo Alto, USA). cDNA was synthesized using the GeneChip WT (Whole Transcript) Amplification kit as described by the manufacturer. The sense cDNA was then fragmented and biotin-labeled with TdT (terminal deoxynucleotidyl transferase) using the GeneChip WT Terminal labeling kit. Approximately 5,5 µg of labeled DNA target was hybridized to the Affymetrix GeneChip Mouse Array at 45°C for 16 h. Hybridized arrays were washed and stained on a GeneChip Fluidics Station 450 and scanned on a GCS3000 Scanner (Affymetrix). Signal values were computed using the Affymetrix® GeneChip™ Command Console software. All Statistical test and visualization of differentially expressed genes was conducted using R statistical language v. 3.1.2. (www.r-project.org).

Gene Ontology (GO) analysis was performed using Gene Ontology resource (<http://geneontology.org/>) (Ashburner *et al.*, 2000; Carbon *et al.*, 2019).

3.2.8. Electron microscopy.

Brown preadipocyte cultures of *Agpat2*^{-/-} and *Agpat2*^{+/+} were grown and differentiated in Thermanox Plastic Coverslip. Next, they were fixed with 2% glutaraldehyde for 2 h,

immersed in 1% OsO₄, dehydrated with ethanol and infiltrated in Epon. The ultra-fine sections were obtained by ultramicrotome (80 nm). The grids were visualized in the Phillips Tecnai 12 electron microscope at the Microscopy Facility UC, Chile.

3.2.9. Histological sections and X-gal staining.

Mice were euthanized by decapitation and fixed in 4% paraformaldehyde for 24 h. Then they were put in sucrose 15% for 12 h and in 30% overnight. They were included in Optimal cutting temperature compound (OCT compound) and 20 μm slices were generated in the Leica CM1860 cryostat.

For X-gal stains, the mice were euthanized by decapitation and included in compound OCT. Cuts 30 μm thick were stained with X-gal solution (30 mM potassium ferricyanide (K₃[Fe(CN)₆]), 30 mM potassium ferrocyanide (K₄[Fe(CN)₆]·3H₂O), 1 mM MgCl₂, 1 mg/mL ONPG) for 24 h at 37°C.

3.2.10. Generation of recombinant adenoviruses.

The coding sequence of mitoNEET was amplified from a plasmid gently donated by Philipp E. Scherer (University of Texas Southwestern Medical Center, Dallas, Texas) and Elov13 from mouse liver cDNA. The PCR products of mitoNEET and Elov13 were cloned into the pENTRTM/D-TOPOTM vector. Orientation and sequence were verified by digestion with restriction enzymes (Not I and Asc I) and by direct sequencing (Macrogen Inc.). Recombinant adenoviral vectors were generated by Clonase II-mediated recombination between mitoNEET-pENTRTM/D-TOPOTM, Elov13-pENTRTM/D-TOPOTM or LacZ-pENTRTM/D-TOPOTM with the vector pAd/CMV/V5-DEST. The resulting plasmids were analyzed by direct sequencing (Macrogen Inc.). 1 μg of the digestion product of mitoNEET-pAd/CMV/V5-DEST, Elov13-

pAd/CMV/V5 -DEST and LacZ-pAd/CMV/V5-DEST were transfected in 293A cells. After 7-10 days, the cells with cytopathic signs were broken by freeze/thaw cycles and then centrifuged at 10,000 x g for 15 min. The supernatant was used to propagate the adenoviruses in 293A cells. Finally, the adenoviral particles were purified by CsCl gradient ultracentrifugation, desalinated and quantified at OD 260 nm. 3×10^8 particles/cm² were used for the infection of the primary cultures of brown preadipocytes.

3.2.11. Fatty acid profile.

Total lipids from plasma samples were extracted with chloroform/methanol (2:1 v/v). Fatty acid methyl esters (FAME) from plasma were prepared with boron trifluoride (12% methanolic solution) according to the (Morrison *et al.*, 1964) and followed by methanolic sodium hydroxide (0,5 N) solution. FAME samples were cooled and extracted with 0,5 mL of hexane. FAME were separated and quantified by gas-liquid chromatography in an Agilent Hewlett-Packard equipment (model 7890 A, CA, USA) using a capillary column (Agilent HP-88, 100 m×0,250 mm; I.D. 0,25 µm) and a flame ionization detector (FID) (Valenzuela *et al.*, 2015; Hernández-Rodas *et al.*, 2017).

3.2.12. Lipotoxicity assays and cell viability measurement.

Sodium palmitate was conjugated with BSA free of fatty acids in a ratio of 1:5, for 1 h at 37°C with shaking (200 rpm). It was filtered by 0,2 µM and dissolved in DMEM-F12 2,5% FBS medium. Primary cultures of brown preadipocytes at day 0 and 5 of differentiation were treated with 0, 250, 500, 750 and 1000 µM of palmitic acid for 12 h. Cell viability was evaluated using LDH Cytotoxicity Assay Kit and MTT reduction.

3.2.13. Statistics.

Two-way ANOVA followed by Sidak's multiple comparisons test was performed using GraphPad Prism version 6.01 for Windows, GraphPad Software, La Jolla California USA, www.graphpad.com. Data are expressed as means \pm SD. * $p < 0.05$ denote statistically significant difference between *Agpat2*^{+/+} and *Agpat2*^{-/-} at the same day of differentiation, and # $p < 0.05$ statistically significant difference compared to day 0 in the same genotype.

3.2.14. Figures.

With the exception of Figure 6, all figures were created with BioRender.com

4. Results.

4.1. Differentiated brown adipocytes of *Agpat2*^{-/-} mice have lower accumulation of lipid droplets.

Our laboratory previously found that the lack of white adipose tissue in the *Agpat2*^{-/-} mice results from a combination of both accelerated adipocyte cell death soon after birth and impaired adipogenesis. In fact, *Agpat2*^{-/-} MEFs differentiated *in vitro* into white adipocytes have lower number of lipid-laden cells and decreased expression levels of key adipogenic transcription factors and mature adipocyte markers (Cautivo *et al.*, 2016). To determine the adipogenic potential of brown preadipocytes derived from *Agpat2*^{-/-} mice, primary cultures of the SVF of iBAT were adipogenically induced with a medium supplemented with 500 nM dexamethasone, 125 nM indomethacin, 0,5 mM IBMX, 5 μM rosiglitazone, 1 nM T3 and 20 nM insulin. Seventy-two hours later, cells were changed to DMEM supplemented with 20 nM insulin and 1 nM T3 (Figure 7A). The abundance of cells accumulating lipid droplets was quantified with an automatized imaging system (Cytation 5, see “Methods” sections for a detailed methodological explanation) at different days after adipogenic induction. Imaging analysis was performed according to “Microscopy-Based High-Content Screening and/or image-based profiling considerations” guidelines (Bray *et al.*, 2004; Boutros *et al.*, 2015; Caicedo *et al.*, 2017).

As shown in Figure 7B, whereas ~80% of cultured *Agpat2*^{+/+} SVF’ cells accumulated lipid droplets at differentiation days 5 and 7, the proportion of *Agpat2*^{-/-} cells laden with lipid droplets were notoriously lower (~40% and ~25% at days 5 and 7, respectively). These results are concordant with the quantification of neutral lipids by Oil Red O staining, where a lower

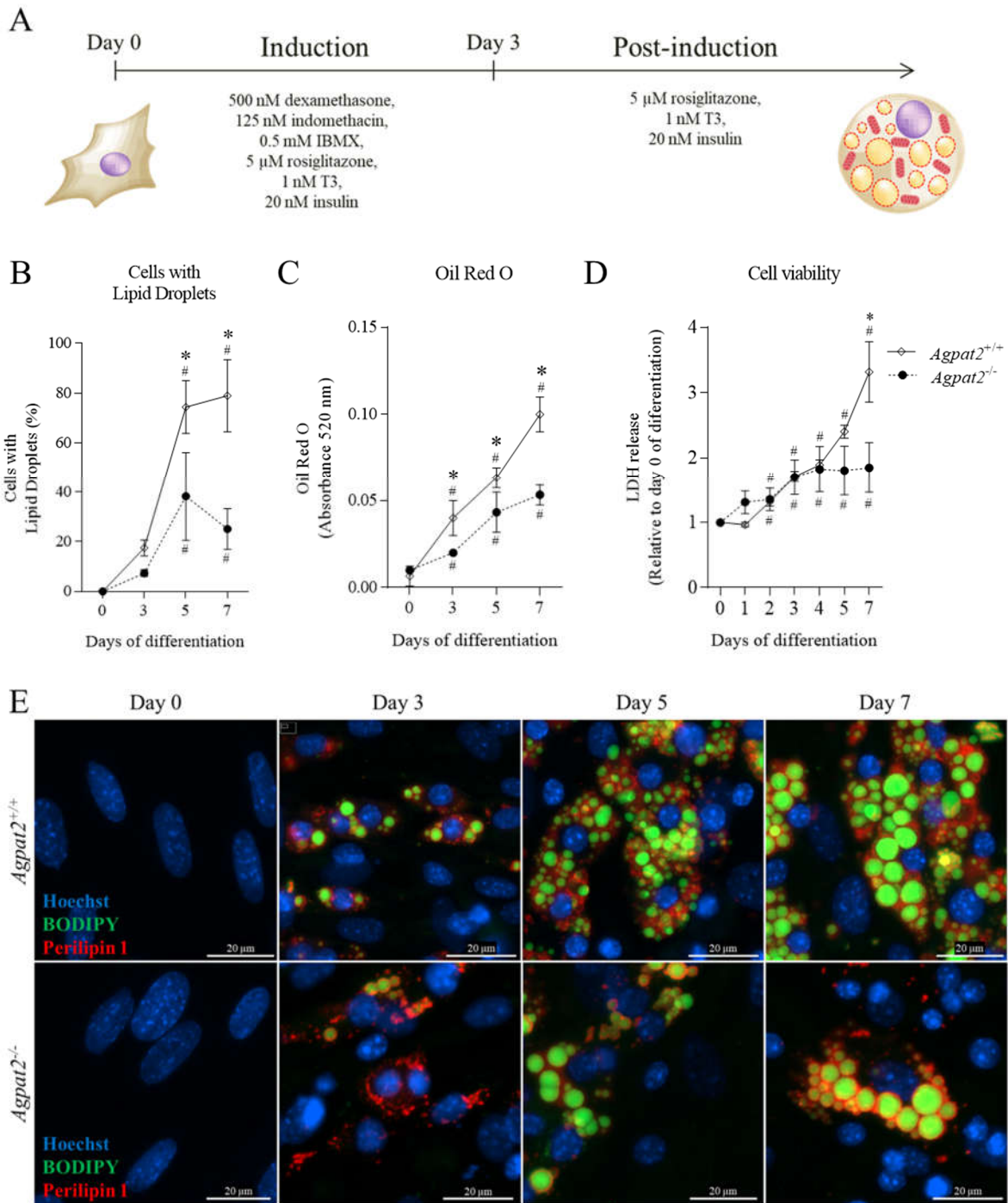


FIGURE 7: The accumulation of lipid droplets in differentiated brown adipocytes of *Agpat2*^{-/-} mice is diminished. (A) Schematic illustration of the adipogenic differentiation in cell cultures of brown preadipocytes. (B) Quantification of cells with lipid droplets (BODIPY). Automated imaging analysis included ~75,000 cells in total. (C) Quantification of neutral lipids by Oil Red O staining. (D) Quantification of LDH release to the media. (E) Representative immunofluorescence images staining perilipin 1 (red), neutral lipids with BODIPY (green) and nuclei with Hoechst 33342 (blue) of wild type and *Agpat2*^{-/-} brown adipocytes at days 0, 3, 5 and 7 of differentiation. Scale bar 20 μ m. Data are expressed as mean \pm SD (N=3 per genotype). * $p < 0.05$ denote statistically significant differences between wild type and *Agpat2*^{-/-} at the same day of differentiation, # $p < 0.05$ denotes statistically significant differences in comparison with day 0 in the same genotype. p values were calculated using two-way ANOVA.

amount of neutral lipids is observed from day 3 to 7 in *Agpat2*^{-/-} cultures compared with *Agpat2*^{+/+} (Figure 7B and C).

Whereas the proportion of *Agpat2*^{-/-} differentiated adipocytes with lipid droplets markedly decreases at day 7 of differentiation, neutral lipids content is higher at day 7 in comparison with day 5 of differentiation. This phenomenon could be the result of an increased lipid content per individual-differentiated *Agpat2*^{-/-} adipocyte, however, this was not quantified in this study.

As indicated above, *Agpat2*^{-/-} mice suffer massive adipocyte death after birth. To determine if this phenomenon occurs *in vitro*, cell viability was evaluated by releasing LDH to the media. Figure 7D shows that no significant differences were found in released LDH between genotypes at day 5, and that *Agpat2*^{-/-} adipocytes have significantly lower LDH at day 7, indicating absence of massive cell death in differentiated brown *Agpat2*^{-/-} adipocytes in culture.

These results, analogous to those reported for us in white *Agpat2*^{-/-} adipocytes (Cautivo *et al.*, 2016), show that AGPAT2 is required for normal lipid droplets and neutral lipid accumulation in *in vitro* differentiated murine brown adipocytes, indicating that in spite of their dissimilar cellular origin, both white and brown adipocytes requires AGPAT2 to proceed onto their normal adipogenic differentiation program.

4.2. Expression levels of adipogenic transcriptional regulators PPAR γ , C/EBP α , PPAR α and PGC1 α but not PRDM16 and C/EBP β are decreased in differentiated brown adipocytes of *Agpat2*^{-/-} mice.

The lower abundance of LDs in differentiated brown adipocytes of *Agpat2*^{-/-} mice (Figure 7) can be the result of impaired adipogenesis. Therefore, we quantified the abundance of classical adipogenic transcription factors and co regulators PPAR γ , PRDM16, C/EBP α , C/EBP β , PPAR α and PGC1 α .

As shown in Figure 8, the proportion of cells with nuclear PPAR γ staining increases at day 3 of differentiation, with no differences between *Agpat2*^{-/-} and wild type cells. At days 5 and 7 of differentiation, the percentage of wild type cells with nuclear PPAR γ signal is further increased, whereas this proportion is not changed (day 5) or it is even decreased (day 7) in *Agpat2*^{-/-} cells (Figure 8A and 8C).

Importantly, the quantification of LDs laden cells that simultaneously have PPAR γ in their nuclei is not different between differentiated brown adipocytes of wild type and *Agpat2*^{-/-} mice (Figure 8B and 8C), suggesting that cells that have nuclear PPAR γ are also the same that build LDs.

In agreement with the lower proportion of differentiated brown adipocytes of *Agpat2*^{-/-} mice with nuclear PPAR γ (Figure 8A), the mRNA and whole cell protein levels of PPAR γ are also lower in these cells at day 5 and 7 (Figure 8D and 8E).

Figure 9A shows that in differentiated brown adipocytes of wild type and *Agpat2*^{-/-} mice, PRDM16 protein levels increases until day 4 of differentiation and that then decreases at day 5. No significant differences were found between both genotypes. C/EBP β , a pro adipogenic

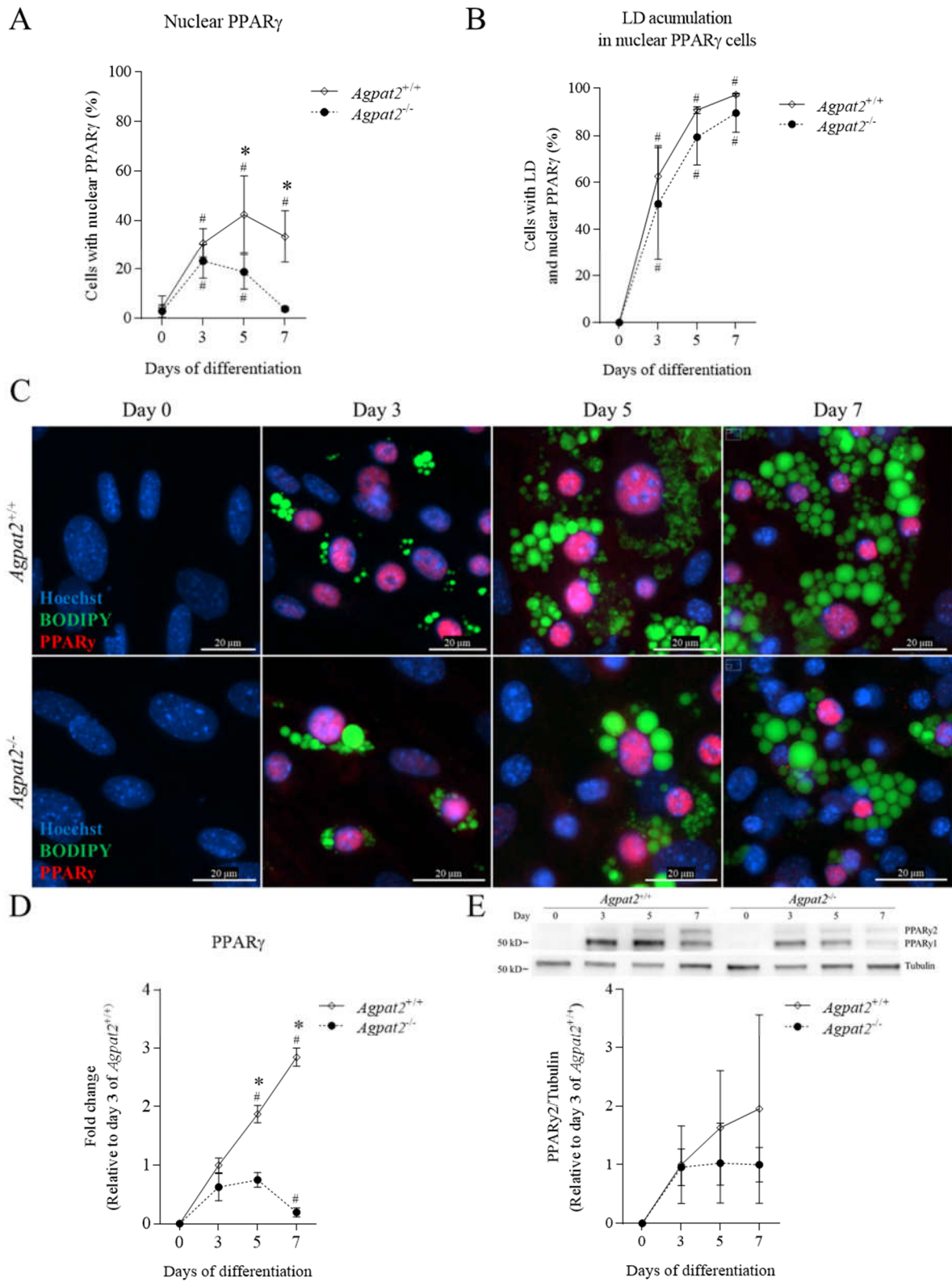


FIGURE 8: PPAR γ is located in the nucleus of cells that accumulate lipid droplets in differentiated brown adipocytes of wild type and *Agpat2*^{-/-} mice. (A) Quantification of cells with nuclear PPAR γ . (B) Quantification of cells with lipid droplets and nuclear PPAR γ . (C) Representative immunofluorescence images staining PPAR γ (red), neutral lipids with BODIPY (green) and nuclei with Hoechst 33342 (blue) of differentiated brown adipocytes of wild type and *Agpat2*^{-/-} mice at days 0, 3, 5 and 7 of differentiation. Scale bar 20 μ m. Automated imaging analysis included ~135,000 cells in total. (D) *Ppar γ* mRNA levels normalized to *36b4* and expressed as relative fold changes to wild type at day 3. (E) Representative immunoblot of PPAR γ and tubulin of differentiated brown adipocytes of wild type and *Agpat2*^{-/-} mice at days 0, 3, 5 and 7 of differentiation and immunoblot quantification of PPAR γ , expressed as fold-change relative the levels of wild type mice at day 3 of differentiation and normalized to tubulin levels. Data are expressed as mean \pm SD (N=3 per genotype). *p < 0.05 denote statistically significant differences between differentiated brown adipocytes of wild type and *Agpat2*^{-/-} mice at the same day of differentiation, # p < 0.05 denotes statistically significant differences in comparison with day 0 in the same genotype. p values were calculated using two-way ANOVA.

transcription factor required for both brown and white adipocyte phenotype determination, has lower expression levels in differentiated brown adipocytes of *Agpat2*^{-/-} mice at day 3 in comparison with wild type cells. At the transcriptional level, C/EBP β mRNA was lower at day 7 of differentiation in differentiated brown adipocytes of *Agpat2*^{-/-} mice (Figure 9B). mRNA levels of C/EBP α , which cooperates with PPAR γ to regulate adipocyte-specific genes after expression of C/EBP β , is lower in differentiated brown adipocytes of *Agpat2*^{-/-} mice at day 3, 5 and 7 in comparison with wild type cells (Figure 9C). mRNA levels of PPAR α , a nuclear hormone receptor that promotes fatty acid uptake, mitochondrial β -oxidation and lipoprotein transport are lower in differentiated brown adipocytes of *Agpat2*^{-/-} mice at days 5 and 7 in comparison with the wild type cells (Figure 9D). Finally, PGC1 α , a transcriptional co-regulator central for mitochondrial biogenesis and brown adipocyte differentiation, is significantly lower in differentiated brown adipocytes of *Agpat2*^{-/-} mice at both protein and mRNA levels (days 4 and 5, respectively) (Figure 9E).

UCP1 is highly expressed in mature brown adipocytes and is a *bona fide* marker of this cell type. Concordantly, it is undetectable at the mRNA and protein levels in undifferentiated preadipocytes of wild type and *Agpat2*^{-/-} mice (cell cultures at day 0 of differentiation). As shown in Figure 10A, brown adipogenic differentiation markedly induced UCP1 at the mRNA and protein levels in wild type cells. In sharp contrast, UCP1 remained undetectable in differentiated brown adipocytes of *Agpat2*^{-/-} mice. Even more, when we exposed differentiated brown adipocytes (day 5 of differentiation) to isoprenaline, a potent beta-adrenergic activator, *Ucp1* mRNA levels in the wild type increase more than ~30-fold, whereas *Agpat2*^{-/-} were completely unresponsive to the stimulus. These results indicate that differentiated brown adipocytes of *Agpat2*^{-/-} mice fail to express UCP1 under a β -adrenergic stimulus (Figure 10B).

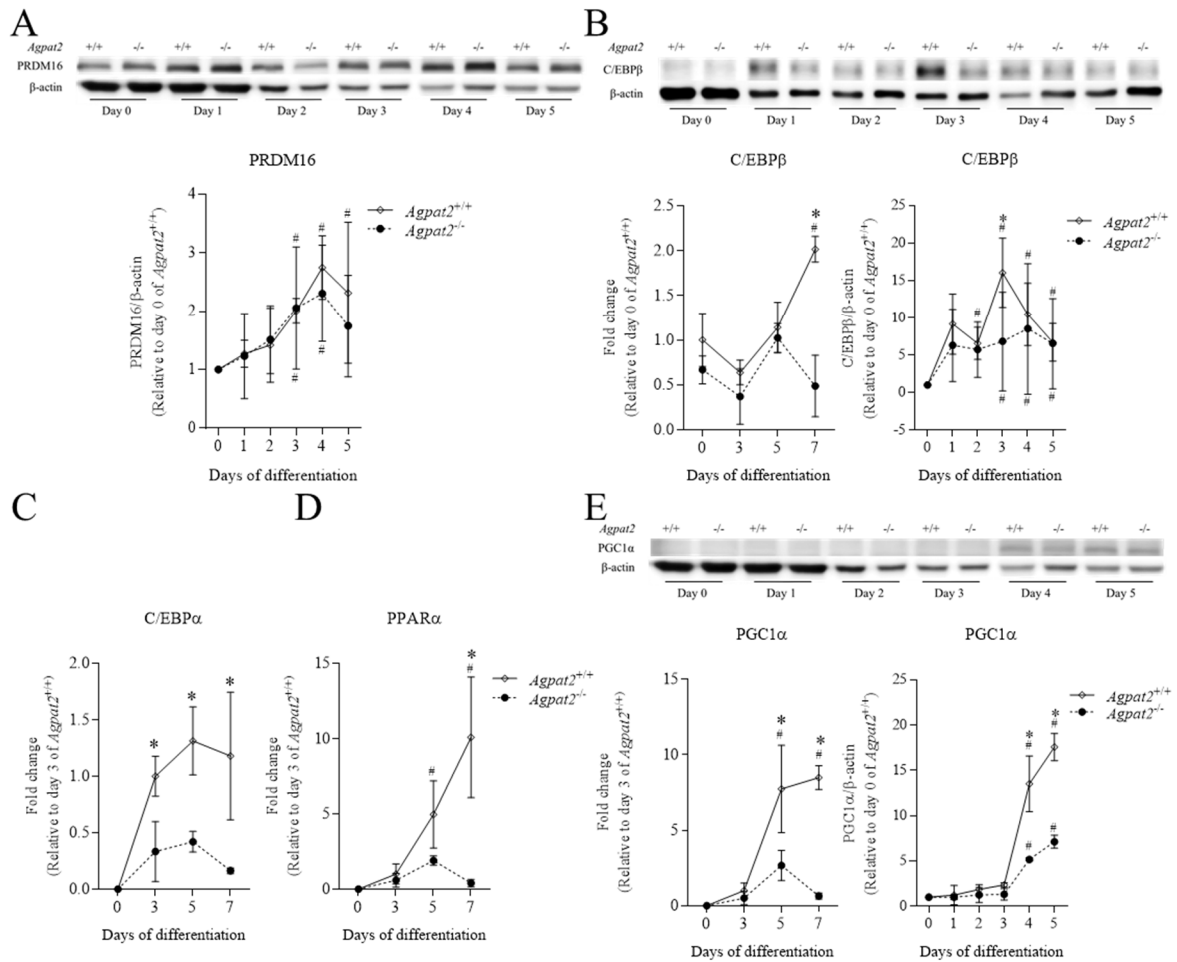


FIGURE 9: Protein and/or mRNA levels of PRDM16, C/EBPβ, C/EBPα, PPARα and PGC1α in differentiated brown adipocytes of wild type and *Agpat2*^{-/-} mice. Representative immunoblot of (A) PRDM16, (B) C/EBPβ and (E) PGC1α and β-actin of differentiated brown adipocytes of wild type and *Agpat2*^{-/-} mice at days 0, 1, 2, 3, 4 and 5 of differentiation and immunoblot quantification expressed as fold-change relative the levels of wild type mice at day 0 of differentiation and normalized to β-actin levels (N=4 per genotype). (B) C/EBPβ, (C) C/EBPα, (D) PPARα and (E) PGC1α mRNA levels normalized to *36b4* and expressed as relative fold changes to wild type at day 0 or 3 (n=3 per genotype). Data are expressed as mean ± SD. *p < 0.05 denote statistically significant differences between differentiated brown adipocytes of wild type and *Agpat2*^{-/-} mice at the same day of differentiation, # p < 0.05 denotes statistically significant differences in comparison with day 0 in the same genotype. p values were calculated using two-way ANOVA.

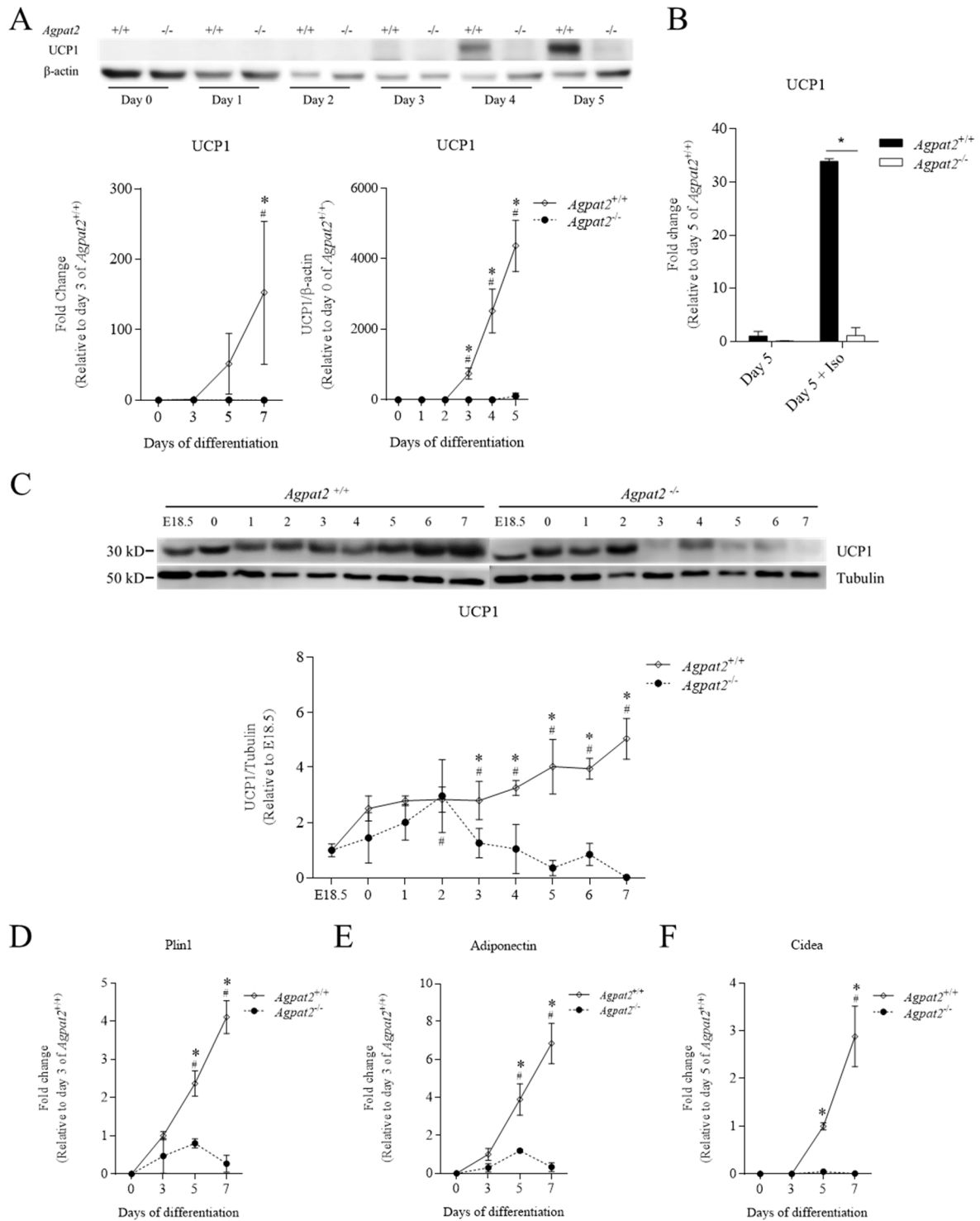


FIGURE 10: Protein and mRNA levels UCP1 and adipocyte markers Plin1, Adiponectin and Cidea are strongly diminished in differentiated brown adipocytes of *Agpat2*^{-/-} mice. (A) Representative immunoblot of UCP1 and β -actin of differentiated brown adipocytes of wild type and *Agpat2*^{-/-} mice at days 0, 1, 2, 3, 4 and 5 of differentiation and immunoblot quantification of UCP1, expressed as fold-change relative the levels of wild type mice at day 0 of differentiation and normalized to β -actin levels (N=4 per genotype) and *Ucp1* mRNA levels normalized to *36b4* and expressed as relative fold changes to wild type at day 3 (n=3 per genotype). (B) UCP1 mRNA levels of differentiated brown adipocytes of wild type and *Agpat2*^{-/-} mice at day 5 in the presence and absence of isoprenaline (10 μ M for 6 h). Data were normalized to *36b4* and expressed as relative fold changes to wild type. (C) Representative immunoblot of UCP1 and tubulin in iBAT of wild type and *Agpat2*^{-/-} mice E18.5 embryos and at days 0, 1, 2, 3, 4, 5, 6 and 7 after birth and immunoblot quantification of UCP1, expressed as fold-change relative the levels of wild type mice E18.5 embryos and normalized to tubulin levels (N=4 per genotype). (D) *Plin1*, (E) *Adiponectin* and (F) *Cidea* mRNA levels normalized to *36b4* and expressed as relative fold changes to wild type at day 3 or 5. Data are expressed as mean \pm SD. *p < 0.05 denote statistically significant differences wild type and *Agpat2*^{-/-} at the same day of differentiation or after birth, # p < 0.05 denotes statistically significant differences in comparison with day 0 or E18.5 in the same genotype. p values were calculated using two-way ANOVA.

We then compared these *in vitro* results with the actual levels of UCP1 in the iBAT of newborn wild type and *Agpat2*^{-/-} mice. As shown in Figure 10C, UCP1 protein levels were equivalent between *Agpat2*^{-/-} and wild type mice until the day 2 after birth. Thereafter, UCP1 mRNA levels are severely decreased in the iBAT of *Agpat2*^{-/-} mice while they increase in wild type mice until the day 7 after birth.

Perilipin 1 (PLIN1) and CIDEA are LD-associated proteins that regulates lipolysis and LDs fusion, respectively, whereas, Adiponectin (ADIPOQ) is an adipokine secreted by WAT and BAT. These three adipocyte markers are significantly lower in differentiated brown adipocytes of *Agpat2*^{-/-} mice at days 5 and 7 in comparison with wild type cells (Figure 10D, 10E and 10F).

Together, these results indicate that brown adipogenic differentiation of *Agpat2*^{-/-} preadipocytes results in a lower proportion of cells laden with lipids and reduced levels of key transcriptional regulators for both general adipocyte (PPAR γ , C/EBP β , C/EBP α and PPAR α) and specific brown adipocyte (PGC1 α) phenotype. Importantly, although some *Agpat2*^{-/-} cells do accumulate lipids and have nuclear PPAR γ , indicating adipogenic differentiation, UCP1 remains undetectable in these cells.

Therefore, we conclude that *Agpat2*^{-/-} preadipocytes undergo an abnormal differentiation process that fails to generate fully mature brown adipocytes *in vitro*.

Alternatively, the low proportion of LD-laden cells in the *Agpat2*^{-/-} differentiated brown adipocytes cultures can also be explained by a lower abundance of preadipocytes in the original SVF cultured from these mice. Therefore, we aimed to quantify the abundance of brown preadipocytes in the cultured SVF and in the iBAT of *Agpat2*^{-/-} and wild type mice.

4.3. Preadipocyte abundance is normal in the interscapular brown adipose tissue of newborn *Agpat2*^{-/-} mice and in their primary cultured stromal vascular fraction (SVF).

To determine whether the preadipocyte content is equivalent in iBAT of newborn mice of *Agpat2*^{-/-} and *Agpat2*^{+/+}, the expression levels of the preadipocyte markers *Fabp4*, *Zfp423* and *Pref-1* were evaluated.

To track *Fabp4* and *Zfp423* expressing cells *in vivo*, new transgenic mouse strains *Agpat2*^{+/-}/*Fabp4-Cre*⁺/*R26R*^{+/+} and *Agpat2*^{+/-}/*Zfp423*^{GFP} were generated, respectively (see “Methods” sections for a detailed explanation of the breeding strategy). To determine the abundance of *Fabp4* and *Zfp423* in the iBAT of *Agpat2*^{-/-} mice, transverse sections of the interscapular region of new born *Agpat2*^{-/-}/*Fabp4-Cre*⁺/*R26R*^{+/+} and *Agpat2*^{-/-}/*Zfp423*^{GFP} mice were stained with X-Gal (Figure 11A) and GFP immunofluorescence (Figure 11C), respectively.

Using these tools, no differences were detected in the abundance of *Fabp4* (a marker for both preadipocytes and mature adipocytes) and *Zfp423* (a marker for brown preadipocytes) between newborn *Agpat2*^{-/-} and wild type mice (day P0.5). Similarly, no differences were found in *Pref-1* (a maker of preadipocytes) and *Zfp423* protein levels in the iBAT of *Agpat2*^{-/-}/*Zfp423*^{GFP} and *Agpat2*^{+/+}/*Zfp423*^{GFP} mice by immunoblotting analysis (Figure 11B).

Next, we estimated the abundance of brown preadipocytes in primary cultured iBAT SVF by quantifying *Pref-1*. As shown in Figure 12, *Pref-1* mRNA and protein levels were equivalent in the cultured SVF derived from *Agpat2*^{-/-} and wild type mice at day 0 of differentiation (Figure 12A and 12B).

Therefore, we conclude that the abundance of preadipocytes iBAT and primary cell cultures of SVF of *Agpat2*^{-/-} and *Agpat2*^{+/+} is equivalent and thus the lower proportion of *Agpat2*^{-/-} differentiated brown adipocytes laden with LD is most likely due to intrinsic adipogenic defects of these cells.

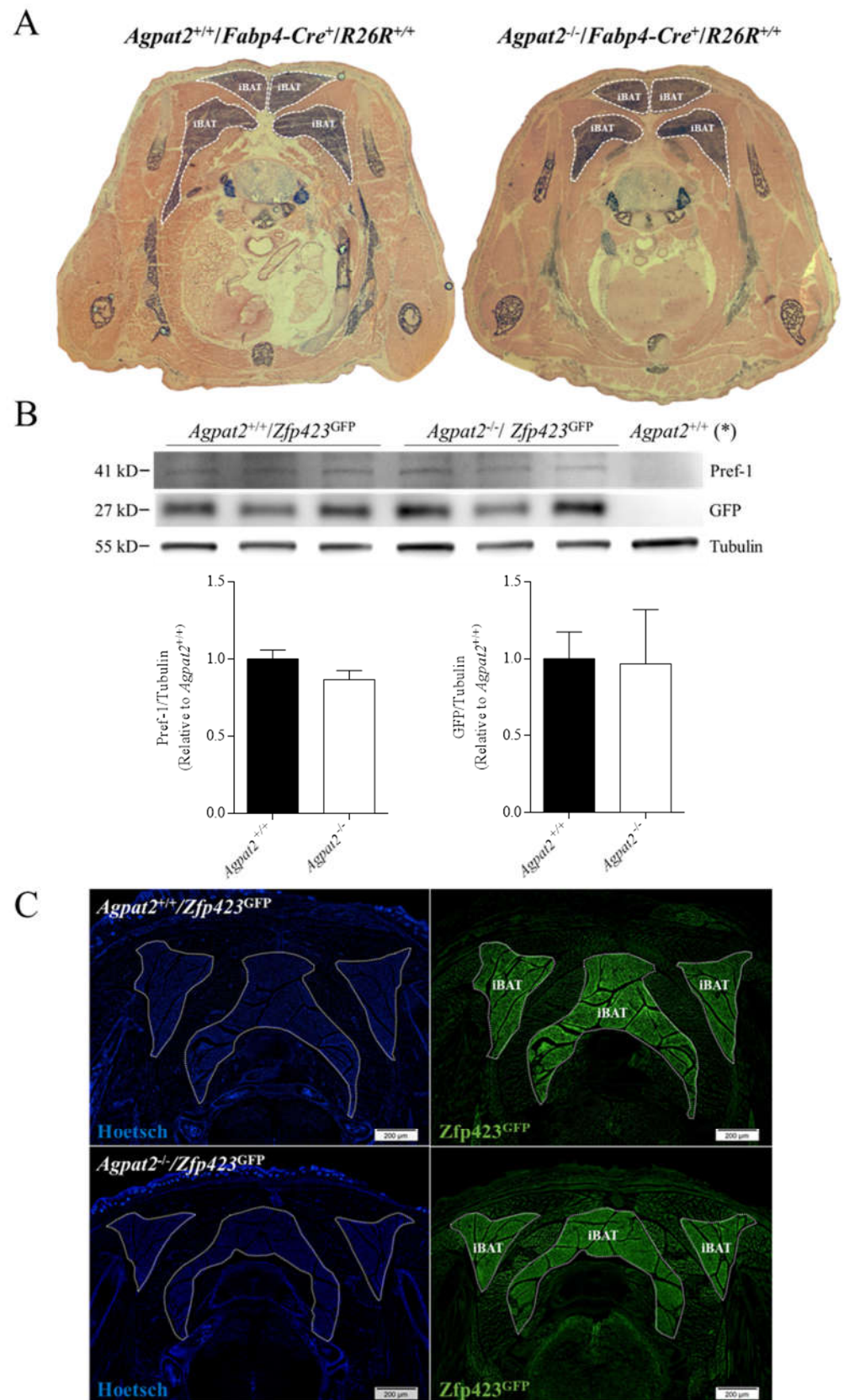


FIGURE 11: Preadipocyte abundance is normal in the iBAT of newborn *Agpat2*^{-/-} mice. (A) Representative transversal cryosections of the scapular region of newborn mice from *Agpat2*^{-/-}/*Fabp4-Cre*⁺/*R26R*^{+/+} and *Agpat2*^{+/+}/*Fabp4-Cre*⁺/*R26R*^{+/+} stained with X-gal. (B) Representative immunoblot of PREF-1, GFP and TUBULIN in iBAT of newborn wild type and *Agpat2*^{-/-} mice and immunoblot quantification of PREF-1 and GFP, expressed as fold-change relative the levels of wild type mice and normalized to tubulin levels (N=3 per genotype). (C) Representative immunofluorescence images staining GFP (green) and nuclei (Hoechst 33342, blue) in the iBAT of newborn wild type and *Agpat2*^{-/-} mice. *Agpat2*^{+/+} (*): Protein sample of differentiated brown adipocytes. Data are expressed as mean ± SD. Statistical analysis was performed using two-tailed unpaired Student's t tests.

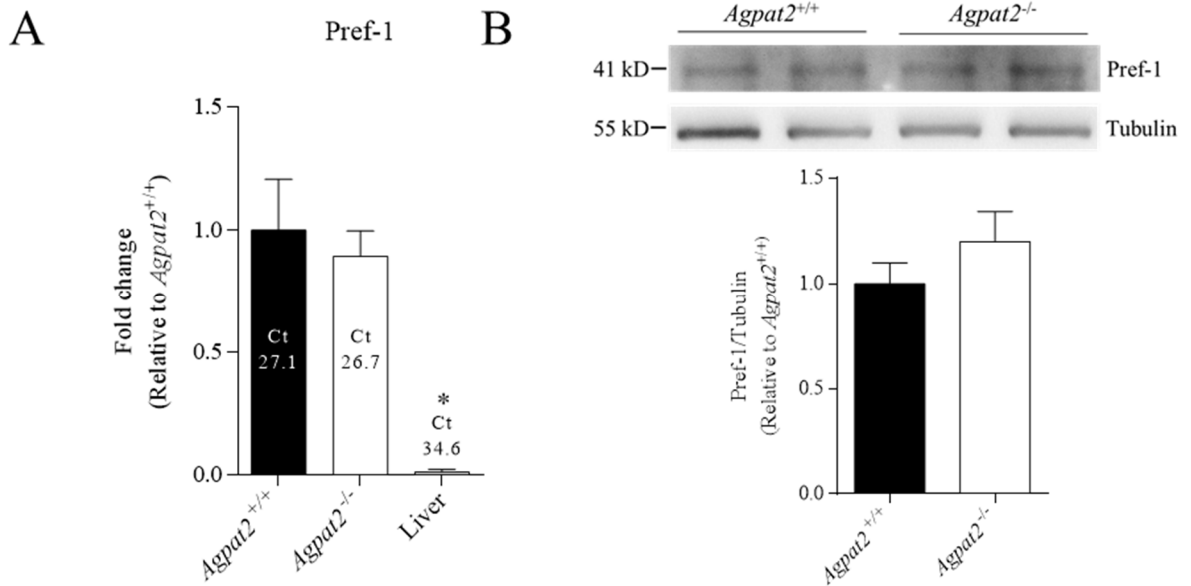


FIGURE 12: Preadipocyte abundance is normal in primary cultured stromal vascular fraction (SVF). (A) *Pref-1* mRNA levels normalized to *36b4* and expressed as relative fold changes to wild type (n=3 per genotype). Liver as a negative control was used. Mean of the cycle threshold (Ct) is shown. (B) Representative immunoblot of PREF-1 and tubulin in SVF of wild type and *Agpat2*^{-/-} mice and immunoblot quantification of PREF-1, expressed as fold-change relative the levels of wild type mice and normalized to tubulin levels. Data are expressed as mean \pm SD (N=3 per genotype). Statistical analysis was performed using (A) one-way ANOVA followed by Dunnett's multiple comparisons test and (B) two-tailed unpaired Student's t tests. * $p < 0.05$ denote statistically significant differences.

4.4. *In vitro* differentiated brown adipocytes of *Agpat2*^{-/-} mice have abnormal expression levels of genes related to type I interferon response and mitochondrial biogenesis/function.

To further explore the transcriptional basis of the failed adipogenesis of differentiated brown adipocytes of *Agpat2*^{-/-} mice we performed unbiased transcriptomic analysis.

Global gene expression of differentiated brown adipocytes was analyzed with microarray technology at days 0, 3 and 5 of differentiation. For this, total RNA of 3 independent cell cultures (each one generated from a different animal) was pooled for each genotype and time of analysis.

As shown in Figure 13A, differentially expressed genes between wild type and *Agpat2*^{-/-} cells were 92, 80 and 647 for days 0, 3 and 5, respectively. In *Agpat2*^{-/-} adipocytes at day 5 of differentiation, the expression of the genes related to the brown adipogenic differentiation *Ucp1*, free fatty acid receptor 4 (*Ffar4*), *Cidea* and cytochrome c oxidase subunit 8B (*Cox8b*) is lower than in wild type adipocytes at the same day of differentiation (Figure 13B). FFAR4 is a receptor for *n*-3 polyunsaturated fatty acids (PUFA) and has been implicated in the activation of thermogenesis in BAT (Kim *et al.*, 2016; Sharma *et al.*, 2019). *Cox8b*, a nuclear gene that encodes a mitochondrial protein that is part of the electron transport chain, is expressed preferentially in brown adipocytes. CIDEA is a LD-associated protein important for LD maturation (Gao *et al.*, 2017).

By contrast, several genes implicated in type-I interferon response are among the most overexpressed genes in *Agpat2*^{-/-} adipocytes at day 5 of differentiation. These include: Interferon-induced protein 44 (*Ifi44*), 2'-5' oligoadenylate synthetase 1G (*Oas1g*), 2'-5' oligoadenylate synthase-like protein 2 (*Oasl2*), interferon-induced protein with tetratricopeptide

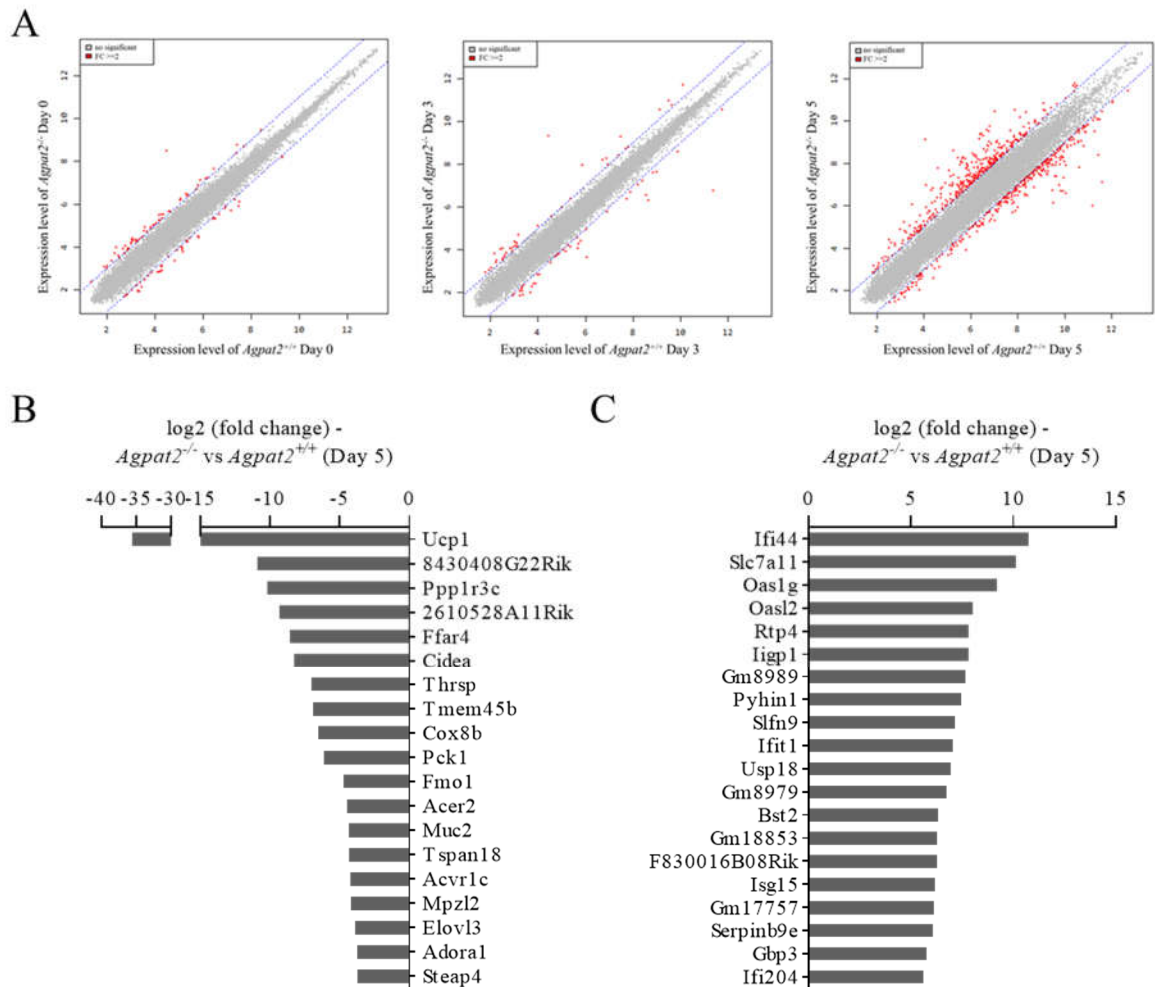


FIGURE 13: Global gene expression analysis of differentiated brown adipocytes of *Agpat2*^{-/-} mice. Interscapular mouse preadipocytes were individually differentiated. In total, 3 animals were used for each genotype and time of analysis. Equal amounts of total RNA from individually differentiated brown adipocytes were pooled and analyzed by microarray technology, as indicated in “Methods” section. (A) Global gene expression level between *Agpat2*^{-/-} versus *Agpat2*^{+/+} at days 0, 3, and 5 of differentiation. Red dots: fold-change (FC) > 2 Grey dots: fold-change < 2. (B) Log₂ fold-change of the top 20 downregulated. (C) Log₂ fold-change of the top 20 upregulated genes between differentiated brown adipocytes of wild type and *Agpat2*^{-/-} mice at day 5 of differentiation.

repeats 1 (*Ifit1*), Ubl carboxyl-terminal hydrolase 18 (*Usp18*) and Interferon-activable protein 204 (*Ifi204*) (Figure 13C).

Gene ontology analysis (GO) of differentially expressed genes revealed no differences between wild type and *Agpat2*^{-/-} cells at days 0 and 3 of differentiation, nor in day 3 versus day 0 in both *Agpat2*^{+/+} and *Agpa2*^{-/-} cells.

By contrast, the comparison between day 5 and day 0 in the wild type differentiated brown adipocytes, revealed enrichment in the gene expression of biological processes related to mitochondria organization (GO: 0007005), fat cell differentiation (GO: 0045444), brown fat cell differentiation (GO: 0050873) and regulation of fat cell differentiation (GO: 0045598) (Figure 14A). In the differentiated brown adipocytes of *Agpat2*^{-/-} mice, there was enrichment in the same processes, although in a lesser extent to the seen in the wild type cells. Interestingly, biological processes related to response to virus (GO: 0009615), cellular response to interferon-beta (GO: 0035458), response to interferon-beta (GO: 0035456) and regulation of type I interferon production (GO: 0032479), were strongly increased, and this was in sharp contrast with the wild type cells, in which these processes are absent (Figure 14B).

In fact, the comparison between wild type and *Agpat2*^{-/-} cells at day 5 of differentiation, showed that biological processes related to response to virus (GO: 0009615), immune system process (GO:0002376) and response to interferon-beta (GO: 0035456), were significantly different between *Agpat2*^{-/-} and wild type cell cultures (Figure 14C). In fact, many differentially expressed genes belong to retinoic acid-inducible gene-I-like receptors (RLRs) and ISGs clusters. Among them highlight DEXH (Asp-Glu-X-His) box polypeptide 58 (*Dhx58*), interferon induced with helicase C domain 1 (*Ifih1*) and DEAD (Asp-Glu-Ala-Asp) box

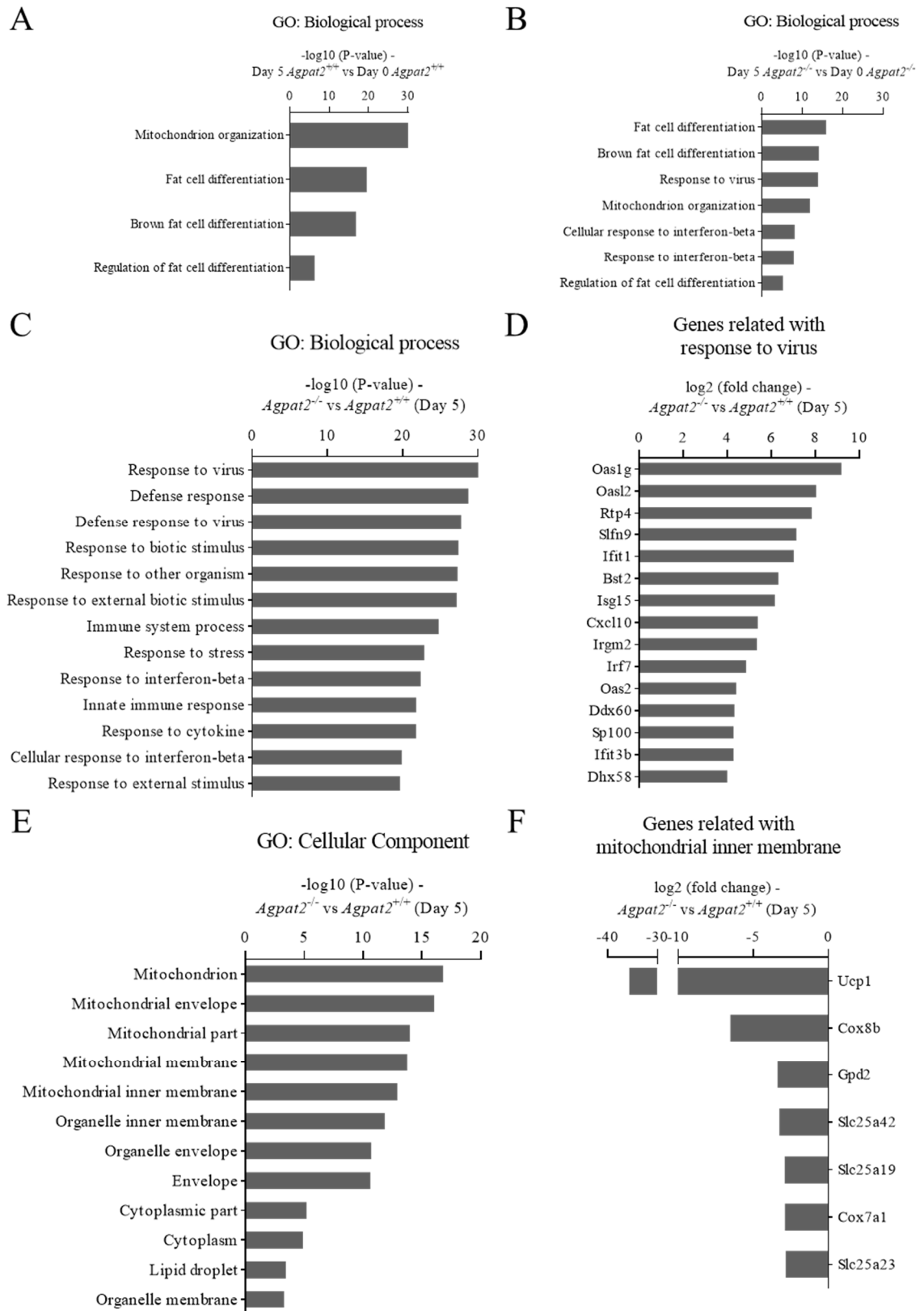


FIGURE 14: Gene ontology (GO) analysis in differentiated brown adipocytes of *Agpat2*^{-/-} mice. Gene ontology (GO) analysis (biological process) of day 5 versus day 0 of (A) *Agpat2*^{+/+} and (B) *Agpat2*^{-/-}. GO analysis of (C) upregulated (biological process) and (E) downregulated (cellular component) genes of *Agpat2*^{-/-} at day 5. Log₂ fold expression change of genes related with (D) cellular response to virus and (F) mitochondrial inner membrane in *Agpat2*^{-/-} versus *Agpat2*^{+/+} at day 5 of differentiation. 3 animals were used per genotype (pool).

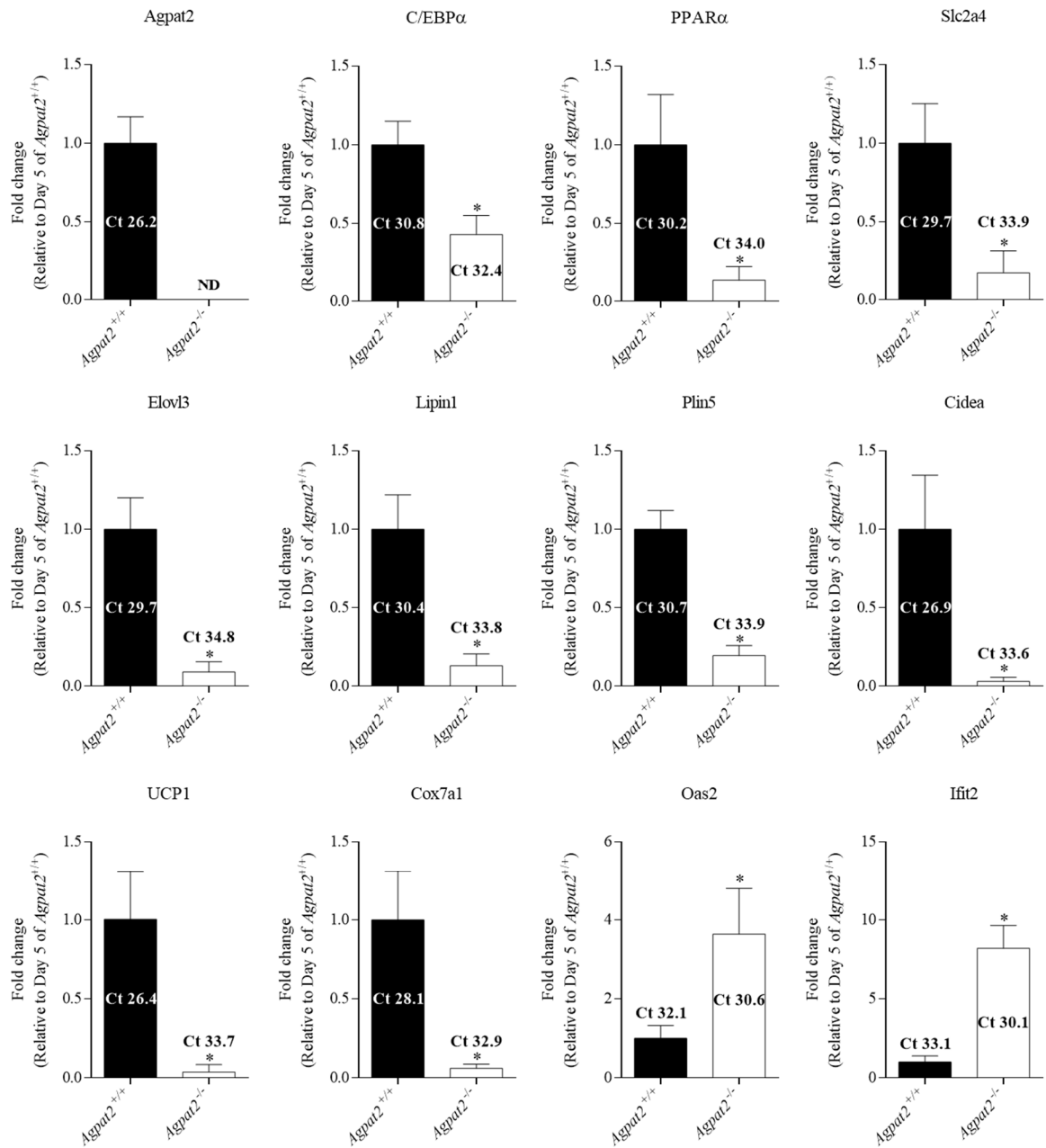


FIGURE 15: qPCR quantification of differentially expressed genes in global gene expression analysis in differentiated brown adipocytes of *Agpat2*^{-/-} mice. mRNA levels of 1-acylglycerol-3-phosphate Oacyltransferase 2 (*Agpat2*), CCAAT enhancer binding protein α (*Cebpa*), peroxisome proliferator activated receptor α (*Ppara*), solute carrier family 2 member 4 (*Slc4a2*), elongation of very long chain fatty acids 3 (*Elovl3*), *Lipin1*, Perilipin 5 (*Plin5*), cell death-inducing DNA fragmentation factor, alpha subunit-like effector A (*Cidea*), uncoupling protein 1 (*Ucp1*), cytochrome c oxidase subunit 7A1 (*Cox7a1*), 2'-5' oligoadenylate synthetase 2 (*Oas2*) and interferon-induced protein with tetratricopeptide repeats 2 (*Ifit2*). Data were normalized to *36b4* and expressed as relative fold changes to wild type at day 5. Mean of the cycle threshold (Ct) is shown. ND: not detected. Data are expressed as mean \pm SD (n=3 per genotype). Statistical analysis was performed using two-tailed unpaired Student's t tests. * p < 0.05 denote statistically significant differences.

polypeptide 58 (*Ddx58*) in the RLRs cluster, and *Irf7*, *Usp18*, *Ifi44* and *Oas2* in the ISGs group (Figures 14D).

Analysis of cellular components between wild type and *Agpat2*^{-/-} cells at day 5 of differentiation, showed that the expression level of genes related to mitochondrion (GO: 0005739), mitochondrial envelope (GO: 0005740), mitochondrial membrane (GO: 0031966), mitochondrial part (GO: 0044429) and mitochondrial inner membrane (GO: 0005743) were significantly decreased in *Agpat2*^{-/-} cells (Figure 14E). Among the genes belonging to these categories highlight *Ucp1*, cytochrome c oxidase subunit 8B (*Cox8b*) and cytochrome c oxidase subunit 7A1 (*Cox7a1*). (Figure 14F).

The mRNA levels of selected genes differentially expressed in the microarray analysis were quantified by qPCR analysis in a new set of differentiated brown adipocytes. For those related with adipogenic differentiation were quantified *Agpat2*, *Cebpa*, *Ppara*, *Slc2a4*, *Elovl3*, *Lipin1*, *Plin5* and *Cidea*. Among those related to ISG we quantified *Ifit2* and *Oas2*, and for those related to mitochondrial function we quantified *Ucp1* and *Cox7a1* (Figure 15).

As shown in the Figure 15, we corroborated that the absence of AGPAT2 in differentiated brown adipocytes decreases the mRNA levels of all the evaluated genes related to brown adipocyte differentiation and specific mitochondrial processes (uncoupled respiration) but increases the mRNA levels of genes related to interferon response.

Interestingly, recent studies have shown that the activation of ISGs impairs thermogenic and mitochondrial function in brown adipocytes (Kissig *et al.*, 2017; Liu *et al.*, 2019). Therefore, it is possible that increased activation of this pathway underlies both abnormal adipogenic brown differentiation of *Agpat2*^{-/-} adipocytes.

4.5. Mitochondrial morphology and distribution are altered at day 5 of differentiation in differentiated brown adipocytes of *Agpat2*^{-/-} mice.

Our global and targeted gene expression analyses suggest that differentiated brown adipocytes of *Agpat2*^{-/-} mice have alterations in mitochondrial biogenesis/function. Since mitochondrial activity is essential for both general adipogenesis and brown adipocyte phenotype, we investigated mitochondrial alterations in differentiated brown adipocytes of *Agpat2*^{-/-} mice. For this, we performed transmission electron microscopy to analyze mitochondrial abundance and ultrastructure in differentiated brown adipocytes of wild type and *Agpat2*^{-/-} mice at days 0 and 5 of differentiation.

We found no differences at day 0 of differentiation (corresponding to “preadipocyte” stage) in the cellular ultrastructure of wild type and *Agpat2*^{-/-} cells, including no changes in the morphology and number of mitochondria (Figure 16A and 16C), as well as other organelles. This result is agreement with our mRNA microarray analysis that showed no global differences in mitochondria-related gene expression level (Figure 13A) and with the abundance of specific adipogenic transcription factors and preadipocytes markers (Figures 9 and 10).

These results were notoriously different from those observed after adipogenic induction. In wild type adipocytes, brown adipogenic differentiation (day 5 after induction) increased the overall abundance of mitochondria changed the overall mitochondrial shape that turned from a “spaghetti”-like to a “bean”-like look. Also, their inner structure was modified, with a denser content of closely packed and parallel cristae, in comparison with undifferentiated preadipocytes (day 0). Importantly, several mitochondria were intimately associated with LDs, such as no

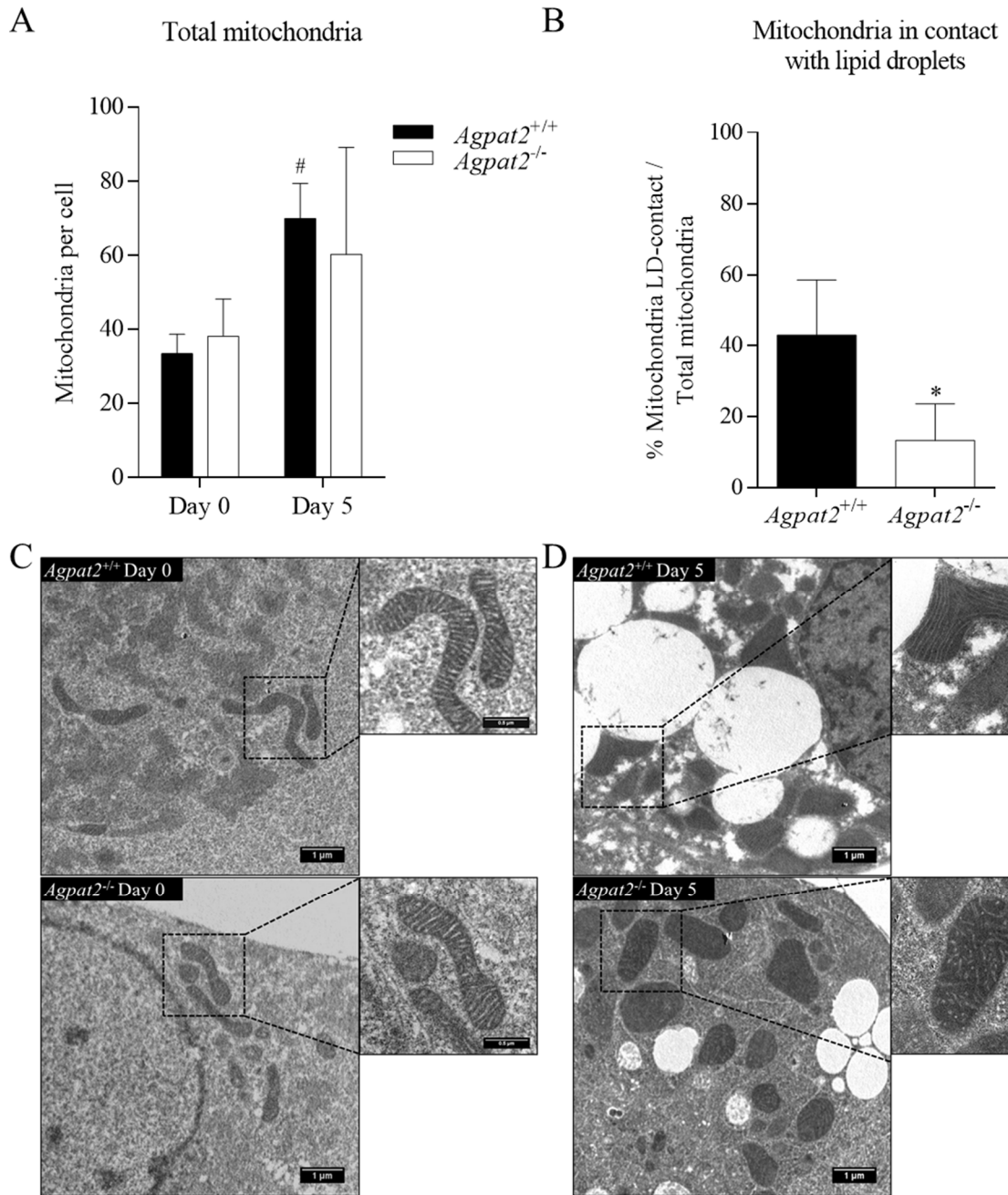


FIGURE 16: Mitochondrial number and morphology is abnormal in differentiated brown adipocytes of *Agpat2*^{-/-} mice. (A) Quantification of total mitochondria of primary cell culture of *Agpat2*^{-/-} and *Agpat2*^{+/+} mice, at days 0 and 5 of differentiation (6-13 cells were counted, n=1 per genotype). (B) Quantification of mitochondria in contact with lipid droplets of primary cell culture of *Agpat2*^{-/-} and *Agpat2*^{+/+} mice, at day 5 of differentiation (11-14 cells were counted, n=1 per genotype). (C) and (D) representative images of transmission electron microscopy (TEM) in brown adipocytes of *Agpat2*^{-/-} and *Agpat2*^{+/+} mice at day 0 and 5 of differentiation. Scale bar 1 and 0,5 μm . Data are expressed as mean \pm SD. *p < 0.05 denote statistically significant differences between differentiated brown adipocytes of wild type and *Agpat2*^{-/-} mice at the same day of differentiation, # p < 0.05 denotes statistically significant differences in comparison with day 0 in the same genotype. p values were calculated using two-way ANOVA.

discernible distance between the mitochondrial outer membrane (OMM) and the surface of LDs could be observed (Figure 16C and 16D).

By contrast, although no differences were noted mitochondrial number between *Agpat2*^{-/-} and wild type brown adipocytes at day 5 of differentiation (Figure 16A), *Agpat2*^{-/-} cells have markedly disorganized cristae, that were never parallel and have fewer packing density than the one observed in wild type cells (Figure 16D). Also, fewer mitochondria were associated to LDs in *Agpat2*^{-/-} cells at day 5 of differentiation.

Regarding this latter finding, recently was reported that the association between mitochondria and lipid droplets requires at least two proteins: Mitofusin 2 (Mfn2) (Boutant *et al.*, 2017) and Perilipin 5 (Plin5) (Benador *et al.*, 2018). Interestingly, whereas our micro array analysis showed no differences in the mRNA levels of Mfn2 between differentiated *Agpat2*^{-/-} and wild type brown adipocytes, *Plin5* mRNA level was lower in *Agpat2*^{-/-} brown adipocytes (~3.4-fold) in comparison with wild type at day 5 of differentiation (Figure 15), suggesting that decreased levels of Plin5 are implicated in the defective association between mitochondria and LDs in *Agpat2*^{-/-} brown adipocytes.

4.6. Differentiated brown adipocytes of *Agpat2*^{-/-} mice have similar STAT1/2 levels in comparison with wild type cells.

As mentioned above, our microarray mRNA analysis showed activation of the response to virus (GO: 0009615) and response to IFN β (GO: 0035456) gene pathways in differentiated *Agpat2*^{-/-} brown adipocytes. Besides to their well-known role in the cellular response to infections, interferon activation has been linked with several other causes of cellular damage (Ivashkiv, 2018) and also with impaired adipogenesis *in vitro* (Lee *et al.*, 2016; Kissig *et al.*, 2017). For these reasons, we decided to further investigate interferon pathways in differentiated brown adipocytes of *Agpat2*^{-/-} mice. As shown in Figure 5, transcriptional regulation of ISGs is complex and involves both redundant and interconnected signaling pathways. Among the key hubs of regulation highlight STAT1/2, that is phosphorylated by type-I interferon receptor and forms complexes with interferon responsive factor 9 (IRF9). After these activating modifications, these proteins translocate to the nucleus and increases interferon responsive element (IRE)-containing genes transcription. Importantly, many of these target genes are overexpressed in differentiated brown adipocytes of *Agpat2*^{-/-} mice (day 5, Figure 13C and 14D).

Therefore, we assessed the abundance and nuclear STAT1 and STAT2 in differentiated brown adipocytes, because it is likely, although not unequivocally correct, that in this location these proteins are transcriptionally active. For quantitative purposes, we captured and analyzed images with an automated high-throughput imaging system (see “Methods” for a detailed explanation).

As shown in Figure 17A, the proportion of cells with nuclear STAT1 staining steadily increased from day 3 in both genotypes, and this proportion was higher in wild type cells in

comparison with differentiated brown adipocytes of *Agpat2*^{-/-} mice only at day 5 differentiation, remaining similar in all the other days analyzed (Figure 17A and 17D). Interestingly, and similar to PPAR γ (Figure 8), if the analysis is restricted to cells that are laden with LDs and that simultaneously have nuclear STAT1 staining, not differences between wild type and *Agpat2*^{-/-} brown adipocytes are found at days 3 and 5 of differentiation. However, at day 7 of differentiation, *Agpat2*^{-/-} cultures have a notorious decrease in the proportion of LDs laden cells with nuclear STAT1 staining whereas in the wild type cultures this proportion was even higher than in the precedent days (Figure 17B and 17D). Importantly, the abundance of total STAT1 protein, quantified by immunoblotting, increased with the adipogenic differentiation in both genotypes but no differences between genotypes were found (Figure 17C). These results do not support our hypothesis that increased STAT1 activity is involved in the lower accumulation of LDs in differentiated brown adipocytes of *Agpat2*^{-/-} mice.

In the case of STAT2, we also performed both immunofluorescence and immunoblotting analysis to quantify nuclear localization and overall protein abundance, respectively. We found that, although the proportion of STAT2 positive cells (Figure 18A) and total STAT2 protein content (Figure 18B) tended to increase in differentiated cultures of both genotypes, with higher levels in *Agpat2*^{-/-} cultures, cellular staining was mostly cytoplasmic (Figure 18C) and no significant differences were reached, possibly owing to the elevated dispersion of the data. In any case, it is highly unlikely that increased levels of STAT2 protein have any role on the adipogenic defect of *Agpat2*^{-/-} brown adipocytes nor increased expression levels of ISGs, since there is no time correspondence between lower LDs accumulation (evident at days 3 and 5 of differentiation) and STAT2 overexpression (day 7).

Although these results suggest that no differences in the activation status of STAT1/2 is present between differentiated brown adipocytes of wild type and *Agpat2*^{-/-} mice, they are in contradiction with the global gene expression analysis, that indicates activation of IFN response. For the correct interpretation of these results, it is important to keep in mind that total and even nuclear content of transcriptional regulators do not necessarily translate in useful information on the transcriptional activity of these proteins. Only the evaluation of the occupancy of IREs by STATs in interferon-targeted genes by of chromatin immunoprecipitation analysis, will provide a more direct information on the activation status of this pathway in differentiated brown adipocytes of *Agpat2*^{-/-} mice.

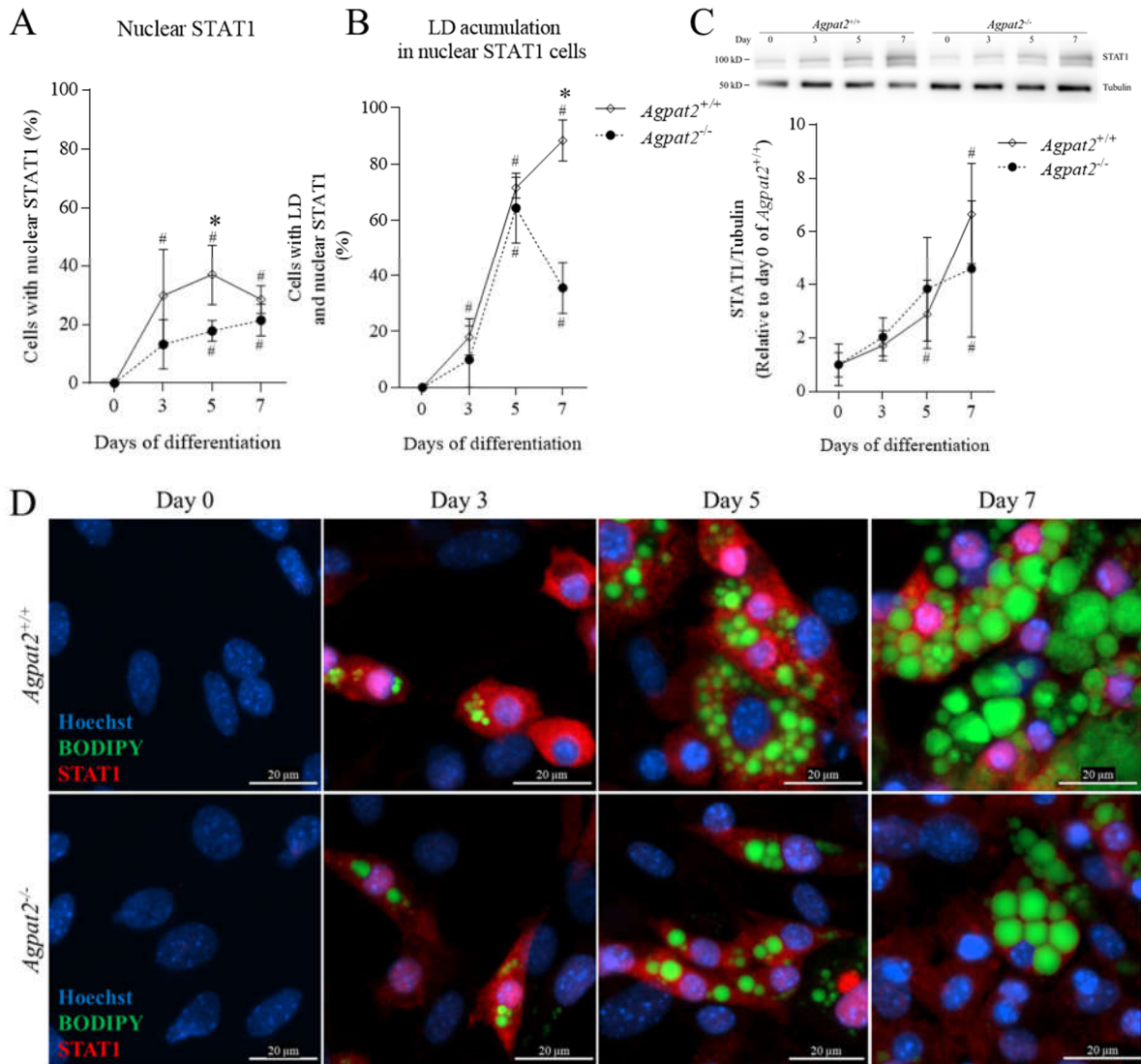


FIGURE 17: Differentiated brown adipocytes of *Agpat2*^{-/-} mice have similar levels of nuclear STAT1 in comparison with wild type cells. (A) Quantification of cells with nuclear STAT1. (B) Quantification of cells with LD and nuclear STAT1. (C) Representative immunoblot of STAT1 and tubulin of differentiated brown adipocytes of wild type and *Agpat2*^{-/-} mice at days 0, 3, 5 and 7 of differentiation and immunoblot quantification of STAT1, expressed as fold-change relative the levels of wild type mice at day 0 of differentiation and normalized to tubulin levels. (D) Representative immunofluorescence images staining STAT1 (red), neutral lipids with BODIPY (green) and nuclei with Hoechst 33342 (blue) of differentiated brown adipocytes of wild type and *Agpat2*^{-/-} mice at days 0, 3, 5 and 7 of differentiation. Scale bar 20 μ m. Automated imaging analysis included ~35,000 cells in total. Data are expressed as mean \pm SD (N=3 per genotype). *p < 0.05 denote statistically significant differences between differentiated brown adipocytes of wild type and *Agpat2*^{-/-} mice at the same day of differentiation, # p < 0.05 denotes statistically significant differences in comparison with day 0 in the same genotype. p values were calculated using two-way ANOVA.

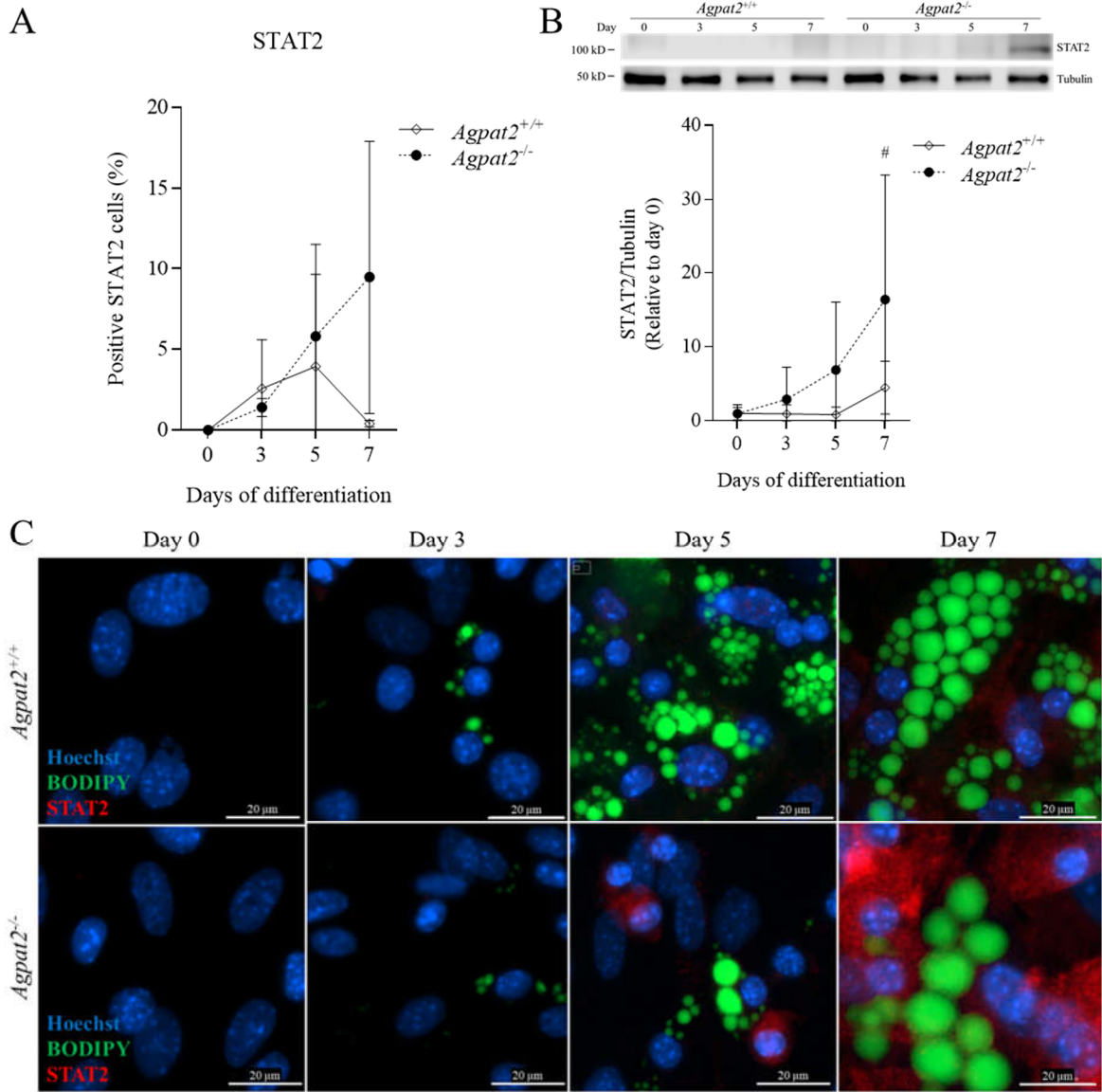


FIGURE 18: Differentiated brown adipocytes of *Agpat2*^{-/-} mice have higher levels of cytoplasmic STAT2 only at advanced stages of differentiation. (A) Quantification of cells with nuclear STAT2. (B) Representative immunoblot of STAT2 and tubulin of differentiated brown adipocytes of wild type and *Agpat2*^{-/-} mice at days 0, 3, 5 and 7 of differentiation and immunoblot quantification of STAT2, expressed as fold-change relative the levels of wild type mice at day 0 of differentiation and normalized to tubulin levels. (C) Representative immunofluorescence images staining STAT2 (red), neutral lipids with BODIPY (green) and nuclei with Hoechst 33342 (blue) of differentiated brown adipocytes of wild type and *Agpat2*^{-/-} mice at days 0, 3, 5 and 7 of differentiation. Scale bar 20 μ m. Automated imaging analysis included ~35,000 cells in total. Data are expressed as mean \pm SD (N=3 per genotype). *p < 0.05 denote statistically significant differences between differentiated brown adipocytes of wild type and *Agpat2*^{-/-} mice at the same day of differentiation, # p < 0.05 denotes statistically significant differences in comparison with day 0 in the same genotype. p values were calculated using two-way ANOVA.

4.2. Elovl3 and mitoNEET forced expression does not restore adipogenic differentiation in differentiated brown adipocytes of *Agpat2*^{-/-} mice.

4.2.1. Elovl3 and mitoNEET are induced in brown adipogenic differentiation of wild type adipocytes but their levels remain low in differentiated brown adipocytes of *Agpat2*^{-/-} mice.

Previous work in our laboratory found that the forced expression of PPAR γ by adenoviral transduction was unable to revert adipogenic impairment of AGPAT2 deficient adipocyte precursor cells upon a “white adipocyte” differentiation paradigm (Cautivo *et al.*, 2016). As mentioned, PPAR γ is a key transcriptional regulator of adipogenesis and its forced overexpression, even in non-adipose cells, increases the expression of genes involved in lipid accumulation and adipocyte phenotype. Thus, our results suggest that AGPAT2 in mouse preadipocytes is, somehow, required for PPAR γ adipogenic activity.

Following that line of thinking, herein we looked for genes downstream PPAR γ and whose expression levels could be forcedly increased to restore the adipogenic capability of *Agpat2*^{-/-} preadipocytes. We choose 2 candidates, Elovl3 and mitoNEET, based on different criteria.

First, we searched our microarray database for those genes with the largest downregulated expression level in differentiated brown adipocytes of *Agpat2*^{-/-} mice in comparison with wild type cells at day 5 of differentiation and that have known functional relevance in adipogenic differentiation and/or mature adipocyte function. Figure 13B shows the top 20 genes with the greater decreased expression level. Among them highlight UCP1 as the top 1 gene, Ffar4, Cidea and Elovl3.

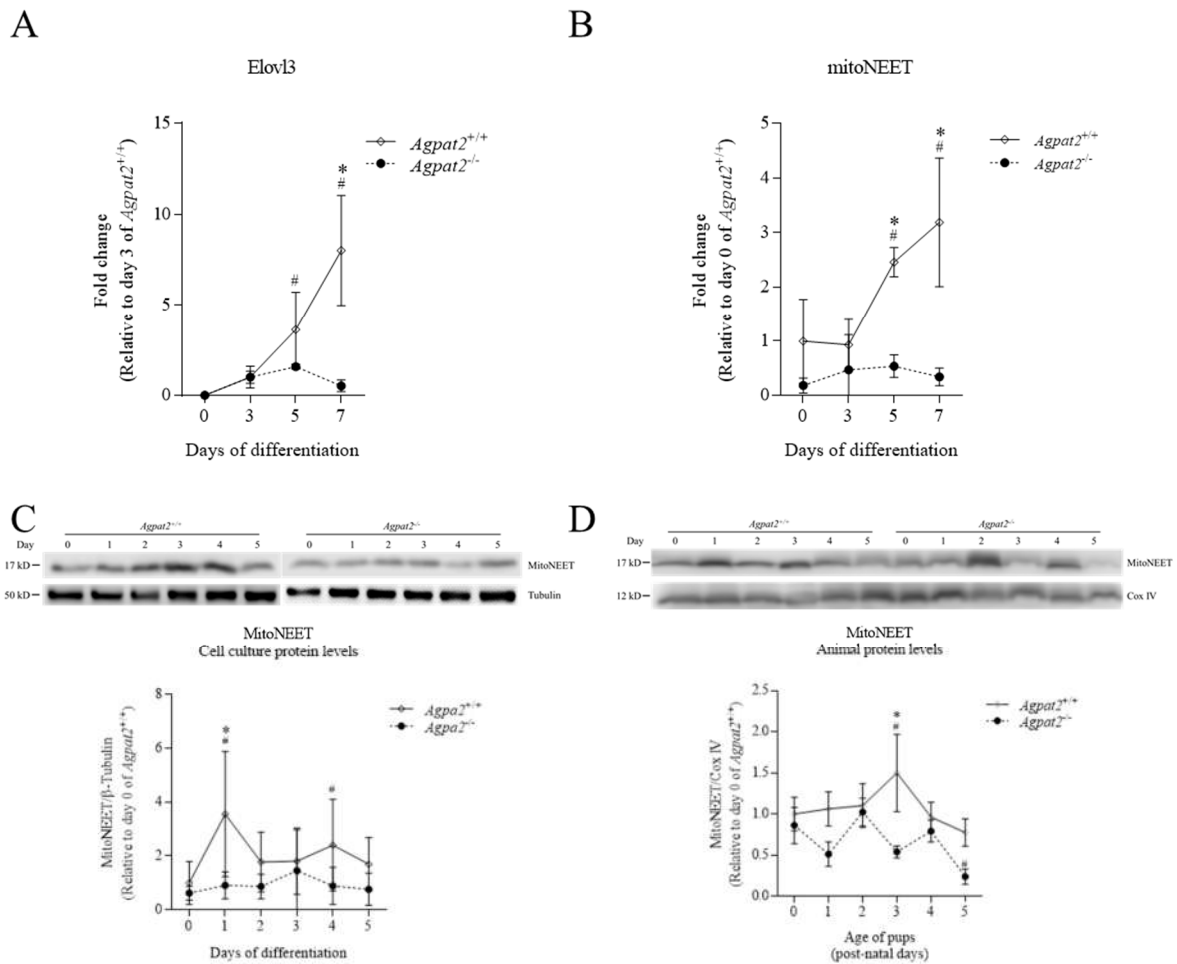


FIGURE 19: *Elov3* and mitoNEET levels are lower in differentiated brown adipocytes of *Agpat2*^{-/-} mice in comparison with wild type cells. (A) *Elov3* mRNA levels normalized to *36b4* and expressed as relative fold changes to wild type mice at day 3. (B) mitoNEET mRNA levels normalized to *36b4* and expressed as relative fold changes to wild type mice at day 0. (C) Representative immunoblot of mitoNEET and tubulin of differentiated brown adipocytes of wild type and *Agpat2*^{-/-} mice at days 0, 1, 2, 3, 4 and 5 of differentiation and immunoblot quantification of mitoNEET, expressed as fold-change relative the levels of wild type mice at day 0 of differentiation and normalized to tubulin levels. (D) Representative immunoblot of mitoNEET and CoxIV in iBAT of wild type and *Agpat2*^{-/-} mice at days 0, 1, 2, 3, 4 and 5 after birth and immunoblot quantification of mitoNEET, expressed as fold-change relative the levels of wild type mice at day 0 after birth and normalized to tubulin levels. Data are expressed as mean \pm SD (N=3 per genotype). *p < 0.05 denote statistically significant differences between wild type and *Agpat2*^{-/-} at the same day of differentiation or after birth, # p < 0.05 denotes statistically significant differences in comparison with day 0 in the same genotype. p values were calculated using two-way ANOVA.

Although UCP1, Cidea and Ffar4 are markers for mature brown adipocyte phenotype, their known function appears to be more a consequence rather than a cause, or a regulator, of adipogenesis. In fact, Cidea has roles in LDs maturation by transferring lipids between these LDs of different sizes (Barneda *et al.*, 2015). Ffar4 has been described as a n-3 polyunsaturated fatty acid (PUFA) receptor and modulates inflammation and glucose sensitivity in white adipocytes (Kim *et al.*, 2016). Finally, UCP1 functions are mostly dedicated to thermogenic activity.

By contrast, Elov13 catalyzes the elongation of C16, C18, or C20 saturated and monounsaturated very long-chain fatty acids (VLCFAs) and is expressed mainly in BAT (Jakobsson, *et al.* 2005; Shapira *et al.*, 2019). Therefore, it is an attractive candidate to modulate PPARs transcriptional activity by generating fatty acid-PPAR lipid ligands that might be important for the regulatory activity of these nuclear receptors in the context of an ongoing brown adipogenic differentiation.

In fact, *Elov13* mRNA levels increase more than 200-fold in iBAT of animals exposed to cold, a physiological stimuli for brown adipogenesis *in vivo* (Tvrdek *et al.*, 1997). Importantly, *Elov13* is transcriptionally regulated by PPAR γ , and in turn, VLCFAs produced by Elov13 may activate the expression of PPAR γ (Kobayashi *et al.*, 2012).

In agreement with our microarray data, *Elov13* mRNA remained unchanged in differentiated brown adipocytes of *Agpat2*^{-/-} mice in comparison with undifferentiated cells and were lower than in wild type differentiated adipocytes (Figure 19A). Since no commercial antibodies are available for mouse *Elov13* detection, we could not quantify the levels of this protein in our experiments.

In addition to *Elovl3*, we also intended to evaluate whether proteins important for mitochondrial function and previously associated to adipogenesis could revert the adipogenic failure of *Agpat2*^{-/-} adipocyte.

MitoNEET is a protein located in the OMM that was originally described as a target of the thiazolidinedione pioglitazone (Colca *et al.*, 2004). Its known function is to transport iron-sulfur clusters into the mitochondria and is a modulator of mitochondrial electron transport and lipid metabolism (Tamir *et al.*, 2015).

Selective overexpression of mitoNEET in adipocytes produces massive increase of adipose tissue mass in *ob/ob* mice, but paradoxically normalization of insulin resistance and diabetic phenotype in these animals, owing to an improved mitochondrial functioning and decreased lipotoxicity. Conversely, suppression of mitoNEET expression *in vitro* produces a profound mitochondrial alteration in hepatocytes, mouse embryonic fibroblasts (MEFs) and 3T3-L1 cells, a cell line with adipogenic potential (Kusminski *et al.*, 2014).

Similar to *Elovl3*, we found that mitoNEET mRNA levels were significantly lower in differentiated brown adipocytes of *Agpat2*^{-/-} mice at days 5 and 7 of differentiation, in comparison with wild type cells (Figure 19B). On the other hand, the abundance of mitoNEET protein was also lower in differentiated brown adipocytes of *Agpat2*^{-/-} mice in comparison with wild type cultures, although these differences were less marked than at the mRNA level (Figure 19C). We also quantified mitoNEET protein in the iBAT of newborn mice. In the first two days after birth, *Agpat2*^{-/-} and wild type mice had equivalent abundance of mitoNEET but they were lower at the third day in *Agpat2*^{-/-} mice (Figure 19D).

Again, the absolute magnitude of these differences at the protein level in iBAT were small; however, since the sole transgenic overexpression of mitoNEET in mice was sufficient to increase adipose tissue mass and improve mitochondrial function in obese mice, we decided to move forward to overexpression experiments in our cell culture model of adipogenesis.

Elov13 and mitoNEET levels were forcedly increased by infection with recombinant adenovirus generated by us in this thesis. An adenovirus encoding LacZ was used as a control of infection. With these adenoviruses, designated as Ad Elov13 and Ad mitoNEET we evaluated whether the forced expression of these gene products was able to improve brown adipogenic differentiation in *Acp1*^{-/-} preadipocytes.

4.2.2. Forced expression of Elovl3 and mitoNEET does not increase lipid droplets accumulation in differentiated brown adipocytes of *Agpat2*^{-/-} mice.

As shown in Figure 20A, *Elovl3* mRNA levels were ~4-fold higher in *Agpat2*^{-/-} brown adipocytes infected with Ad Elovl3, in comparison with *Agpat2*^{-/-} adipocytes infected with an adenovirus encoding LacZ (day 5 of differentiation). No differences in the mRNA levels of *Elovl3* were observed between wild type and *Agpat2*^{-/-} adipocytes infected with Ad Elovl3 (data not shown), indicating that infection with Ad Elovl3 was able to reverse the decreased levels of *Elovl3* in differentiated brown adipocytes of *Agpat2*^{-/-} mice, at least at the mRNA level.

Wild type brown adipocytes infected with Ad Elovl3 presented ~80% of cells laden with LDs at day 5 and 7 of differentiation, and this proportion was not different from the one in wild type cells infected with Ad LacZ, indicating that the sole overexpression of Elovl3 is not sufficient to increase the content of LDs in differentiated brown adipocytes.

Differentiated brown adipocytes of *Agpat2*^{-/-} mice infected with Ad Elovl3 or Ad LacZ had ~40% of cells laden with LDs, and no differences were observed in this proportion between *Agpat2*^{-/-} infected with either adenovirus (Figure 20B and 20C), indicating that overexpressed Elovl3 does not reverse the adipogenic failure of *Agpat2*^{-/-} adipocytes.

Infection of *Agpat2*^{-/-} adipocytes with Ad mitoNEET increased the abundance of mitoNEET mRNA by ~10-fold higher in *Agpat2*^{-/-} cells in comparison with *Agpat2*^{-/-} cells infected with Ad LacZ at days 3 and 5 of differentiation, resulting in equivalent mitoNEET mRNA levels in differentiated brown adipocytes of wild type and *Agpat2*^{-/-} mice (data not shown).

Forced expression of mitoNEET did not increase the proportion of LDs laden cells in both wild type and *Agpat2*^{-/-} adipocytes in comparison with the cells of the same genotype but infected with Ad LacZ, and thus did not rescue *Agpat2*^{-/-} adipocytes adipogenic failure (Figure 21B and 21C).

These results indicate the sole overexpression of Elovl3 or mitoNEET is not sufficient to restore the number of cells with lipid droplets in differentiated *Agpat2*^{-/-} brown adipocytes. Combining with our previously published result that PPAR γ overexpression also failed to improve adipogenesis in preadipocytes lacking AGPAT2, we hypothesize that the absence of AGPAT2 determines either the lack of an endogenous activator of PPAR γ or promotes a state of cellular “resistance” to the actions of this nuclear receptor.

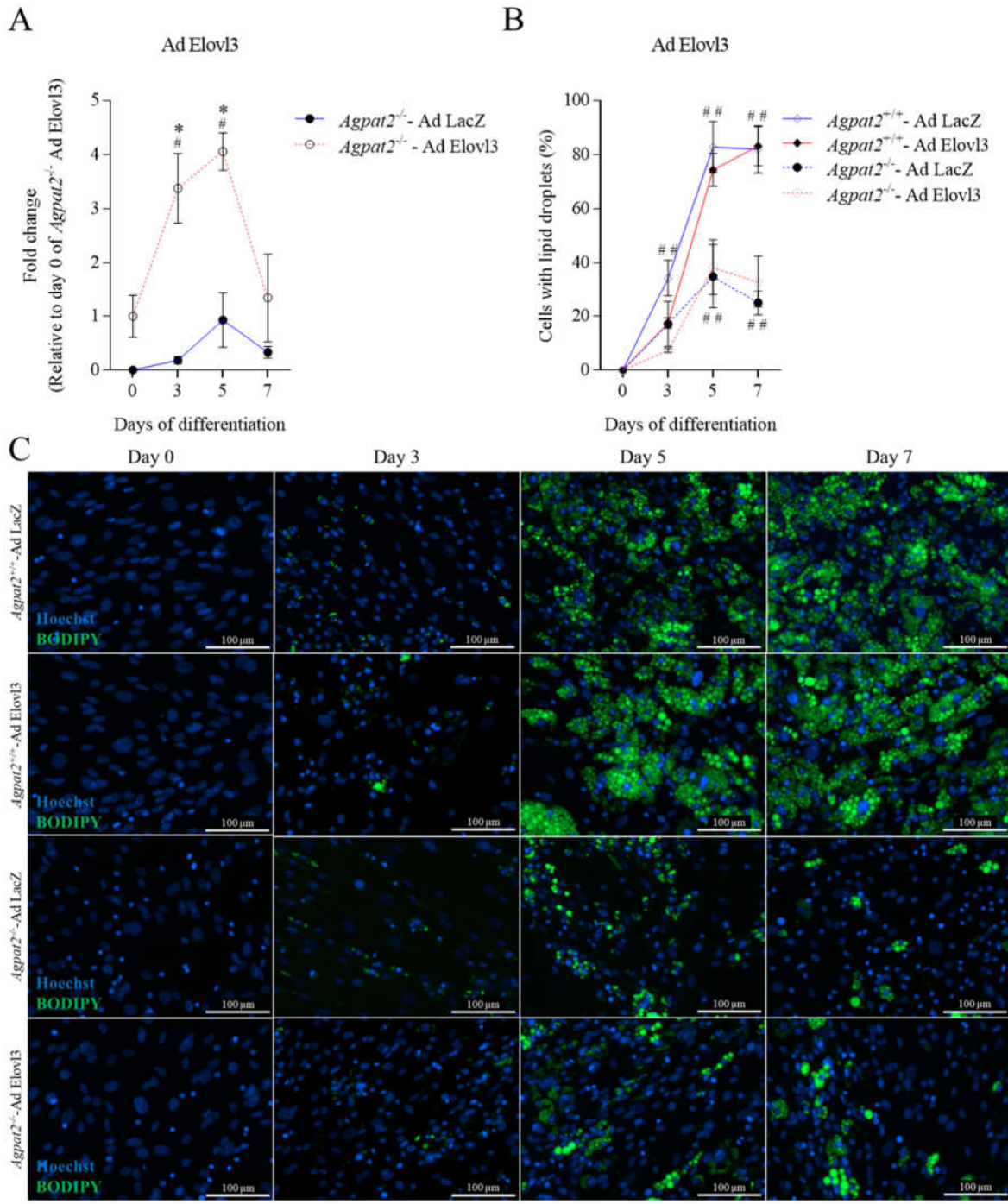


FIGURE 20: The forced overexpression of Elovl3 does not restore lipid droplets accumulation in differentiated brown adipocytes of *Agpat2*^{-/-} mice. (A) *Elovl3* mRNA levels of differentiated brown adipocytes of *Agpat2*^{-/-} mice infected with Ad Elovl3. Data were normalized to *36b4* and expressed as relative fold changes to *Agpat2*^{-/-} Ad Elovl3 at day 0. (B) Quantification of cells with lipid droplets (BODIPY) in differentiated brown adipocytes of wild type and *Agpat2*^{-/-} mice infected with Ad Elovl3. Automated imaging analysis included ~130,000 cells in total. (C) Representative images of neutral lipid (BODIPY, green) and nuclei (Hoechst 33342, blue) staining in differentiated brown adipocytes of wild type and *Agpat2*^{-/-} mice infected with Ad Elovl3, at days 0, 3, 5 and 7 of differentiation. Scale bar 100 μ m. Data are expressed as mean \pm SD (n=3 per genotype). *p < 0.05 denote statistically significant differences between differentiated brown adipocytes of wild type and *Agpat2*^{-/-} mice at the same day of differentiation, # p < 0.05 denotes statistically significant differences in comparison with day 0 in the same genotype. p values were calculated using two-way ANOVA.

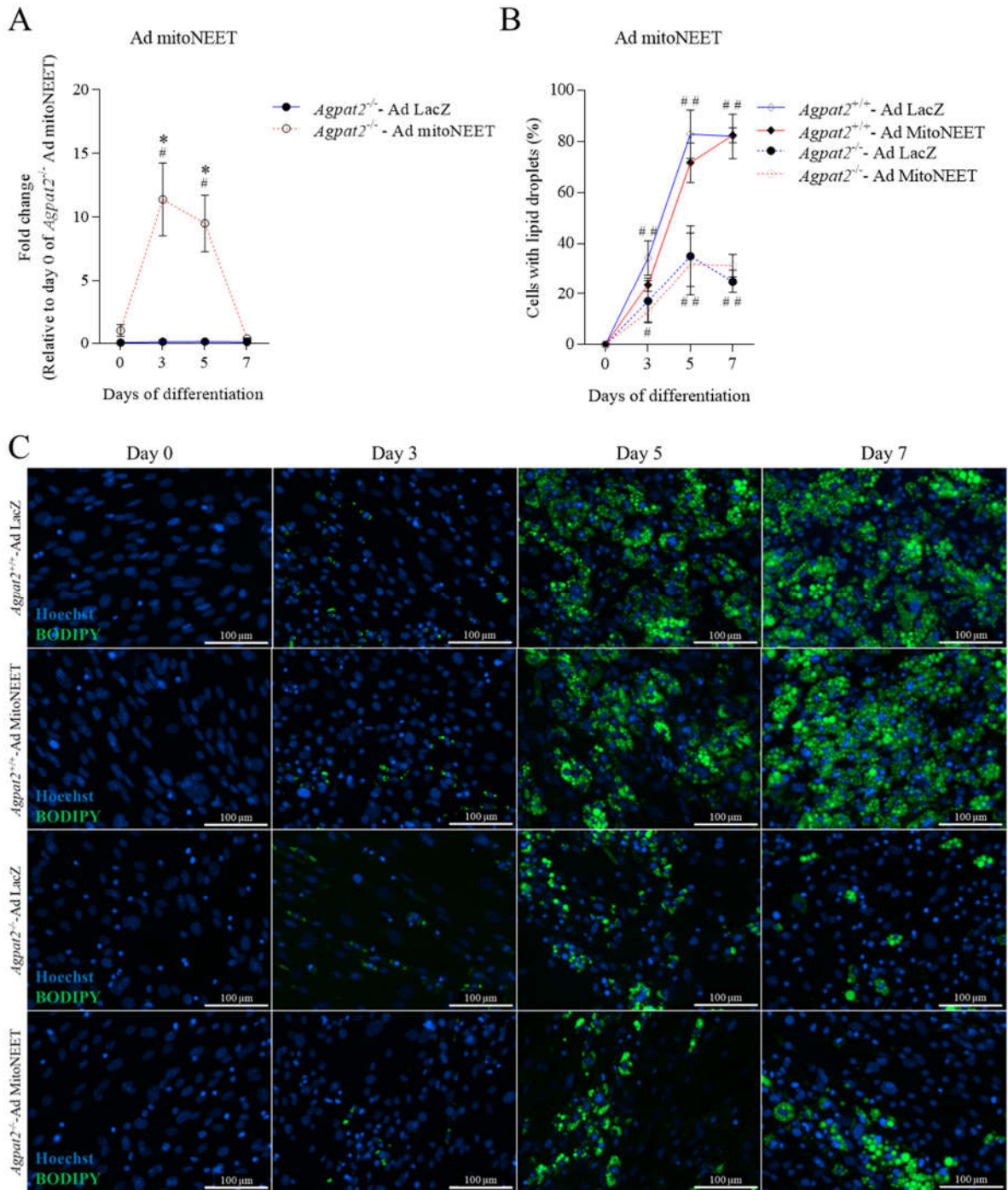


FIGURE 21: The forced overexpression of mitoNEET does not restore lipid droplets accumulation in differentiated brown adipocytes of *Agpat2*^{-/-} mice. (A) mitoNEET mRNA levels of differentiated brown adipocytes of *Agpat2*^{-/-} mice infected with Ad mitoNEET. Data were normalized to *36b4* and expressed as relative fold changes to *Agpat2*^{-/-} Ad mitoNEET at day 0. (B) Quantification of cells with lipid droplets (BODIPY) in differentiated brown adipocytes of wild type and *Agpat2*^{-/-} mice infected with Ad mitoNEET. Automated imaging analysis included ~130,000 cells in total. (C) Representative images of neutral lipid (BODIPY, green) and nuclei (Hoechst 33342, blue) staining in differentiated brown adipocytes of wild type and *Agpat2*^{-/-} mice infected with Ad mitoNEET, at days 0, 3, 5 and 7 of differentiation. Scale bar 100 μ m. Data are expressed as mean \pm SD (n=3 per genotype). *p < 0.05 denote statistically significant differences between differentiated brown adipocytes of wild type and *Agpat2*^{-/-} mice at the same day of differentiation, # p < 0.05 denotes statistically significant differences in comparison with day 0 in the same genotype. p values were calculated using two-way ANOVA.

4.3. Palmitic acid overload determines excessive cell death in differentiated brown adipocytes of *Agpat2*^{-/-} mice.

Agpat2^{-/-} mice completely loss adipose tissue during the first week of life as a consequence of selective adipocytes cell death and adipose tissue inflammation (Cautivo *et al.*, 2016). In addition, adult *Agpat2*^{-/-} mice have increased plasma levels of triglycerides (Cortés *et al.*, 2009). Herein we hypothesize that adipocytes of *Agpat2*^{-/-} in mice die because of inability to adapt to the elevated levels of circulating fatty acids in the days that follow birth. To evaluate this possibility, we first quantified plasma levels of saturated, monounsaturated and polyunsaturated fatty acids at different ages after birth in these mice. Given the scarce amount of blood that can be retrieved from individual animals at this age, we determined fatty acid composition by gas–liquid chromatography in pooled mouse plasma samples.

As shown in the Figure 22 and Table 1, circulating levels of saturated, monounsaturated and polyunsaturated fatty acids in *Agpat2*^{-/-} and wild type mice are equivalent at the day of birth. Importantly, as soon as the second day *post partum*, *Agpat2*^{-/-} mice have a marked increase in all measured fatty acid species, and this difference is maintained to the fourth day after birth.

In particular, levels of palmitic acid, a saturated 16-carbon fatty acid with known cellular toxicity by activating apoptotic mechanisms (Paumen *et al.*, 1997) and that has been implicated in insulin resistance *in vivo* (Paumen *et al.*, 1997), are ~6-fold higher in *Agpat2*^{-/-} mice in comparison with wild type animals on days 2 and 4 after birth (Figure 22D). To evaluate the effects of elevated palmitic acid on the viability of differentiated *Agpat2*^{-/-} adipocytes, we exposed cell cultures of undifferentiated preadipocytes (day 0 of differentiation) and differentiated brown adipocytes (day 5 of differentiation) to growing concentrations of palmitic

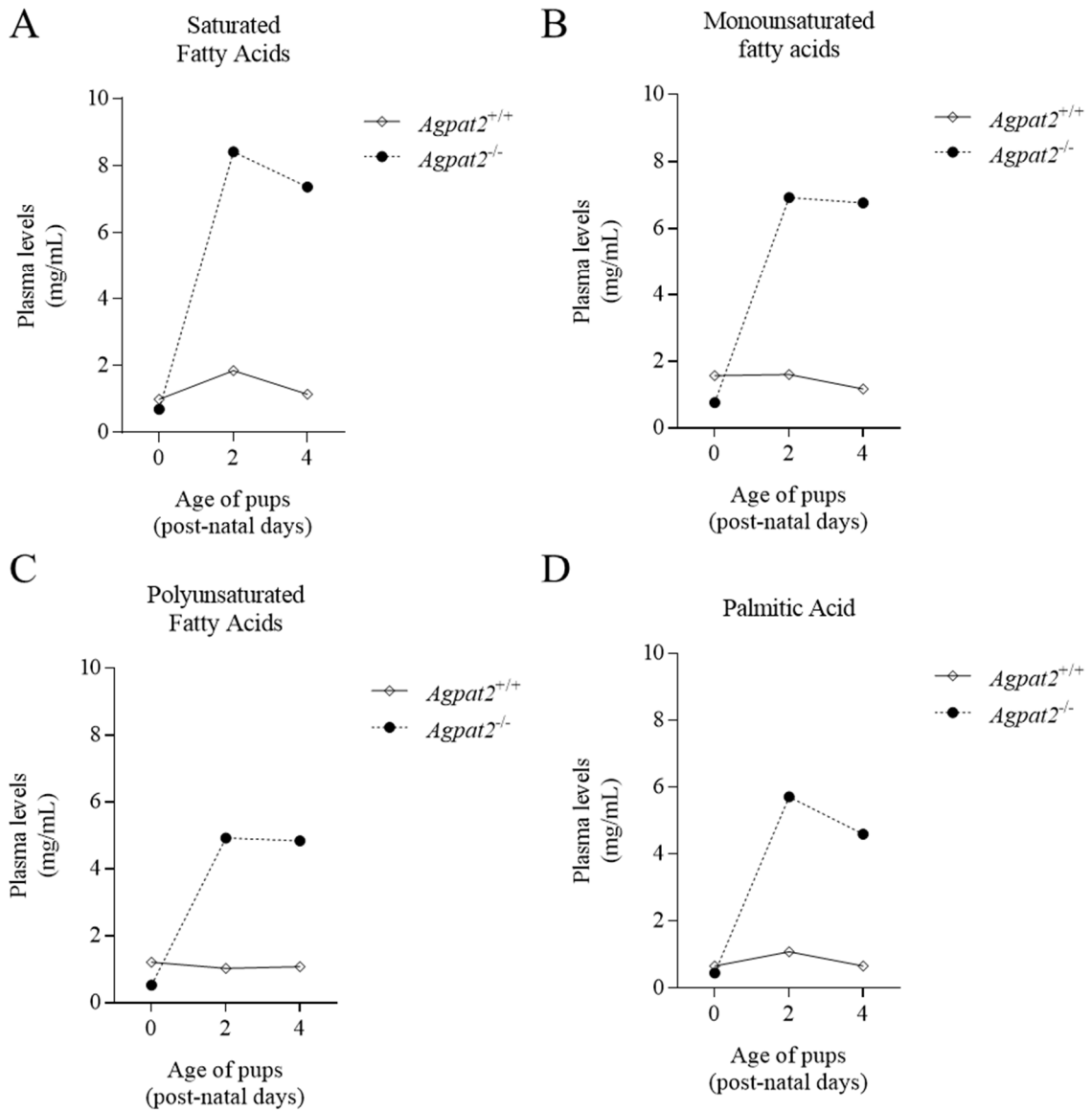


FIGURE 22: Levels of saturated, monounsaturated and polyunsaturated fatty acids are markedly increased in *Agpat2*^{-/-} mice. Graphs of total levels of (B) saturated, (C) monounsaturated, (D) polyunsaturated fatty acids and (E) palmitic acid of wild type and *Agpat2*^{-/-} mice at days 0, 2, and 4 after birth. Between 2 to 8 animals were used per genotype (pool).

	Post-natal days [$\mu\text{g/mL}$]					
	P0.5		P2.5		P4.5	
	<i>Agpat2</i> ^{+/+} Pool n=8	<i>Agpat2</i> ^{-/-} Pool n=6	<i>Agpat2</i> ^{+/+} Pool n=2	<i>Agpat2</i> ^{-/-} Pool n=3	<i>Agpat2</i> ^{+/+} Pool n=2	<i>Agpat2</i> ^{-/-} n=2
Saturated Fatty Acids						
C10:0 Capric acid	0,0	0,0	17,2	138,9	10,0	106,2
C12:0 Dodecanoic acid	15,5	12,9	54,5	520,1	33,9	393,0
C14:0 Tetradecanoic acid	84,2	38,8	202,6	1274,0	134,3	1071,8
C16:0 Palmitic Acid	658,2	453,0	1082,9	5708,4	665,3	4278,2
C18:0 Stearic acid	211,4	180,0	471,5	725,1	286,5	623,1
C20:0 Eicosanoic acid	11,8	4,9	18,2	26,8	12,6	28,3
C22:0 Docosanoic acid	7,1	3,7	4,4	15,1	5,8	13,4
C24:0 Tetracosanoic acid	3,7	0,0	0,0	14,8	0,0	15,9
Total Saturated Fatty Acids	991,9	693,4	1851,3	8423,2	1148,4	6529,9
Monounsaturated fatty acids						
C12:1 Dodecenoic acid	0,0	0,0	0,0	0,0	0,0	4,5
C14:1 Tetradecenoic acid	0,0	0,0	0,0	40,9	0,0	34,0
C16:1 Palmitoleic acid	125,9	63,5	186,9	1113,3	112,3	831,8
C18:1 Oleic acid	1394,3	647,2	1288,1	5517,9	981,2	4099,2
C20:1n9 Eicosanoic acid	35,4	15,4	69,0	172,4	42,7	134,7
C22:1n9 Erucic acid	9,8	30,8	52,1	43,5	25,1	42,3
C24:1 Tetracosanoic acid	6,4	3,7	8,2	36,4	10,8	38,3
Total Monounsaturated Fatty Acids	1571,7	760,6	1604,2	6924,4	1172,0	5184,7
Polyunsaturated Fatty Acids						
C18:2n6 Linoleic acid	669,4	310,0	465,9	2739,6	471,5	2089,5
C18:3n6 Linolenic acid	8,8	4,3	21,3	137,6	11,7	89,9
C18:3n3 Linolenic acid	173,1	50,5	42,0	173,0	77,8	192,8
C20:2n6 Eicosadienoic acid	7,1	3,1	6,3	95,1	10,4	79,9
C20:3n6 Eicosatrienoic acid	7,7	3,7	25,1	158,6	25,7	130,0
C20:3n3 Eicosatetrienoic acid	0,0	0,0	0,0	8,0	0,0	2,2
C20:4n6 Eicosatetraenoic acid	106,4	71,5	219,4	623,8	178,8	464,3
C20:5n3 Eicosapentaenoic acid	113,1	32,7	63,4	222,3	111,1	290,0
C22:2n6 Docosadienoic acid	0,0	0,0	0,0	0,0	0,0	0,0
C22:4n6 Docosatetraenoic Acid	6,1	3,7	4,4	86,4	2,4	54,4
C22:5n3 Docosapentaenoic Acid	22,2	7,4	18,8	136,7	23,6	92,0
C22:6n3 Docosahexaenoic acid	101,7	45,6	159,3	536,4	164,1	333,7
Total Polyunsaturated Fatty Acids	1215,5	532,5	1026,1	4917,4	1077,0	3818,6

TABLE 2: Levels of saturated, monounsaturated, polyunsaturated fatty acids in plasma of wild type and *Agpat2*^{-/-} mice at days 0, 2, and 4 after birth. Between 2 to 8 animals were used per genotype (pool).

acid (0, 250, 500, 750 and 1000 μ M) for 12 hours and determined cellular ability to reduce MTT and the amount of LDH released to culture media, as indicators of cell viability/death.

As shown in Figure 23, at day 0 of differentiation, *Agpat2*^{-/-} and wild type preadipocytes viability is equally sensitive to the increased levels of palmitic acid, since no differences in MTT reduction or release of LDH to the media were found between genotypes (Figure 23A and 23B).

By contrast, at day 5 of differentiation, we found significant differences in the adipocyte viability. Whereas wild type cells were completely resistant to elevated palmitic acid, in differentiated brown adipocytes of *Agpat2*^{-/-} mice, MTT reduction and LDH release were inversely and directly correlated, respectively, with palmitic acid concentration (Figure 23C and 23D).

We also evaluated cleaved caspase 3 levels in *Agpat2*^{-/-} and wild type cell cultures at days 0 and 5 differentiation after incubation with growing concentrations of palmitic acid (0, 500 and 1000 μ M). For quantification purposes, we used an automated imaging acquisition system to identify and count cells that simultaneously have presence of cleaved caspase 3 and present intense and dense nuclear Hoechst 33342 staining, as a morphological sign of pycnosis (Anilkumar *et al.*, 2017; Mandavilli *et al.*, 2018).

Using this operative definition for apoptosis, we found that at day 0 of differentiation, when cells mostly correspond to preadipocytes, *Agpat2*^{-/-} and wild type cultures were equally sensitive to palmitic acid-induced apoptosis, with ~25% of apoptotic cells after incubation with palmitic acid 1000 μ M (Figure 24A and 24B). By contrast, at day 5 of differentiation, when cells are a model of mature brown adipocytes, we found that whereas wild type cells did not increase the proportion of apoptotic cells at any of the tested concentration of palmitic acid,

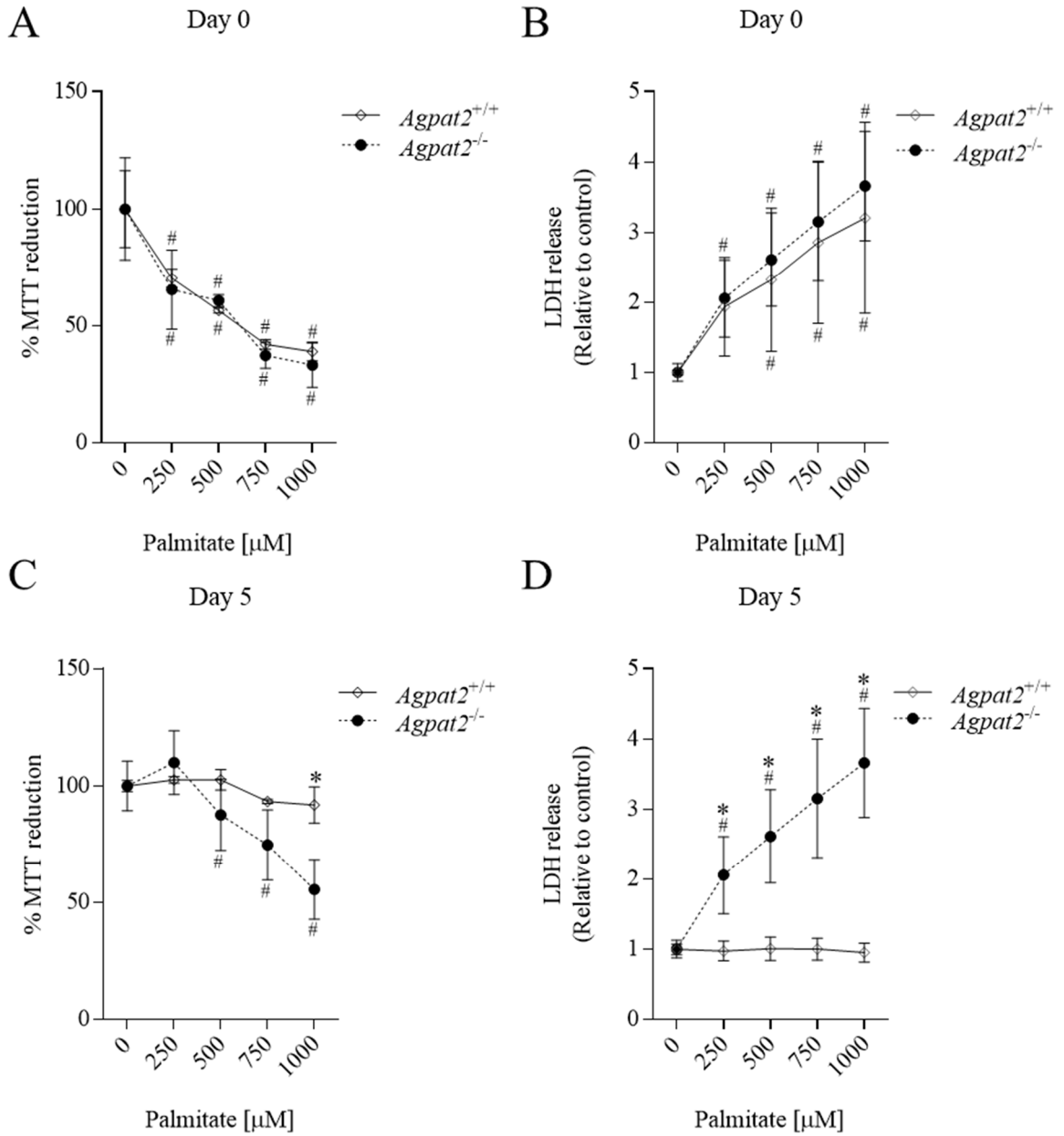


FIGURE 23: Differentiated brown adipocytes of *Agpat2*^{-/-} mice have increased susceptibility to palmitic acid-induced cell death at day 5 of differentiation. Viability of cell cultures of undifferentiated preadipocytes (day 0 of differentiation) and differentiated brown adipocytes (day 5 of differentiation) measured by MTT reduction (A and C) or release of LDH to the media (B and D). Cell cultures were incubated with different concentrations of palmitic acid (0, 250, 500, 750 and 1000 μ M) for 12 hours. Data are expressed as mean \pm SD (n=3 per genotype). *p < 0.05 denote statistically significant differences between differentiated brown adipocytes of wild type and *Agpat2*^{-/-} mice at the same day of differentiation, # p < 0.05 denotes statistically significant differences in comparison with day 0 in the same genotype. p values were calculated using two-way ANOVA.

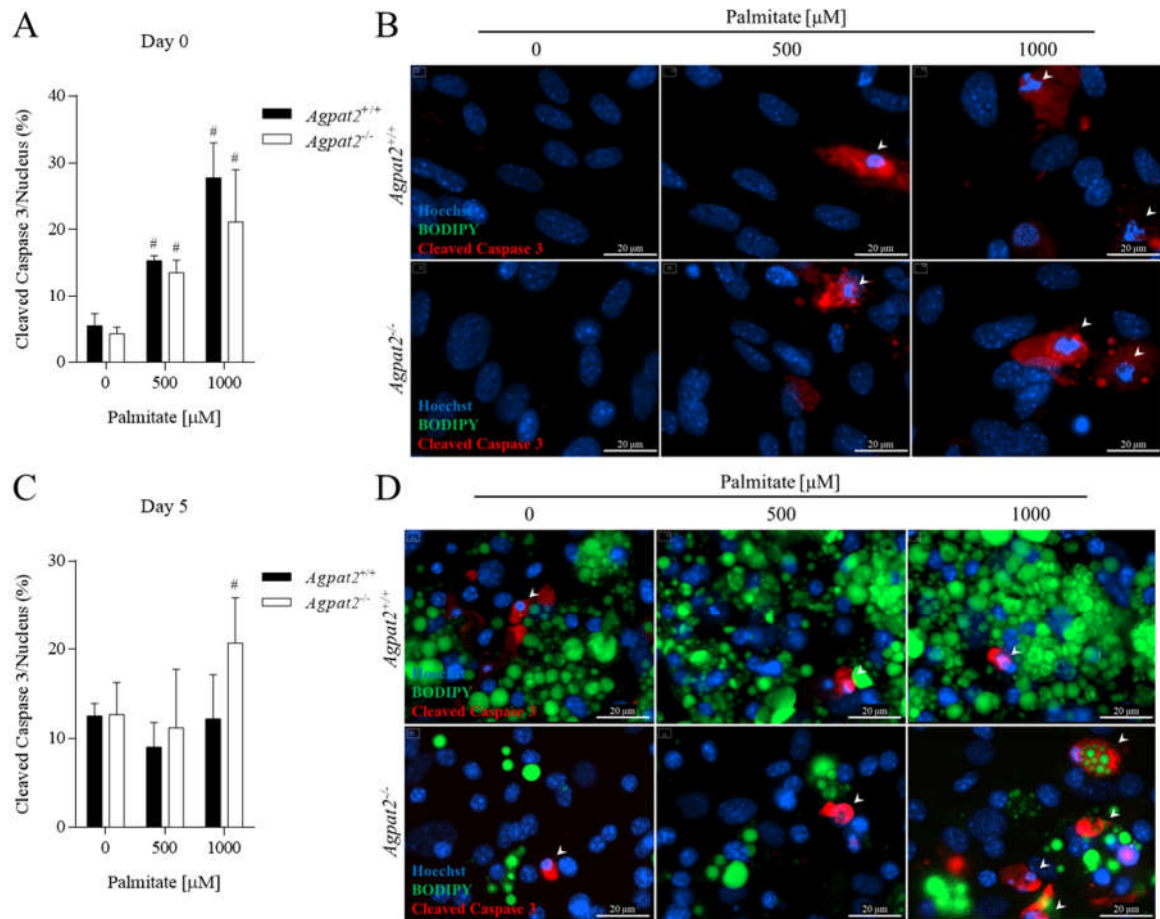


FIGURE 24: Activated caspase 3 is not different between differentiated brown adipocytes of wild type and *Agpat2*^{-/-} mice at day 0 differentiation but is higher in *Agpat2*^{-/-} cells at day 5 after incubation with palmitic acid. Quantification of cells with cleaved caspase 3 and small/dense nuclear staining at (A) day 0 and (C) 5 (n=3 per genotype). Representative immunofluorescence images staining cleaved caspase 3 (red), neutral lipids with BODIPY (green) and nuclei with Hoechst 33342 (blue) of differentiated brown adipocytes of wild type and *Agpat2*^{-/-} mice at (B) day 0 and (D) 5 of differentiation. Scale bar 20 μm . Cell cultures were incubated with different concentrations of palmitic acid (0, 500 and 1000 μM) for 12 hours before images capture. Automated imaging analysis included $\sim 175,000$ cells in total. Data are expressed as mean \pm SD. *p < 0.05 denote statistically significant differences between differentiated brown adipocytes of wild type and *Agpat2*^{-/-} mice at the same day of differentiation, # p < 0.05 denotes statistically significant differences in comparison with day 0 in the same genotype. p values were calculated using two-way ANOVA.

apoptotic cells were significantly more abundant in *Agpat2*^{-/-} adipocytes incubated with palmitic acid 1000 μ M in comparison with those incubated with not palmitic acid (Figure 24C and 24D).

The discrepancy between MTT and LDH results, that suggested a much higher proportion of cell death in *Agpat2*^{-/-} differentiated adipocytes after palmitic acid incubation than the one suggested by apoptosis detection based on cleaved caspase 3/nuclear changes, lead us to investigate a third method for cell death determination. Cytochrome c, a component of the mitochondrial electron transport chain, is normally located in the mitochondrial intermembrane space. Upon apoptosis, cytochrome c detaches from mitochondrial phospholipid cardiolipin and diffuses into the cytosol through OMM pores. In the cytosol, it triggers several mechanisms of apoptosis, including caspases 3 and 7 activation and massive release of endoplasmic reticulum calcium (Singh, *et al.*, 2019).

For this additional method, we defined apoptotic cells by a combination of intense cytosolic cytochrome c and intense/dense nuclear Hoechst 33342 staining. Imaging analysis was also performed by an automatic system (see “Methods” section for details).

Similar to the results with caspase 3 and MTT and LDH determination (Figure 23 and 24), we found that, based on cytochrome c changes, at day 0 of differentiation palmitic acid 1000 μ M significantly increased the frequency of apoptotic cells, with a \sim 25% of apoptotic cells and no differences noted between wild type and *Agpat2*^{-/-} cells (Figure 25A and 25B). By contrast, at day 5 of differentiation, palmitic acid exclusively increased the proportion of apoptotic cells in differentiated brown adipocytes of *Agpat2*^{-/-} mice (Figure 25C and 25D) whereas differentiated brown adipocytes of wild type were completely resistant to palmitic acid-induced cell death. However, it is important to note that differentiated brown adipocytes of

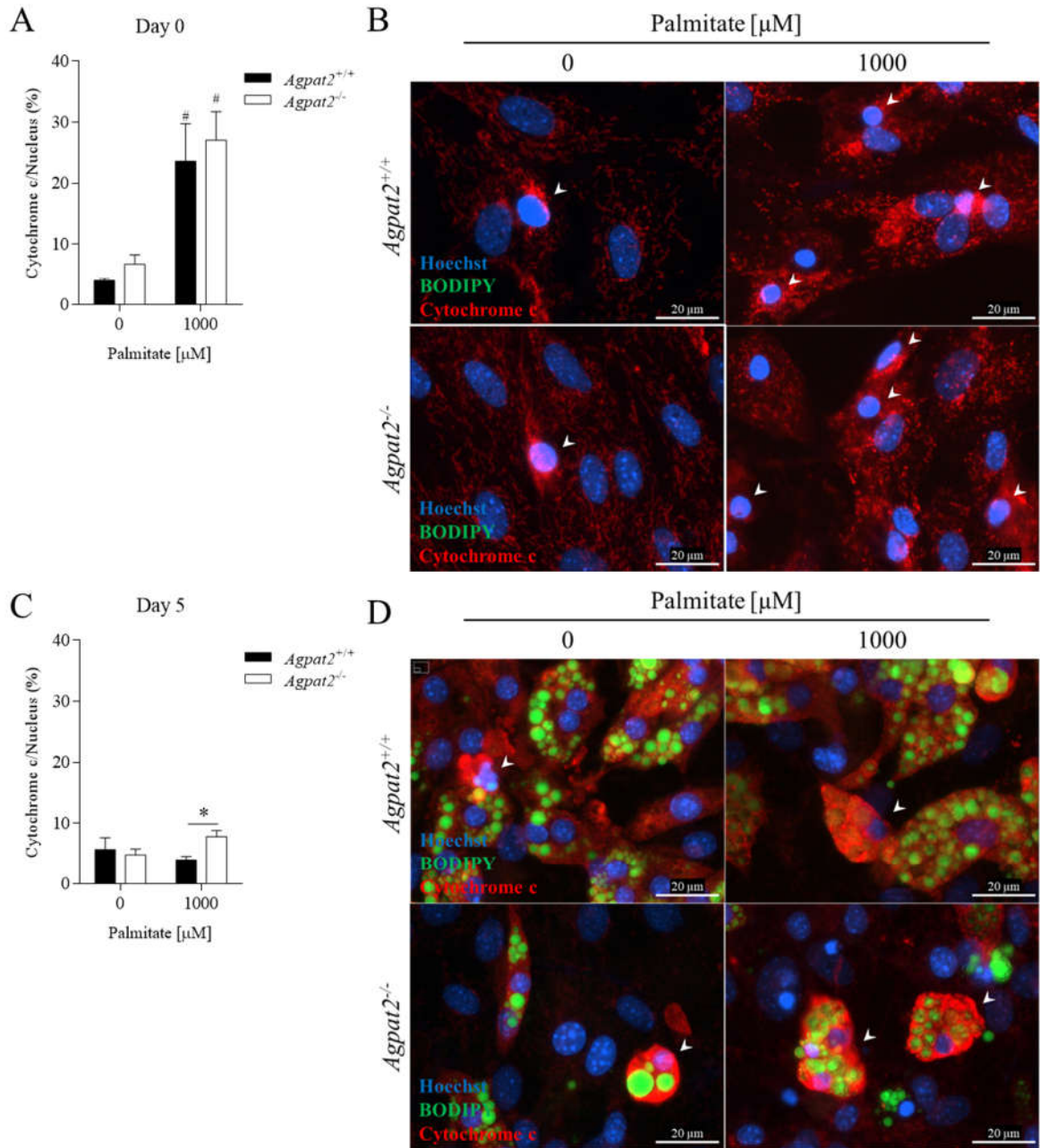


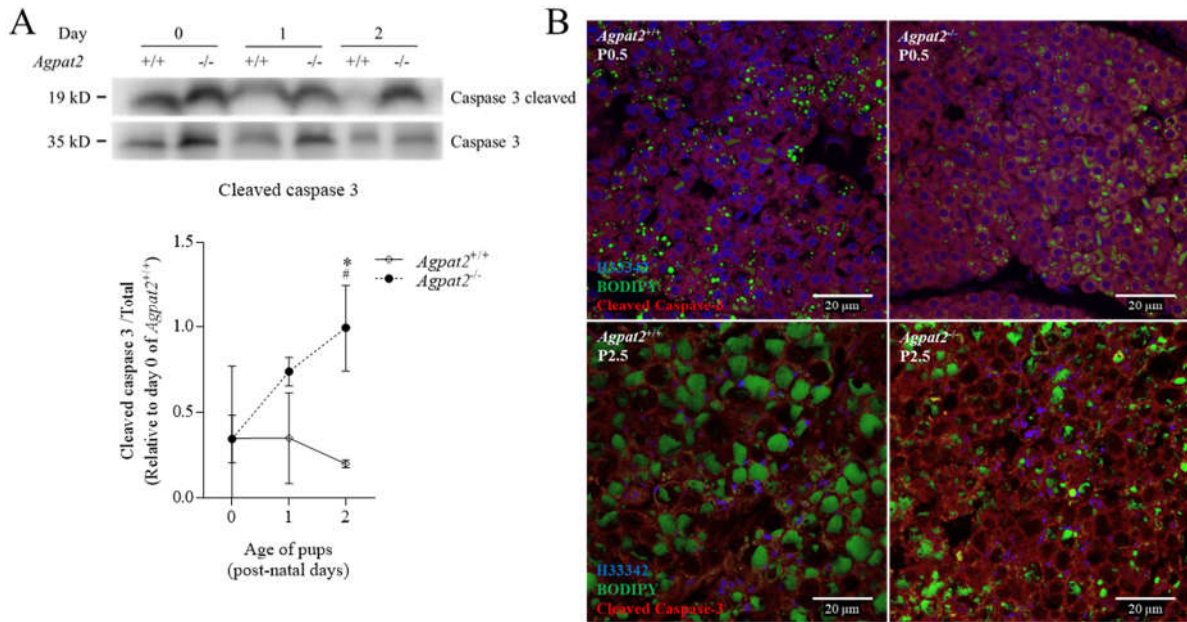
FIGURE 25: Palmitic acid increases cytosolic cytochrome c in preadipocytes of both genotypes, but only in differentiated brown adipocytes of *Agpat2*^{-/-} mice at day 5 of differentiation. (A) and (C) quantification of cells with cytochrome c and small/dense nuclear staining at days 0 and 5 of differentiation (n=3 per genotype). (B) and (D) are representative immunofluorescence images staining cytochrome c (red), neutral lipids with BODIPY (green) and nuclei with Hoechst 33342 (blue) of differentiated brown adipocytes of wild type and *Agpat2*^{-/-} mice at days 0 and 5 of differentiation. Scale bar 20 μ m. Cell cultures were incubated with different concentrations of palmitic acid (0, 500 and 1000 μ M) for 12 hours. Automated imaging analysis included ~65,000 cells in total. Data are expressed as mean \pm SD. *p < 0.05 denote statistically significant differences between differentiated brown adipocytes of wild type and *Agpat2*^{-/-} mice at the same day of differentiation, # p < 0.05 denotes statistically significant differences in comparison with day 0 in the same genotype. p values were calculated using two-way ANOVA.

Agpat2^{-/-} mice were also, partially resistant to lipotoxic cell death, as palmitic acid (1000 μ M) only increased the proportion of apoptotic cells to ~10%. Therefore, our results indicate that differentiated brown adipocytes of *Agpat2*^{-/-} mice are more sensitive to lipotoxic cell death than wild type adipocytes, possibly owing to their relative incapacity to store fatty acids esterified in LDs triglycerides. In fact, it has been reported that defects in LDs formation determine accumulation of saturated membrane glycerolipids that trigger ER stress and cell death (Olzmann *et al.*, 2018).

Finally, to contextualize the above *in vitro* observations with the situation *in vivo*, where adipocytes in newborn *Agpat2*^{-/-} mice suffer massive death in association with severe hypertriglyceridemia, we assessed apoptosis in the iBAT of newborn mice.

We found a significant increase in the levels of both total caspase 3 and cleaved caspase 3 in the iBAT of *Agpat2*^{-/-} mice 2 days after birth, by confocal microscopy and western blotting, in comparison with wild type mice of the same age (Figure 26A and 26B). Importantly, while the ratio between active and total caspase 3 remained unchanged in the iBAT of wild type mice as the animals age, this ratio progressively increased in the *Agpat2*^{-/-} mice, suggesting further apoptosis of brown adipocytes in these animals.

Taken as a whole, our results indicate that *Agpat2*^{-/-} brown adipocytes are sensitive to lipotoxicity unlike wild type adipocytes, and that this mechanism can have a role in the loss of iBAT in *Agpat2*^{-/-} mice after birth.



In summary, the results of this thesis show that differentiated *Agpat2*^{-/-} brown adipocytes have a lower proportion of lipid-laden cells with decreased levels of transcription factors PPAR γ , PPAR α , C/EBP α and PGC1 α and of the markers of mature adipocytes UCP1, Adipoq, Cidea and Plin1. Along with the above, differentiated *Agpat2*^{-/-} brown adipocytes at day 5 of differentiation show an altered mitochondrial morphology, a high expression of ISGs and an increase in sensitivity to lipotoxicity by palmitic acid. On the other hand, the ectopic expression of Elovl3 and mitoNEET in *Agpat2*^{-/-} preadipocytes is not able to restore the population of cells with lipid drops with respect to the wild type.

5. Discussion.

5.1. Considerations of the quantitative analysis of lipid-laden adipocytes and the evaluation of the adipogenic markers in the primary cultures of brown preadipocytes of *Agpat2*^{+/+} and *Agpat2*^{-/-} mice.

The quantification of lipid-laden adipocytes by an automated imaging system evidences a lower population of lipid-laden cells in the *Agpat2*^{-/-} cultures compared to the wild type. Leaving aside that the cause of this is a differential proportion of adipogenic precursors, it is observed that in both genotypes there are two populations, one that differentiates in lipid-laden cells, and another that does not. This phenomenon, which occurs in MEFs of *Agpat2*^{-/-} and *Agpat2*^{+/+} (Cautivo *et al.*, 2016), pre-adipocyte 3T3-L1 cell culture line (Diep *et al.*, 2018), as well as in practically all differentiations of mouse and human preadipocytes, is inherent in adipogenic differentiation *in vitro*. The cause is unknown, however experimental evidences of measurements in individual cells by atomic force microscopy (AFM) suggest that *in vitro* adipogenesis is probably generated in cells as an all-or-nothing phenomenon (Labriola *et al.*, 2015). On the other hand, similar to our wild type cultures, the adipogenic differentiations of other studies show that adipocytes present in cell cultures do not reach 100% *in vitro* (Diep *et al.*, 2018). The reason is that the optimal differentiation protocol is not being used. However, the high variability in literature of the composition and incubation times, of the adipogenic differentiation media (Wang *et al.*, 2018), makes it difficult to develop an optimal protocol. In this thesis the protocol originally used was modified because it did not induce the expression of the UCP1 marker, despite being described as a brown adipogenic differentiation protocol (Gerhart-Hines *et al.*, 2013).

Given the above, it is relevant to take into consideration the impact of the different populations in the comparative analysis of western blotting and mRNA levels of the adipogenic markers between the cell cultures of *Agpat2*^{+/+} and *Agpat2*^{-/-} mice. For example, PPAR γ protein and mRNA levels decrease by day 5 of differentiation in *Agpat2*^{-/-}, but not in all cells, there are cells that express PPAR γ and others that do not. While this might indicate that there is a group of cells in *Agpat2*^{-/-} that normally differentiates, this is not the case. UCP1 levels are undetectable in *Agpat2*^{-/-}, indicating that PPAR γ lipid-laden cells are abnormal. In addition, TEM results show that lipid-laden cells in *Agpat2*^{-/-} have abnormal mitochondria.

To overcome this limitation, both populations must be analyzed separately. It has now been described that physical separation by density is sufficient to isolate the cells that carry lipids (Benador *et al.*, 2018). Also, by means of microscopy it is possible to identify the cells that load lipids, however, the limitation of the technique is given by the available markers.

5.2. Causes of impaired adipogenesis in *Agpat2*^{-/-} cultures.

Adipogenesis is a highly complex process, which unlike other differentiations such as osteogenesis, involves the expression and repression of genes, as well as the remodeling of chromatin (Rauch *et al.*, 2019). Therefore, to understand the implications of the absence of AGPAT2 in the primary cultures of brown preadipocytes, in this section of the discussion we will sequentially analyze the implications of the alterations in the transcription factors, together with other phenomena that could be affecting the differentiation adipogenic.

PPAR γ , master regulator of adipogenesis that promotes brown differentiation by forming a complex with PRDM16 and C/EBP β (Seale *et al.*, 2008) and binds to a regulatory enhancing region distant from the UCP1 gene (Villarroya *et al.*, 2017), it is present in the cells with lipid droplets and absent in the cells that do not have them, suggesting that its expression allows the accumulation of lipid droplets in both *Agpat2*^{-/-} and wild type cells. However, the lower number of cells with lipid droplets is not only due to a lower expression of PPAR γ in *Agpat2*^{-/-} cultures, since the ectopic expression of PPAR γ in MEFs *Agpat2*^{-/-} cultures, does not restore the failed adipogenesis (Cautivo *et al.*, 2016). In addition, the induction of PPAR γ with rosiglitazone can reverse the failed adipogenesis related to its lower expression (Liu *et al.*, 2019). While these results do not suggest that failed adipogenesis is caused only by the low expression of PPAR γ , it is not ruled out that post-translational modifications, such as phosphorylation, SUMOylation, Acetylation, Ubiquitination and O-GlcNAcylation, are altering their function in these cultures (de sá *et al.*, 2017; Brunmeir *et al.*, 2018).

In the case of PRDM16, which acts together with PPAR γ and C/EBP β as a key transcriptional co-regulator for brown adipogenic differentiation (Seale *et al.*, 2007, 2008), it

does not show differences at the protein level in *Agpat2*^{-/-} cultures. However, the limitation of only measuring the expression of PRDM16 is that it does not fully demonstrate its function. For example, it has been described that PRDM16 interacts with mediator complex subunit 1 (MED1) by remodeling chromatin and allowing the expression of genes related to brown differentiation as well as the expression of UCP1 (Harms *et al.*, 2015; Iida *et al.*, 2015). In addition, a wide range of microRNAs modulate PRDM16, either increasing or decreasing its activity: miR-133, miR-27, miR-150 and miR-499 inhibit its expression and Mir193b-365 potency (Chi *et al.*, 2016; Jiang *et al.*, 2018).

C/EBP β , which forms a complex with PPAR γ and PRDM16, allows the expression of brown adipogenesis genes and interacts with a proximal regulatory region of UCP1 (Seale *et al.*, 2008; Villarroya *et al.*, 2017), increases its expression at 4 hours after adipogenic induction in 3T3-L1 cells (Salma *et al.*, 2004), indicating that its main adipogenic function is initially performed in the differentiation process as well as PRDM16 and PPAR γ . Therefore, the alteration of C/EBP β protein levels at day 3 may be a consequence and not the cause of the failed differentiation in these cultures. In any case, as in PRM16 and PPAR γ , the absence of significant differences in expression levels does not exclude the existence of other processes associated with C/EBP β that may be playing a fundamental role in their function.

The expression of C/EBP α is triggered by PPAR γ (Elberg, 2000), and it has been reported that together they are able to synergistically activate key genes of white adipogenesis (Zuo *et al.*, 2006; Madsen *et al.*, 2014). However, in the mouse *Cebpa*^{-/-}, iBAT are relatively unaffected, indicating that its absence is not critical for brown differentiation *in vivo* (Linhart *et*

al., 2001). This suggests that the low levels of C/EBP α in *Agpat2*^{-/-} cultures may be caused by the lower levels of PPAR γ .

The low levels of PPAR α in *Agpat2*^{-/-} cultures can be explained in part because their expression is regulated by PPAR γ (Shapira *et al.*, 2019), as well as by PRDM16 (Harms *et al.*, 2015) and EBF2 (Shapira *et al.*, 2017). The main effect of the low expression of PPAR α is in PGC1 α , since it induces its expression in differentiated brown adipocyte cultures generating an increase in the expression of UCP1 (Hondares *et al.*, 2011). However, brown adipocytes without PPAR α have normal levels of UCP1 (Lasar *et al.*, 2018).

Next, in the adipogenic differentiation arises the transcriptional coactivator PGC1 α , which has a central role in mitochondrial biogenesis and in cold-induced thermogenesis. As indicated above, its expression is mainly regulated by PRDM16, PPAR α and PPAR γ , partly explaining its low levels in *Agpat2*^{-/-} cultures. The main effect of PGC1 α would be on the low levels of UCP1. PGC1 α acts at the UCP1 promoter gene in the exposure to cold, so that deficient brown adipocytes of PGC1 α have reduced levels of UCP1, thus failing in thermogenic activation, but not in brown adipogenic differentiation (Lin *et al.*, 2004; Uldry *et al.*, 2006).

Interestingly, along with the low expression levels of adipogenic transcriptional factors, the expression of ISGs is strongly induced in *Agpat2*^{-/-} cultures at day 5 of differentiation. The relationship between the increase in ISGs and the inhibition of adipogenesis has been described in 3T3-L1 cell lines, where adipose differentiation is inhibited in the presence of IFN- α by decreasing the expression at the protein level of PPAR γ , C/EBP α and C/EBP β , being the deletion of STAT1 sufficient to counteract this inhibition (Lee *et al.*, 2016). Also primary iWAT preadipocytes differentiated in the presence of IFN α severely inhibited lipid accumulation,

decreasing the expression of Fabp4, PPAR γ and C/EBP α (Liu *et al.*, 2019). Along with this, the absence of PRDM16, which suppresses IRF1, increases the sensitivity of cultures of brown preadipocytes to INF α (Kissig *et al.*, 2017) and that of ATF7, which binds directly to the *Stat1* promoter, stimulates the expression of ISGs and inhibits adipogenesis (Liu *et al.*, 2019). However, the exposure of brown preadipocytes to INF α does not inhibit adipogenesis, maintaining the levels of PPAR γ 2 and Fabp4 similar to the untreated control (Kissig *et al.*, 2017). Our results show that, although there is an increase in ISGs, there is no increase in STAT1/2 levels in *Agpat2*^{-/-} cultures at days 0, 3, 5 and 7 of differentiation compared to wild type. This may be due to the fact that STAT1/2 could be activating briefly in the hours after induction of differentiation (day 1-2), as occurs in 3T3-L1 cells treated with INF α (Lee *et al.*, 2016). Independent of this, to determine if ISGs play a fundamental role in inhibiting differentiation, other studies must be carried out.

It should be noted that although there is a strong decrease in several key transcription factors in adipogenesis, there are lipid-laden cells in *Agpat2*^{-/-} cultures. However, UCP1 is undetectable and the markers of mature adipocytes Cidea, Adiponectin and Perilipin1 are strongly diminished at day 5 in *Agpat2*^{-/-} cultures.

In the case of UCP1, its absence could be caused both by the low levels of PGC1 α , as well as by the low expression of its PPAR α and PPAR γ inducers. However, the transcriptional problem does not explain the total absence of UCP1 in *Agpat2*^{-/-} cultures, because in models where transcription factors are strongly affected, there is at least a low expression of UCP1 (Seale *et al.*, 2008). Interestingly, several transporters of the large family of nuclear-encoded transporters embedded in the inner mitochondrial membrane SLC25 (solute carrier 25), to which

UCP1 (SLC25A7) belongs, are diminished (Slc25a19, Slc25a20, Slc25a23, Slc25a34, Slc25a35 and Slc25a42). This, together with the low expression of Cox7a1 and Cox8b, indicates that the absence of UCP1 is not only due to transcriptional problems that affect its expression, but also due to a problem of mitochondrial integrity that could be affecting its presence in mitochondria of *Agpat2*^{-/-} cultures. On the other hand, when β -adrenergic stimulation occurs, the expression of UCP1 is strongly triggered by PGC1 α and PPAR α , and its transport activated by the release of fatty acids from the lipid droplet, however and consistent with transcriptional (PPAR α and PGC1 α) and mitochondrial problems, our results show that in *Agpat2*^{-/-} cultures at day 5 of differentiation stimulated with isoprenaline, there is no increase in UCP1 mRNA levels similar to wild type, indicating that the system is unable to respond to this stimulus.

Interestingly, unlike the *Agpat2*^{-/-} cultures at day 5 of differentiation, in the mice the levels of UCP1 in iBAT in *Agpat2*^{-/-} are similar to the wild type until day 3 after birth, both at the mRNA level and of protein (Cautivo *et al.*, 2016). Although the causes of this phenomenon are complex, similar phenomena occur in other murine models. *In vitro* the absence of PRDM16 in brown preadipocytes inhibits brown adipogenesis, with low expression levels of UCP1, Cidea, Pgc1 α and Elovl3 (Seale *et al.*, 2007), however, *in vivo* PRDM16 is dispensable for the development of BAT in embryogenesis (Harms *et al.*, 2014).

Alterations in morphology and mitochondrial markers in *Agpat2*^{-/-} cultures can be caused by several effects. The differentiation of brown preadipocytes in the presence of IFN α causes the levels of UCP1, Cidea and Cox7a1 to be drastically reduced, and although the levels of mitochondrial DNA are similar to the control, IFN- α has a profound impact on mitochondrial morphology (Kissig *et al.*, 2017). Also, the absence of UCP1 in animals exposed to adrenergic

stimulation (4°C) generates mitochondria with highly disorganized crests and in some cases absent, being extraordinarily sensitive to ROS-induced dysfunction and possesses impaired ability to buffer calcium. Interestingly, the expression of the markers Ifi204, Ifi205, Ifih1, and Ddx58, as well as the transcription factors Stat1, Stat2, and Irf3 are increased, however, exposure to thermoneutrality (30°C) completely eliminates the expression of these markers (Kazak *et al.*, 2017). On the other hand, mitochondrial DNA stress (mtDNA) enhances the expression of a subset of interferon-stimulated genes (Ifi44, Ifit1, Ifit3, Oasl2 and Rtp4), and the expression of cytoplasmic DNA and RNA sensors, such as Ddx58, Ifih1 and the p200 Ifi203, Ifi204 and Ifi205 family proteins, as well as the transcription factors Irf7, Stat1 and Stat2, similar to our *Agpat2*^{-/-} cultures at differentiation day 5 (West *et al.*, 2015). Also, mitochondrial double-stranded RNA accumulation increases the expression of interferon-stimulated genes and other markers of immune activation (Cxcl10, Ifi44, Tgpt1, Ccl5, Ifit1, Cmpk2 among others) (Dhir *et al.*, 2018). Considering these phenomena, it is important to determine if the mitochondrial dysfunction is caused by the increase in the expression of the ISGs caused by transcriptional problems (similar to those of PRDM16 and ATF7), or if the mitochondrial dysfunction in itself is the cause of the increase in the expression of the ISGs (Figure 27).

In summary, apparently the main cause that the number of differentiated brown adipocytes is lower in the *Agpat2*^{-/-} cultures, are the diminished levels in the transcription factors PPAR γ , PPAR α , C/EBP α and PGC1 α . On the other hand, although it is not clear that the increase in ISGs has a fundamental role in the inhibition of adipogenesis, everything indicates that their presence is related to either causing the mitochondrial dysfunction or the consequence of it.

5.3. Lipotoxicity

Our results show that *Agpat2*^{-/-} animals are born with circulating lipid levels similar to wild type, however, at day 2 after birth, a strong increase is generated. The cause of this phenomenon is dual: in lipodystrophy there is an inability to store circulating triglycerides (both those ingested and those produced endogenously) and the ingestion of breast milk begins. The alteration in lipid composition of breast milk, which represents the main source of calories and essential fatty acids for membrane synthesis and neonatal development of the brain (Giovannini *et al.*, 1991), can have a direct impact on iBAT. It has been observed that maternal HFD feeding during lactation affected *Ucp1* expression in BAT of offspring at weaning (Liang *et al.*, 2016), indicating that the alteration of circulating lipids in neonatal mice can have a direct impact on iBAT.

Palmitic acid, which increases drastically in the plasma of neonates *Agpat2*^{-/-} together with saturated, monounsaturated and polyunsaturated fatty acids, has been described as a potent inducer of lipotoxicity in several cell types (de Vries *et al.*, 1997; Paumen *et al.*, 1997). Consistent with this, when cultures of brown preadipocytes are exposed to high concentrations of palmitic acid, a significant cell death occurs associated with lipotoxicity in both genotypes. However, when brown adipocytes are incubated with high concentrations of brown adipocytes at day 5 of differentiation, it is observed that the *Agpat2*^{-/-} cultures are more sensitive to the lipotoxic effect. Since palmitic acid lipotoxicity is mediated by ER stress, which in turn is diminished by the generation of the lipid drop that occurs in adipocytes (Olzmann *et al.*, 2018), it would be expected that the cause of *Agpat2*^{-/-} cultures are more sensitive to lipotoxicity is the lower proportion of cells with lipid drops. However, in the analyzes of cleaved caspase 3 and cytochrome c it is observed that not only the cells that do not possess lipid drops are affected by

the increase of palmitic acid, suggesting that all cells of this culture are significantly more sensitive to lipotoxicity. There are at least two reasons that could explain the increased sensitivity in *Agpat2*^{-/-} cultures. First, it has been described in myoblasts that lipotoxicity caused by palmitic acid damages mitochondrial DNA and decreases the respiratory rate (Patková *et al.*, 2014). Given that the mitochondria of the *Agpat2*^{-/-} cultures at day 5 has an altered morphology that is associated with a dysfunction, these could be affected to a greater extent than those of the wild type cultures. Second, it has recently been described that the depletion of RNF213 which encodes a protein with AAA-ATPase and RING-finger E3 ubiquitin-ligase domains with little-known function, protects against lipotoxicity and normalizes changes in the expression of induced genes by palmitic acid (Piccolis *et al.*, 2019). Interestingly, *Agpat2*^{-/-} cultures present in the global gene analysis the increase of RNF213 expression (4.2 times to day 5 compared to wild type), suggesting that basally on day 5, *Agpat2*^{-/-} cultures are more sensitive to lipotoxicity by palmitic acid (Figure 28).

On the other hand, cell death caused by high concentrations of palmitic acid at day 0 of differentiation in both genotypes and at day 5 in *Agpta2*^{-/-} and evaluated by MTT and LDH, is significantly higher than that detected by cleaved caspase 3 and cytochrome c. Since measurements of MTT, which measures viable cells with an active metabolism, and LDH, which measures the activity of the LDH enzyme that is released into the cell culture medium by damage to the plasma membrane, are unable to discriminate between different types of cell death, it is likely that in cell culture are occurring other types of cell death in addition to apoptosis. In fact, it has been described that the presence of palmitic acid can trigger necrosis in macrophages through the activation of RIP1/RIP3 (Kim *et al.*, 2017), and pyroptosis promoting inflammation and activation of caspase 1 (Wen *et al.*, 2011), suggesting that these

types of death may also be present. Likewise, in iBAT it is observed that apoptosis is a pathway of death present in the tissue, however, it is also possible that other types of death are occurring.

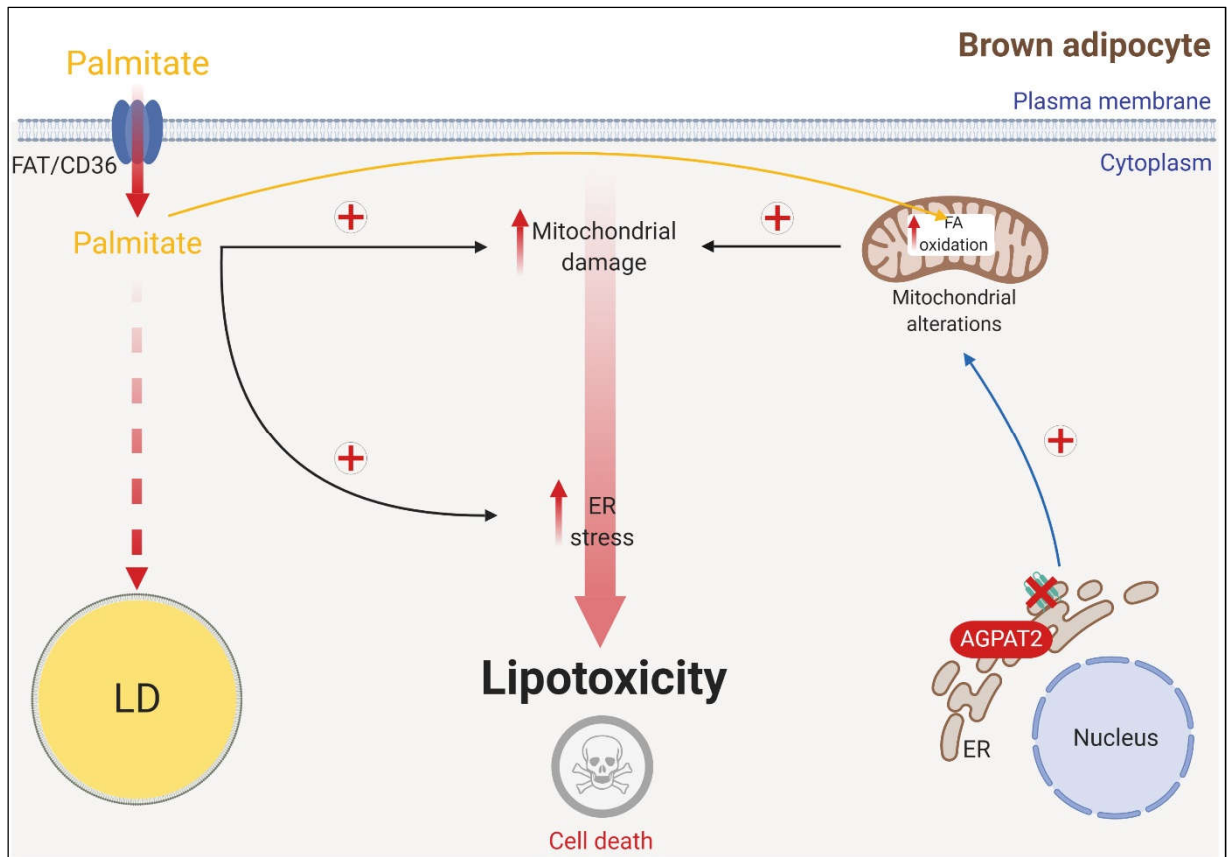


FIGURE 28: Model illustrating the potential causes of lipotoxicity in differentiated brown adipocytes of *Agpat2*^{-/-} mice. Palmitic acid enters to the adipocytes by FAT/CD36 transporter (not studied in this thesis but supported by Abumrad *et al.*, 1993) and can be oxidized in the mitochondria or esterified and stored in the LDs. When this buffering functions (oxidation and storage in LD triglycerides) are overpassed, cell death can be triggers by lipotoxic mechanisms that depend on ER stress and mitochondrial damage (not studied in this thesis but supported by Zou *et al.*, 2017). ER: endoplasmic reticulum; FAT/CD36: fatty acid translocase/ cluster of differentiation 36; LD: lipid droplets. Tapia *et al*, unpublished.

6. Conclusions.

- 1.- In the brown adipogenic differentiation of *Agpat2*^{-/-} cells there is a lower proportion of lipid-laden cells and decreased levels of PPAR γ , PPAR α , C/EBP α and PGC1 α compared to the wild type. Interestingly, levels of brown adipogenic regulators PRMD16 and C/EBP β remain unchanged in these cells. In addition, *Agpat2*^{-/-} brown adipocytes have decreased levels of markers of mature adipocytes such as Adipoq, Cidea and Plin1.
- 2.- Differentiated *Agpat2*^{-/-} brown adipocytes present mitochondria with an altered morphology at the ultrastructural level, as well as undetectable levels of UCP1 and lower levels of several genes of mitochondrial transporters with respect to the wild type.
- 3.- Differentiated *Agpat2*^{-/-} brown adipocytes have a selective enrichment in the mRNA levels of genes that are target of interferon type I response. Although the cause of this phenomenon remains to be determined, it is likely that mitochondrial dysfunction might be implicated. Also, it is likely that elevated levels of ISGs might interfere with brown adipogenic differentiation in *Agpat2*^{-/-} brown adipocytes; however, this remains to be determined.
- 3.- Ectopic expression of ELOVL3 and mitoNEET in *Agpat2*^{-/-} cells does not restore the population of lipid-laden cells similar to the wild type, suggesting that upstream metabolic and/or transcriptional defects are commanding the adipogenic impairment of *Agpat2*^{-/-} brown adipocytes.
- 4.- Differentiated *Agpat2*^{-/-} brown adipocytes have an increased sensitivity to lipotoxicity caused by palmitic acid with respect to the wild type. This increased sensitivity could be caused by the lower capacity of these cell to store fatty acids in LDs as well as mitochondrial dysfunction that results in impaired fatty acid oxidation and thus increased exposure to toxic palmitic acid.

Increased levels of *Rnf213* in *Agpat2*^{-/-} brown adipocytes might also be increasing the lipotoxic susceptibility of these cells, although this remains to be studied.

5.- The results of this thesis indicate that AGPAT2 is necessary for normal brown adipose differentiation, since its absence generates a lower proportion of lipid-laden cells; which in turn have alterations in mitochondrial morphology, an increase in the expression of the ISGs and sensitivity to lipotoxicity caused by palmitic acid. We believe that the combination of these mechanisms is the underlying cause of adipocyte destruction that drives lipodystrophy in both *Agpat2*^{-/-} mice and CGL1 patients.

7. References.

- Abumrad, N. A. *et al.* (1993) 'Cloning of a rat adipocyte membrane protein implicated in binding or transport of long-chain fatty acids that is induced during preadipocyte differentiation. Homology with human CD36.', *The Journal of biological chemistry*, 268(24), pp. 17665–8. Available at: <http://www.jbc.org.gate2.inist.fr/content/268/24/17665.full.pdf>.
- Adams, J. M. *et al.* (2004) 'Ceramide Content Is Increased in Skeletal Muscle From Obese Insulin-Resistant Humans', *Diabetes*, 53(1), pp. 25–31. doi: 10.2337/diabetes.53.1.25.
- Agarwal, A. K. *et al.* (2002) 'AGPAT2 is mutated in congenital generalized lipodystrophy linked to chromosome 9q34', *Nature Genetics*, 31(1), pp. 21–23. doi: 10.1038/ng880.
- Agarwal, A. K. (2012) 'Lysophospholipid acyltransferases: 1-acylglycerol-3-phosphate O-acyltransferases. from discovery to disease', *Current Opinion in Lipidology*, 23(4), pp. 290–302. doi: 10.1097/MOL.0b013e328354fcf4.
- Agarwal, A. K. and Garg, A. (2003) 'Congenital generalized lipodystrophy: significance of triglyceride biosynthetic pathways', *Trends in Endocrinology & Metabolism*, 14(5), pp. 214–221. doi: 10.1016/S1043-2760(03)00078-X.
- Agarwal, A. K. and Garg, A. (2010) 'Enzymatic activity of the human 1-acylglycerol-3-phosphate-O-acyltransferase isoform 11: upregulated in breast and cervical cancers', *Journal of Lipid Research*, 51(8), pp. 2143–2152. doi: 10.1194/jlr.m004762.
- Aherne, W. and Hull, D. (1966) 'Brown adipose tissue and heat production in the newborn infant', *The Journal of Pathology and Bacteriology*, 91(1), pp. 223–234. doi: 10.1002/path.1700910126.
- Akerblad, P. *et al.* (2002) 'Early B-Cell Factor (O/E-1) Is a Promoter of Adipogenesis and Involved in Control of Genes Important for Terminal Adipocyte Differentiation', *Molecular and Cellular Biology*, 22(22), pp. 8015–8025. doi: 10.1128/MCB.22.22.8015-8025.2002.
- Anilkumar, U. *et al.* (2017) 'Defining external factors that determine neuronal survival, apoptosis and necrosis during excitotoxic injury using a high content screening imaging platform', *PLOS ONE*. Edited by V. Ceña, 12(11), p. e0188343. doi: 10.1371/journal.pone.0188343.
- Arch, J. R. *et al.* (1984) 'Atypical beta-adrenoceptor on brown adipocytes as target for anti-obesity drugs.', *Nature*, 309(5964), pp. 163–5. Available at: <http://www.ncbi.nlm.nih.gov/pubmed/2838602>.
- Ashburner, M. *et al.* (2000) 'Gene Ontology: tool for the unification of biology', *Nature Genetics*, 25(1), pp. 25–29. doi: 10.1038/75556.
- Atit, R. *et al.* (2006) 'β-catenin activation is necessary and sufficient to specify the dorsal dermal fate in the mouse', *Developmental Biology*. Elsevier GmbH, 296(1), pp. 164–176. doi: 10.1016/j.ydbio.2006.04.449.
- Barak, Y. *et al.* (1999) 'PPARγ Is Required for Placental, Cardiac, and Adipose Tissue Development', *Molecular Cell*, 4(4), pp. 585–595. doi: 10.1016/S1097-2765(00)80209-9.
- Barneda, D. *et al.* (2015) 'The brown adipocyte protein CIDEA promotes lipid droplet fusion via a phosphatidic acid-binding amphipathic helix', *eLife*, 4, pp. 1–24. doi: 10.7554/eLife.07485.
- Benador, I. Y. *et al.* (2018) 'Mitochondria Bound to Lipid Droplets Have Unique Bioenergetics, Composition, and Dynamics that Support Lipid Droplet Expansion', *Cell Metabolism*, 27(4), pp. 869–885.e6. doi: 10.1016/j.cmet.2018.03.003.
- Berardinelli, W. (1954) 'An undiagnosed endocrinometabolic syndrome: report of 2 cases.',

- The Journal of clinical endocrinology and metabolism*, 14(2), pp. 193–204. doi: 10.1210/jcem-14-2-193.
- Bertholet, A. M. and Kirichok, Y. (2017) ‘UCP1: A transporter for H⁺ and fatty acid anions’, *Biochimie*. Elsevier B.V, 134, pp. 28–34. doi: 10.1016/j.biochi.2016.10.013.
- Boutant, M. *et al.* (2017) ‘Mfn2 is critical for brown adipose tissue thermogenic function’, *The EMBO Journal*, 36(11), pp. 1543–1558. doi: 10.15252/embj.201694914.
- Boutros, M., Heigwer, F. and Laufer, C. (2015) ‘Microscopy-Based High-Content Screening’, *Cell*. Elsevier Inc., 163(6), pp. 1314–1325. doi: 10.1016/j.cell.2015.11.007.
- Bray, M.-A. and Carpenter, A. (2004) *Advanced Assay Development Guidelines for Image-Based High Content Screening and Analysis, Assay Guidance Manual*. Available at: <http://www.ncbi.nlm.nih.gov/pubmed/23469374>.
- Brookheart, R. T., Michel, C. I. and Schaffer, J. E. (2009) ‘As a Matter of Fat’, *Cell Metabolism*, 10(1), pp. 9–12. doi: 10.1016/j.cmet.2009.03.011.
- Brunmeir, R. and Xu, F. (2018) ‘Functional Regulation of PPARs through Post-Translational Modifications’, *International Journal of Molecular Sciences*, 19(6), p. 1738. doi: 10.3390/ijms19061738.
- Caicedo, J. C. *et al.* (2017) ‘Data-analysis strategies for image-based cell profiling’, *Nature Methods*, 14(9), pp. 849–863. doi: 10.1038/nmeth.4397.
- Cannon, B. and Nedergaard, J. (2004) ‘Brown Adipose Tissue: Function and Physiological Significance’, *Physiological Reviews*, 84(1), pp. 277–359. doi: 10.1152/physrev.00015.2003.
- Cao, W. *et al.* (2001) ‘ β -adrenergic activation of p38 MAP kinase in adipocytes: cAMP induction of the uncoupling protein 1 (UCP1) gene requires p38 map kinase’, *Journal of Biological Chemistry*, 276(29), pp. 27077–27082. doi: 10.1074/jbc.M101049200.
- Cao, W. *et al.* (2004) ‘p38 mitogen-activated protein kinase is the central regulator of cyclic AMP-dependent transcription of the brown fat uncoupling protein 1 gene.’, *Molecular and cellular biology*, 24(7), pp. 3057–67. doi: 10.1128/MCB.24.7.3057.
- Carbon, S. *et al.* (2019) ‘The Gene Ontology Resource: 20 years and still GOing strong’, *Nucleic Acids Research*. Oxford University Press, 47(D1), pp. D330–D338. doi: 10.1093/nar/gky1055.
- Cautivo, K. M. *et al.* (2016) ‘AGPAT2 is essential for postnatal development and maintenance of white and brown adipose tissue’, *Molecular Metabolism*. Elsevier GmbH, 5(7), pp. 491–505. doi: 10.1016/j.molmet.2016.05.004.
- Chaudhry, A. and Granneman, J. G. (1999) ‘Differential regulation of functional responses by beta-adrenergic receptor subtypes in brown adipocytes.’, *The American journal of physiology*, 277(1), pp. R147-53. doi: 10.1152/ajpregu.1999.277.1.R147.
- Chaurasia, B. *et al.* (2016) ‘Adipocyte Ceramides Regulate Subcutaneous Adipose Browning, Inflammation, and Metabolism’, *Cell Metabolism*. Elsevier Inc., 24(6), pp. 820–834. doi: 10.1016/j.cmet.2016.10.002.
- Chavez, J. A. and Summers, S. A. (2012) ‘A Ceramide-Centric View of Insulin Resistance’, *Cell Metabolism*. Elsevier Inc., 15(5), pp. 585–594. doi: 10.1016/j.cmet.2012.04.002.
- Chi, J. and Cohen, P. (2016) ‘The Multifaceted Roles of PRDM16: Adipose Biology and Beyond’, *Trends in Endocrinology & Metabolism*. Elsevier Ltd, 27(1), pp. 11–23. doi: 10.1016/j.tem.2015.11.005.
- Colca, J. R. *et al.* (2004) ‘Identification of a novel mitochondrial protein (“mitoNEET”) cross-linked specifically by a thiazolidinedione photoprobe’, *American Journal of Physiology-Endocrinology and Metabolism*, 286(2), pp. E252–E260. doi: 10.1152/ajpendo.00424.2003.

- Cortés, V. A. *et al.* (2009) ‘Molecular Mechanisms of Hepatic Steatosis and Insulin Resistance in the AGPAT2-Deficient Mouse Model of Congenital Generalized Lipodystrophy’, *Cell Metabolism*, 9(2), pp. 165–176. doi: 10.1016/j.cmet.2009.01.002.
- Cortés, V. A. and Fernández-Galilea, M. (2015) ‘Lipodystrophies: adipose tissue disorders with severe metabolic implications’, *Journal of Physiology and Biochemistry*, 71(3), pp. 471–478. doi: 10.1007/s13105-015-0404-1.
- Cottle, Nash, Veress, F. (1967) ‘Release of noradrenaline from brown fat of cold-acclimated rats’, *Life Sciences*, 6(7), pp. 2267–2271.
- Cousin, B. *et al.* (1992) ‘Occurrence of brown adipocytes in rat white adipose tissue: molecular and morphological characterization.’, *Journal of cell science*, 103 (Pt 4(2), pp. 931–42. Available at: <http://www.ncbi.nlm.nih.gov/pubmed/10313640>.
- Cypess, A. M. *et al.* (2009) ‘Identification and Importance of Brown Adipose Tissue in Adult Humans A BS TR AC T’, *N Engl J Med*, 360, pp. 1509–1526. Available at: <http://faculty>.
- Dempersmier, J. *et al.* (2015) ‘Cold-Inducible Zfp516 Activates UCP1 Transcription to Promote Browning of White Fat and Development of Brown Fat’, *Molecular Cell*. Elsevier Inc., 57(2), pp. 235–246. doi: 10.1016/j.molcel.2014.12.005.
- Dhir, A. *et al.* (2018) ‘Mitochondrial double-stranded RNA triggers antiviral signalling in humans’, *Nature*. doi: 10.1038/s41586-018-0363-0.
- Diep, D. T. V. *et al.* (2018) ‘Anti-adipogenic effects of KD025 (SLx-2119), a ROCK2-specific inhibitor, in 3T3-L1 cells’, *Scientific Reports*. Springer US, 8(1), p. 2477. doi: 10.1038/s41598-018-20821-3.
- Elberg, G. (2000) ‘Modulation of the Murine Peroxisome Proliferator-Activated Receptor gamma 2 Promoter Activity by CCAAT/Enhancer Binding Proteins’, *Journal of Biological Chemistry*, 275(36), pp. 27815–27822. doi: 10.1074/jbc.M003593200.
- Fernández-Galilea, M. *et al.* (2015) ‘AGPAT2 deficiency impairs adipogenic differentiation in primary cultured preadipocytes in a non-autophagy or apoptosis dependent mechanism’, *Biochemical and Biophysical Research Communications*. Elsevier Ltd, 467(1), pp. 39–45. doi: 10.1016/j.bbrc.2015.09.128.
- Fredriksson, J. M. *et al.* (2001) ‘Analysis of inhibition by H89 of UCP1 gene expression and thermogenesis indicates protein kinase A mediation of β 3-adrenergic signalling rather than β 3-adrenoceptor antagonism by H89’, *Biochimica et Biophysica Acta - Molecular Cell Research*, 1538(2–3), pp. 206–217. doi: 10.1016/S0167-4889(01)00070-2.
- Gale, S. E. *et al.* (2006) ‘A Regulatory Role for 1-Acylglycerol-3-phosphate- O -acyltransferase 2 in Adipocyte Differentiation’, *Journal of Biological Chemistry*, 281(16), pp. 11082–11089. doi: 10.1074/jbc.M509612200.
- Gao, G. *et al.* (2017) ‘Control of lipid droplet fusion and growth by CIDE family proteins’, *Biochimica et Biophysica Acta (BBA) - Molecular and Cell Biology of Lipids*, 1862(10), pp. 1197–1204. doi: 10.1016/j.bbalip.2017.06.009.
- Garg, A. *et al.* (1999) ‘A Gene for Congenital Generalized Lipodystrophy Maps to Human Chromosome 9q34’, *The Journal of Clinical Endocrinology & Metabolism*, 84(9), pp. 3390–3394. doi: 10.1210/jcem.84.9.6103.
- Garg, A. (2004) ‘Acquired and Inherited Lipodystrophies’, *New England Journal of Medicine*, 350(12), pp. 1220–1234. doi: 10.1056/NEJMra025261.
- Garg, A. (2011) ‘Lipodystrophies: Genetic and acquired body fat disorders’, *Journal of Clinical Endocrinology and Metabolism*, 96(11), pp. 3313–3325. doi: 10.1210/jc.2011-1159.
- Garg, A. and Agarwal, A. K. (2009) ‘Lipodystrophies: Disorders of adipose tissue biology’,

- Biochimica et Biophysica Acta (BBA) - Molecular and Cell Biology of Lipids*. Elsevier B.V., 1791(6), pp. 507–513. doi: 10.1016/j.bbalip.2008.12.014.
- Gerhart-Hines, Z. *et al.* (2013) ‘The nuclear receptor Rev-erba controls circadian thermogenic plasticity’, *Nature*, 503(7476), pp. 410–413. doi: 10.1038/nature12642.
- Giovannini, M., Agostoni, C. and Salari, P. C. (1991) ‘The Role of Lipids in Nutrition during the First Months of Life’, *Journal of International Medical Research*, 19(5), pp. 351–362. doi: 10.1177/030006059101900501.
- Goh, T. T. *et al.* (2007) ‘Lipid-induced β -cell dysfunction in vivo in models of progressive β -cell failure’, *American Journal of Physiology-Endocrinology and Metabolism*, 292(2), pp. E549–E560. doi: 10.1152/ajpendo.00255.2006.
- Granneman, J. G. (1988) ‘Norepinephrine infusions increase adenylate cyclase responsiveness in brown adipose tissue.’, *The Journal of pharmacology and experimental therapeutics*, 245(3), pp. 1075–80. Available at: <http://www.ncbi.nlm.nih.gov/pubmed/2838602>.
- Grujic, D. *et al.* (1997) ‘Beta3-adrenergic receptors on white and brown adipocytes mediate beta3-selective agonist-induced effects on energy expenditure, insulin secretion, and food intake. A study using transgenic and gene knockout mice.’, *The Journal of biological chemistry*, 272(28), pp. 17686–93. Available at: <http://www.ncbi.nlm.nih.gov/pubmed/9211919>.
- Guillou, H. *et al.* (2010) ‘The key roles of elongases and desaturases in mammalian fatty acid metabolism: Insights from transgenic mice’, *Progress in Lipid Research*. Elsevier Ltd, 49(2), pp. 186–199. doi: 10.1016/j.plipres.2009.12.002.
- Harms, M. J. *et al.* (2014) ‘Prdm16 Is Required for the Maintenance of Brown Adipocyte Identity and Function in Adult Mice’, *Cell Metabolism*. Elsevier Inc., 19(4), pp. 593–604. doi: 10.1016/j.cmet.2014.03.007.
- Harms, M. J. *et al.* (2015) ‘PRDM16 binds MED1 and controls chromatin architecture to determine a brown fat transcriptional program’, *Genes and Development*, 29(3), pp. 298–307. doi: 10.1101/gad.252734.114.
- Hayashi, Y. K. *et al.* (2009) ‘Human PTRF mutations cause secondary deficiency of caveolins resulting in muscular dystrophy with generalized lipodystrophy’, *Journal of Clinical Investigation*, 119(9), pp. 2623–2633. doi: 10.1172/JCI38660.
- Heaton, J. M. (1972) ‘The distribution of brown adipose tissue in the human.’, *Journal of anatomy*, 112(Pt 1), pp. 35–9. Available at: <http://www.ncbi.nlm.nih.gov/pubmed/5086212>.
- Hernández-Rodas, M. C. *et al.* (2017) ‘Supplementation with Docosahexaenoic Acid and Extra Virgin Olive Oil Prevents Liver Steatosis Induced by a High-Fat Diet in Mice through PPAR- α and Nrf2 Upregulation with Concomitant SREBP-1c and NF- κ B Downregulation’, *Molecular Nutrition and Food Research*, 61(12). doi: 10.1002/mnfr.201700479.
- Hertzog, P. J. and Williams, B. R. G. (2013) ‘Fine tuning type I interferon responses’, *Cytokine & Growth Factor Reviews*. Elsevier Ltd, 24(3), pp. 217–225. doi: 10.1016/j.cytogfr.2013.04.002.
- Holland, W. L. *et al.* (2011) ‘Receptor-mediated activation of ceramidase activity initiates the pleiotropic actions of adiponectin’, *Nature Medicine*. Nature Publishing Group, 17(1), pp. 55–63. doi: 10.1038/nm.2277.
- Hondares, E. *et al.* (2011) ‘Peroxisome Proliferator-activated Receptor α (PPAR α) Induces PPAR γ Coactivator 1 α (PGC-1 α) Gene Expression and Contributes to Thermogenic Activation of Brown Fat’, *Journal of Biological Chemistry*, 286(50), pp. 43112–43122. doi: 10.1074/jbc.M111.252775.

- Iida, S. *et al.* (2015) 'PRDM16 enhances nuclear receptor-dependent transcription of the brown fat-specific Ucp1 gene through interactions with Mediator subunit MED1', *Genes & Development*, 29(3), pp. 308–321. doi: 10.1101/gad.252809.114.
- Inagaki, T., Sakai, J. and Kajimura, S. (2016) 'Transcriptional and epigenetic control of brown and beige adipose cell fate and function', *Nature Reviews Molecular Cell Biology*. Nature Publishing Group, 17(8), pp. 480–495. doi: 10.1038/nrm.2016.62.
- Ivashkiv, L. B. (2018) 'IFN γ : signalling, epigenetics and roles in immunity, metabolism, disease and cancer immunotherapy', *Nature Reviews Immunology*, pp. 545–558. doi: 10.1038/s41577-018-0029-z.
- Ivashkiv, L. B. and Donlin, L. T. (2014) 'Regulation of type I interferon responses', *Nature Reviews Immunology*. Nature Publishing Group, 14(1), pp. 36–49. doi: 10.1038/nri3581.
- Jakobsson, A., Jørgensen, J. A. and Jacobsson, A. (2005) 'Differential regulation of fatty acid elongation enzymes in brown adipocytes implies a unique role for Elovl3 during increased fatty acid oxidation', *American Journal of Physiology-Endocrinology and Metabolism*, 289(4), pp. E517–E526. doi: 10.1152/ajpendo.00045.2005.
- Jiang, C. *et al.* (2015) 'Intestine-selective farnesoid X receptor inhibition improves obesity-related metabolic dysfunction', *Nature Communications*. Nature Publishing Group, 6(1), p. 10166. doi: 10.1038/ncomms10166.
- Jiang, J. *et al.* (2018) 'MiR-499/PRDM16 axis modulates the adipogenic differentiation of mouse skeletal muscle satellite cells', *Human Cell*. Springer Japan, 31(4), pp. 282–291. doi: 10.1007/s13577-018-0210-5.
- Jimenez-Preitner, M. *et al.* (2011) 'Plac8 Is an Inducer of C/EBP β Required for Brown Fat Differentiation, Thermoregulation, and Control of Body Weight', *Cell Metabolism*, 14(5), pp. 658–670. doi: 10.1016/j.cmet.2011.08.008.
- Jimenez, M. A. *et al.* (2007) 'Critical Role for Ebf1 and Ebf2 in the Adipogenic Transcriptional Cascade', *Molecular and Cellular Biology*, 27(2), pp. 743–757. doi: 10.1128/MCB.01557-06.
- Kajimura, S. *et al.* (2009) 'Initiation of myoblast to brown fat switch by a PRDM16–C/EBP β transcriptional complex', *Nature*, 460(7259), pp. 1154–1158. doi: 10.1038/nature08262.
- Kalinovich, A. V. *et al.* (2017) 'UCP1 in adipose tissues: two steps to full browning', *Biochimie*. Elsevier B.V., 134, pp. 127–137. doi: 10.1016/j.biochi.2017.01.007.
- Kazak, L. *et al.* (2017) 'UCP1 deficiency causes brown fat respiratory chain depletion and sensitizes mitochondria to calcium overload-induced dysfunction', *Proceedings of the National Academy of Sciences*, 114(30), pp. 7981–7986. doi: 10.1073/pnas.1705406114.
- Kim, C. A. *et al.* (2008) 'Association of a Homozygous Nonsense Caveolin-1 Mutation with Berardinelli-Seip Congenital Lipodystrophy', *The Journal of Clinical Endocrinology & Metabolism*, 93(4), pp. 1129–1134. doi: 10.1210/jc.2007-1328.
- Kim, J. *et al.* (2016) 'Eicosapentaenoic Acid Potentiates Brown Thermogenesis through FFAR4-dependent Up-regulation of miR-30b and miR-378', *Journal of Biological Chemistry*, 291(39), pp. 20551–20562. doi: 10.1074/jbc.M116.721480.
- Kim, S. K. *et al.* (2017) 'Palmitate induces RIP1/RIP3-dependent necrosis via MLKL-mediated pore formation in the plasma membrane of RAW 264.7 cells', *Biochemical and Biophysical Research Communications*. Elsevier Ltd, 482(2), pp. 359–365. doi: 10.1016/j.bbrc.2016.11.068.
- Kissig, M. *et al.* (2017) 'PRDM16 represses the type I interferon response in adipocytes to promote mitochondrial and thermogenic programming', *The EMBO Journal*, 36(11), pp. 1528–

1542. doi: 10.15252/emj.201695588.

Kobayashi, T. and Fujimori, K. (2012) 'Very long-chain-fatty acids enhance adipogenesis through coregulation of Elovl3 and PPAR γ in 3T3-L1 cells', *American Journal of Physiology-Endocrinology and Metabolism*, 302(12), pp. E1461–E1471. doi: 10.1152/ajpendo.00623.2011.

Kozak, U. C. *et al.* (1994) 'An upstream enhancer regulating brown-fat-specific expression of the mitochondrial uncoupling protein gene.', *Molecular and Cellular Biology*, 14(1), pp. 59–67. doi: 10.1128/MCB.14.1.59.

Krief, S. *et al.* (1993) 'Tissue distribution of beta 3-adrenergic receptor mRNA in man.', *Journal of Clinical Investigation*, 91(1), pp. 344–349. doi: 10.1172/JCI116191.

Krssak, M. *et al.* (1999) 'Intramyocellular lipid concentrations are correlated with insulin sensitivity in humans: a ^1H NMR spectroscopy study', *Diabetologia*, 42(1), pp. 113–116. doi: 10.1007/s001250051123.

Kusminski, C. M., Park, J. and Scherer, P. E. (2014) 'MitoNEET-mediated effects on browning of white adipose tissue', *Nature Communications*. Nature Publishing Group, 5(1), p. 3962. doi: 10.1038/ncomms4962.

Labriola, N. R. and Darling, E. M. (2015) 'Temporal heterogeneity in single-cell gene expression and mechanical properties during adipogenic differentiation', *Journal of Biomechanics*. Elsevier, 48(6), pp. 1058–1066. doi: 10.1016/j.jbiomech.2015.01.033.

Lasar, D. *et al.* (2018) 'Peroxisome Proliferator Activated Receptor Gamma Controls Mature Brown Adipocyte Inducibility through Glycerol Kinase', *Cell Reports*, 22(3), pp. 760–773. doi: 10.1016/j.celrep.2017.12.067.

Law, B. A. *et al.* (2018) 'Lipotoxic very-long-chain ceramides cause mitochondrial dysfunction, oxidative stress, and cell death in cardiomyocytes', *The FASEB Journal*, 32(3), pp. 1403–1416. doi: 10.1096/fj.201700300R.

Lee, K. *et al.* (2016) 'Interferon-alpha inhibits adipogenesis via regulation of JAK/STAT1 signaling', *Biochimica et Biophysica Acta - General Subjects*. Elsevier B.V., 1860(11), pp. 2416–2427. doi: 10.1016/j.bbagen.2016.07.009.

Lepper, C. and Fan, C. M. (2010) 'Inducible lineage tracing of Pax7-descendant cells reveals embryonic origin of adult satellite cells', *Genesis*, 48(7), pp. 424–436. doi: 10.1002/dvg.20630.

Liang, X. *et al.* (2016) 'Maternal high-fat diet during lactation impairs thermogenic function of brown adipose tissue in offspring mice', *Scientific Reports*. Nature Publishing Group, 6(1), p. 34345. doi: 10.1038/srep34345.

Lin, J. *et al.* (2004) 'Defects in Adaptive Energy Metabolism with CNS-Linked Hyperactivity in PGC-1 α Null Mice', *Cell*, 119(1), pp. 121–135. doi: 10.1016/j.cell.2004.09.013.

Linhart, H. G. *et al.* (2001) 'C/EBP is required for differentiation of white, but not brown, adipose tissue', *Proceedings of the National Academy of Sciences*, 98(22), pp. 12532–12537. doi: 10.1073/pnas.211416898.

Listenberger, L. L. *et al.* (2003) 'Triglyceride accumulation protects against fatty acid-induced lipotoxicity', *Proceedings of the National Academy of Sciences*, 100(6), pp. 3077–3082. doi: 10.1073/pnas.0630588100.

Listenberger, L. L., Ory, D. S. and Schaffer, J. E. (2001) 'Palmitate-induced Apoptosis Can Occur through a Ceramide-independent Pathway', *Journal of Biological Chemistry*, 276(18), pp. 14890–14895. doi: 10.1074/jbc.M010286200.

Liu, Y. *et al.* (2019) 'The Transcription Factor ATF7 Controls Adipocyte Differentiation and

- Thermogenic Gene Programming', *iScience*. Elsevier Inc., 13, pp. 98–112. doi: 10.1016/j.isci.2019.02.013.
- Madsen, M. S. *et al.* (2014) 'Peroxisome Proliferator-Activated Receptor and C/EBP Synergistically Activate Key Metabolic Adipocyte Genes by Assisted Loading', *Molecular and Cellular Biology*, 34(6), pp. 939–954. doi: 10.1128/MCB.01344-13.
- Maedler, K. *et al.* (2001) 'Distinct effects of saturated and monounsaturated fatty acids on beta-cell turnover and function.', *Diabetes*, 50(1), pp. 69–76. Available at: <http://www.ncbi.nlm.nih.gov/pubmed/11147797>.
- Maedler, K. *et al.* (2003) 'Monounsaturated fatty acids prevent the deleterious effects of palmitate and high glucose on human pancreatic beta-cell turnover and function.', *Diabetes*, 52(3), pp. 726–33. doi: 10.2337/diabetes.52.3.726.
- Magré, J. *et al.* (2001) 'Identification of the gene altered in Berardinelli-Seip congenital lipodystrophy on chromosome 11q13', *Nature Genetics*, 28(4), pp. 365–370. doi: 10.1038/ng585.
- Mandavilli, B. S., Aggeler, R. J. and Chambers, K. M. (2018) 'Tools to Measure Cell Health and Cytotoxicity Using High Content Imaging and Analysis', in Johnston, P. A. and Trask, O. J. (eds). New York, NY: Springer New York (Methods in Molecular Biology), pp. 33–46. doi: 10.1007/978-1-4939-7357-6_3.
- Manthiram, K. *et al.* (2017) 'The monogenic autoinflammatory diseases define new pathways in human innate immunity and inflammation', *Nature Immunology*, 18(8), pp. 832–842. doi: 10.1038/ni.3777.
- van Marken Lichtenbelt, W. D. *et al.* (2009) 'Cold-Activated Brown Adipose Tissue in Healthy Men', *New England Journal of Medicine*, 360(15), pp. 1500–1508. doi: 10.1056/NEJMoa0808718.
- Merklin, R. J. (1974) 'Growth and distribution of human fetal brown fat', *The Anatomical Record*, 178(3), pp. 637–645. doi: 10.1002/ar.1091780311.
- Morrison, W. and Smith, L. (1964) 'PREPARATION OF FATTY ACID METHYL ESTERS AND DIMETHYLACETALS FROM LIPIDS WITH BORON FLUORIDE--METHANOL.', *Journal of lipid research*, 5(1 3), pp. 600–8. Available at: <http://www.ncbi.nlm.nih.gov/pubmed/14221106>.
- Nahmias, C. *et al.* (1991) 'Molecular characterization of the mouse , B3-adrenergic receptor : relationship with the atypical receptor of adipocytes', 10(12), pp. 3721–3727.
- Nicholls, D. G. (1976) 'Hamster Brown-Adipose-Tissue Mitochondria. Purine Nucleotide Control of the Ion Conductance of the Inner Membrane, the Nature of the Nucleotide Binding Site', *European Journal of Biochemistry*, 62(2), pp. 223–228. doi: 10.1111/j.1432-1033.1976.tb10151.x.
- Ohno, H. *et al.* (2013) 'EHMT1 controls brown adipose cell fate and thermogenesis through the PRDM16 complex', *Nature*. Nature Publishing Group, 504(7478), pp. 163–167. doi: 10.1038/nature12652.
- Olzmann, J. A. and Carvalho, P. (2018) 'Dynamics and functions of lipid droplets', *Nature Reviews Molecular Cell Biology*. Springer US. doi: 10.1038/s41580-018-0085-z.
- Ordoñez, M. *et al.* (2017) 'Implication of Ceramide Kinase in Adipogenesis', *Mediators of Inflammation*, 2017, pp. 1–7. doi: 10.1155/2017/9374563.
- Ordoñez, M. *et al.* (2018) 'Regulation of adipogenesis by ceramide 1-phosphate', *Experimental Cell Research*. Elsevier Inc., 372(2), pp. 150–157. doi: 10.1016/j.yexcr.2018.09.021.

- Park, J. H. *et al.* (2013) 'A Multifunctional protein, EWS, is essential for early brown fat lineage determination', *Developmental Cell*. Elsevier, 26(4), pp. 393–404. doi: 10.1016/j.devcel.2013.07.002.
- Patková, J., Anděl, M. and Trnka, J. (2014) 'Palmitate-Induced Cell Death and Mitochondrial Respiratory Dysfunction in Myoblasts are Not Prevented by Mitochondria-Targeted Antioxidants', *Cellular Physiology and Biochemistry*, 33(5), pp. 1439–1451. doi: 10.1159/000358709.
- Patni, N. and Garg, A. (2015) 'Congenital generalized lipodystrophies - New insights into metabolic dysfunction', *Nature Reviews Endocrinology*. Nature Publishing Group, 11(9), pp. 522–534. doi: 10.1038/nrendo.2015.123.
- Paumen, M. B. *et al.* (1997) 'Inhibition of Carnitine Palmitoyltransferase I Augments Sphingolipid Synthesis and Palmitate-induced Apoptosis', *Journal of Biological Chemistry*, 272(6), pp. 3324–3329. doi: 10.1074/jbc.272.6.3324.
- Perseghin, G. *et al.* (1999) 'Intramyocellular triglyceride content is a determinant of in vivo insulin resistance in humans: a 1H-13C nuclear magnetic resonance spectroscopy assessment in offspring of type 2 diabetic parents.', *Diabetes*, 48(8), pp. 1600–6. Available at: <http://www.ncbi.nlm.nih.gov/pubmed/10426379>.
- Petrovic, N. *et al.* (2010) 'Chronic Peroxisome Proliferator-activated Receptor γ (PPAR γ) Activation of Epididymally Derived White Adipocyte Cultures Reveals a Population of Thermogenically Competent, UCP1-containing Adipocytes Molecularly Distinct from Classic Brown Adipocytes', *Journal of Biological Chemistry*, 285(10), pp. 7153–7164. doi: 10.1074/jbc.M109.053942.
- Piccolis, M. *et al.* (2019) 'Probing the Global Cellular Responses to Lipotoxicity Caused by Saturated Fatty Acids Molecular Cell Article Probing the Global Cellular Responses to Lipotoxicity Caused by Saturated Fatty Acids', *Molecular Cell*. Elsevier Inc., 74, pp. 1–13. doi: 10.1016/j.molcel.2019.01.036.
- Puigserver, P. *et al.* (1998) 'A Cold-Inducible Coactivator of Nuclear Receptors Linked to Adaptive Thermogenesis', *Cell*, 92(6), pp. 829–839. doi: 10.1016/S0092-8674(00)81410-5.
- Raichur, S. *et al.* (2019) 'The role of C16:0 ceramide in the development of obesity and type 2 diabetes: CerS6 inhibition as a novel therapeutic approach', *Molecular Metabolism*. Elsevier GmbH, 21(xxxx), pp. 36–50. doi: 10.1016/j.molmet.2018.12.008.
- Rajakumari, S. *et al.* (2013) 'EBF2 Determines and Maintains Brown Adipocyte Identity', *Cell Metabolism*. Elsevier Inc., 17(4), pp. 562–574. doi: 10.1016/j.cmet.2013.01.015.
- Rauch, A. *et al.* (2019) 'Osteogenesis depends on commissioning of a network of stem cell transcription factors that act as repressors of adipogenesis', *Nature Genetics*. Springer US, 51(4), pp. 716–727. doi: 10.1038/s41588-019-0359-1.
- Rius, B. *et al.* (2017) 'The specialized proresolving lipid mediator maresin 1 protects hepatocytes from lipotoxic and hypoxia-induced endoplasmic reticulum stress', *The FASEB Journal*, 31(12), pp. 5384–5398. doi: 10.1096/fj.201700394R.
- Rosen, E. D. *et al.* (1999) 'PPAR γ Is Required for the Differentiation of Adipose Tissue In Vivo and In Vitro', *Molecular Cell*, 4(4), pp. 611–617. doi: 10.1016/S1097-2765(00)80211-7.
- de sá, P. M. *et al.* (2017) 'Transcriptional regulation of adipogenesis', *Comprehensive Physiology*, 7(2), pp. 635–674. doi: 10.1002/cphy.c160022.
- Sajan, M. P. *et al.* (2015) 'Hepatic insulin resistance in ob/ob mice involves increases in ceramide, aPKC activity, and selective impairment of Akt-dependent FoxO1 phosphorylation', *Journal of Lipid Research*, 56(1), pp. 70–80. doi: 10.1194/jlr.M052977.

- Salma, N. *et al.* (2004) ‘Temporal Recruitment of Transcription Factors and SWI/SNF Chromatin-Remodeling Enzymes during Adipogenic Induction of the Peroxisome Proliferator-Activated Receptor Nuclear Hormone Receptor’, *Molecular and Cellular Biology*, 24(11), pp. 4651–4663. doi: 10.1128/MCB.24.11.4651-4663.2004.
- Sankella, S., Garg, A. and Agarwal, A. K. (2017) ‘Activation of Sphingolipid Pathway in the Livers of Lipodystrophic *Aagpat2*^{-/-} Mice’, *Journal of the Endocrine Society*, 1(7), pp. 980–993. doi: 10.1210/js.2017-00157.
- Schneider, W. M., Chevillotte, M. D. and Rice, C. M. (2014) ‘Interferon-Stimulated Genes: A Complex Web of Host Defenses’, *Annual Review of Immunology*, 32(1), pp. 513–545. doi: 10.1146/annurev-immunol-032713-120231.
- Seale, P. *et al.* (2007) ‘Transcriptional Control of Brown Fat Determination by PRDM16’, *Cell Metabolism*, 6(1), pp. 38–54. doi: 10.1016/j.cmet.2007.06.001.
- Seale, P. *et al.* (2008) ‘PRDM16 controls a brown fat/skeletal muscle switch’, *Nature*, 454(7207), pp. 961–967. doi: 10.1038/nature07182.
- Seip, M. (1959) ‘Lipodystrophy and gigantism with associated endocrine manifestations. A new diencephalic syndrome?’, *Acta paediatrica*, 48, pp. 555–74. Available at: <http://www.ncbi.nlm.nih.gov/pubmed/14444642>.
- Shapira, S. N. *et al.* (2017) ‘EBF2 transcriptionally regulates brown adipogenesis via the histone reader DPF3 and the BAF chromatin remodeling complex’, *Genes & Development*, 31(7), pp. 660–673. doi: 10.1101/gad.294405.116.
- Shapira, S. N. and Seale, P. (2019) ‘Transcriptional Control of Brown and Beige Fat Development and Function’, *Obesity*, 27(1), pp. 13–21. doi: 10.1002/oby.22334.
- Sharma, R. *et al.* (2019) ‘Octacosanol and policosanol prevent high-fat diet-induced obesity and metabolic disorders by activating brown adipose tissue and improving liver metabolism’, *Scientific Reports*. Springer US, 9(1), p. 5169. doi: 10.1038/s41598-019-41631-1.
- Shimabukuro, M. *et al.* (1998) ‘Fatty acid-induced cell apoptosis: A link between obesity and diabetes’, *Proceedings of the National Academy of Sciences*, 95(5), pp. 2498–2502. doi: 10.1073/pnas.95.5.2498.
- Shinoda, K. *et al.* (2015) ‘Genetic and functional characterization of clonally derived adult human brown adipocytes’, *Nature Medicine*, 21(4), pp. 389–394. doi: 10.1038/nm.3819.
- Simha, V. *et al.* (2003) ‘Effect of Leptin Replacement on Intrahepatic and Intramyocellular Lipid Content in Patients With Generalized Lipodystrophy’, *Diabetes Care*, 26(1), pp. 30–35. doi: 10.2337/diacare.26.1.30.
- Singh, R., Letai, A. and Sarosiek, K. (2019) ‘Regulation of apoptosis in health and disease: the balancing act of BCL-2 family proteins’, *Nature Reviews Molecular Cell Biology*. Springer US. doi: 10.1038/s41580-018-0089-8.
- Subauste, A. R. *et al.* (2012) ‘Alterations in Lipid Signaling Underlie Lipodystrophy Secondary to AGPAT2 Mutations’, *Diabetes*, 61(11), pp. 2922–2931. doi: 10.2337/db12-0004.
- Susulic, V. S. *et al.* (1995) ‘Targeted disruption of the beta 3-adrenergic receptor gene.’, *The Journal of biological chemistry*, 270(49), pp. 29483–92. Available at: <http://www.ncbi.nlm.nih.gov/pubmed/7493988>.
- Szczepaniak, L. S. *et al.* (1999) ‘Measurement of intracellular triglyceride stores by H spectroscopy: validation in vivo’, *American Journal of Physiology-Endocrinology and Metabolism*, 276(5), pp. E977–E989. doi: 10.1152/ajpendo.1999.276.5.E977.
- Tamir, S. *et al.* (2015) ‘Structure–function analysis of NEET proteins uncovers their role as

- key regulators of iron and ROS homeostasis in health and disease', *Biochimica et Biophysica Acta (BBA) - Molecular Cell Research*, 1853(6), pp. 1294–1315. doi: 10.1016/j.bbamcr.2014.10.014.
- Tapia, P. *et al.* (2018) 'Biology and pathological implications of brown adipose tissue: promises and caveats for the control of obesity and its associated complications', *Biological Reviews*, 93(2), pp. 1145–1164. doi: 10.1111/brv.12389.
- Teruel, T., Hernandez, R. and Lorenzo, M. (2001) 'Ceramide mediates insulin resistance by tumor necrosis factor-alpha in brown adipocytes by maintaining Akt in an inactive dephosphorylated state.', *Diabetes*, 50(11), pp. 2563–71. Available at: <http://www.ncbi.nlm.nih.gov/pubmed/11679435>.
- Timmons, J. A. *et al.* (2007) 'Myogenic gene expression signature establishes that brown and white adipocytes originate from distinct cell lineages', *Proceedings of the National Academy of Sciences*, 104(11), pp. 4401–4406. doi: 10.1073/pnas.0610615104.
- Tsukahara, T. *et al.* (2010) 'Phospholipase D2-dependent inhibition of the nuclear hormone receptor PPAR γ by cyclic phosphatidic acid', *Molecular Cell*. Elsevier Ltd, 39(3), pp. 421–432. doi: 10.1016/j.molcel.2010.07.022.
- Tsushima, K. *et al.* (2018) 'Mitochondrial Reactive Oxygen Species in Lipotoxic Hearts Induce Post-Translational Modifications of AKAP121, DRP1, and OPA1 That Promote Mitochondrial Fission', *Circulation Research*, 122(1), pp. 58–73. doi: 10.1161/CIRCRESAHA.117.311307.
- Tvrđik, P. *et al.* (1997) 'Cig30, a Mouse Member of a Novel Membrane Protein Gene Family, Is Involved in the Recruitment of Brown Adipose Tissue', *Journal of Biological Chemistry*, 272(50), pp. 31738–31746. doi: 10.1074/jbc.272.50.31738.
- Uldry, M. *et al.* (2006) 'Complementary action of the PGC-1 coactivators in mitochondrial biogenesis and brown fat differentiation', *Cell Metabolism*, 3(5), pp. 333–341. doi: 10.1016/j.cmet.2006.04.002.
- Unger, R. H. (1995) 'Lipotoxicity in the pathogenesis of obesity-dependent NIDDM. Genetic and clinical implications.', *Diabetes*, 44(8), pp. 863–70. Available at: <http://www.ncbi.nlm.nih.gov/pubmed/7621989>.
- Unger, R. H. (2002) 'Lipotoxic Diseases', *Annual Review of Medicine*, 53(1), pp. 319–336. doi: 10.1146/annurev.med.53.082901.104057.
- Unger, R. H. and Scherer, P. E. (2010) 'Gluttony, sloth and the metabolic syndrome: a roadmap to lipotoxicity', *Trends in Endocrinology & Metabolism*. Elsevier Ltd, 21(6), pp. 345–352. doi: 10.1016/j.tem.2010.01.009.
- Ussher, J. R. *et al.* (2010) 'Inhibition of De Novo Ceramide Synthesis Reverses Diet-Induced Insulin Resistance and Enhances Whole-Body Oxygen Consumption', *Diabetes*, 59(10), pp. 2453–2464. doi: 10.2337/db09-1293.
- Valenzuela, R. *et al.* (2015) 'Reduction in the desaturation capacity of the liver in mice subjected to high fat diet: Relation to LCPUFA depletion in liver and extrahepatic tissues', *Prostaglandins, Leukotrienes and Essential Fatty Acids*. Elsevier, 98, pp. 7–14. doi: 10.1016/j.plefa.2015.04.002.
- Villarroya, F., Peyrou, M. and Giralt, M. (2017) 'Transcriptional regulation of the uncoupling protein-1 gene', *Biochimie*. Elsevier Ltd, 134, pp. 86–92. doi: 10.1016/j.biochi.2016.09.017.
- Virtanen, K. A. *et al.* (2009) 'Functional Brown Adipose Tissue in Healthy Adults', *New England Journal of Medicine*, 360(15), pp. 1518–1525. doi: 10.1056/NEJMoa0808949.
- de Vries, J. E. *et al.* (1997) 'Saturated but not mono-unsaturated fatty acids induce apoptotic

- cell death in neonatal rat ventricular myocytes.’, *Journal of lipid research*, 38(7), pp. 1384–94. Available at: <http://www.ncbi.nlm.nih.gov/pubmed/9254064>.
- Walls, S. M. *et al.* (2018) ‘Ceramide-Protein Interactions Modulate Ceramide-Associated Lipotoxic Cardiomyopathy’, *Cell Reports*. Elsevier Company., 22(10), pp. 2702–2715. doi: 10.1016/j.celrep.2018.02.034.
- Wang, Q. A. *et al.* (2013) ‘Tracking adipogenesis during white adipose tissue development, expansion and regeneration’, *Nature Medicine*. Nature Publishing Group, 19(10), pp. 1338–1344. doi: 10.1038/nm.3324.
- Wang, W. *et al.* (2014) ‘Ebf2 is a selective marker of brown and beige adipogenic precursor cells’, *Proceedings of the National Academy of Sciences*, 111(40), pp. 14466–14471. doi: 10.1073/pnas.1412685111.
- Wang, W. and Seale, P. (2016) ‘Control of brown and beige fat development’, *Nature Reviews Molecular Cell Biology*. Nature Publishing Group, 17(11), pp. 691–702. doi: 10.1038/nrm.2016.96.
- Wang, XingYun *et al.* (2018) ‘Evaluation and optimization of differentiation conditions for human primary brown adipocytes’, *Scientific Reports*. Springer US, 8(1), p. 5304. doi: 10.1038/s41598-018-23700-z.
- de Weerd, N. A. and Nguyen, T. (2012) ‘The interferons and their receptors-distribution and regulation’, *Immunology and Cell Biology*. Nature Publishing Group, 90(5), pp. 483–491. doi: 10.1038/icb.2012.9.
- Wen, H. *et al.* (2011) ‘Fatty acid-induced NLRP3-ASC inflammasome activation interferes with insulin signaling’, *Nature Immunology*. Nature Publishing Group, 12(5), pp. 408–415. doi: 10.1038/ni.2022.
- West, A. P. *et al.* (2015) ‘Mitochondrial DNA stress primes the antiviral innate immune response’, *Nature*, 520(7548), pp. 553–557. doi: 10.1038/nature14156.
- Wu, J. *et al.* (2012) ‘Beige Adipocytes Are a Distinct Type of Thermogenic Fat Cell in Mouse and Human’, *Cell*, 150(2), pp. 366–376. doi: 10.1016/j.cell.2012.05.016.
- Yamashita, A. *et al.* (2014) ‘Glycerophosphate/Acylglycerophosphate Acyltransferases’, *Biology*, 3(4), pp. 801–830. doi: 10.3390/biology3040801.
- Yang, S. *et al.* (2014) ‘Defective mitophagy driven by dysregulation of rheb and KIF5B contributes to mitochondrial reactive oxygen species (ROS)-induced nod-like receptor 3 (NLRP3) dependent proinflammatory response and aggravates lipotoxicity’, *Redox Biology*. Elsevier, 3, pp. 63–71. doi: 10.1016/j.redox.2014.04.001.
- Yin, J. *et al.* (2015) ‘Palmitate induces endoplasmic reticulum stress and autophagy in mature adipocytes: Implications for apoptosis and inflammation’, *International Journal of Molecular Medicine*, 35(4), pp. 932–940. doi: 10.3892/ijmm.2015.2085.
- Yubero, P. *et al.* (1998) ‘Dominant Negative Regulation by c-Jun of Transcription of the Uncoupling Protein-1 Gene through a Proximal cAMP-Regulatory Element: A Mechanism for Repressing Basal and Norepinephrine-Induced Expression of the Gene before Brown Adipocyte Differentiation’, *Molecular Endocrinology*, 12(7), pp. 1023–1037. doi: 10.1210/mend.12.7.0137.
- Zdravec, D. *et al.* (2010) ‘Ablation of the very-long-chain fatty acid elongase ELOVL3 in mice leads to constrained lipid storage and resistance to diet-induced obesity’, *The FASEB Journal*, 24(11), pp. 4366–4377. doi: 10.1096/fj.09-152298.
- Zechner, R. *et al.* (2009) ‘Adipose triglyceride lipase and the lipolytic catabolism of cellular fat stores’, *Journal of Lipid Research*, 50(1), pp. 3–21. doi: 10.1194/jlr.R800031-JLR200.

Zhou, Y. *et al.* (2019) 'Lipotoxicity reduces β cell survival through islet stellate cell activation regulated by lipid metabolism-related molecules', *Experimental Cell Research*, 380(1), pp. 1–8. doi: 10.1016/j.yexcr.2019.04.012.

Zou, L. *et al.* (2017) 'Palmitate induces myocardial lipotoxic injury via the endoplasmic reticulum stress-mediated apoptosis pathway', *Molecular Medicine Reports*, 16(5), pp. 6934–6939. doi: 10.3892/mmr.2017.7404.

Zuo, Y., Qiang, L. and Farmer, S. R. (2006) 'Activation of CCAAT/Enhancer-binding Protein (C/EBP) α Expression by C/EBP β during Adipogenesis Requires a Peroxisome Proliferator-activated Receptor- γ -associated Repression of HDAC1 at the C/ebp α Gene Promoter', *Journal of Biological Chemistry*, 281(12), pp. 7960–7967. doi: 10.1074/jbc.M510682200.

.

Biology and pathological implications of brown adipose tissue: promises and caveats for the control of obesity and its associated complications

Pablo Tapia¹, Marta Fernández-Galilea¹, Fermín Robledo¹, Pablo Mardones², José E. Galgani^{1,3,*} and Víctor A. Cortés^{1,*} 

¹*Department of Nutrition, Diabetes and Metabolism, School of Medicine, Pontificia Universidad Católica de Chile, Marcoleta 367, Santiago, 8330024, Chile*

²*Research and Innovation Office, School of Engineering, Pontificia Universidad Católica de Chile, Marcoleta 367, Santiago, 8330024, Chile*

³*Departamento Ciencias de la Salud, Carrera de Nutrición y Dietética, Pontificia Universidad Católica de Chile, Marcoleta 367, Santiago, 8330024, Chile*

ABSTRACT

The discovery of metabolically active brown adipose tissue (BAT) in adult humans has fuelled the research of diverse aspects of this previously neglected tissue. BAT is solely present in mammals and its clearest physiological role is non-shivering thermogenesis, owing to the capacity of brown adipocytes to dissipate metabolic energy as heat. Recently, a number of other possible functions have been proposed, including direct regulation of glucose and lipid homeostasis and the secretion of a number of factors with diverse regulatory actions. Herein, we review recent advances in general biological knowledge of BAT and discuss the possible implications of this tissue in human metabolic health. In particular, we confront the claimed thermogenic potential of BAT for human energy balance and body mass regulation, mostly based on animal studies, with the most recent quantifications of human BAT.

Key words: brown adipose tissue, adipogenesis, thermogenesis, obesity, insulin resistance.

CONTENTS

I. Introduction	2
II. BAT morphology and function requires adrenergic stimulation	3
III. UCP1 is regulated by overlapping and redundant pathways	3
IV. Brown adipocyte development and regulation	5
V. The cellular lineage of BAT	7
VI. Interscapular BAT and skeletal muscle have a convergent developmental origin	7
VII. Beige/brite and iBAT adipocytes have different developmental origins	9
VIII. White and brown adipocytes derive from specialized vascular-wall cells in adipose depots	11
IX. BAT is a secretory organ	11
(1) FGF21	11
(2) BMP8B	11
(3) NRG4	11

* Address for correspondence (E-mail: vcortesm@uc.cl; jgalgani@uc.cl; Tel: +56 2 23546389).

(4) VEGF-A	12
(5) IL-6	12
(6) RBP4	12
(7) IGF-1	12
(8) miRNAs	12
X. The importance of BAT for metabolic regulation	12
XI. The impact of BAT in human health and disease	13
XII. Activating brown adipose tissue thermogenesis as a target to induce weight loss	13
XIII. Conclusions	14
XIV. Acknowledgements	15
XV. REFERENCES	15

I. INTRODUCTION

An estimated ~2 billion adult people are currently overweight and more than 600 million are clinically obese worldwide (World Health Organization, 2017). Accordingly, research directed to understand the biological basis of excessive adiposity as well as to uncover novel therapeutic approaches has expanded steadily. The interplay between white and brown adipose tissue classes (WAT and BAT, respectively) has received growing attention as a relevant mechanism for the pathogenesis of obesity and its related metabolic complications (Speakman & O'Rahilly, 2012).

Adipose tissue stores vast amounts of energy (~9000 cal/kg) in highly specialized cells (Wells, 2006). While WAT mainly buffers calorie intake fluctuations, the intracellular triglycerides stored in BAT are burnt off to generate heat. BAT is a highly specialized thermogenic system that uncouples fatty acid oxidation and mitochondrial respiration from ATP synthesis to dissipate energy. This process, known as non-shivering thermogenesis, is induced in response to cold *via* β -adrenergic stimulation and requires uncoupling protein 1 (UCP1, thermogenin), which is present in the inner mitochondrial membrane and is recognized as a *bona fide* molecular marker of BAT. BAT-dependent thermogenesis has clear physiological implications for small mammals, such as rodents or newborn animals, because of their increased susceptibility to hypothermia, owing to an elevated surface-to-volume ratio (Dawkins & Hull, 1964; Cannon & Nedergaard, 2004), however, its functional relevance for adult humans remains debated. Recent correlational findings suggest that BAT activation regulates insulin sensitivity (Chondronikola *et al.*, 2014; Lee *et al.*, 2014b), lipid homeostasis (Chondronikola *et al.*, 2016), and body mass/composition (Yoneshiro *et al.*, 2013). These facts have led to proposals that pharmacological activation of BAT-dependent thermogenesis could be an effective therapy against obesity and its metabolic complications (Nedergaard & Cannon, 2010). Nevertheless, this still lacks empirical demonstration and the actual thermogenic potential of human BAT remains to be determined.

Anatomically, BAT is a discrete organ located in the interscapular region of small mammals and newborn humans (Aherne & Hull, 1966; Merklin, 1974). Based on the presence of UCP1 orthologues, brown-like adipocytes have been

described in all newborn mammals studied to date, including ovine and bovine species (Casteilla *et al.*, 1987; Cypess & Kahn, 2010; Nedergaard & Cannon, 2010; Birerdinc *et al.*, 2013), and African elephant shrews (*Elephantulus myurus*), a species belonging to the Afrotheria, a group of animals thought to be at the base of the eutherian clade (Mzilikazi *et al.*, 2007).

Interscapular BAT (iBAT) is currently known as 'classical BAT' in contrast to the interspersed clusters of brown-like adipocytes found inside WAT of the supraclavicular space, mediastinum, pericardium, and perirenal/adrenal and intercostal arteries, which are denominated 'beige' or 'brite (brown-in-white)' adipose tissue (Enerback, 2010). As discussed in Section V, despite their morphological and functional similarities, classical and beige/brite adipocytes have a distinct developmental origin and regulation (Spiegelman, 2013).

BAT mass diminishes with age in humans ultimately to become indistinguishable from WAT (Heaton, 1972). Seminal studies based on [¹⁸F]-fluorodeoxyglucose-positron emission tomography-computed tomography (FDG-PET-CT) revealed that BAT is present (Cypess *et al.*, 2009; van Marken Lichtenbelt *et al.*, 2009; Saito *et al.*, 2009; Virtanen *et al.*, 2009) and is efficiently activated by cold in most adults (Cypess *et al.*, 2012; Ouellet *et al.*, 2012), renewing interest in understanding BAT biology.

Importantly, transcriptional analysis of FDG-PET-CT-detectable brown fat in adult humans revealed that these depots are composed of beige adipocytes instead of classical brown adipocytes, as they express characteristic genes of murine beige adipocytes such as *CD137*, *TMEM26* and *TBX1* but not classical brown adipocytes markers *EBF3*, *EVA1* and *FBXO31* (Spiegelman, 2013). These findings led to the conclusion that most BAT in adult humans corresponds to beige/brite fat rather than classical BAT.

Herein our goal is to review key aspects of normal BAT biology as well as recent advances that link this tissue to human disease. We also discuss the potential limitations and caveats that novel obesity therapies based on BAT activation must face before moving towards clinical trials. This latter issue has been largely overlooked in the literature possibly because of the urgency of finding new pharmacological targets for obesity; however, important concerns on the potential efficacy of such therapies have been raised because

of inconsistencies in key experimental studies (Wu *et al.*, 2012; Spiegelman, 2013) and the absence of compelling evidence that the magnitude of BAT-dependent thermogenesis can determine sustained negative energy balance in obese humans at thermoneutral conditions (Section XII).

II. BAT MORPHOLOGY AND FUNCTION REQUIRES ADRENERGIC STIMULATION

Brown adipocytes have a number of distinguishing features, including: (i) multiple and relatively small lipid droplets (LDs), (ii) large and numerous mitochondria with highly laminar cristae, and (iii) expression of UCP1 (Cannon & Nedergaard, 2004). By contrast, white adipocytes have a large unilocular LD; few, small and elongated mitochondria with randomly oriented cristae, and undetectable uncoupling activity (Frontini & Cinti, 2010).

BAT thermogenesis is controlled by norepinephrine (NE), which is released from sympathetic terminals under the control of hypothalamic thermal/metabolic sensors (Lowell & Bachman, 2003). In brown adipocytes, NE activates cell-surface G-protein-coupled β -adrenoceptors (mainly β_3 in mice and β_1 in humans), increasing intracellular cyclic AMP (cAMP) levels (Sundin, Mills & Fain, 1984; Connolly, Nanberg & Nedergaard, 1986) and activating protein kinase A (PKA), which further amplifies the adrenergic thermogenic signal through a series of transcriptional and post-transcriptional mechanisms (Oldfield *et al.*, 2002). PKA also promotes triglyceride lipolysis by phosphorylating LD-associated regulatory proteins and lipases, therefore coordinating fatty acid release, mitochondrial β -oxidation and thermogenesis (Fig. 1).

The physiological relevance of adrenergic stimulation on BAT biology was recognized in very early studies of adipose tissue. Hausberger (1934) reported that denervation of the 'hibernating gland' (iBAT) transforms multilocular to unilocular adipose cells, indicating that adrenergic stimulation is required for normal BAT morphology. Correspondingly, it was noted that the adipose tissue surrounding catecholamine-secreting pheochromocytoma tumours is composed mostly of multiloculated adipocytes (Rona, 1964), suggesting for the first time that intense paracrine adrenergic stimulation promotes the conversion of WAT to BAT *in vivo*.

More recent experimentation has further supported the role of adrenergic stimulation in brown adipocyte differentiation. In mice, the combined deletion of all three β -adrenoceptor genes leads to thermogenically inactive brown adipocytes filled with a single LD and decreased UCP1 levels (Bachman *et al.*, 2002). These mice fail to upregulate UCP1 expression and oxygen consumption in response to isoproterenol, a pan- β -adrenoceptor agonist, or cold exposure, and become obese under regular chow diet and standard housing conditions (Bachman *et al.*, 2002). Moreover, mice lacking adrenaline and noradrenaline because of dopamine β -hydroxylase gene deletion, have

BAT with abnormally large LDs, are cold intolerant and are incapable of increasing UCP1 levels after cold exposure (Thomas & Palmiter, 1997).

These results suggest that adrenergic stimulation is critical for BAT normal morphology and function in mice and possibly in humans, given the reported cases of pheochromocytoma.

Interestingly, and in contrast to the effects of cold-dependent adrenergic stimulation on BAT, pharmacological β -adrenergic activation fails to increase the uptake of FDG in BAT, while still increasing the metabolic rate in adult humans (Cypess *et al.*, 2012; Vosselman *et al.*, 2012). This phenomenon suggests that activation of BAT requires specific sympathetic pathways that are selectively dependent on cold stimulation and that are not activated by systemic non-selective β -adrenergic stimulation.

III. UCP1 IS REGULATED BY OVERLAPPING AND REDUNDANT PATHWAYS

The understanding of BAT-dependent thermogenesis has progressed greatly in recent years. UCP1 gene expression relies on multiple and interlinked transcriptional regulators that include nuclear receptors peroxisome proliferator-activated receptor gamma (PPAR γ), retinoic acid receptors (RARs), thyroid hormone receptor (TR), and retinoid X receptor (RXR) (Fig. 2). Putative binding sites for these proteins have been identified in a 220-base pair enhancer element located 2.4 kilobases upstream of the murine UCP1 gene (Kozak, 2010). UCP1 gene expression is also dependent on the PKA target cAMP response element-binding protein (CREB), as well as members of the fibroblast growth factor (FGF), bone morphogenetic protein (BMP), and Wnt families (Lowell & Spiegelman, 2000; Cannon & Nedergaard, 2004; Fisher *et al.*, 2012).

PPAR γ is essential for UCP1 enhancer activation but, interestingly, this seems to be a specific effect for brown adipocytes (Lowell & Spiegelman, 2000). *In vivo* studies have shown that chronic (14 days) treatment with thiazolidinedione PPAR γ activators increases UCP1 at the mRNA and protein level exclusively in brown adipocytes of rats and mice (Sears *et al.*, 1996) and whole-body transgenic overexpression of PPAR γ 2 increases UCP1 levels in brown adipocytes but not in white adipocytes or skeletal muscle in mice (Kelly *et al.*, 1998). The reason for this selective action of PPAR γ on UCP1 expression in BAT is not known but likely indicates that additional transcriptional regulators are required for UCP1 gene expression specifically in brown adipocytes.

An interesting new regulatory circuit for UCP1 expression links the thyroid hormone axis with circulating bile acids (BAs). BAs are cholesterol derivatives that reach the systemic circulation and activate both nuclear and cell surface receptors in cell types important for the physiological regulation of lipid, glucose and energy metabolism (Zhou *et al.*, 2014). TGR5/Gpbar1 is a G-protein-coupled receptor

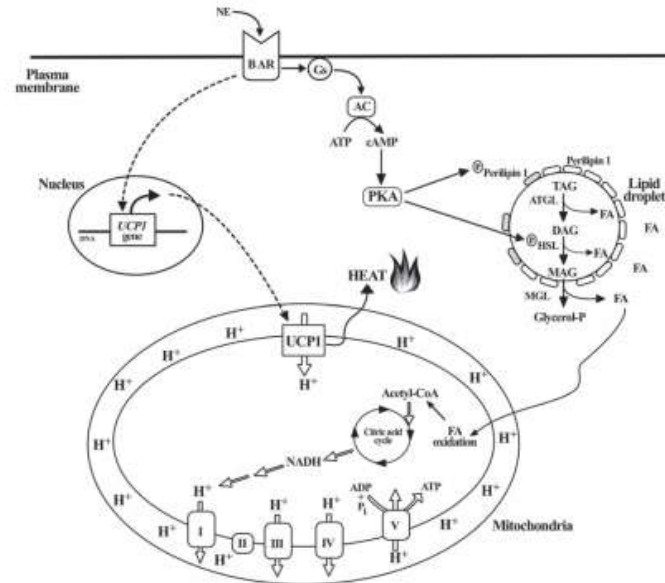


Fig. 1. β -adrenergic receptors coordinate triglyceride lipolysis, mitochondrial fatty acid oxidation and uncoupling protein 1 (UCP1) abundance in brown adipocytes. Sympathetic stimulation of interscapular brown adipose tissue (iBAT) is the main physiological mechanism for regulating non-shivering thermogenesis in response to cold exposure. Three receptors are the most abundant adrenoceptors in murine classical brown adipocytes whereas one seems to be the main adrenoceptor in human BAT. After norepinephrine (NE) binding, β -adrenoceptor (BAR) activates adenylyl cyclase (AC) and thus increases cyclic AMP (cAMP) intracellular concentration through protein Gs-dependent mechanisms. cAMP binds to protein kinase A (PKA) and thus promotes the phosphorylation of direct PKA target proteins. These include perilipin 1, a structural protein present on the lipid droplet (LD) surface and hormone-sensitive lipase (HSL), a required enzyme for LD triglyceride (TAG) lipolysis. In its non-phosphorylated state, perilipin 1 prevents the interaction between HSL as well as other lipases adipose triglyceride lipase (ATGL) and monoacylglycerol lipase (MGL) with the LD. By contrast, phosphorylated perilipin 1 allows the physical interaction between these enzymes and the LD. In parallel, PKA-mediated phosphorylation of HSL triggers the translocation of this enzyme from the cytoplasm to the LD to mediate hydrolysis of sn-2,3 diacylglycerols (DAG). The resulting monoacylglycerols (MAG) are finally deacylated by MGL. The released fatty acids (FAs) are imported to the mitochondria where they are oxidized to acetyl-coenzyme A (acetyl Co-A) and ultimately fuel the oxidative phosphorylation of ADP to ATP. Adrenergic stimulation also increases the abundance of UCP1 in the inner mitochondrial membrane (IMM) by transcriptional mechanisms that also depend on cAMP levels and PKA activation. This ultimately results in dissipation of the electrochemical H^+ gradient across the IMM and regulated heat generation. MGL, monoacylglycerol lipase.

present in the plasma membrane of brown adipocytes, among other cell types, and its activation by BAs increases type 2 deiodinase (DIO2) levels, which converts metabolically inactive tetraiodothyronine/thyroxine (T4) into active triiodothyronine (T3) (Watanabe *et al.*, 2006). This results in higher levels of mitochondrial UCP1 (Fig. 2), elevated uncoupled fatty acid oxidation and energy expenditure, and ultimately, protection against diet-induced obesity in mice (Watanabe *et al.*, 2006). Consequently, TGR5 has been envisioned as a new pharmacological target for increasing thermogenesis in obese patients (Thomas, Auwerx & Schoonjans, 2008). Supporting this proposition, oral treatment with chenodeoxycholic acid, a naturally occurring BA, for 2 days increases BAT activity, as detected by FDG-PET-CT, and resting energy expenditure

at thermoneutral conditions in lean and healthy women (Chavez-Talavera *et al.*, 2017). The effectiveness of this strategy to chronically elevate thermogenesis and decrease body adiposity in obese subjects remains to be determined.

UCP1 gene transcription is regulated by TR isoform beta (TR β) both in mice (Ribeiro *et al.*, 2001) and cultured human adipocytes (Lee *et al.*, 2012). Also, circulating levels of T4 correlate with the expression level of UCP1 and other beige/brite adipocyte gene markers in WAT depots of obese humans (Broeders *et al.*, 2015), suggesting that thyroid hormones physiologically regulate the abundance of BAT in humans. Considering that thyroid hormone and thyromimetic compounds potently decrease body adiposity (Martagón *et al.*, 2015) and that cardiovascular actions of thyroid hormones are dependent on TR α , the selective

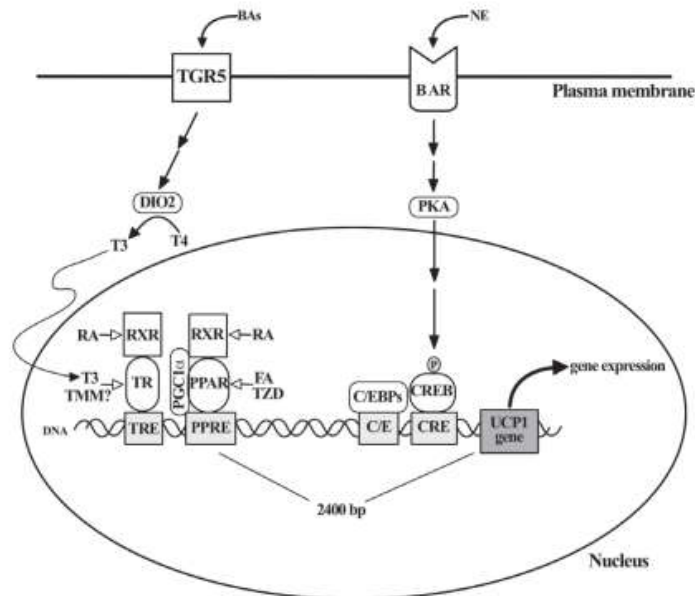


Fig. 2. Uncoupling protein 1 (UCP1) gene expression is regulated by multiple factors in brown adipocytes. After binding their respective ligand activators, both peroxisome proliferator-activated receptor (PPAR) and thyroid hormone receptor (TR) heterodimerize with retinoid X receptor (RXR) and bind to PPAR- and TR-responsive elements (PPRE and TRE, respectively) present on an enhancer region 2400 base pairs upstream of the UCP1-encoding gene. PPAR γ coactivator 1 α (PGC1 α) binds to PPAR and recruits transcriptional coactivators and excludes corepressors (not shown) that seem to be critical for the specific expression of UCP1 in brown adipocytes. Closer to the origin of UCP1 gene transcription, CCAAT/enhancer binding proteins (C/EBPs) and cyclic AMP response element binding protein (CREB) bind to their specific responsive sequences (C/E and CRE, respectively). In response to β -adrenergic stimulation [norepinephrine (NE) binding to β -adrenoceptors (BARs)], protein kinase A (PKA) directly phosphorylates CREB and promotes its translocation from the cytoplasm to the nucleus to trigger UCP1 transcription. Independently, G-protein coupled bile acid receptor Gpbar1 (TGR5) increases the conversion of tetraiodothyronine/thyroxine (T4) to triiodothyronine (T3) mediated by deiodinase 2 (DIO2). Elevated intracellular T3 activates TR and thus increases UCP1 gene transcription.

elevation of UCP1 levels by TR β appears to be an interesting therapeutic opportunity for increasing thermogenesis in humans. Nonetheless, formal assessments of the clinical potential of TR β selective activation on thermogenesis, body composition, or metabolic regulation in humans are awaited. Interestingly, it was reported that pharmacological supplementation with T4 potently increased UCP1, DIO2 and other beige/brown adipocyte gene markers as well as FDG-PET-CT-detectable BAT mass, in association with improved glycaemic control, in a patient with genetic severe insulin resistance and thyroidectomy for thyroid cancer (Martínez-Sánchez *et al.*, 2017).

IV. BROWN ADIPOCYTE DEVELOPMENT AND REGULATION

Current knowledge on adipocyte differentiation (adipogenesis) largely derives from the study of established pre-adipocyte

cell lines (Rosen & MacDougald, 2006). Based on these models, adipogenesis has been conceptualized as a multi-stage process driven by the sequential activation and repression of transcription factors, co-activators, co-repressors and cell-cycle regulatory molecules (Lefterova & Lazar, 2009) (Fig. 3).

PPAR γ is recognized as the master regulator of white and brown adipogenesis (Tontonoz & Spiegelman, 2008) as its sole ectopic expression in non-adipogenic mouse fibroblasts triggers adipogenic differentiation and development of white adipocyte-like cells (Tontonoz, Hu & Spiegelman, 1994). In addition, multiple gene-deletion experiments in mice and the identification of mutations in the PPAR γ gene in lipodystrophic patients have confirmed the key role of PPAR γ in adipogenesis *in vivo* (Barak *et al.*, 1999; Rosen *et al.*, 1999; Agarwal & Garg, 2002; He *et al.*, 2003). CCAAT/enhancer binding proteins (C/EBPs) is another group of essential adipogenic transcription factors. C/EBP β and C/EBP δ are expressed early in adipogenesis

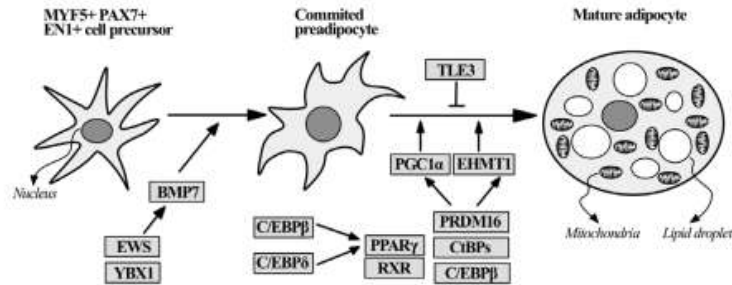


Fig. 3. Transcriptional regulation of brown adipogenesis. Classical brown adipocytes reside mostly in the interscapular adipose tissue of rodents and newborn humans. They derive from mesenchymal precursors that express myogenic factor 5 (Myf5) and that also originates skeletal muscle myocytes. Adipogenic stimuli favour the conversion of these undifferentiated precursors to committed preadipocytes that progressively transform into fully differentiated brown adipocytes upon the transcriptional control of several regulatory proteins and microRNAs (miRNAs) (not shown for simplicity). Peroxisome proliferator-activated receptor γ (PPAR γ) is absolutely necessary but not sufficient for brown adipogenesis. PRD1-BF-1RIZ1 homologous-containing protein 16 (PRDM16) is a co-regulatory factor that interacts with other proteins to assemble transcriptional complexes that coordinate to suppress WAT and activate BAT adipogenesis. BMP7: bone morphogenetic protein 7; C/EBP: CCAAT/enhancer binding protein; CtBPs: C-terminal binding proteins; EHMT1: euchromatic histone lysine methyltransferase 1; EN1: Engrailed homeobox 1; EWS: Ewing sarcoma; PAX7: Paired box 7; PGC1 α : PPARG coactivator 1 alpha; RXR: Retinoid X receptor; TLE3: Transducin like enhancer of split 3; YBX1: Y-Box binding protein 1.

and command the transcription of PPAR γ and C/EBP α , which mediate later steps of the program and whose ectopic expression induces adipogenic differentiation in pre-adipocyte cell lines (Yeh *et al.*, 1995). Importantly, neither PPAR γ nor C/EBPs are sufficient for triggering the brown adipogenic transcriptional program.

In vitro experimentation has shown that, in spite of their morphological, metabolic and developmental differences, WAT and BAT share a similar adipogenic transcriptional program (Kajimura, Seale & Spiegelman, 2010). PPAR γ is necessary for both white and brown fat differentiation (Nedergaard *et al.*, 2005), but it is clearly insufficient for a complete brown cell lineage determination. Additional factors that are selectively involved in brown adipogenesis have been recently described, including PPAR γ coactivator 1 α (PGC1 α) (Puigserver *et al.*, 1998), Forkhead box C2 (FOXO2) (Cederberg *et al.*, 2001), PRD1-BF-1-RIZ1 homologous-containing protein (PRDM) 16 (Seale *et al.*, 2007), T-box 15 (TBX15) (Gburcik *et al.*, 2012), euchromatic histone-lysine-N-methyltransferase 1 (EHMT1) (Ohno *et al.*, 2013) and Ewing sarcoma (EWS) (Park *et al.*, 2013).

PRDM16 is a required factor for BAT differentiation *in vitro*, since its gene deletion precludes brown adipogenesis in immortalized brown preadipocytes (Seale *et al.*, 2007). Conversely, overexpression of PRDM16 in cultured preadipocytes and its transgenic expression in mouse adipose tissue induce classic BAT gene expression, including UCP1 and other mitochondrial proteins, while inhibiting typical WAT markers (Seale *et al.*, 2007). Nonetheless, *in vivo* PRDM16 deletion studies suggest that this factor is not absolutely required for BAT formation since PRDM16-deficient mice, that have lethal craniofacial defects (Skarulis *et al.*, 2010), still present substantial amounts of

UCP1-expressing adipocytes (Bjork *et al.*, 2010). Similarly, PRDM16 selective suppression in mature adipocytes does not prevent the expression of classical brown adipocyte markers, including UCP1, in iBAT but largely decreases the ability of WAT to increase the expression of these markers upon cold stimulation (Seale *et al.*, 2008), indicating that PRDM16 is a required factor for the physiological cold acclimation of the adipose tissue in mice.

To promote brown adipogenesis, PRDM16, a zinc finger protein itself, does not bind to the DNA but rather interacts with other regulatory proteins, such as C-terminal-binding proteins (CtBPs) and PGC1 α , to coordinately repress WAT and promote BAT gene-expression profiles (Cohen *et al.*, 2014). On the promoter regions of WAT-selective genes PRDM16 forms complexes with corepressor CtBPs to inhibit the expression of those genes; by contrast, it forms complexes with coactivator PGC1 α to activate the transcription of BAT-specific genes (Kajimura *et al.*, 2009).

Several BMP family members enhance adipogenesis *in vitro*; however, only BMP7 fully activates the brown adipogenic program. EWS induces *Bmp7* transcription by forming a complex with Y-box binding protein 1 (YBX1) on *Bmp7* promoter (Park *et al.*, 2013). Importantly, mice with engineered deletions of either BMP7 (Tseng *et al.*, 2008) or EWS (Park *et al.*, 2013) display reduced iBAT mass and UCP1 expression, indicating that this regulatory circuit is physiologically relevant for these animals.

The Groucho family member transducin-like enhancer of split 3 (TLE3) actively antagonizes brown adipogenesis by blocking the interaction between PRDM16 and PPAR γ and reducing the transcription of BAT-specific gene determinants *in vivo* (Villanueva *et al.*, 2013).

Micro RNAs (miRNAs) are small non-coding RNAs that control gene expression by targeting specific messenger RNAs and have been implicated in multiple biological processes and diseases, including obesity (Cruz *et al.*, 2017). In mice, adipocyte-selective gene deletion of enzymes involved in the processing of miRNAs DICER (Mori *et al.*, 2014) or DiGeorge syndrome critical region 8 (DGCR8) (Kim *et al.*, 2014) results in general lipodystrophy, lower abundance of brown adipocytes in iBAT mass and impaired insulin sensitivity, indicating that normal processing of miRNAs in adipocytes is required for adipose tissue development and function. On the other hand, selective overexpression of micro RNA miR-133 in brown preadipocytes prevents their differentiation to mature brown adipocytes by targeting PRDM16 (Trajkovski *et al.*, 2012), suggesting that specific miRNAs are physiological regulators of brown adipogenesis. Accordingly, additional miRNAs have been implicated in adipogenesis (reviewed by Cruz *et al.*, 2017), including: miR-365, miR-346 and miR-362 (Mori *et al.*, 2014), miR-182 and miR-203 (Kim *et al.*, 2014), miR-193b and miR365 (Sun *et al.*, 2011).

In a survey of miRNAs that may be relevant for the development of beige/brite adipocytes in WAT depots, Giroud *et al.* (2016) recently found that miR-125b-5p expression is lower in BAT than in WAT and that it correlates inversely with mitochondrial biogenesis. By contrast, miR-106b and miR-93 levels were higher under diet-induced obesity and inhibited the expression of thermogenic genes in murine BAT (Wu *et al.*, 2013), suggesting that miRNAs have a determinant role for both brown and white adipocyte abundance *in vivo*.

Currently, the therapeutic potential of the transcriptional regulators of brown adipogenesis to increase whole body mass of brown adipocytes and hence promote non-shivering thermogenesis in humans, remain uncertain, mostly given the intrinsic difficulties of directly targeting nuclear proteins. Nonetheless, even assuming the effectiveness of such potential drugs, clinically relevant weight loss will only be obtained by the simultaneous prevention of compensatory increases of energy intake (Polidori *et al.*, 2016).

Recently, a multiplicity of natural and synthetic compounds have been claimed to promote brown adipogenesis in *in vivo* or *in vitro* systems (reviewed by Wankhade *et al.*, 2016) (Table 1). With the exception of some thiazolidinediones (Wankhade *et al.*, 2016) and capsinoids (Digby *et al.*, 1998), none of these compounds have demonstrated browning effects in humans. More importantly, clinical effectiveness and security of these candidate molecules to control body mass in obese patients have yet to be demonstrated.

V. THE CELLULAR LINEAGE OF BAT

It was long assumed that white and brown adipocytes shared a common developmental origin owing to their similar intracellular lipid-storage capacity and gene expression

profiles. Interestingly, even though some early investigators argued that brown adipocytes merely corresponded to immature white adipose cells (Sheldon, 1924) other contemporary authors contended that BAT was an already mature and functional tissue (Rasmussen, 1923). Notably, compelling experimental evidence that adipose tissue has committed cellular precursors that differ from other mesodermal-derived tissues was generated early in BAT studies (Hausberger, 1955).

The classical adipogenic model posits that adipose tissue has a single mesodermal origin and that a common mesenchymal stem cell (MSC) gives rise to WAT and BAT, as well as bone, muscle, and cartilage (Yoneshiro *et al.*, 2012). Accordingly, it was thought that MSCs generate common adipose cell precursors ('adipoblasts') that, in turn, differentiate into committed white or brown preadipocytes under appropriate stimulatory conditions. Even though this is no longer the prevailing hypothesis (see below), the model was long supported by the simultaneous absence of both WAT and BAT depots in several lipodystrophic mouse models, including those deficient for PPAR γ (Koutnikova *et al.*, 2003), 1-acylglycerol-3-phosphate O-acyltransferase 2 (AGPAT2) (Cortés *et al.*, 2009) and Berardinelli-Seip congenital lipodystrophy 2 (seipin) BSCL2 (Liu *et al.*, 2014).

Recent developmental and evolutionary studies show that WAT and classical BAT have, indeed, diverging origins. Temporal considerations support this idea: BAT originates early during fetal life and is morphologically and molecularly mature at birth (Cannon & Nedergaard, 1986; Cautivo *et al.*, 2016), whereas WAT develops at mid-gestation in humans and postnatally in mice (Wang & Scherer, 2014). In addition, BAT appeared significantly later in evolution compared with WAT, along with non-shivering thermogenesis and homeothermic regulation in mammals (Gesta, Tseng & Kahn, 2007).

Interestingly, WAT from different anatomical sites shows distinctive gene expression patterns (Gesta *et al.*, 2007), and lineage-tracing studies show that, whereas WAT in the trunk derives from the mesoderm, WAT in the cephalic region derives from the neural crest and thus belongs to the ectodermal lineage (Billon *et al.*, 2007), suggesting that white adipocytes have several distinct embryonic/developmental origins. BAT also seems to be developmentally diverse, with different cell precursors for interscapular classical iBAT and for beige/brite adipocytes (Spiegelman, 2013).

VI. INTERSCAPULAR BAT AND SKELETAL MUSCLE HAVE A CONVERGENT DEVELOPMENTAL ORIGIN

Using genetic fate mapping, Atit *et al.* (2006) first showed that in mice iBAT brown adipocytes originate from Engrailed 1 (En1)-expressing cells in the central dermomyotome, along with the dorsal dermis and epaxial skeletal muscle. Supporting these findings, Timmons *et al.* (2007) showed that

Table 1. Natural and synthetic compounds that increase uncoupling protein 1 (UCP1) levels in white adipose tissue (WAT) or promote brown adipose tissue (BAT) activity *in vivo*

Compound	Molecular target	Mechanism	Reference
Thiazolidinediones	Peroxisome proliferator-activated receptor γ (PPAR γ)	Synthetic PPAR γ agonist; transcriptional activation of brown adipogenesis	Fukui <i>et al.</i> (2000)
Capsinoids	Transient receptor potential cation channel subfamily V member 1 (TRPV1)	Mechanisms for their effects on brown adipogenesis undetermined; increases UCP1 levels and BAT activity in cultured adipocytes, mice and humans, likely by increasing central adrenergic activity	Baboota <i>et al.</i> (2014) and Yoneshiro <i>et al.</i> (2012)
Irisin	Unknown cell surface receptor; requires Peroxisome proliferator-activated receptor α (PPAR α) and p38 mitogen activated kinase (MAPK)	Protein product secreted by skeletal muscle in response to exercise induces transcriptional activation of brown adipogenesis in mice	Bostrom <i>et al.</i> (2012) and Zhang <i>et al.</i> (2014)
Resveratrol	AMP activated protein kinase (AMPK), sirtuin 1 (SIRT1)	Natural phenol antioxidant; mechanisms for its effects on brown adipogenesis unknown	Wang <i>et al.</i> (2015) and Alberdi <i>et al.</i> (2013)
Melatonin	Undetermined, possibly metallothionein-1 (MT1/MT), RAR related orphan receptor (ROR)	Hormone secreted by pineal gland and a natural plant product; mechanisms for its effects on brown adipogenesis are unknown, possibly central activation of sympathetic system	Jimenez-Aranda <i>et al.</i> (2013) and Tan <i>et al.</i> (2011)
10,12 Conjugated linoleic acid	Unknown, possibly G-protein coupled receptor (GPR) 120 and GPR40	Natural long-chain fatty acid enriched in dairy products; mechanisms for its effects on brown adipogenesis unknown	Shen <i>et al.</i> (2013)
Glucagon-like peptide 1	Glucagon-like peptide 1 receptor (GLP1R)	Peptide hormone secreted by enteroendocrine L-cells in response to feeding; hypothalamic AMPK activation that possibly increases sympathetic output	Lockie <i>et al.</i> (2012) and Beiroa <i>et al.</i> (2014)
β -aminoisobutyric acid	Unknown cell surface receptor; requires PPAR α	Non-protein β -amino acid released by muscle in response to exercise; mechanisms for its effects on brown adipogenesis unknown	Roberts <i>et al.</i> (2014)
Tamoxifen	Unknown, possibly oestrogen receptor (ER) in adipocytes	Synthetic ER antagonist; intraperitoneal injection increases UCP1 protein levels in subcutaneous WAT in mice after 5 days; unknown mechanism	Hesselbarth <i>et al.</i> (2015)
Chrysin	Unknown; requires AMPK	Natural flavonoid found in flowers and mushrooms that increases UCP1 protein levels in cultured 3T3L1 cells	Choi & Yun (2016)
Imatinib/Gleevec®	PPAR γ	Synthetic molecule that inhibits cyclin-dependent kinase (CDK)5-mediated PPAR γ phosphorylation in S273 and increases UCP1 protein levels in subcutaneous WAT of mice	Choi <i>et al.</i> (2016a)
β -Lapachone	Micro RNA 32 (miR32) and indirectly iodothyronine deiodinase 2 (DIO2)	Natural plant naphthoquinone that increases UCP1 protein levels and thermogenesis in WAT of mice	Choi <i>et al.</i> (2016b)
Uroguanylin	Guanilate cyclase 2C receptor (GUCY2C) in the hypothalamus	Peptide hormone secreted by duodenal epithelial cells in response to feeding; increases UCP1 protein levels in WAT by central adrenergic activation	Folgueira <i>et al.</i> (2016)
Curcumin	Unknown	Natural phenolic compound of plant origin that increases UCP1 mRNA levels in cultured mouse adipocytes	Kim <i>et al.</i> (2016)
D-Limonene	Unknown; possibly requires β 3 adrenoceptor activation	Natural monoterpene mainly present in citrus fruits; activates AMPK and increases UCP1 protein levels in cultured 3T3L1 cells	Lone & Yun (2016)

Table 1. Continued

Compound	Molecular target	Mechanism	Reference
Artepillin C	Unknown; possibly binds and directly activates PPAR γ	Natural phenolic component of Brazilian propolis; increases UCP1 in WAT of mice and cultured adipocytes likely by direct transcriptional mechanisms	Nishikawa <i>et al.</i> (2016)
Cannabidiol	Unknown; requires PPAR γ and phosphatidylinositol-4,5-bisphosphate 3-kinase (PI3K)	Major phytocannabinoid of <i>Cannabis sativa</i> ; increases UCP1 protein levels in cultured 3T3L1 cells by unknown mechanisms	Parray & Yun (2016)
Butein	PR domain-containing protein 4 (PRDM4)	Natural chalcone of plant origin and antioxidant activity that increases UCP1 protein levels in WAT of mice and cultured adipocytes, possibly by transcriptional mechanisms	Song <i>et al.</i> (2016)
Seliciclib/Roscovitine®	PPAR γ	Synthetic compound that inhibits CDK5 phosphorylation of PPAR γ at S273 and increases UCP1 protein levels in the WAT of mice, possibly by transcriptional mechanisms	Wang <i>et al.</i> (2016)
Quercetin in combination with resveratrol	Unknown	Natural polyphenolic compound that potentiates the effect of resveratrol to increase UCP1 protein levels in the WAT of rats by unknown mechanisms	Arias <i>et al.</i> (2017)
Pentamethylquercetin	Unknown	Natural polymethoxylated flavonoid of plant origin that increases UCP1 mRNA levels in cultured 3T3L1 cells	Han <i>et al.</i> (2017)
Cyanidin-3-glucoside	Unknown	Plant polyphenolic anthocyanin that increases UCP1 protein levels in 3T3-L1 cells by unknown mechanisms but mediated by cyclic AMP (cAMP) elevation	Matsukawa <i>et al.</i> (2017)
Glucoraphanin	Unknown; requires nuclear factor, erythroid 2 like 2 (NRF2)	Increases UCP1 protein levels in WAT of mice by unknown mechanisms that likely involve mitochondrial biogenesis	Nagata <i>et al.</i> (2017)

brown preadipocytes have a gene expression profile highly similar to myogenic precursors, including elevated levels of the myogenic regulator myogenin, typically regarded as a 'master' transcriptional regulator of muscle development, myoblast determination protein (MyoD), and myogenic factor 5 (Myf5). Global analysis of miRNA abundance showed that myogenic miR-1, miR-133a and miR-206 were specifically expressed in brown pre- and mature adipocytes in mice but were absent in white adipocytes (Walden *et al.*, 2009), further supporting the notion that classical brown adipocytes derive from a cell precursor shared with skeletal myocytes.

Both the C2C12 myoblast cell line and primary mouse myoblasts isolated from postnatal skeletal muscle robustly differentiate into lipid-filled adipocyte-like cells when transduced with PRDM16 (Seale *et al.*, 2008). These cells express common adipocyte markers such as PPAR γ and adipocyte fatty acid binding protein 2 (aP2) as well as the BAT markers UCP1, elongation of very long chain fatty acids 3 (ELOVL3) and cell death-inducing DFFA-like effector A (CIDEA), while repressing myogenic genes for MyoD and myogenin (Seale *et al.*, 2008). Conversely, PRDM16 knockdown in primary brown fat cells potently induces

skeletal myogenesis *in vitro*, and its deletion in mice determines morphologically abnormal BAT, with reduced levels of brown adipocyte markers and higher expression of myogenic markers (Seale *et al.*, 2008).

Notably, myogenin-deficient mice, which are devoid of mature skeletal muscle fibres, have increased BAT mass, especially at the cervical–dorsal–interscapular region (Hasty *et al.*, 1993), suggesting that precursor cells that are incapable of completing muscle differentiation are directed, perhaps by default, to the brown adipocyte differentiation program.

By contrast, whereas iBAT brown adipocytes derive from Myf5-expressing mesenchymal precursors in mice, WAT and the pockets of brown-like adipocytes inside WAT (i.e. brite/beige fat cells) derive from precursors that do not belong to the Myf5-expressing cell lineage (Seale *et al.*, 2008).

VII. BEIGE/BRITE AND IBAT ADIPOCYTES HAVE DIFFERENT DEVELOPMENTAL ORIGINS

The actual origin of beige/brite adipocytes is still a matter of debate. Cinti (2009) and Frontini & Cinti (2010) suggested

that white adipocytes (or at least a specific subset of these cells) can convert reversibly into beige/brite cells. Since murine mature adipocytes can undergo reversible mammary epithelial transdifferentiation *in vivo* (Morrone *et al.*, 2004; De Matteis *et al.*, 2009), these investigators propose that analogous processes may occur within the adipose tissue. In fact, upon prolonged exposure to cold or β -adrenergic agonists, selected white adipocytes apparently do convert into brown-like fat cells (Himms-Hagen *et al.*, 2000; Granneman *et al.*, 2005). Similarly, thiazolidinedione PPAR γ activators clearly induce beige/brite sprouts in murine WAT (Wilson-Fritch *et al.*, 2004), possibly as a result of sirtuin 1 (SIRT1)-dependent post-translational modifications of PPAR γ (Qiang *et al.*, 2012) and stabilization of the PRDM16–PPAR γ interaction (Ohno *et al.*, 2012).

A second hypothesis for beige/brite adipocytes origin states that they differentiate *de novo* from precursor cells (preadipocytes) already present in specific areas of WAT. The invariable anatomical pattern of beige cell abundance among WAT depots (Murano *et al.*, 2009) strongly suggests that beige preadipocytes mass is anatomically defined.

Wu *et al.* (2012) subcloned multiple adipose cell lines from immortalized stromal cells derived from subcutaneous inguinal WAT. Comparative transcriptomic analysis showed a subgroup of adipocytes that was more similar to classical brown adipocytes (iBAT) than to white adipocytes inside WAT (Wu *et al.*, 2012), suggesting that distinct classes of cell precursors may give rise to beige/brite cells whereas others remain committed to the white adipocyte lineage. In a clinically relevant result, the same authors found that adipocytes from biopsied BAT depots in healthy human volunteers had higher molecular similarity to murine beige/brite cells than to classic murine iBAT (high expression levels of beige markers cluster differentiation 127 (CD127), transmembrane protein 26 (TMEM26) and t-box 1 (TBX1), and lower levels of iBAT markers early B-cell factor 3 (EBF3), epithelial V-like antigen 1 (EVA1) and F-box only protein 31 (FBXO31) (Wu *et al.*, 2012).

Therefore, the most consolidated current evidence suggests that humans have at least two types of brown adipocytes: one is iBAT present in newborns and infants (Aherne & Hull, 1966; Lidell, Betz & Enerback, 2014) whereas the other corresponds to beige/brite adipose tissue, interspersed between the subcutaneous adipose tissue that surrounds the large blood vessels of the neck and supraclavicular space (Cypess *et al.*, 2009).

Nevertheless, very recent studies have found that this neat anatomical and ontogenic distinction might not be completely correct. In-depth transcriptional analysis of supraclavicular adipose tissue in humans showed simultaneous expression of markers from both iBAT [miR-206, miR-133b, lim homeobox gene 8 (LHX8), and zinc finger protein of cerebellum 1 (ZIC1)] and beige/brite adipocytes (TBX1 and TMEM26) (Jespersen *et al.*, 2013), suggesting either coexistence of these two classes of adipose cells in that depot or, alternatively, complex gene expression and regulation patterns in human BAT.

From a functional standpoint, it remains to be determined whether classical iBAT and beige/brite adipocytes have equivalent thermogenic potentials. Beyond the physiological implications of this definition, its importance lies in the fact that beige/brite adipocytes are the likely cellular substrate of all anti-obesity therapies based on BAT activation in humans. While no direct functional comparison between iBAT and beige/brite adipocytes is available, this question can be approached by considering the relative content of UCP1 in both tissues. It has been estimated that UCP1 corresponds to 5–8% of rat iBAT mitochondrial protein (Lin & Klingenberg, 1980). Analogous quantifications are not available for human BAT or beige/brite fat cells, nevertheless, analysis of intra-abdominal BAT in three patients with pheochromocytoma, in which neoplastic cells from the adrenal medulla secrete excessive amounts of catecholamines, revealed that UCP1 abundance in that adipose depot was similar to that in murine iBAT (~30 $\mu\text{g/g}$) (Lean *et al.*, 1986a). Importantly, the abundance of UCP1 in the BAT of normal individuals appears to be at least ten times lower than in pheochromocytoma-associated BAT (Lean *et al.*, 1986b), shedding doubts on the actual maximal thermogenic potential of BAT in adult humans as a therapeutic option for obesity. A more recent work studied UCP1 content in WAT depots of children subjected to major inflammatory and metabolic stress because of severe burning. A 37 ± 25 (mean \pm SD) days after burning, UCP1 content was ~8-fold higher in comparison with healthy control children (22.8 versus 2.7 $\mu\text{g/g}$) (Sidossis *et al.*, 2014). Supporting the molecular evidence of acute browning of WAT in humans, total mitochondrial functional mass (estimated by citrate synthase activity) and uncoupled respiration were ~4- and ~3-fold increased, respectively, in the WAT of late-burn in comparison with early-burn patients (Sidossis *et al.*, 2015).

The question of how stable beige/brite adipocytes are after browning induction is equally relevant with respect to future BAT-based therapies. To investigate the kinetics of browning processes, Rosenwald *et al.* (2013) exposed mice to 8°C for 7 days and then moved them to warm (23°C) housing conditions. Cold stimulation increased UCP1 mRNA and protein levels as well as other brown adipocyte markers, in subcutaneous (inguinal) but not in visceral (epididymal) WAT, indicating depot-specific browning. Importantly, they found that these phenotypic changes lasted for 5 weeks after moving animals to warm conditions (Rosenwald *et al.*, 2013). However, cell-lineage-tracing studies with a genetic labelling system that permanently tagged cells expressing UCP1 revealed that beige/brite cells persisted for at least 8 weeks after warm-housing adaptation, but this time with a white adipocyte phenotype (Rosenwald *et al.*, 2013), suggesting long-lasting remodelling of WAT in response to cold activation. Analogous results have been generated by other investigators, which have also revealed the critical role of β -adrenergic signalling (Chabowska-Kita *et al.*, 2015; Lee *et al.*, 2015) and the genetic background of the mice (Guerra

et al., 1998; Lasar *et al.*, 2013) for cold-induced browning activation.

VIII. WHITE AND BROWN ADIPOCYTES DERIVE FROM SPECIALIZED VASCULAR-WALL CELLS IN ADIPOSE DEPOTS

The ultimate origin of white and brown preadipocytes remains to be confirmed *in vivo* in humans. Cell-sorting-based methods successfully identified a small subset of stromal vascular cells in the WAT of mice that exhibits elevated adipogenic and proliferative potential *in vitro* (Rodeheffer, Birsoy & Friedman, 2008). Moreover, these cells have the ability to differentiate spontaneously into mature WAT in lipodystrophic mice *in vivo* (Rodeheffer *et al.*, 2008). Similarly, by ectopically expressing green fluorescent protein (GFP) under the transcriptional control of zinc finger protein 423 (*Zfp423*), a transcriptional regulator of white and brown adipogenic determination (Gupta *et al.*, 2010), it was demonstrated that a subset of capillary pericytes and endothelial cells (ECs) in mature and developing WAT or iBAT have characteristics of preadipocytes in mice (Gupta *et al.*, 2012). Supporting this notion, Tran *et al.* (2012) determined that murine ECs of both WAT and BAT have ultrastructural features of pericytes. By lineage-tracing experiments with VE-cadherin promoter-controlled reporters, these investigators found that these cells have molecular characteristics of preadipocytes, including *Zfp423* expression (Tran *et al.*, 2012). Lineage-tracing studies, using genetically labelled adipocyte progenitors with *lacZ* reporter gene under the transcriptional control of PPAR γ promoter in mice, confirmed that the vascular wall of adipose tissue capillaries is a physiological niche of adipocyte precursors (Tang *et al.*, 2008).

These findings agree with the hypothesis that adipose progenitors reside in or near capillary vessels in adipose tissue, however, they appear to contradict the idea of a common cellular progenitor for myocytes and brown adipocytes. Interestingly, a subgroup of cells in the murine dorsal aorta expresses myogenic and endothelial markers, including Myf5 and VE-cadherin (De Angelis *et al.*, 1999), suggesting that Myf5⁺ progenitor cells also reside in the capillary wall of both adipogenic and myogenic niches.

IX. BAT IS A SECRETORY ORGAN

BAT depletion by specific inactivation of the insulin receptor gene in UCP1-expressing adipocytes impairs insulin secretion and triggers diabetes with no associated changes in insulin resistance, WAT mass, or levels of circulating free fatty acids and triglycerides (Guerra *et al.*, 2001), suggesting that BAT can regulate β -cell function and mass, perhaps through still-unidentified secreted factors. Although these seminal findings have not yet been independently confirmed, they launched a search for new endocrine roles of BAT. Indeed,

brown adipocytes secrete several factors that influence critical tissues for metabolic regulation and that might help to explain the metabolic actions claimed for BAT activation (reviewed in Villarroya *et al.*, 2017).

(1) FGF21

Circulating fibroblast growth factor 21 (FGF21) is secreted by the liver (Markan *et al.*, 2014) and its physiological effects are mediated by fibroblast growth factor receptor 1 (FGFR1) and β -Klotho co-receptor (Ogawa *et al.*, 2007). Pharmacological administration of FGF21 decreases body mass, increases energy expenditure, and lowers blood glucose and insulin levels in mice and non-human primates (Gimeno & Moller, 2014). Active BAT and brite/beige adipocytes are able to release FGF21 (Chartoumpakis *et al.*, 2011; Lee *et al.*, 2014c). In humans, levels of circulating FGF21 correlate with BAT activity after acute exposure to cold (Hanssen *et al.*, 2015), suggesting that BAT-derived FGF21 could also reach the circulation. Nonetheless, it seems more plausible that adipose-derived FGF21 works as an autocrine/paracrine factor, increasing the expression of UCP1 and other thermogenic genes, and thus promoting browning (Fisher *et al.*, 2012; Lee *et al.*, 2014a).

(2) BMP8B

BMPs belong to the transforming growth factor β (TGF- β) superfamily and some members are relevant regulators of adipogenesis (Tseng *et al.*, 2008). BMP8B-deficient mice have a reduced metabolic rate and increased susceptibility to diet-induced obesity (Whittle *et al.*, 2012), suggesting a role for this protein in the regulation of BAT mass/activity. BMP8B is expressed in BAT mature adipocytes along with thermogenic markers and it enhances lipolysis in brown adipocytes *via* a P38 mitogen-activated protein kinase (MAPK)/CREB-dependent pathway (Whittle *et al.*, 2012). BMP8B also mediates WAT browning through mechanisms that rely on AMP-activated protein kinase (AMPK) inhibition and increased signalling through orexin receptor 1 in specific hypothalamic nuclei (Martins *et al.*, 2016).

(3) NRG4

Neuregulin 4 (NRG4) is a member of the epidermal growth factor (EGF) family and is expressed in the murine lung, heart, and adipose tissues, with the highest expression level in BAT (Pfeifer, 2015). NRG4 expression in BAT is increased by cold exposure (Rosell *et al.*, 2014) and its gene deletion determines increased body mass, insulin resistance and fatty liver production in mice (Wang *et al.*, 2014). Conversely, by hydrodynamic *in vivo* transfection, hepatic NRG4 overexpression prevents high-fat-diet-induced mass gain and decreases obesity-induced chronic inflammation and insulin resistance in mice (Ma, Gao & Liu, 2016). These and other results led to suggestions that NRG4 is a potential therapeutic tool to increase BAT in obesity,

although the relevance for this molecule in human BAT physiology remains unknown (Christian, 2015).

(4) VEGF-A

Vascular endothelial growth factor A (VEGF-A) is a key regulator of angiogenesis and tissue remodelling (Neufeld *et al.*, 1999). Its selective transgenic overexpression in white adipocytes increases vascularization, mitochondrial mass, UCP1 levels and thermogenic capacity in mice (Sun *et al.*, 2012). Transgenic overexpression of VEGF-A in classical brown adipocytes further increased UCP1 levels in iBAT and both basal and cold-stimulated non-shivering thermogenesis in mice (Sun *et al.*, 2014). Although the physiological translation of these results remains unknown, it is interesting to note that cold exposure increases iBAT angiogenesis in association with increased expression levels of VEGF-A, suggesting a role for VEGF-A in normal iBAT thermogenic capacity (Xue *et al.*, 2009) and WAT browning (Sun *et al.*, 2012).

(5) IL-6

Interleukin-6 (IL-6) is a proinflammatory cytokine produced by immune and non-immune cells, mainly in the skeletal muscle and adipose tissue; however, the role of this cytokine in obesity remains controversial (Ma *et al.*, 2015; Braune *et al.*, 2017). Interestingly, transplantation of BAT that is deficient in IL-6 prevents the metabolic benefits of increasing BAT mass in mice (Stanford *et al.*, 2013), suggesting that IL-6 is an essential mediator of BAT actions on insulin sensitivity and glucose regulation.

(6) RBP4

Retinol binding protein 4 (RBP4) is a serum protein involved in the transport of vitamin A and has been associated with insulin resistance in humans (Graham *et al.*, 2006). It is mainly produced by the liver and WAT (Asha *et al.*, 2016), and although it remains unknown whether it plays a pathogenic role in human insulin resistance, its transgenic overexpression or direct injection causes insulin resistance in mice (Yang *et al.*, 2005). To address the role of RBP4 in insulin resistance, Zemany *et al.* (2014) specifically deleted *Stra6*, the gene encoding the high-affinity receptor for RBP4, in white adipocytes. They found that *Stra6*-deficient mice were leaner and had increased energy expenditure relative to wild-type controls, in association with elevated UCP1 mRNA levels in WAT, suggesting enhanced browning (Zemany *et al.*, 2014). Intriguingly, it was described that BAT may contribute to RBP4 circulating levels *via* cAMP-, PPAR α - and PPAR γ -mediated pathways (Rosell *et al.*, 2012), however, the physiological significance of these findings remains unknown.

(7) IGF-1

Insulin like growth factor 1 (IGF-1) is produced by the liver in response to growth hormone and insulin stimulation. IGF-1

deficiency consistently associates with insulin resistance and therefore it is a prospective pharmacological target for this condition (reviewed in Aguirre *et al.*, 2016). In streptozotocin-induced diabetic mice, BAT transplantation results in higher IGF-1 levels and improved glucose regulation (Gunawardana & Piston, 2012), suggesting that BAT can be a physiological source of circulating IGF-1.

(8) miRNAs

Recent studies suggest that, in addition to their direct roles in adipogenesis, miRNAs can be secreted in exosomes by brown adipocytes and thus possibly exert regulatory roles in distant tissues (Zemany *et al.*, 2014). In vitro, adrenergic stimulation increases the release of miRNA-loaded exosomes by cultured murine brown adipocytes and iBAT explants by five- and ninefold, respectively (Chen *et al.*, 2016), indicating that miRNA secretion could be physiologically regulated. Adipocyte-specific gene deletion of DICER1, an enzyme necessary for the processing of miRNAs, results in lower levels of circulating exosomal miRNAs, indicating that BAT and WAT are physiological sources of miRNAs in the blood (Thomou *et al.*, 2017).

X. THE IMPORTANCE OF BAT FOR METABOLIC REGULATION

Mouse models of BAT (Lowell *et al.*, 1993) and UCP1 (Enerback *et al.*, 1997) ablation provided evidence that stimulated studies on the physiological role of BAT in energy homeostasis and body composition, particularly its roles in thermogenic adaptation to cold exposure.

Genotoxic deletion of brown adipocytes by transgenic expression of diphtheria toxin-A under the transcriptional control of UCP1 promoter resulted in overt obesity and insulin resistance in mice, importantly without changes in food intake (Lowell *et al.*, 1993). Interestingly, studies of UCP1-deficient mice did not replicate these results, shedding doubt on the functional role of UCP1-driven thermogenesis on body composition, since resting energy expenditure and body mass remained unaffected in mice lacking UCP1 (Enerback *et al.*, 1997).

Subsequent reports claimed that UCP1-deficient animals spontaneously developed obesity when housed under thermoneutral conditions ($\sim 30^{\circ}\text{C}$) (Feldmann *et al.*, 2009), possibly indicating that differences in metabolic efficiency, masked by 'normal' housing conditions ($18\text{--}22^{\circ}\text{C}$), may underlie the absence of obesity found by Enerback *et al.* (1997). However, other investigators could not replicate these findings. Liu *et al.* (2003) showed that in congenic C57BL/6J mice, a lack of UCP1 paradoxically resulted in protection from diet-induced obesity when the animals were housed at 20°C . This response is possibly due to the use of less metabolically efficient alternative mechanisms for non-shivering thermogenesis, as suggested by the fact that body mass differences were not observed when animals

were housed at thermoneutral conditions (Liu *et al.*, 2003; Anunciado-Koza *et al.*, 2008).

Therefore, it is currently thought that BAT-dependent thermogenesis can have at least two distinct functional roles: adaptive thermoregulation and metaboloregulation. Whereas the former has reached scientific consensus (Enerback *et al.*, 1997; Hofmann *et al.*, 2001; Meyer *et al.*, 2010), the latter, i.e. that BAT thermogenesis burns off excess calories in states of positive energy balance to maintain energy homeostasis and protect against obesity and insulin resistance, remains controversial (Kozak, 2010).

The known inverse correlation between BAT mass and total adiposity in humans (Cypess *et al.*, 2009; van Marken Lichtenbelt *et al.*, 2009; Saito *et al.*, 2009) favours the metaboloregulation hypothesis as does the observation that total mass of beige/brite adipocytes, which is strongly dependent on genetic factors (Almind *et al.*, 2007; Xue *et al.*, 2007), also inversely correlates with the susceptibility to develop obesity in mice (Almind *et al.*, 2007). In contradiction is the likelihood that obesity was a very rare condition in premodern humans, owing to food scarcity and elevated energy expenditure (Hayes *et al.*, 2005), therefore burning off excess calories by means of BAT activation is in clear conflict with evolutionary arguments.

Nevertheless, although the physiological actions of BAT on basal metabolic regulation are controversial, the capacity of activated BAT to generate heat by dissipating metabolic energy, either by cold exposure or adrenergic stimulation, and thus increase whole-body energy expenditure, is beyond doubt (Dawkins & Hull, 1964). In high-fat-fed mice, intermittent exposure to severe cold (4°C for 1–8 h, 3× a week for 10 weeks) consistently increases whole-body and iBAT heat generation but, since there are compensatory increases in food intake, no changes in body mass are detectable (Ravussin *et al.*, 2014). Notably, in spite of its lack of effects on body adiposity, cold exposure improves glucose tolerance and insulin sensitivity in obese mice (Ravussin *et al.*, 2014).

In agreement with the above observations, pharmacological β -adrenergic activation results in a substantial reduction of adiposity in rats, dogs and mice, likely by stimulating BAT-mediated energy dissipation (Robidoux, Martin & Collins, 2004) and BAT transplantation to genetically obese mice decreases body mass and hepatic steatosis, improves adipose tissue hypertrophy and inflammation, and increases whole-body insulin sensitivity (Liu *et al.*, 2015).

However, it is equally important to recognize that metaboloregulatory roles for BAT in humans remain hypothetical. Human populations have a broad distribution of BAT mass (as determined by FDG-PET-CT scan), which consistently correlates negatively with body adiposity. This association, combined with larger BAT mass in cold than in warm seasons (Saito *et al.*, 2009) and its acute activity regulation by cold exposure (van Marken Lichtenbelt *et al.*, 2009; Saito *et al.*, 2009), do suggest that BAT may be physiologically implicated in whole-body energy balance in humans. This has inspired the suggestion that the excessive

periods spent in thermoneutral environments in modern human populations is a determinant of obesity (Johnson *et al.*, 2011).

Blondin *et al.* (2015) showed that cold exposure can increase energy expenditure by 82% and raise plasma free fatty acid concentration by 1.4-fold in association with a 2.3-fold elevation of BAT oxidative activity in lean healthy men, suggesting that WAT lipolysis is physiologically linked to BAT metabolic activation and that BAT-dependent thermogenesis could be substantial in humans. Reinforcing the notion that BAT activity increases fat mobilization and oxidation in humans, Hibi *et al.* (2016) showed that patients with FDG-PET-CT-detectable BAT after acute exposure to cold have higher diet-induced thermogenesis and a lower respiratory quotient than subjects without detectable BAT.

It is noteworthy that in spite of these and analogous correlation-based studies, actual demonstrations of the physiological significance of BAT as a determinant of energy expenditure in adult humans are lacking.

XI. THE IMPACT OF BAT IN HUMAN HEALTH AND DISEASE

Besides its effects on body composition/mass regulation, BAT may have a direct impact on other determinants of disease in humans. This idea was inspired by the observation that pharmacological or genetic activation of BAT, or its surgical implantation, improve circulating levels of glucose (Stanford *et al.*, 2013), triglycerides (Bartelt *et al.*, 2011) and cholesterol (Berbée *et al.*, 2015) as well as whole-body insulin sensitivity (Cederberg *et al.*, 2001; Liu *et al.*, 2013; Stanford *et al.*, 2013) in mice, independently of significant changes in body mass. Whether these findings extrapolate to humans and can be used in clinical applications to treat diseases connected with obesity and insulin resistance remains to be determined. Important questions to be answered are: (i) what is the relative power of BAT activation to reduce both body adiposity and insulin resistance in comparison with currently available therapies, and (ii) what are the risks associated with chronic BAT activation?

XII. ACTIVATING BROWN ADIPOSE TISSUE THERMOGENESIS AS A TARGET TO INDUCE WEIGHT LOSS

The observed inverse correlation between body mass index and BAT activity (see Sections I and X) lead us to investigate the extent to which maximally activated BAT can influence whole-body energy expenditure. Eventually, enhanced thermogenesis may prevent weight gain (or even induce weight loss) if a compensatory increase in energy intake does not take place.

However, the precise mass and metabolic activity of human BAT remains undetermined. This is partly because

Table 2. Resting metabolic activity of principal organs in humans

Organ	Resting metabolic activity (kcal/kg/day)
Heart	440
Kidneys	440
Brain	240
Liver	200
Skeletal muscle	13
Adipose tissue	5
Residual mass	7

of the diffuse anatomical distribution of this tissue but also, because of great heterogeneity in published PET-CT-based detection protocols and intrinsic variability in BAT mass, even at the individual level (Pardo *et al.*, 2017). For example, in one study only considering individuals with FDG-PET-CT-detectable BAT (81 out of 1644 patients), the volume of BAT ranged between ~ 12 and ~ 300 ml; i.e. 11–285 g, assuming a tissue density of 0.95 g/ml in normal volunteers (Gerngross *et al.*, 2017). These authors suggested that the total mass of BAT could have been greatly underestimated, by a factor of ~ 4 , in adult humans and thus its total thermogenic capacity could also be underappreciated.

Classical studies have estimated that maximally activated BAT can produce up to 300 W/kg tissue of heat in comparison with 1–2 W/kg tissue by other organs (Power, 1989). If we speculate that whole-body metabolically active BAT is 2–3 times the mass reported in the supraclavicular and neck by FDG-PET of healthy adults (60 g) (Virtanen *et al.*, 2009) and assume that BAT may have a resting metabolic activity similar to the heart or the kidneys, the two organs with the highest reported resting metabolic activity in humans (Muller *et al.*, 2011) (Table 2), then total BAT mass (~ 180 g) should account for only ~ 80 kcal/day. Another calculation, taking a total BAT mass of ~ 200 g and a resting metabolic activity equivalent to the liver (Table 2) (Wang *et al.*, 2012), provides a thermogenic yield of only 40 kcal/day.

Our estimations of the contribution of BAT to whole-body thermogenesis is in sharp contrast with previous analyses based on animal findings (Rothwell & Stock, 1983; Rosenbaum & Leibel, 2010) that speculated that 50 g of maximally stimulated BAT could account for up to 20% of total energy expenditure in humans. For an adult human with a resting metabolic rate of 1500 kcal/day, 50 g of BAT therefore would account for an energy expenditure of 300 kcal/day, giving a specific metabolic activity of 6000 kcal/kg of BAT per day, or 13-fold higher than the resting metabolic activity of heart or kidneys which seems highly unlikely.

An absolute magnitude of dissipated energy of 40–80 kcal/day seems of negligible importance for long-term energy balance and body-mass determination (Weinsier, Bracco & Schutz, 1993; Butte & Ellis, 2003;

Swinburn *et al.*, 2006), although it may be that such small but persistent energy imbalances may have triggered the observed increased body mass of westernized populations over the last three decades (Hill, 2006).

A direct role of BAT on thermogenesis and body mass appears to be strongly limited by the small mass of this tissue and the seemingly low plausibility of maintaining BAT permanently activated for prolonged periods of time. Nonetheless, therapeutic activation of BAT could still be beneficial to metabolic health by increasing the clearance rate of circulating lipids and glucose and thus preventing ectopic toxic lipid buildup in tissues, which is a leading cause of insulin resistance (ter Horst *et al.*, 2017). It is also possible that BAT activation could increase whole-body energy expenditure beyond the limits imposed by its own mass by means of secreted factors that regulate thermogenesis in distant target tissues.

XIII. CONCLUSIONS

(1) The existence of BAT in infants has been known for a long time, but the demonstration of metabolically active BAT in adults was only documented in 2009. This finding has reinvigorated the investigation of different aspects of BAT, mainly driven by the expectation of developing new therapeutic tools against obesity.

(2) In small mammals, BAT-dependent thermogenesis is pivotal to prevent hypothermia; however, its physiological relevance in larger organisms, such as adult humans, remains uncertain. It has been proposed, mostly based on animal studies, that BAT may help to prevent or reverse excessive adiposity and improve glucose and triglyceride clearance from blood; however, direct and convincing evidence from human studies is lacking.

(3) The cellular lineage and the developmental pathways of BAT are diverse in humans. Interscapular BAT, which is abundant in newborns and infants, is similar to classical BAT of small rodents. By contrast, beige/brite adipose tissue, the most abundant form of BAT in adult humans, is developmentally closer to white adipose tissue. Recent findings suggest that both types of brown adipocytes can coexist in some BAT depots of adults.

(4) BAT can also secrete several protein and RNA factors that are likely to influence thermogenic activity by autocrine mechanisms or regulate insulin sensitivity in distant tissues by endocrine actions.

(5) Accurate quantification of the mass and specific thermogenic activity of BAT in living humans remains a technical challenge. Furthermore, metabolically active BAT detected by FDG-PET-CT methods seems to be highly variable, at both the inter-individual and individual level, possibly owing to intrinsic properties of this tissue but also to the high heterogeneity of the detection protocols used.

(6) Our estimation of the contribution of BAT to whole-body resting thermogenesis indicates that it is unlikely that BAT has a significant role in the determination of

Brown adipose tissue in health and disease

15

body adiposity in the long term, mostly due to its small relative mass and the difficulty of maintaining it in a state of continual maximal activation. Furthermore, it remains unknown whether this mode of activation, if feasible, has any adverse effects on human health.

XIV. ACKNOWLEDGEMENTS

Grant funding: Fondecyt 1141134 (V.A.C.), Fondecyt 1170117 (J.E.G.).

XV. REFERENCES

AGARWAL, A. K. & GARG, A. (2002). A novel heterozygous mutation in peroxisome proliferator-activated receptor- γ gene in a patient with familial partial lipodystrophy. *The Journal of Clinical Endocrinology and Metabolism* 87, 408–411.

AGUIRRE, G. A., DE ITA, J. R., DE LA GARZA, R. G. & CASTILLA-CORTAZAR, I. (2016). Insulin-like growth factor-1 deficiency and metabolic syndrome. *Journal of Translational Medicine* 14, 3.

AHERNE, W. & HULL, D. (1966). Brown adipose tissue and heat production in the newborn infant. *The Journal of Pathology and Bacteriology* 91, 223–234.

ALBERDI, G., RODRIGUEZ, V. M., MIRANDA, J., MACARULLA, M. T., CHURRUACA, I. & PORTILLO, M. P. (2015). Thermogenesis is involved in the body-fat lowering effects of resveratrol in rats. *Food Chemistry* 141, 1530–1535.

ALMIND, K., MANIERI, M., SVITZ, W. I., CINTI, S. & KAHN, C. R. (2007). Ectopic brown adipose tissue in muscle provides a mechanism for differences in risk of metabolic syndrome in mice. *Proceedings of the National Academy of Sciences of the United States of America* 104, 2366–2371.

ANUNCIADO-KOZA, R., UKROPEC, J., KOZA, R. A. & KOZAK, L. P. (2008). Inactivation of UCP1 and the glycerol phosphate cycle synergistically increases energy expenditure to resist diet-induced obesity. *The Journal of Biological Chemistry* 283, 27688–27697.

ARIAS, N., PICO, C., TERESA MACARULLA, M., OLIVER, P., MIRANDA, J., PALOU, A. & PORTILLO, M. P. (2017). A combination of resveratrol and quercetin induces browning in white adipose tissue of rats fed an obesogenic diet. *Obesity* 25, 111–121.

ASHA, G. V., RAJA GOPAL REDDY, M., MAHESH, M., VAJRESWARI, A. & JYAKUMAR, S. M. (2016). Male mice are susceptible to high fat diet-induced hyperglycaemia and display increased circulatory retinol binding protein 4 (RBP4) levels and its expression in visceral adipose depositions. *Archives of Physiology and Biochemistry* 122, 19–26.

ATTI, R., SGAIER, S. K., MOHAMED, O. A., TAKETO, M. M., DUFOUR, D., JOYNER, A. L., NISWANDER, L. & CONLON, R. A. (2006). Beta-catenin activation is necessary and sufficient to specify the dorsal dermal fate in the mouse. *Developmental Biology* 296, 164–176.

BAROOTA, R. K., SINGH, D. P., SARMA, S. M., KAUR, J., SANDHIR, R., BOPARAI, R. K., KONDEPUDI, K. K. & BISHNOI, M. (2014). Capsaicin induces “brite” phenotype in differentiating 3T3-L1 preadipocytes. *PLoS One* 9, e103093.

BACHMAN, E. S., DHILLON, H., ZHANG, C. Y., CINTI, S., BIANCO, A. C., KORILEK, B. K. & LOWELL, B. B. (2002). betaAR signaling required for diet-induced thermogenesis and obesity resistance. *Science* 297, 843–845.

BARAK, Y., NELSON, M. C., ONG, E. S., JONES, Y. Z., RUIZ-LOZANO, P., CHEN, K. R., KODER, A. & EVANS, R. M. (1999). PPAR gamma is required for placental, cardiac, and adipose tissue development. *Molecular Cell* 4, 585–595.

BARTELT, A., BRUNS, O. T., REIMER, R., HOHENBERG, H., ITRICHI, H., PELDSCHUS, K., KAUL, M. G., TROMSDORF, U. I., WELLER, H., WAURISCH, C., EYCHMULLER, A., GORDTS, P. L., RINNINGER, F., BRUEGELMANN, K., FREUND, B., NIELSEN, P., MERREL, M. & HEEREN, J. (2011). Brown adipose tissue activity controls triglyceride clearance. *Nature Medicine* 17, 200–205.

BEIROA, D., ISHIBRSON, M., GALLEGO, R., SENRA, A., HERRANZ, D., VILLARROYA, F., SERRANO, M., FERRO, J., SALVADOR, J., ESCALADA, J., DIEGUEZ, C., LOPEZ, M., FRUTIER, G. & NOGUEIRAS, R. (2014). GLP-1 agonist stimulates brown adipose tissue thermogenesis and browning through hypothalamic AMPK. *Diabetes* 63, 3346–3358.

BERRÉ, J. F. P., BOON, M. R., KHEDOE, P. S. J., BARTELT, A., SCHLEIN, C., WORTHIMANN, A., KOIJMAN, S., HOEK, G., MOL, I. M., JOHN, C., JUNG, C., VAZIRPANAHI, N., BROUWERS, L. P. J., GORDTS, P. L. S. M., ESKO, J. D., et al. (2015). Brown fat activation reduces hypercholesterolemia and protects from atherosclerosis development. *Nature Communications* 6, 6356.

BILLON, N., IANNARELLI, P., MONTEIRO, M. C., GLAVIEUX-PARDANAUD, C., RICHARDSON, W. D., KESSARIN, N., DANI, C. & DUPIN, E. (2007). The generation of adipocytes by the neural crest. *Development* 134, 2283–2292.

BIRERDING, A., JARRAR, M., STOTTISH, T., RANDHAWA, M. & BARANOVA, A. (2013). Manipulating molecular switches in brown adipocytes and their precursors: a therapeutic potential. *Progress in Lipid Research* 52, 51–61.

BLONDIN, D. P., LABRÉ, S. M., PHOENIX, S., GUÉRIEN, B., TURCOTTE, É. E., RICHARD, D., CARPENTIER, A. C. & HAMAN, F. (2015). Contributions of white and brown adipose tissues and skeletal muscles to acute cold-induced metabolic responses in healthy men. *The Journal of Physiology* 593, 701–714.

BJORCK, B. C., TURRIS-DOAN, A., PRYSAK, M., HERRON, B. J. & BEIER, D. R. (2010). Pcdh16 is required for normal palatogenesis in mice. *Human Molecular Genetics* 19, 774–789.

BOSTROM, P., WU, J., JEDRYCHOWSKI, M. P., KORBE, A. Y., LI, L., LO, J. C., RASBACH, K. A., BOSTROM, E. A., CHOI, J. H., LONG, J. Z., KAJIMURA, S., ZINGARETTI, M. C., VIND, B. F., TU, H., CINTI, S., HOJLUND, K., GYGI, S. P. & SPIEGELMAN, B. M. (2012). A PGC1- α -dependent myokine that drives brown-fat-like development of white fat and thermogenesis. *Nature* 481, 463–468.

BRAUNE, J., WEYER, U., HOBUSCH, C., MAUER, J., BRUNING, J. C., BECHMANN, I. & GERICK, M. (2017). IL-6 regulates M2 polarization and local proliferation of adipose tissue macrophages in obesity. *Journal of Immunology* 198, 2927–2934. <https://doi.org/10.4049/jimmunol.1600476>.

BROEDERS, E. P. M., NASCIMENTO, E. B. M., HAVEKEN, B., BRANS, B., ROUMANS, K. H. M., TAILLEUX, A., SCHAART, G., KOUACH, M., CHARTON, J., DEPREZ, B., BOUVY, N. D., MOTTAGHY, F., STALLS, B., VAN MARREN LICHTENELT, W. D. & SCHRAUWEN, P. (2015). The bile acid chenodeoxycholic acid increases human brown adipose tissue activity. *Cell Metabolism* 22, 418–426.

BUTTE, N. F. & ELLIS, K. J. (2003). Comment on “Obesity and the environment: where do we go from here?”. *Science* 301, 598 author reply 598.

CANNON, B. & NEDERGAARD, J. (1998). Brown adipose tissue thermogenesis in neonatal and cold-adapted animals. *Biochemical Society Transactions* 14, 233–236.

CANNON, B. & NEDERGAARD, J. (2004). Brown adipose tissue: function and physiological significance. *Physiological Reviews* 84, 277–359.

CASTILLA, I., FOREST, C., ROBELIN, J., RICQUIER, D., LOMBET, A. & AILHAUD, G. (1997). Characterization of mitochondrial uncoupling protein in bovine fetus and newborn calf. *The American Journal of Physiology* 272, E627–E636.

CAUTIVO, K. M., LIZAMA, C. O., TAPIA, P. J., AGARWAL, A. K., GARG, A., HORTON, J. D. & CORTÉS, V. A. (2016). AGPAT2 is essential for postnatal development and maintenance of white and brown adipose tissue. *Molecular Metabolism* 5, 491–505.

CEDEBERG, A., GRONNING, L. M., AHERNE, B., TANKEN, K., CARLSSON, P. & ENNERACK, S. (2001). FOXO2 is a winged helix gene that counteracts obesity, hypertriglyceridemia, and diet-induced insulin resistance. *Cell* 106, 563–573.

CHABOWSKA-KITA, A., TRARGZYNSKA, A., KORYTKO, A., KACZMAREK, M. M. & KOZAK, L. P. (2015). Low ambient temperature during early postnatal development fails to cause a permanent induction of brown adipocytes. *FASEB Journal* 29, 3238–3252.

CHIARTOMPERI, D. V., HAREKOS, I. G., ZIROS, P. G., PSYTHROGIANNIS, A. I., KYRIAZOPOULOU, V. E. & PAPAVALLELOU, A. G. (2011). Brown adipose tissue responds to cold and adrenergic stimulation by induction of FGF21. *Molecular Medicine* 17, 736–740.

CHAVEZ-TALAVERA, O., TAILLEUX, A., LEJEVRE, P. & STALLS, B. (2017). Bile acid control of metabolism and inflammation in obesity, type 2 diabetes, dyslipidemia, and nonalcoholic fatty liver disease. *Gastroenterology* 152, 1679–1694.

CHEN, Y., BUYEL, J. J., HANSSSEN, M. J., SIEGEL, F., PAN, R., NAUMANN, J., SCHELL, M., VAN DER LANS, A., SCHLEIN, C., FROELICHT, H., HEEREN, J., VIRTANEN, K. A., VAN MARREN LICHTENELT, W. & PYFFER, A. (2016). Exosomal microRNA miR-92a concentration in serum reflects human brown fat activity. *Nature Communications* 7, 11420.

CHOI, J. H. & YUN, J. W. (2016). Chrysin induces brown fat-like phenotype and enhances lipid metabolism in 3T3-L1 adipocytes. *Nutrition* 32, 1002–1010.

CHOI, S. S., KIM, E. S., JUNG, J. E., MARCIANO, D. P., JO, A., KOO, J. Y., CHOI, S. Y., YANG, Y. R., JANG, H. J., KIM, E. K., PARK, J., KWON, H. M., LEE, I. H., PARK, S. B., MYUNG, K. J., SUH, P. G., GRIFFIN, P. R. & CHOI, J. H. (2016a). PPARgamma antagonist gleevec improves insulin sensitivity and promotes the browning of white adipose tissue. *Diabetes* 65, 829–839.

CHOI, W. H., AHN, J., JUNG, C. H., JANG, Y. J. & HA, T. Y. (2016b). Beta-lapachone prevents diet-induced obesity by increasing energy expenditure and stimulating the browning of white adipose tissue via downregulation of miR-382 expression. *Diabetes* 65, 2490–2501.

CHONDRONIKOLA, M., VOLPI, E., BÖRSHEIM, E., PORTER, C., ANNAMALAI, P., ENNERÄCK, S., LIDL, M. E., SARAF, M. K., LABRÉ, S. M., HURREN, N. M., FYANT, C., CHAO, T., ANDERSEN, C. R., CESANI, F., HAWKINS, H. & SIDOSSIS, I. S. (2014). Brown adipose tissue improves whole-body glucose homeostasis and insulin sensitivity in humans. *Diabetes* 63, 4089–4099.

CHONDRONIKOLA, M., VOLPI, E., BÖRSHEIM, E., PORTER, C., SARAF, M. K., ANNAMALAI, P., FYANT, C., CHAO, T., WONG, D., SHINODA, K., LABRÉ, S. M., HURREN, N. M., CESANI, F., KAJIMURA, S. & SIDOSSIS, I. S. (2016). Brown adipose

- tissue activation is linked to distinct systemic effects on lipid metabolism in humans. *Cell Metabolism* 23, 1200–1206.
- CHRISTIAN, M. (2015). Transcriptional fingerprinting of "browning" white fat identifies NRG4 as a novel adipokine. *Adipocytes* 4, 50–54.
- CINTI, S. (2009). Transdifferentiation properties of adipocytes in the adipose organ. *American Journal of Physiology, Endocrinology and Metabolism* 297, E977–E986.
- COHEN, P., LEVY, J. D., ZHANG, Y., FRONTINI, A., KOLODNY, D. P., SVENSSON, K. J., LO, J. C., ZENG, X., YE, L., KHANDEKAR, M. J., WU, J., GUNAWARDANA, S. C., BANKS, A. S., CAMPOREZ, J. P. G., JURCZAK, M. J., KAJIMURA, S., PISTON, D. W., MATHIS, D., CINTI, S., SHULMAN, G. I., SEALE, P. & SPIEGELMAN, B. M. (2014). Ablation of PRDM16 and beige adipose causes metabolic dysfunction and a subcutaneous to visceral fat switch. *Cell* 156, 304–316.
- CONNOLLY, E., NANBERG, E. & NEDERGAARD, J. (1996). Norepinephrine-induced Na^+ influx in brown adipocytes is cyclic AMP-mediated. *The Journal of Biological Chemistry* 261, 14377–14385.
- CORTÉS, V. A., CURTIS, D. E., SUKUMARAN, S., SHAO, X., PARAMESWARA, V., RASHID, S., SMITH, A. R., REN, J., ESSER, V., HAMMER, R. E., AGARWAL, A. K., HORTON, J. D. & GARG, A. (2009). Molecular mechanisms of hepatic steatosis and insulin resistance in the AGPAT2-deficient mouse model of congenital generalized lipodystrophy. *Cell Metabolism* 9, 165–176.
- CRUZ, K. J., DE OLIVEIRA, A. R., MORAIS, J. B., SEVERO, J. S. & MARREIRO PII, D. D. (2017). Role of microRNAs on adipogenesis, chronic low-grade inflammation, and insulin resistance in obesity. *Nutrition* 35, 28–35.
- CYPRESS, A. & KAHN, C. (2010). Brown fat as a therapy for obesity and diabetes. *Current Opinion in Endocrinology, Diabetes, and Obesity* 17, 143–149.
- CYPRESS, A., LEIDMAN, S., WILLIAMS, G., TAL, L., RODMAN, D., GOLDFINE, A., KUO, F., PALMER, E., TSENG, Y. & DORIA, A. (2009). Identification and importance of brown adipose tissue in adult humans. *The New England Journal of Medicine* 360, 1509–1517.
- CYPRESS, A. M., CHEN, Y. C., SZE, C., WANG, K., ENGLISH, J., CHAN, O., HOLMAN, A. R., TAL, L., PALMER, M. R., KOLODNY, G. M. & KAHN, C. R. (2012). Cold but not sympathomimetics activates human brown adipose tissue in vivo. *Proceedings of the National Academy of Sciences of the United States of America* 109, 10001–10005.
- DAWKINS, M. J. & HULL, D. (1964). Brown adipose tissue and the response of newborn rabbits to cold. *The Journal of Physiology* 172, 216–238.
- DE ANGELIS, L., BERGHELLA, L., COLETTA, M., LATTANZI, L., ZANCI, M., CUSILLA-DE ANGELIS, M. G., PONZETTO, C. & COSSU, G. (1999). Skeletal myogenic progenitors originating from embryonic dorsal aorta coexpress endothelial and myogenic markers and contribute to postnatal muscle growth and regeneration. *The Journal of Cell Biology* 147, 869–878.
- DE MATTIIS, R., ZINGARETTI, M. C., MURANO, I., VITALI, A., FRONTINI, A., GIANNULI, I., BARBATELLI, G., MARCUCCI, F., BORDICCHIA, M., SARZANI, R., RAVIOLA, E. & CINTI, S. (2009). *In vivo* physiological transdifferentiation of adult adipose cells. *Stem Cells* 27, 2761–2768.
- DIGBY, J. E., MONTAGUE, C. T., SEWTER, C. P., SANDERS, L., WILKINSON, W. O., RAHILLY, S. & PRINS, J. B. (1998). Thiazolidinedione exposure increases the expression of uncoupling protein 1 in cultured human preadipocytes. *Diabetes* 47, 138.
- ENERBACK, S. (2010). Human brown adipose tissue. *Cell Metabolism* 11, 248–252.
- ENERBACK, S., JACOBSSON, A., SIMPSON, E. M., GUERRA, C., YAMASHITA, H., HARPER, M. E. & KOZAK, L. P. (1997). Mice lacking mitochondrial uncoupling protein are cold-sensitive but not obese. *Nature* 387, 90–94.
- FELDMANN, H. M., GOLOZOUBOVA, V., CANNON, B. & NEDERGAARD, J. (2009). UCP1 ablation induces obesity and abolishes diet-induced thermogenesis in mice exempt from thermal stress by living at thermoneutrality. *Cell Metabolism* 9, 203–209.
- FISHER, F. M., KLEINER, S., DOURIS, N., FOX, E. C., MEPANI, R. J., VERDEGUE, F., WU, J., KHARTONENKOV, A., FLIER, J. S., MARATOS-FLIER, E. & SPIEGELMAN, B. M. (2012). FGF21 regulates PGC-1 α and browning of white adipose tissues in adaptive thermogenesis. *Genes & Development* 26, 271–281.
- FOLGUEIRA, C., BEIROA, D., CALLON, A., AL-MASSADI, O., BARJA-FERNANDEZ, S., SENRA, A., FERRO, J., LOPEZ, M., DIEGUEZ, C., CASANUEVA, F. F., ROHNER-JEANRENAUD, F., SEDANE, L. M. & NOGUEIRAS, R. (2016). Uroguanylin action in the brain reduces weight gain in obese mice via different efferent autonomic pathways. *Diabetes* 65, 421–432.
- FRONTINI, A. & CINTI, S. (2010). Distribution and development of brown adipocytes in the murine and human adipose organ. *Cell Metabolism* 11, 253–256.
- FUKU, Y., MASUI, S., OSADA, S., UMESONO, K. & MOTOJIMA, K. (2000). A new thiazolidinedione, NC-2100, which is a weak PPAR- γ agonist, exhibits potent antidiabetic effects and induces uncoupling protein 1 in white adipose tissue of KK Ay obese mice. *Diabetes* 49, 759–767.
- GRUBIC, V., CAWTHORN, W. P., NEDERGAARD, J., TIMMONS, J. A. & CANNON, B. (2012). An essential role for Thr15 in the differentiation of brown and "brite" but not white adipocytes. *American Journal of Physiology, Endocrinology and Metabolism* 303, E1053–E1060.
- GERNGROSS, C., SCHRETTNER, J., KLINGENSPOR, M., SCHWABER, M. & FROMMELT, T. (2017). Active brown fat during 18FDG-PET/CT imaging defines a patient group with characteristic traits and an increased probability of brown fat rededuction. *Journal of Nuclear Medicine* 58, 1104–1110.
- GESTA, S., TSENG, Y. H. & KAHN, C. R. (2007). Developmental origin of fat: tracking obesity to its source. *Cell* 131, 242–256.
- GIMENO, R. E. & MOLLER, D. E. (2014). FGF21-based pharmacotherapy—potential utility for metabolic disorders. *Trends in Endocrinology and Metabolism* 25, 303–311.
- GIROUD, M., PISANI, D. F., KARRIENER, M., BARQUINSAU, V., GHANDOUR, R. A., TEWS, D., FISCHER-POSOVSZKY, P., CHAMBAUD, J. C., KNIPPSCHILD, U., NIEMI, T., TAITTONEN, M., NUUTILA, P., WABITSCH, M., HERZIG, S., VIRTANEN, K. A., LANGEN, D., SCHEIDLER, M. & AMRI, E. Z. (2016). miR-125b affects mitochondrial biogenesis and impairs brite adipocyte formation and function. *Molecular Metabolism* 5, 615–625.
- GRAHAM, T. E., YANG, Q., BLUHER, M., HAMMARSTEDT, A., CIARALDI, T. P., HENRY, R. R., WASON, C. J., OBERBACH, A., JANSSON, P. A., SMITH, U. & KAHN, B. B. (2006). Retinobinding protein 4 and insulin resistance in lean, obese, and diabetic subjects. *The New England Journal of Medicine* 354, 2552–2563.
- GRANNEMAN, J. G., LI, P., ZHU, Z. & LI, Y. (2005). Metabolic and cellular plasticity in white adipose tissue I: effects of beta3-adrenergic receptor activation. *American Journal of Physiology, Endocrinology and Metabolism* 289, E608–E616.
- GUERRA, C., KOZA, R. A., YAMASHITA, H., WALSH, K. & KOZAK, L. P. (1998). Emergence of brown adipocytes in white fat in mice is under genetic control. Effects on body weight and adiposity. *The Journal of Clinical Investigation* 102, 412–420.
- GUERRA, C., NAVARRO, P., VALVERDE, A. M., ARRIBAS, M., BRUNING, J., KOZAK, L. P., KAHN, C. R. & BENITO, M. (2001). Brown adipose tissue-specific insulin receptor knockout shows diabetic phenotype without insulin resistance. *The Journal of Clinical Investigation* 108, 1205–1213.
- GUNAWARDANA, S. C. & PISTON, D. W. (2012). Reversal of type 1 diabetes in mice by brown adipose tissue transplant. *Diabetes* 61, 674–682.
- GUPTA, R. K., ARANY, Z., SEALE, P., MEPANI, R. J., YE, L., CONROE, H. M., ROBY, Y. A., KULAGA, H., REED, R. R. & SPIEGELMAN, B. M. (2010). Transcriptional control of preadipocyte determination by Zfp423. *Nature* 464, 619–623.
- GUPTA, R. K., MEPANI, R. J., KLEINER, S., LO, J. C., KHANDEKAR, M. J., COHEN, P., FRONTINI, A., BHOWMICK, D. C., YE, L., CINTI, S. & SPIEGELMAN, B. M. (2012). Zfp423 expression identifies committed preadipocytes and localizes to adipose endothelial and perivascular cells. *Cell Metabolism* 15, 230–239.
- HAN, Y., WU, J. Z., SHEN, J. Z., CHEN, L., HE, T., JIN, M. W. & LIU, H. (2017). Pentamethylpterostein induces adipose browning and exerts beneficial effects in 3T3-L1 adipocytes and high-fat diet-fed mice. *Scientific Reports* 7, 1123.
- HANSEN, M. J., BROEDERS, E., SAMMS, R. J., VONSELNAN, M. J., VAN DER LANS, A. A., CHENG, C. C., ADAMS, A. C., VAN MARREN LICHTENHELT, W. D. & SCHRAUWEN, P. (2015). Serum FGF21 levels are associated with brown adipose tissue activity in humans. *Scientific Reports* 5, 10275.
- HASTY, P., BRADLEY, A., MORRIS, J. H., EDMONDSON, D. G., VENUTTI, J. M., OLSON, E. N. & KLEIN, W. H. (1993). Muscle deficiency and neonatal death in mice with a targeted mutation in the myogenin gene. *Nature* 364, 501–506.
- HAUSBERGER, F. X. (1934). Über die innervation der Fettorgane. *Zeitschrift für Mikroskopisch-Anatomische Forschung* 36, 231–266.
- HAUSBERGER, F. X. (1955). Quantitative studies on the development of autotransplants of immature adipose tissue of rats. *The Anatomical Record* 122, 507–515.
- HAYS, M., CHUNTER, M., HESHKA, S., WANG, Z., PIETROBELLI, A. & HEYMSFIELD, S. B. (2005). Low physical activity levels of modern *Homo sapiens* among free-ranging mammals. *International Journal of Obesity* 29, 151–156.
- HE, W., BARAK, Y., HEYNER, A., OLSON, P., LIAO, D., LE, J., NELSON, M., ONG, E., OLEFSKY, J. M. & EVANS, R. M. (2003). Adipose-specific peroxisome proliferator-activated receptor γ knockout causes insulin resistance in fat and liver but not in muscle. *Proceedings of the National Academy of Sciences of the United States of America* 100, 15712–15717.
- HEATON, J. M. (1972). The distribution of brown adipose tissue in the human. *Journal of Anatomy* 112, 35–39.
- HENSELBARTH, N., PETTINELLI, C., GERBICK, M., BERGER, C., KUNATH, A., STUMVOLL, M., BLUHER, M. & KLÖTING, N. (2015). Tardosifen affects glucose and lipid metabolism parameters, causes browning of subcutaneous adipose tissue and transient body composition changes in C57BL/6NTac mice. *Biochemical and Biophysical Research Communications* 464, 724–729.
- HIBI, M., OISHI, S., MATSUHITA, M., YONESHIRO, T., YAMAGUCHI, T., USUI, C., YASUNAGA, K., KATSURAGI, Y., KUBOTA, K., TANAKA, S. & SATTO, M. (2016). Brown adipose tissue is involved in diet-induced thermogenesis and whole-body fat utilization in healthy humans. *International Journal of Obesity* 40, 1655–1661.
- HILL, J. O. (2006). Understanding and addressing the epidemic of obesity: an energy balance perspective. *Endocrine Reviews* 27, 750–761.
- HIMMS-HAGEN, J., MELNYK, A., ZINGARETTI, M. C., CERESI, E., BARBATELLI, G. & CINTI, S. (2000). Multilocular fat cells in WAT of CL-316243-treated rats derive directly from white adipocytes. *American Journal of Physiology, Cell Physiology* 279, C670–C681.
- HOFMANN, W. E., LIU, X., BEARDEN, C. M., HARPER, M. E. & KOZAK, L. P. (2001). Effects of genetic background on thermoregulation and fatty acid-induced

- uncoupling of mitochondria in UCP1-deficient mice. *The Journal of Biological Chemistry* 276, 12460–12465.
- TER HORST, K. W., GILJAMSE, P. W., VERSTEEG, R. I., ACKERMANN, M. T., NEDERVEEN, A. J., LA FLEUR, S. E., ROMIJN, J. A., NIEUWDOORP, M., ZHANG, D., SAMUEL, V. T., VATNER, D. F., PETERSEN, K. F., SHULMAN, G. I. & SERLIE, M. J. (2017). Hepatic diacylglycerol-associated protein kinase ζ translocation links hepatic steatosis to hepatic insulin resistance in humans. *Cell Reports* 19, 1997–2004.
- JENSEN, N. Z., LARSEN, T. J., PEIJS, L., DAUGAARD, S., HOMOE, P., LOFT, A., DE JONG, J., MATHUR, N., CANNON, B., NEDERGAARD, J., PEDERSEN, B. K., MOLLER, K. & SCHELLE, C. (2013). A classical brown adipose tissue mRNA signature partly overlaps with brite in the supraclavicular region of adult humans. *Cell Metabolism* 17, 798–805.
- JIMENEZ-ARANDA, A., FERNANDEZ-VAZQUEZ, G., CAMPOS, D., TASSI, M., VELASCO-PEREZ, I., TAN, D. X., REITER, R. J. & AGUI, A. (2013). Melatonin induces browning of inguinal white adipose tissue in Zucker diabetic fatty rats. *Journal of Pineal Research* 55, 416–423.
- JOHNSON, F., MAVROGIANNI, A., UCCI, M., VIDAL-PUIG, A. & WARDLE, J. (2011). Could increased time spent in a thermal comfort zone contribute to population increases in obesity? *Obesity Reviews* 12, 543–551.
- KAJIMURA, S., SEALE, P., KUBOTA, K., LUNSFORD, E., FRANGIONI, J. V., GYGI, S. P. & SPIEGELMAN, B. M. (2009). Initiation of myoblast to brown fat switch by a PRDM16/C/EBP β transcriptional complex. *Nature* 460, 1154–1158.
- KAJIMURA, S., SEALE, P. & SPIEGELMAN, B. M. (2010). Transcriptional control of brown fat development. *Cell Metabolism* 11, 257–262.
- KELLY, L. J., VICARIO, P. P., THOMPSON, G. M., CANDELORE, M. R., DOEBBER, T. W., VENTRE, J., WU, M. S., MEURER, R., FORREST, M. J., CONNER, M. W., CASCIARI, M. A. & MOLLER, D. E. (1998). Peroxisome proliferator-activated receptors gamma and alpha mediate *in vivo* regulation of uncoupling protein (UCP-1, UCP-2, UCP-3) gene expression. *Endocrinology* 139, 4920–4927.
- KIM, H. J., CHO, H., ALEXANDER, R., PATTERSON, H. C., GU, M., LO, K. A., XU, D., GOH, V. J., NGUYEN, L. N., CHAI, X., HUANG, C. X., KOVALIK, J. P., GHOSH, S., TRAJKOVSKI, M., SILVER, D. L., LODISH, H. & SUN, L. (2014). MicroRNAs are required for the feature maintenance and differentiation of brown adipocytes. *Diabetes* 63, 4045–4056.
- KIM, S. W., CHOI, J. H., MUKHERJEE, R., HWANG, K. C. & YUN, J. W. (2016). Proteomic identification of fat-browning markers in cultured white adipocytes treated with curcumin. *Molecular and Cellular Biochemistry* 415, 51–66.
- KOUTNIKOVA, H., COCK, T. A., WATANABE, M., HOUTEN, S. M., CHAMPY, M. F., DIERICH, A. & ALTWATER, J. (2003). Compensation by the muscle limits the metabolic consequences of lipodystrophy in PPAR gamma hypomorphic mice. *Proceedings of the National Academy of Sciences of the United States of America* 100, 14457–14462.
- KOZAK, L. P. (2010). Brown fat and the myth of diet-induced thermogenesis. *Cell Metabolism* 11, 263–267.
- LASAR, D., JULIUS, A., FROMME, T. & KLINGENSPOR, M. (2013). Browning attenuates murine white adipose tissue expansion during postnatal development. *Biochimica et Biophysica Acta* 1831, 960–968.
- LEAN, M. E., JAMES, W. P., JENNINGS, G. & TRAYHURN, P. (1986a). Brown adipose tissue in patients with pheochromocytoma. *International Journal of Obesity* 10, 219–227.
- LEAN, M. E., JAMES, W. P., JENNINGS, G. & TRAYHURN, P. (1986b). Brown adipose tissue uncoupling protein content in human infants, children and adults. *Clinical Science* 71, 291–297.
- LEE, J.-Y., TAKAHASHI, N., YASUBUCHI, M., KIM, Y.-I., HASHIZAKI, H., KIM, M.-J., SARAMOTO, T., GOTO, T. & KAWADA, T. (2012). Triiodothyronine induces UCP-1 expression and mitochondrial biogenesis in human adipocytes. *American Journal of Physiology—Cell Physiology* 302, C463–C472.
- LEE, P., LINDERMAN, J. D., SMITH, S., BRYCHTA, R. J., WANG, J., IDELSON, C., PERRON, R. M., WERNER, C. D., PHAN, G. Q., KAMMULA, U. S., KERREW, E., PACAK, K., CHEN, K. Y. & CELI, F. S. (2014a). Irisin and FGF21 are cold-induced endocrine activators of brown fat function in humans. *Cell Metabolism* 19, 302–309.
- LEE, P., SMITH, S., LINDERMAN, J., COURVILLE, A. B., BRYCHTA, R. J., DIECKMANN, W., WERNER, C. D., CHEN, K. Y. & CELI, F. S. (2014b). Temperature-acclimated brown adipose tissue modulates insulin sensitivity in humans. *Diabetes* 63, 3686–3698.
- LEE, P., WERNER, C. D., KERREW, E. & CELI, F. S. (2014c). Functional thermogenic beige adipogenesis is inducible in human neck fat. *International Journal of Obesity* 38, 170–176.
- LEE, Y. H., PETROVA, A. P., KONKAR, A. A. & GRANNEMAN, J. G. (2013). Cellular origins of cold-induced brown adipocytes in adult mice. *FASEB Journal* 29, 286–299.
- LEFFEROVA, M. I. & LAZAR, M. A. (2009). New developments in adipogenesis. *Trends in Endocrinology and Metabolism* 20, 107–114.
- LIDELL, M. E., BETZ, M. J. & ENNERBACK, S. (2014). Two types of brown adipose tissue in humans. *Adipocytes* 3, 63–66.
- LIN, C. S. & KLINGENBERG, M. (1980). Isolation of the uncoupling protein from brown adipose tissue mitochondria. *FEBS Letters* 113, 299–303.
- LIU, L., JIANG, Q., WANG, X., ZHANG, Y., LIN, R. C., LAM, S. M., SHUI, G., ZHOU, L., LI, P., WANG, Y., CHU, X., GAO, M., ZHANG, L., LV, Y., XU, G., LIU, G., ZHAO, D. & YANG, H. (2014). Adipose-specific knockout of *Seipin/Bcl2* results in progressive lipodystrophy. *Diabetes* 63, 2320–2331.
- LIU, X., ROSSMEISL, M., McCLAIN, J. & KOZAK, L. P. (2003). Paradoxical resistance to diet-induced obesity in UCP1-deficient mice. *The Journal of Clinical Investigation* 111, 399–407.
- LIU, X., WANG, S., YOU, Y., MENG, M., ZHENG, Z., DONG, M., LIN, J., ZHAO, Q., ZHANG, C., YUAN, X., HU, T., LIU, L., HUANG, Y., ZHANG, L., WANG, D., ZHAN, J., JONG LEE, H., SPEAKMAN, J. R. & JIN, W. (2015). Brown adipose tissue transplantation reverses obesity in Ob/Ob Mice. *Endocrinology* 156, 2461–2469.
- LIU, X., ZHENG, Z., ZHU, X., MENG, M., LI, L., SHEN, Y., CHU, Q., WANG, D., ZHANG, Z., LI, C., LI, Y., XUE, Y., SPEAKMAN, J. R. & JIN, W. (2013). Brown adipose tissue transplantation improves whole-body energy metabolism. *Cell Research* 23, 851–854.
- LOCKIE, S. H., HEPPNER, K. M., CHAUDHARY, N., CHARENNE, J. R., MORGAN, D. A., VEYRAT-DUREBEX, C., ANANTHAKRISHNAN, G., ROHNER-JEANRENAUD, F., DRUCKER, D. J., DiMARCHI, R., RAHMOUNI, K., Oldfield, B. J., TSCHOP, M. H. & PEREZ-TILVE, D. (2012). Direct control of brown adipose tissue thermogenesis by central nervous system glucagon-like peptide-1 receptor signaling. *Diabetes* 61, 2753–2762.
- LONE, J. & YUN, J. W. (2016). Monoterpene limonene induces brown fat-like phenotype in 3T3-L1 white adipocytes. *Life Sciences* 153, 198–206.
- LOWELL, B. B. & BACHMAN, E. S. (2003). Beta-Adrenergic receptors, diet-induced thermogenesis, and obesity. *The Journal of Biological Chemistry* 278, 29385–29388.
- LOWELL, B. B. & SPIEGELMAN, B. M. (2000). Towards a molecular understanding of adaptive thermogenesis. *Nature* 404, 652–660.
- LOWELL, B. B., S-SUSULIC, V., HAMANN, A., LAWITTS, J. A., HIMMS-HAGEN, J., BOYER, B. B., KOZAK, L. P. & FLIER, J. S. (1993). Development of obesity in transgenic mice after genetic ablation of brown adipose tissue. *Nature* 366, 740–742.
- MA, Y., GAO, M. & LIU, D. (2016). Preventing high fat diet-induced obesity and improving insulin sensitivity through neuregulin 4 gene transfer. *Scientific Reports* 6, 26242. <https://doi.org/10.1038/srep26242>.
- MA, Y., GAO, M., SUN, H. & LIU, D. (2015). Interleukin-6 gene transfer reverses body weight gain and fatty liver in obese mice. *Biochimica et Biophysica Acta* 1852, 1001–1011.
- MARKAN, K. R., NABER, M. C., AMEKA, M. K., ANDEREGG, M. D., MANGELSDORF, D. J., KLEWER, S. A., MOHAMMADI, M. & POTTHOFF, M. J. (2014). Circulating FGF21 is liver derived and enhances glucose uptake during refeeding and overfeeding. *Diabetes* 63, 4057–4063.
- VAN MARKEN LICHTENBELT, W. D., VANHOMMERIG, J. W., SMAILERS, N. M., DROSSAERTS, J. M., KEMERINK, G. J., BOUYV, N. D., SCHRAUWEN, P. & TEULE, G. J. (2009). Cold-activated brown adipose tissue in healthy men. *The New England Journal of Medicine* 360, 1500–1508.
- MARTAGÓN, A. J., LIN, J. Z., CIMINI, S. L., WEBB, P. & PHILLIPS, K. J. (2015). The amelioration of hepatic steatosis by thyroid hormone receptor agonists is insufficient to restore insulin sensitivity in Ob/Ob mice. *PLoS One* 10, e0122987.
- MARTÍNEZ-SÁNCHEZ, N., MORENO-NAVARETTE, J. M., CONTRERAS, C., RIAL-PENSADO, E., FERNO, J., NOGUEIRAS, R., DEGUÉZ, C., FERNÁNDEZ-REAL, J.-M. & LÓPEZ, M. (2017). Thyroid hormones induce browning of white fat. *Journal of Endocrinology* 232, 351–362.
- MARTINS, L., SEDANO-COLLAZO, P., CONTRERAS, C., GONZALEZ-GARCIA, I., MARTINEZ-SANCHEZ, N., GONZALEZ, F., ZALVIDE, J., GALLEGO, R., DIEGUEZ, C., NOGUEIRAS, R., TENA-SEMPERE, M. & LOPEZ, M. (2016). A functional link between AMPK and orexin mediates the effect of BMP8B on energy balance. *Cell Reports* 16, 2231–2242.
- MATSUKAWA, T., VILLAREAL, M. O., MOTOJIMA, H. & ISODA, H. (2017). Increasing cAMP levels of preadipocytes by cyanidin-3-glucoside treatment induces the formation of beige phenotypes in 3T3-L1 adipocytes. *The Journal of Nutritional Biochemistry* 40, 77–85.
- MERKLIN, R. J. (1974). Growth and distribution of human fetal brown fat. *The Anatomical Record* 178, 637–645.
- MEYER, C. W., WILLERSHAUSER, M., JASTROCH, M., ROUBICE, B. C., FROMME, T., OELKRUG, R., HELDMAIER, G. & KLINGENSPOR, M. (2010). Adaptive thermogenesis and thermal conductance in wild-type and UCP1-KO mice. *American Journal of Physiology* 299, R1396–R1406.
- MORI, M. A., THOMAS, T., BOUCHER, J., LEE, K. Y., LALLUKKA, S., KIM, J. K., TORRIANI, M., YKI-JARVINEN, H., GRINSPOON, S. K., CYPRESS, A. M. & KAHN, C. R. (2014). Altered miRNA processing disrupts brown/white adipocyte determination and associates with lipodystrophy. *The Journal of Clinical Investigation* 124, 3339–3351.
- MORRONI, M., GIORDANO, A., ZINGARETTI, M. C., BOIANI, R., DE MATTEIS, R., KAHN, B. B., NESOLI, E., TONELLO, C., PISOSCHI, C., LUCHETTI, M. M., MARELLI, M. & CINTI, S. (2004). Reversible transdifferentiation of secretory epithelial cells into adipocytes in the mammary gland. *Proceedings of the National Academy of Sciences of the United States of America* 101, 16801–16806.

- MULLER, M. J., LANGEMANN, D., GEHRKE, I., LATER, W., HELLER, M., GLUER, C. C., HEYMSFIELD, S. B. & BOSY-WESTPHAL, A. (2011). Effect of constitution on mass of individual organs and their association with metabolic rate in humans—a detailed view on allometric scaling. *PLoS One* 6, e22732.
- MURANO, I., BARRATELLI, G., GIORDANO, A. & CINTI, S. (2009). Noradrenergic parenchymal nerve fiber branching after cold acclimatisation correlates with brown adipocyte density in mouse adipose organ. *Journal of Anatomy* 214, 171–178.
- MZILIKAZI, N., JASTROCH, M., MEYER, C. W. & KLINGENSPOR, M. (2007). The molecular and biochemical basis of nonshivering thermogenesis in an African endemic mammal, *Elephantulus nyanus*. *American Journal of Physiology* 293, R2120–R2127.
- NAGATA, N., XU, L., KOHNO, S., USHIDA, Y., AOKI, Y., UMEMA, R., FUKU, N., ZHUGE, F., NI, Y., NAGASHIMADA, M., TAKAHASHI, C., SUGANUMA, H., KANEKO, S. & OYA, T. (2017). Glucocorticoid ameliorates obesity and insulin resistance through adipose tissue browning and reduction of metabolic endotoxaemia in mice. *Diabetes* 66, 1222–1236.
- NEDERGAARD, J. & CANNON, B. (2010). The changed metabolic world with human brown adipose tissue: therapeutic visions. *Cell Metabolism* 11, 268–272.
- NEDERGAARD, J., PETROVIC, N., LINDGREN, E. M., JACOBSSON, A. & CANNON, B. (2005). PPAR γ in the control of brown adipocyte differentiation. *Biochimica et Biophysica Acta* 1740, 293–304.
- NEUFELD, G., COHEN, T., GENGRINOVITCH, S. & POLTORAK, Z. (1999). Vascular endothelial growth factor (VEGF) and its receptors. *FASEB Journal* 13, 9–22.
- NISHIKAWA, S., AOYAMA, H., KAMIYA, M., HIGUCHI, J., KATO, A., SOGA, M., KAWAI, T., YOSHIMURA, K., KUMAZAWA, S. & TSUDA, T. (2016). Artepillin c, a typical brazilian propolis-derived component, induces brown-like adipocyte formation in c3h10t1/2 cells, primary inguinal white adipose tissue-derived adipocytes, and mice. *PLoS One* 11, e0162512.
- OGAWA, Y., KUROKI, H., YAMAMOTO, M., NANDI, A., ROSENBLATT, K. P., GOETZ, R., ELISEENKOVA, A. V., MOHAMMADI, M. & KURO-O, M. (2007). BetaKlotho is required for metabolic activity of fibroblast growth factor 21. *Proceedings of the National Academy of Sciences of the United States of America* 104, 7432–7437.
- OHNO, H., SHINODA, K., OHYAMA, K., SHARP, L. Z. & KAJIMURA, S. (2013). EHMT1 controls brown adipocyte cell fate and thermogenesis through the PRDM16 complex. *Nature* 504, 163–167.
- OHNO, H., SHINODA, K., SPIEGELMAN, B. M. & KAJIMURA, S. (2012). PPAR γ agonists induce a white-to-brown fat conversion through stabilization of PRDM16 protein. *Cell Metabolism* 15, 395–404.
- OLDFIELD, B. J., GILES, M. E., WATSON, A., ANDERSON, C., COLVILL, L. M. & MCKINLEY, M. J. (2002). The neurochemical characterisation of hypothalamic pathways projecting polysynaptically to brown adipose tissue in the rat. *Neuroscience* 110, 515–526.
- OUELLET, V., LABRÉ, S. M., BLONDIN, D. P., PHOENIX, S., GUÉRIN, B., HAMAN, F., TURCOTT, E. E., RICHARD, D. & CARPENTIER, A. C. (2012). Brown adipose tissue oxidative metabolism contributes to energy expenditure during acute cold exposure in humans. *The Journal of Clinical Investigation* 122, 545–552.
- PAREDO, J. V., LEE, J. T., LARSON, R. C., THURAS, P. & LARSON, A. A. (2017). Automated quantification of cold-inducible human brown adipose tissue with FDG PET/CT with application to fibromyalgia. *American Journal of Nuclear Medicine and Molecular Imaging* 7, 24–32.
- PARK, J. H., KANG, H. J., KANG, S. I., LEE, J. E., HUR, J., GE, K., MUELLER, E., LI, H., LEE, B. C. & LEE, S. B. (2013). A multifunctional protein, EWS, is essential for early brown fat lineage determination. *Developmental Cell* 26, 393–404.
- PAREY, H. A. & YUN, J. W. (2016). Cannabidiol promotes browning in 3T3-L1 adipocytes. *Molecular and Cellular Biochemistry* 416, 131–139.
- PFYFER, A. (2015). NRG4: an endocrine link between brown adipose tissue and liver. *Cell Metabolism* 21, 13–14.
- POLLIDORI, D., SANGHVI, A., SEELEY, R. J. & HALL, K. D. (2016). How strongly does appetite counter weight loss? Quantification of the feedback control of human energy intake. *Obesity* 24, 2289–2295.
- POWELL, G. G. (1989). Biology of temperature: the mammalian fetus. *Journal of Developmental Physiology* 12, 295–304.
- PUGSENYER, P., WU, Z., PARK, C. W., GRAVES, R., WRIGHT, M. & SPIEGELMAN, B. M. (1998). A cold-inducible coactivator of nuclear receptors linked to adaptive thermogenesis. *Cell* 92, 829–839.
- QIANG, L., WANG, L., KON, N., ZHAO, W., LEE, S., ZHANG, Y., ROSENBAUM, M., ZHAO, Y., GU, W., FARMER, S. R. & ACCILI, D. (2012). Brown remodeling of white adipose tissue by SirT1-dependent deacetylation of Ppargamma. *Cell* 150, 620–632.
- RASMUSSEN, A. T. (1923). The so-called hibernating gland. *Journal of Morphology* 38, 147–205.
- RAVUSSEN, Y., XIAO, C., GAVRILOVA, O. & REITMAN, M. L. (2014). Effect of intermittent cold exposure on brown fat activation, obesity, and energy homeostasis in mice. *PLoS One* 9, e85876.
- RIBEIRO, M. O., CARVALHO, S. D., SCHULTZ, J. J., CHIPELLINI, G., SCANLAN, T. S., BIANCO, A. C. & BRENT, G. A. (2001). Thyroid hormone–sympathetic interaction and adaptive thermogenesis are thyroid hormone receptor isoform-specific. *The Journal of Clinical Investigation* 108, 97–105.
- ROBERTS, I. D., BOKTHOM, P., O'SULLIVAN, J. F., SCHINZEL, R. T., LEWIS, G. D., DEJAM, A., LEE, Y. K., PALMA, M. J., CALHOON, S., GEORGIADI, A., CHEN, M. H., RAMACHANDRAN, V. S., LARSON, M. G., BOUCHARD, C., RANKINEN, T., et al. (2014). Beta-aminoisobutyric acid induces browning of white fat and hepatic beta-oxidation and is inversely correlated with cardiometabolic risk factors. *Cell Metabolism* 19, 96–108.
- ROBIDOUX, J., MARTIN, T. L. & COLLINS, S. (2004). Beta-adrenergic receptors and regulation of energy expenditure: a family affair. *Annual Review of Pharmacology and Toxicology* 44, 297–323.
- RODEHEFFER, M. S., BIRSOY, K. & FRIEDMAN, J. M. (2008). Identification of white adipocyte progenitor cells *in vivo*. *Cell* 135, 240–249.
- RONA, G. (1964). Changes in adipose tissue accompanying pheochromocytoma. *Canadian Medical Association Journal* 91, 303–305.
- ROSELLI, M., HONDARES, E., IWAMOTO, S., GONZALEZ, F. J., WARTSCH, M., STALLS, B., OLMO, Y., MONSALVE, M., GIRALT, M., IGLESIAS, R. & VILLARROYA, F. (2012). Peroxisome proliferator-activated receptors- α and - γ , and cAMP-mediated pathways, control retinoid-binding protein-4 gene expression in brown adipose tissue. *Endocrinology* 153, 1162–1173.
- ROSELLI, M., KAFOROU, M., FRONTINI, A., OKOLO, A., CHAN, Y. W., NIKOLOPOULOU, E., MILLERSHIP, S., FENCICH, M. E., MACINTYRE, D., TURNER, J. O., MOORE, J. D., BLACKBURN, E., GULLICK, W. J., CINTI, S., MONTANA, G., PARKER, M. G. & CHRISTIAN, M. (2014). Brown and white adipose tissues: intrinsic differences in gene expression and response to cold exposure in mice. *American Journal of Physiology, Endocrinology and Metabolism* 306, E945–E964.
- ROSEN, E. & MACDOUGALD, O. (2006). Adipocyte differentiation from the inside out. *Nature Reviews Molecular Cell Biology* 7, 885–896.
- ROSEN, E. D., SARRAF, P., TROY, A. E., BRADWIN, G., MOORE, K., MILSTONE, D. S., SPIEGELMAN, B. M. & MORTENSEN, R. M. (1999). PPAR γ is required for the differentiation of adipose tissue *in vivo* and *in vitro*. *Molecular Cell* 4, 611–617.
- ROSENBAUM, M. & LEIBEL, R. L. (2010). Adaptive thermogenesis in humans. *International Journal of Obesity* 34(Suppl. 1), S47–S55.
- ROSENWALD, M., PERDIKARI, A., RULICKE, T. & WOLFRUM, C. (2013). Bi-directional interconversion of brite and white adipocytes. *Nature Cell Biology* 15, 659–667.
- ROTHWELL, N. J. & STOCK, M. J. (1983). Luxuskonsumption, diet-induced thermogenesis and brown fat: the case in favour. *Clinical Science* 64, 19–23.
- SAITO, M., OKAMATSU-OGURA, Y., MATSUSHITA, M., WATANABE, K., YONESHIRO, T., NIO-KOBAYASHI, J., IWANAGA, T., MIYAGAWA, M., KAMIYA, T., NAKADA, K., KAWAI, Y. & TSUJIMAKI, M. (2009). High incidence of metabolically active brown adipose tissue in healthy adult humans: effects of cold exposure and adiposity. *Diabetes* 58, 1526–1531.
- SEALE, P., BJORK, B., YANG, W., KAJIMURA, S., CHIN, S., KUANG, S., SCIME, A., DEVARAKONDA, S., CONROE, H. M., ERDJUMENT-BROMAGE, H., TEMPT, P., RUDNICKI, M. A., BEIER, D. R. & SPIEGELMAN, B. M. (2008). PRDM16 controls a brown fat/skeletal muscle switch. *Nature* 454, 961–967.
- SEALE, P., KAJIMURA, S., YANG, W., CHEN, S., ROHAS, L. M., ULDRY, M., TAVERNIER, G., LANGIN, D. & SPIEGELMAN, B. M. (2007). Transcriptional control of brown fat determination by PRDM16. *Cell Metabolism* 6, 38–54.
- SEARS, I. B., MACGINNITTE, M. A., KOVACS, L. G. & GRAVES, R. A. (1996). Differentiation-dependent expression of the brown adipocyte uncoupling protein gene: regulation by peroxisome proliferator-activated receptor gamma. *Molecular and Cellular Biology* 16, 3410–3419.
- SHELDON, E. F. (1924). The so-called hibernating gland in mammals: a form of adipose tissue. *The Anatomical Record* 28, 331–347.
- SHEN, W., CHUANG, C. C., MARTINEZ, K., REID, T., BROWN, J. M., XI, L., HINSON, L., HOPKINS, R., STARNES, J. & MCINTOSH, M. (2013). Conjugated linoleic acid reduces adiposity and increases markers of browning and inflammation in white adipose tissue of mice. *Journal of Lipid Research* 54, 909–922.
- SIDOSSIS, I., PORTER, C., SARAF, M., CHAO, T., FINNERTY, C., CHONDRONIKOLA, M., BORNHEIM, E., HAWKINS, H. & HERNDON, D. (2014). Browning of subcutaneous white adipose tissue in humans after severe adrenergic stress (1160.5). *The FASEB Journal* 28. <http://www.fasebj.org/content/28/1/1160.5>
- SIDOSSIS, I. S., PORTER, C., SARAF, M. K., BORNHEIM, E., RADHAKRISHNAN, R. S., CHAO, T., ALI, A., CHONDRONIKOLA, M., MILCAR, R., FINNERTY, C. C., HAWKINS, H. K., TOLIVER-KINSKY, T. & HERNDON, D. N. (2015). Browning of subcutaneous white adipose tissue in humans. *Cell Metabolism* 22, 219–227.
- SKARULIS, M. C., CELI, F. S., MUELLER, E., ZEMSKOVA, M., MALEK, R., HUGENDUBLER, L., COCHRAN, C., SOLOMON, J., CHEN, C. & GORDEN, P. (2010). Thyroid hormone induced brown adipose tissue and amelioration of diabetes in a patient with extreme insulin resistance. *The Journal of Clinical Endocrinology & Metabolism* 95, 256–262.
- SONG, N. J., CHOI, S., RAJBHANDARI, P., CHANG, S. H., KIM, S., VERGNES, L., KWON, S. M., YOON, J. H., LEE, S., KU, J. M., LEE, J. S., REUI, K., KOO, S. H.,

- TONTONOV, P. & PARK, K. W. (2016). Prdm16 induction by the small molecule butein promotes white adipose tissue browning. *Nature Chemical Biology* 12, 479–481.
- SPEARMAN, J. R. & O'RAHILLY, S. (2012). Fat: an evolving issue. *Diabetic Medicine & Metabolism* 5, 569–573.
- SPIEGELMAN, B. M. (2013). Banting lecture 2012: regulation of adipogenesis: toward new therapeutics for metabolic disease. *Diabetes* 62, 1774–1782.
- STANFORD, K. L., MIDDLEBEEK, R. J., TOWNSEND, K. L., AN, D., NYGAARD, E. B., HITCHCOX, K. M., MARKAN, K. R., NAKANO, K., HIRSHMAN, M. F., TSENG, Y. H. & GOODYEAR, L. J. (2013). Brown adipose tissue regulates glucose homeostasis and insulin sensitivity. *The Journal of Clinical Investigation* 123, 215–223.
- SUN, K., KUSMINSKI, C. M., LUBY-PHELPS, K., SPURGIN, S. B., AN, Y. A., WANG, Q. A., HOLLAND, W. L. & SCHIERER, P. E. (2014). Brown adipose tissue derived VEGF-A modulates cold tolerance and energy expenditure. *Molecular Metabolism* 3, 474–483.
- SUN, K., WERNSTEDT-ÅSTERHOLM, I., KUSMINSKI, C. M., BUENO, A. C., WANG, Z. V., POLLARD, J. W., BRÆKKE, R. A. & SCHIERER, P. E. (2012). Dichotomous effects of VEGF-A on adipose tissue dysfunction. *Proceedings of the National Academy of Sciences of the United States of America* 109, 5874–5879.
- SUN, L., XIE, H., MORI, M. A., ALEXANDER, R., YUAN, B., HATTANGADI, S. M., LIU, Q., KAHN, C. R. & LODISH, H. F. (2011). Mir193b-365 is essential for brown fat differentiation. *Nature Cell Biology* 13, 958–965.
- SUNDEIN, U., MILLS, I. & FAIR, J. N. (1984). Thyroid-catecholamine interactions in isolated rat brown adipocytes. *Metabolism: Clinical and Experimental* 33, 1028–1033.
- SWINBURN, B. A., JOLLEY, D., KREMER, P. J., SALBE, A. D. & RAVUSSIN, E. (2006). Estimating the effects of energy imbalance on changes in body weight in children. *The American Journal of Clinical Nutrition* 83, 859–863.
- TAN, D. X., MANCHESTER, L. C., FUENTES-BROTO, L., PAREDES, S. D. & REITER, R. J. (2011). Significance and application of melatonin in the regulation of brown adipose tissue metabolism: relation to human obesity. *Obesity Reviews* 12, 167–188.
- TANG, W., ZEVE, D., SUI, J. M., BOSNAKOVSKI, D., KYBA, M., HAMMER, R. E., TALLQVIST, M. D. & GRAFF, J. M. (2008). White fat progenitor cells reside in the adipose vasculature. *Science* 322, 583–586.
- THOMAS, C., AUVIER, J. & SCHOONJANS, K. (2009). Bile acids and the membrane bile acid receptor TGR5—connecting nutrition and metabolism. *Thyroid* 18, 167–174.
- THOMAS, S. A. & PALMITER, R. D. (1997). Thermoregulatory and metabolic phenotypes of mice lacking noradrenaline and adrenaline. *Nature* 387, 94–97.
- THOMOU, T., MORI, M. A., DREYFUSS, J. M., KONISHI, M., SAKAGUCHI, M., WOLFRUM, C., RAO, T. N., WENNA, J. N., GARCIA-MARTIN, R., GREENSPAN, S. K., GORDEN, P. & KAHN, C. R. (2017). Adipose-derived circulating miRNAs regulate gene expression in other tissues. *Nature* 542, 450–455.
- TIMMONS, J. A., WENNEMALM, K., LARSSON, O., WALDEN, T. B., LASSMANN, T., PETROVIC, N., HAMILTON, D. L., GIMENO, R. E., WAHLESTEDT, C., BAAK, K., NEDERGAARD, J. & CANNON, B. (2007). Myogenic gene expression signature establishes that brown and white adipocytes originate from distinct cell lineages. *Proceedings of the National Academy of Sciences of the United States of America* 104, 4401–4406.
- TONTONOV, P., HU, E. & SPIEGELMAN, B. M. (1994). Stimulation of adipogenesis in fibroblasts by PPAR gamma 2, a lipid-activated transcription factor. *Cell* 79, 1147–1156.
- TONTONOV, P. & SPIEGELMAN, B. M. (2008). Fat and beyond: the diverse biology of PPARgamma. *Annual Review of Biochemistry* 77, 289–312.
- TRAJKOVSKI, M., AHMED, K., ESAU, C. C. & STOFFEL, M. (2012). MyomiR-133 regulates brown fat differentiation through Prdm16. *Nature Cell Biology* 14, 1330–1335.
- TRAN, K.-V., GALEKMAN, O., FRONTINI, A., ZINGARETTI, M. C., MORIYANI, M., GIORDANO, A., SMORLES, A., PERUGINI, J., DE MATTEIS, R., SERRATI, A., CORVERA, S. & CINTI, S. (2012). The vascular endothelium of the adipose tissue gives rise to both white and brown fat cells. *Cell Metabolism* 15, 222–229.
- TSENG, Y. H., KOKKOTOU, E., SCHULZ, T. J., HUANG, T. L., WINNAY, J. N., TANGUCHI, C. M., TRAN, T. T., SUZUKI, R., ESPINOZA, D. O., YAMAMOTO, Y., AHRENS, M. J., DUDLEY, A. T., NORRIS, A. W., KULKARNI, R. N. & KAHN, C. R. (2008). New role of bone morphogenetic protein 7 in brown adipogenesis and energy expenditure. *Nature* 454, 1000–1004.
- VILLANUEVA, C. J., VERGNES, L., WANG, J., DREW, B. G., HONG, C., TU, Y., HU, Y., PENG, X., XU, F., SAEZ, E., WROBLEWSKI, K., HEYNER, A. L., REIF, K., FONG, L. G., YOUNG, S. G. & TONTONOV, P. (2013). Adipose subtype-selective recruitment of TLE3 or Prdm16 by PPARgamma specifies lipid storage versus thermogenic gene programs. *Cell Metabolism* 17, 423–435.
- VILLARROVA, F., CERREJO, R., VILLARROVA, J. & GREALT, M. (2017). Brown adipose tissue as a secretory organ. *Nature Reviews. Endocrinology* 13, 26–35.
- VIRTANEN, K., LIDELL, M., ORAVA, J., HEGGLIND, M., WESTERGRÉN, R., NIEMI, T., TAITTONEN, M., LAINE, J., SAVISTO, N., ENERBACK, S. & NUUTILA, P. (2009). Functional brown adipose tissue in healthy adults. *The New England Journal of Medicine* 360, 1518–1525.
- VOSSELMAN, M. J., VAN DER LANS, A. A., BRANS, B., WIERTS, R., VAN BAAK, M. A., SCHIRAUWEN, P. & VAN MARREN LICHTENBELT, W. D. (2012). Systemic β -adrenergic stimulation of thermogenesis is not accompanied by brown adipose tissue activity in humans. *Diabetes* 61, 3106–3113.
- WALDEN, T. B., TIMMONS, J. A., KELLER, P., NEDERGAARD, J. & CANNON, B. (2009). Distinct expression of muscle-specific microRNAs (myomiRs) in brown adipocytes. *Journal of Cellular Physiology* 218, 444–449.
- WANG, G. X., ZHAO, X. Y., MENG, Z. X., KERN, M., DIETRICH, A., CHEN, Z., COZACOV, Z., ZHOU, D., OKUNADE, A. L., SU, X., LI, S., BLUHER, M. & LIN, J. D. (2014). The brown fat-enriched secreted factor Nrg1 preserves metabolic homeostasis through attenuation of hepatic lipogenesis. *Nature Medicine* 20, 1436–1443.
- WANG, H., LIU, L., LIN, J. Z., APRAHAMIAN, T. R. & FARMER, S. R. (2016). Browning of white adipose tissue with rosiglitazone induces a distinct population of UCP1+ adipocytes. *Cell Metabolism* 24, 835–847.
- WANG, Q. A. & SCHIERER, P. E. (2014). The AdipoChaser mouse: a model tracking adipogenesis *in vivo*. *Adipocytes* 3, 146–150.
- WANG, S., LIANG, X., YANG, Q., FU, X., ROGERS, C. J., ZHU, M., RODGERS, B. D., JIANG, Q., DOBSON, M. V. & DU, M. (2015). Resveratrol induces brown-like adipocyte formation in white fat through activation of AMP-activated protein kinase (AMPK) alpha 1. *International Journal of Obesity* 39, 967–976.
- WANG, Z., YING, Z., BOSNY-WESTPHAL, A., ZHANG, J., HELLER, M., LATZ, W., HEYMSFIELD, S. B. & MÜLLER, M. J. (2012). Evaluation of specific metabolic rates of major organs and tissues: comparison between nonobese and obese women. *Obesity* 20, 95–100.
- WANKHADE, U. D., SHEN, M., YADAV, H. & THAKALI, K. M. (2016). Novel browning agents, mechanisms, and therapeutic potentials of brown adipose tissue. *BioMed Research International* 2016, 2365609. <https://doi.org/10.1155/2016/2365609>.
- WATANABE, M., HOUTEN, S. M., MATSUKI, C., CHRISTOFOLITTE, M. A., KIM, B. W., SATO, H., MESSADDEQ, N., HARNETT, J. W., EZARI, O., KODAMA, T., SCHOONJANS, K., BIANCO, A. C. & AUWERX, J. (2006). Bile acids induce energy expenditure by promoting intracellular thyroid hormone activation. *Nature* 439, 484–489.
- WEINER, R. L., BRACCO, D. & SCHUTZ, Y. (1993). Predicted effects of small decreases in energy expenditure on weight gain in adult women. *International Journal of Obesity and Related Metabolic Disorders* 17, 693–700.
- WELLS, J. C. (2006). The evolution of human fatness and susceptibility to obesity: an ethnological approach. *Biological Reviews of the Cambridge Philosophical Society* 81, 183–205.
- WHITTLE, A. J., CAROBBIO, S., MARTINS, L., SLAWIK, M., HONDARES, E., VAZQUEZ, M. J., MORGAN, D., CSIKASZ, R. L., GALLEGO, R., RODRIGUEZ-CUENCA, S., DALE, M., VIRTUE, S., VILLARROVA, F., CANNON, B., RAHMOUNI, K., LOPEZ, M. & VIDAL-PEIG, A. (2012). BMP8B increases brown adipose tissue thermogenesis through both central and peripheral actions. *Cell* 149, 871–885.
- WILSON-FRITZCH, L., NICOLORO, S., CHOUINAUD, M., LAZAR, M. A., CHUI, P. C., LESZYK, J., STRAUBHAAR, J., CZECH, M. P. & CORVERA, S. (2004). Mitochondrial remodeling in adipose tissue associated with obesity and treatment with rosiglitazone. *The Journal of Clinical Investigation* 114, 1281–1289.
- World Health Organization (2017). Obesity and overweight – Fact sheet. Available at <http://www.who.int/mediacentre/factsheets/fs311/en/>. Accessed October 29, 2017.
- WU, J., BOSTROM, P., SPARKS, L. M., YE, L., CHOI, J. H., GIAN, A. H., KHANDEKAR, M., VIRTANEN, K. A., NUUTILA, P., SCHAART, G., HUANG, K., TU, H., VAN MARREN LICHTENBELT, W. D., HOEKES, J., ENERBACK, S., SCHIRAUWEN, P. & SPIEGELMAN, B. M. (2012). Beige adipocytes are a distinct type of thermogenic fat cell in mouse and human. *Cell* 150, 366–376.
- WU, Y., ZUO, J., ZHANG, Y., XIE, Y., HU, F., CHEN, L., LIU, B. & LIU, F. (2013). Identification of miR-106b-93 as a negative regulator of brown adipocyte differentiation. *Biochemical and Biophysical Research Communications* 438, 575–580.
- XUE, B., RIM, J. S., HOGAN, J. C., COULTER, A. A., KOZA, R. A. & KOZAK, L. P. (2007). Genetic variability affects the development of brown adipocytes in white fat but not in interscapular brown fat. *Journal of Lipid Research* 48, 41–51.
- XUE, Y., PETROVIC, N., CAO, R., LARSSON, O., LIM, S., CHEN, S., FELDMANN, H. M., LIANG, Z., ZHU, Z., NEDERGAARD, J., CANNON, B. & CAO, Y. (2009). Hypoxia-independent angiogenesis in adipose tissues during cold acclimation. *Cell Metabolism* 9, 99–109.
- YANG, Q., GRAHAM, T. E., MODY, N., PREITNER, F., PERONI, O. D., ZAROLOITNY, J. M., KOTANI, K., QUADRO, L. & KAHN, B. B. (2005). Serum retinol binding protein 4 contributes to insulin resistance in obesity and type 2 diabetes. *Nature* 436, 356–362.
- YEH, W. C., CAO, Z., CLASSON, M. & MCKNIGHT, S. L. (1995). Cascade regulation of terminal adipocyte differentiation by three members of the C/EBP family of leucine zipper proteins. *Genes & Development* 9, 168–181.
- YONESHIRO, T., AITA, S., KAWAI, Y., IWANAGA, T. & SAITO, M. (2012). Nonpungent capsaicin analogs (capsinoids) increase energy expenditure through the activation of brown adipose tissue in humans. *The American Journal of Clinical Nutrition* 95, 845–850.
- YONESHIRO, T., AITA, S., MATSUSHITA, M., KATAYAMA, T., KAMEYA, T., KAWAI, Y., IWANAGA, T. & SAITO, M. (2013). Recruited brown adipose tissue as an antidiabetic agent in humans. *The Journal of Clinical Investigation* 123, 3404–3408.

- ZEMANY, L., KRAUS, B. J., NORSEEN, J., SATTO, T., PERONI, O. D., JOHNSON, R. L. & KAHN, B. B. (2014). Downregulation of *strab* in adipocytes and adipose stromovascular fraction in obesity and effects of adipocyte-specific STRA6 knockdown *in vivo*. *Molecular and Cellular Biology* **34**, 1170–1186.
- ZHANG, Y., LI, R., MENG, Y., LI, S., DONELAN, W., ZHAO, Y., QI, L., ZHANG, M., WANG, X., CUI, T., YANG, L.-J. & TANG, D. (2014). Irisin stimulates browning of white adipocytes through mitogen-activated protein kinase p38 MAP kinase and ERK MAP kinase signaling. *Diabetes* **63**, 514.
- ZHOU, Y., YANG, J., HUANG, J., LI, T., XU, D., ZUO, B., HOU, L., WU, W., ZHANG, L., XIA, X., MA, Z., REN, Z. & XIONG, Y. (2014). The formation of brown adipose tissue induced by transgenic over-expression of PPARgamma2. *Biochemical and Biophysical Research Communications* **446**, 959–964.

(Received 18 May 2017; revised 10 November 2017; accepted 14 November 2017)



AGPAT2 is essential for postnatal development and maintenance of white and brown adipose tissue

Kelly M. Cautivo^{1,2,3}, Carlos O. Lizama⁴, Pablo J. Tapia¹, Anil K. Agarwal⁵, Abhimanyu Garg⁵, Jay D. Horton^{2,3,*}, Victor A. Cortés^{1,*}

ABSTRACT

Objective: Characterize the cellular and molecular events responsible for lipodystrophy in AGPAT2 deficient mice.

Methods: Adipose tissue and differentiated MEF were assessed using light and electron microscopy, followed by protein (immunoblots) and mRNA analysis (qPCR). Phospholipid profiling was determined by electrospray ionization tandem mass spectrometry (ESI-MS/MS).

Results: In contrast to adult *Agpat2*^{-/-} mice, fetuses and newborn *Agpat2*^{-/-} mice have normal mass of white and brown adipose tissue. Loss of both the adipose tissue depots occurs during the first week of postnatal life as a consequence of adipocyte death and inflammatory infiltration of the adipose tissue. At the ultrastructural level, adipose tissue of newborn *Agpat2*^{-/-} mice is virtually devoid of caveolae and has abnormal mitochondria and lipid droplets. Autophagic structures are also abundant. Consistent with these findings, differentiated *Agpat2*^{-/-} mouse embryonic fibroblasts (MEFs) also have impaired adipogenesis, characterized by a lower number of lipid-laden cells and ultrastructural abnormalities in lipid droplets, mitochondria and plasma membrane. Overexpression of PPAR γ , the master regulator of adipogenesis, increased the number of *Agpat2*^{-/-} MEFs that differentiated into adipocyte-like cells but did not prevent morphological abnormalities and cell death. Furthermore, differentiated *Agpat2*^{-/-} MEFs have abnormal phospholipid compositions with 3-fold increased levels of phosphatidic acid.

Conclusion: We conclude that lipodystrophy in *Agpat2*^{-/-} mice results from postnatal cell death of adipose tissue in association with acute local inflammation. It is possible that AGPAT2 deficient adipocytes have an altered lipid filling or a reduced capacity to adapt the massive lipid availability associated with postnatal feeding.

© 2016 The Authors. Published by Elsevier GmbH. This is an open access article under the CC BY-NC-ND license (<http://creativecommons.org/licenses/by-nc-nd/4.0/>).

Keywords AGPAT2; Adipose tissue; Adipogenesis; Phospholipid; Lipodystrophy

1. INTRODUCTION

Congenital generalized lipodystrophy (CGL, Berardinelli-Seip syndrome) is a rare autosomal recessive disorder characterized by a lack of adipose tissue (AT). Affected individuals are prone to metabolic complications including insulin resistance, diabetes mellitus, hepatic steatosis and hypertriglyceridemia [1,2].

Mutations in the *AGPAT2* gene, encoding 1-acylglycerol-3-phosphate O-acyltransferase 2, cause the most common form of CGL, designated CGL-1 [3]. Patients with CGL-1 have total absence of metabolically active adipose tissue, which is present in most subcutaneous regions, intra-abdominal and intra-thoracic regions and bone marrow; mechanical adipose tissue, which is present in the palms, soles, scalp, peri-articular regions and orbits, is completely preserved [4]. Similarly,

mice lacking AGPAT2 (*Agpat2*^{-/-} mice) have complete loss of both white and brown adipose tissue and manifest severe insulin resistance and hyperglycemia [5,6]. The mechanisms underlying the loss of adipose tissue in *Agpat2*^{-/-} mice remain unknown.

AGPAT2 belongs to a family of enzymes catalyzing the *sn*-2 acylation of the glycerol-3-phosphate backbone. This reaction converts lysophosphatidic acid (LPA) to phosphatidic acid (PA) in the *de novo* glycerolipid synthesis pathway [7]. In humans and mice, AGPAT2 is a ~31 kDa protein with four predicted transmembrane domains [8] and specificity for LPA and acyl-CoA substrates [9,10]. Epitope tagged AGPAT2 localizes to the endoplasmic reticulum (ER) of CHO cells and primary mouse hepatocytes [10].

Lipodystrophy can result from either insufficient generation of mature adipocytes, i.e. defective adipogenesis, or accelerated adipocytes loss,

¹Department of Nutrition, Diabetes and Metabolism, School of Medicine, Pontificia Universidad Católica de Chile, Santiago 8331150, Chile ²Department of Molecular Genetics, University of Texas Southwestern Medical Center, Dallas, TX 75390, USA ³Department of Internal Medicine, University of Texas Southwestern Medical Center, Dallas, TX 75390, USA ⁴Cardiovascular Research Institute, University of California, San Francisco, San Francisco, CA 94158, USA ⁵Division of Nutrition and Metabolic Diseases, Center for Human Nutrition, Department of Internal Medicine, University of Texas Southwestern Medical Center at Dallas, TX 75390, USA

*Corresponding author. Department of Nutrition, Diabetes and Metabolism, School of Medicine, Pontificia Universidad Católica de Chile, Av. Libertador Bernardo O'Higgins 340, Santiago 8331150, Chile. Tel.: +56 2 23546389; fax: +56 2 26338298. E-mail: vcortes@med.puc.cl (V.A. Cortés).

**Corresponding author. Department of Molecular Genetics, University of Texas Southwestern Medical Center, Dallas, TX 75390, USA. Tel.: +1 214 648 3644; fax: +1 214 648 6388. E-mail: jay.horton@utsouthwestern.edu (J.D. Horton).

Received February 13, 2016 • Revision received April 29, 2016 • Accepted May 6, 2016 • Available online 13 May 2016

<http://dx.doi.org/10.1016/j.molmet.2016.05.004>

Original article

i.e., defective adipose maintenance. Previous work with cell lines [11,12] and muscle-derived multipotent cells isolated from subjects harboring AGPAT2 mutations [12] has suggested that AGPAT2 is required for adipogenic differentiation; however, the roles of AGPAT2 for *in vivo* adipose tissue dynamics is unknown. Herein, we characterized morphological, ultrastructural, and molecular changes of AT from *Agpat2*^{-/-} mice and assessed adipogenic differentiation in *Agpat2*^{-/-} mouse embryonic fibroblasts (MEFs).

2. MATERIALS AND METHODS

2.1. Mice

Agpat2^{-/-} mice were generated as described previously [5]. *Agpat2*^{-/-} and *Agpat2*^{+/-} mice were obtained by mating of *Agpat2*^{+/-} mice. Genotyping was performed by the PCR protocol as described [5]. Adult mice were fed chow ad libitum. All mouse procedures were reviewed and approved by the Institutional Animal Care and Use Committee at Pontificia Universidad Católica de Chile and University of Texas Southwestern Medical Center (UTSW).

2.2. Mouse embryonic fibroblasts (MEFs)

Agpat2^{-/-} pregnant females (14.5 d.p.c.) were sacrificed by isoflurane overdose. The embryos were removed, washed with ice cold sterile PBS, and sacrificed by decapitation. Maternal tissues, placental membranes, and internal organs were removed, and carcasses were rinsed with PBS and manually minced. The resulting material was digested with 0.25% trypsin/1 mM EDTA for 3 h at 4 °C and centrifuged. Cells were resuspended in DMEM 4.5 g/L glucose, supplemented with 10% heat-inactivated fetal bovine serum (FBS), 2 mM L-glutamine, 0.1 mM nonessential amino acids, 100 µg/ml penicillin/streptomycin, and 0.1 mM 2-β-mercaptoethanol and seeded onto 150 mm plastic dishes. Because of *Agpat2*^{+/-} mice mating, the embryos are of all three genotypes: *Agpat2*^{+/+}, *Agpat2*^{+/-} and *Agpat2*^{-/-}. Genomic DNA was isolated from tail biopsies of each embryo and only those of *Agpat2*^{+/+} and *Agpat2*^{-/-} genotypes were further processed. Genotyping PCR conditions are similar as mentioned before [5]. MEFs were cultured until 100% confluence and frozen in liquid nitrogen at passage 1. All the experiments were performed at passage 3.

2.3. MEFs adipogenic differentiation

4 × 10⁵ MEFs/well were seeded on 12-well plates and cultured in DMEM 4.5 g/L glucose, supplemented with 10% heat-inactivated FBS, 2 mM L-glutamine, 0.1 mM nonessential amino acids, 100 µg/ml penicillin/streptomycin, and 0.1 mM 2-β-mercaptoethanol. Adipogenesis was induced 2 days after confluency with induction medium (standard medium plus 1 µM dexamethasone, 0.5 mM 3-isobutyl-1-methylxanthine (IBMX), 10 µg/ml insulin) for 3 days. After induction, MEFs were fed an adipogenic differentiation medium (standard medium plus 10 µg/ml insulin and 10 µM rosiglitazone) for 2 additional days and then cultured in adipogenic maintenance medium (standard medium supplemented with 10 µg/ml insulin).

2.4. Histology and immunofluorescence

E18.5 embryos and newborn mice were euthanized by CO₂ anesthesia following cervical decapitation. Immediately, they were rinsed with 1X PBS and fixed overnight in 4% PFA/PBS and then transferred into 30–18% sucrose/PBS gradient. For histological studies in dorsal skin and interscapular BAT (IBAT) of P0-P6.5 mice, tissues were fixed in 4% PFA/PBS and then embedded in paraffin. Cryo and paraffin embedding, sectioning, H&E and Oil Red O staining were performed at UTSW

Molecular Pathology Core. For Perilipin-1 and MAC-2 immunofluorescence in AT, sections were deparaffinized in xylene and rehydrated in a graded series of ethanol followed by dH₂O. Antigen unmasking was carried out by heating slices in 10 mM sodium citrate buffer (pH 6.0) at 95–99 °C for 10 min. Tissue sections were blocked and then incubated overnight at 4 °C with primary antibodies. After the washing steps, fluorochrome-conjugated secondary antibodies were incubated for 1 h at room temperature. For immunofluorescence detection in cultured cells, MEFs were seeded on glass coverslips and adipogenic differentiation was induced as described above. At the indicated days, differentiated MEFs were fixed in 4% PFA, washed with PBS and permeabilized/blocked in 0.3% Triton X-100; 3% BSA/PBS. Primary and secondary antibody incubation steps were performed as described above. Finally, all stained slides and coverslips were mounted with ProLong[®] Gold Antifade Reagent with 4',6'-diamidino-2-phenylindole (DAPI) (Molecular Probes). Images were captured with Leica SP5 Tandem Scanner Spectral 2-photon confocal microscope (Leica Microsystems, Inc., Buffalo Grove, IL) and processed with ImageJ (NIH, Bethesda, MD, US) and Bitplane Imaris software v. 7.3.1 (Andor Technology PLC, Belfast, N. Ireland). The following antibodies and dilutions were used: rabbit anti-Perilipin-1 (1:300, Cell Signalling), rabbit anti-Caveolin-1 (1:100, Cell Signalling), rabbit anti-PPARγ (1:100, Cell Signalling) and rat anti-MAC-2 (1:200, Cedarlane), Alexa Fluor[®] 488 or 594 goat anti-rabbit IgG (H + L) and Alexa Fluor[®] 488 goat anti-rat IgG (Molecular Probes) were diluted 1:300 in blocking buffer. F-actin was stained with rhodamine phalloidin (1:30 in PBS, Molecular Probes). For neutral lipid staining in MEFs, samples were incubated with 1 µg/ml BODIPY 493/503 (Molecular Probes).

2.5. TUNEL assay

Apoptotic cells were detected by the terminal deoxynucleotidyltransferase-mediated deoxyuridine-triphosphate-biotin nick-end labeling (TUNEL) method using DeadEnd Fluorometric TUNEL System (Promega, Madison, WI) according to the manufacturer's protocol. For TUNEL/Perilipin-1 double-labeled assay, paraffin sections of adipose tissue were first treated for TUNEL staining followed by immunofluorescent detection of Perilipin-1. Nuclei were counterstained with propidium iodide or DAPI as indicated. Stained samples were examined by confocal scanning laser microscopy.

2.6. Transmission electron microscopy

Dissected tissues from anterior subcutaneous regions and differentiated MEFs were fixed in 2% glutaraldehyde; 0.1 M cacodylate buffer and processed at the UTSW Electron Microscopy Core Facility. Sections were examined with a TEM Tecnai Spirit electron microscope and photographed with a Morada CCD camera.

2.7. Immunoblot analysis and antibodies

MEF protein extracts were prepared in RIPA buffer (50 mM Tris pH 8.0, 180 mM NaCl, 1% NP-40, 1% sodium deoxycholic acid, 0.1 mM EGTA and 0.1% sodium dodecyl sulfate (SDS)) supplemented with protease and phosphatase inhibitor cocktails (Roche) and 1 mM phenylmethylsulfonyl fluoride (PMSF). Proteins (50 µg) were denatured in Laemmli's sample buffer (62.5 mM Tris, pH 6.8, 2% SDS, 25% glycerol, 0.01% bromophenol blue, and 5% β-mercaptoethanol), separated in a SDS-polyacrylamide gel and electrotransferred onto a nitrocellulose membrane. Membranes were blocked with 5% bovine serum albumin (BSA)/tris phosphate buffer 0.1% Tween 20 (TBS-T) and incubated overnight at 4 °C with primary antibodies diluted in 5% BSA/TBS-T solution. Rabbit antibodies against PPARγ, C/EBPα, C/EBPβ, C/EBPγ, β-actin, ATG12, Beclin, Akt (pan) and anti-rabbit IgG,

HRP-linked antibodies were all purchased from Cell Signalling. Blots were visualized by chemiluminescence detection using Super Signal[®] West Pico Reagents (Pierce).

2.8. Real-time reverse transcription PCR

Total RNA was extracted from iBAT, posterior subcutaneous AT and MEFs using RNA STAT-60 reagent (TEL-TEST). 2 µg of total RNA were reverse transcribed with High Capacity cDNA Reverse Transcription Kit (Applied Biosystems). Real-time PCR was performed on ABI Prism[®] 7900 HT thermalcycler (Applied Biosystems) using SYBR[®] Green PCR Master Mix (Applied Biosystems) as reported [5]. Individual mRNA levels were normalized to 36B4 and expressed as fold-change relative to non-differentiated *Agpat2*^{+/+} MEFs or wild type mice AT, with the $\Delta\Delta C_t$ method. Primer sequences used for real time PCR are provided in Supplementary Table 1.

2.9. Recombinant adenovirus

PPAR γ 2 encoding adenovirus was generated with ViraPower adenoviral expression system (Invitrogen). The PPAR γ 2 cDNA was amplified with Phusion high fidelity DNA polymerase (New England Biolabs) from a mouse liver cDNA library. PCR products were gel-purified and cloned into pENTR/D-TOPO vector (Invitrogen). The orientation and the sequence of the inserted cDNAs were confirmed by sequencing. Recombinant adenoviral vectors were generated by Clonase II mediated recombination between PPAR γ 2-pENTR/D-TOPO and pAd/CMV/V5-DEST vector (Invitrogen). Resulting recombinant plasmids were confirmed by sequencing. Infecting adenoviral particles were generated by transfecting 1 µg of PacI digested PPAR γ 2-pAD/CMV/V5-DEST in 293A cells using FuGENE 6 reagent (Roche Diagnostics). Adenoviral particles were purified in CsCl gradients and quantified by OD at 260 nm. 6×10^9 adenoviral particles were used to transduce MEFs in 60 mm dishes.

2.10. Lipid extraction and phospholipid composition analysis

Total triglycerides from differentiated MEFs were extracted and measured using Triglyceride Colorimetric Assay Kit (Cayman Chemicals) according to the manufacturer's instructions. To extract total glycerophospholipids, differentiated MEFs were collected and snap-frozen immediately in liquid nitrogen. Next, samples were homogenized with 2 ml of ice-cold Tris-HCl 20 mM containing protease inhibitors. Then, 0.8 ml the homogenized sample was vigorously mixed with CHCl_3 and 0.1 N HCl:CH₃OH methanol in a 0.8:1:1 ratio. Next, an equal amount of CHCl_3 was added to the mix, manually shaken and centrifuged at $600 \times g$ for 10 min at 4 °C. The lower phase was carefully removed and washed with a small volume of 1 M KCl. Extracted lipids were sent to Kansas Lipidomics Research Center (KLRC) for quantitation of phospholipid species. Automated electrospray ionization-tandem mass spectrometry approach was used, and data acquisition, analysis and identification were carried out as KLRC described previously [13,14]. The data are presented as mol % of the total lipids analyzed.

2.11. Imaging analysis

To quantify the number and size of adipocytes in histological sections of adipose tissue, adipocyte area was measured on hematoxylin and eosin stained slides using Adiposoft and ImageJ software as previously described [15]. To determine the relative percentage of lipid-laden cells (cells containing LDs) after 6 days of differentiation, MEFs were grown on glass coverslips and differentiated. At day 6, cells were fixed and stained with BODIPY 493/503 to detect neutral lipids, rhodamine-phalloidin to detect cortical actin lining the inner surface of the plasma membrane in adipocytes [16,17], and DAPI to stain cell nuclei.

Samples were imaged using a confocal microscope. For cell counting, five non-overlapping fields were analyzed and quantified using Image J software (each field contained approximately 150 cells). The relative percentage of lipid-laden cells was determined as the ratio of BODIPY/cortical F-actin labeled cells to the total cell number per field. For time-course experiments, lipid-laden cells were monitored under an inverted microscope with phase contrast objectives at different days of differentiation. Images from the sample fields were captured at each time and then analyzed with Image J software. Quantitative image analysis of fluorescence intensity was performed with Image J software as previously described [18].

2.12. Statistical analysis

GraphPad Prism 5.00 (GraphPad, La Jolla, CA) was used for plotting and statistical analyses. Unpaired, two-sided Student's t-test was used to determine the statistical significance of the differences observed in two-group experiments. One-way ANOVA was used to compare three or more groups in some experiments. P-values of <0.05 were considered significant. (*), 0.01 (**), and 0.001 (***)

3. RESULTS

3.1. Newborn *Agpat2*^{-/-} mice are born with subcutaneous white and brown adipose tissues, which are lost during the first week of life

As we previously reported, AGPAT2 deficient adult mice are completely devoid of all white adipose tissue (WAT) and brown adipose tissue (BAT) depots [5]. Surprisingly, and in contrast, fetuses and newborn *Agpat2*^{-/-} mice have preserved adipose tissue, as indicated by Oil Red O and Perilipin-1 staining of thoracic transversal section of E18.5 and newborn mice (Figure 1). Indeed, BAT was observed in the interscapular, subscapular, intercostal, and neck regions and had similar anatomic distribution and mass in both genotypes (Figure 1A). Analysis of the dorsal area showed a well-defined layer of subcutaneous Oil-red O stained (Figure 1B), Perilipin-1 expressing adipocytes (Figure 1C) located throughout the hypodermis as well as the dermis of all examined *Agpat2*^{+/+} and *Agpat2*^{-/-} mice. The thin layer of anterior-subcutaneous WAT (scWAT) was nearly intact in the *Agpat2*^{-/-} mice (Figure 1B–C). Interestingly, interscapular WAT, which normally covers the two lobes of interscapular BAT in adult mice [19,20], was absent in E18.5 embryos and newborn (P0.5) *Agpat2*^{+/+} and *Agpat2*^{-/-} mice but it was detectable soon after birth exclusively in *Agpat2*^{+/+} (data not shown). This suggests that this particular WAT depot is always absent in the *Agpat2*^{-/-} mice, possibly because most of its development is postnatal and coincides with times when adipose degeneration is already active in these animals. Interestingly, depots of posterior-subcutaneous WAT, which are located mainly in the dorsolumbar and lower ventral regions of the adult mice [20–23], were observed in transverse sections of the inguinal region of both *Agpat2*^{+/+} and *Agpat2*^{-/-} newborn mice (Supplementary Figure 1A–B). Histological analysis at postnatal times showed that subcutaneous adipocytes in wild type mice continuously increased their cell volume over the course of the first week (Figure 2A, upper panels). In *Agpat2*^{-/-} newborn mice at day P0.5, subcutaneous adipocytes were smaller and their size did not increase during the following days (Figure 2A, lower panels). Instead, the subcutaneous space of *Agpat2*^{-/-} mice was filled with multilocular cells that lacked adipocyte morphology (Figure 2A, lower panels). In contrast to scWAT, abundant BAT was present in newborn *Agpat2*^{-/-} mice. Analysis of interscapular BAT (iBAT) showed normal multilocular brown adipocytes in the *Agpat2*^{-/-} mice at the time of birth (P0.5)

Original article

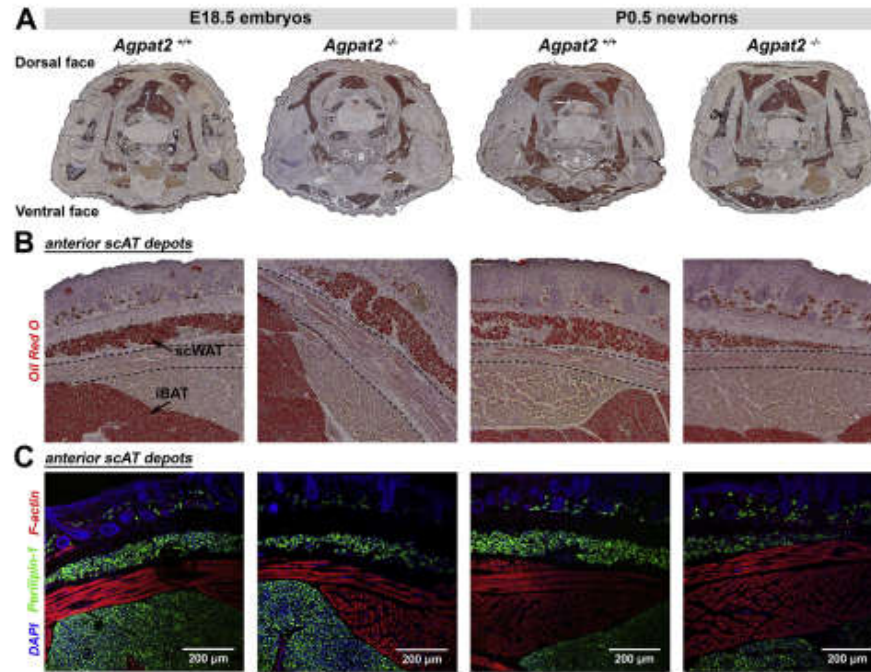


Figure 1: Late fetuses and newborn *Agpat2*^{-/-} mice have normal adipose tissue mass, anatomical distribution and Perilipin-1 expression. (A) Oil red O/hematoxylin stained transversal thoracic sections revealed normal distribution of adipose tissue in E18.5 fetuses and newborn *Agpat2*^{+/+} and *Agpat2*^{-/-} mice. (B) Higher magnification of the dorsal areas stained with Oil red O showed a thin layer of lipid-laden cells in the hypodermis corresponding to developing subcutaneous white adipose tissue (scWAT) in animals of both genotypes. scWAT is separated from the interscapular brown adipose tissue (iBAT) by the panniculus carnosus muscle (outlined by dashed line). (C) Perilipin-1 immunofluorescence staining (green) revealed that lipid-laden cells correspond to adipocytes expressing Perilipin-1. F-actin was detected with Phalloidin/rhodamine (red), indicating skeletal muscle. Nuclei were stained with DAPI (blue). Images are representative of 6 embryos or fetuses per genotype and age.

(Figure 2B), indicating that brown adipocyte commitment and differentiation is normal in *AGPAT2* deficient fetuses. Starting from P2.5, the iBAT of *Agpat2*^{-/-} mice showed aberrant lipid accumulation in brown adipocytes and progressive tissue deterioration, including a reduced number of multilocular adipocytes, abundant unilocular lipid laden cells, and inflammatory cell infiltration. At day P6.5, BAT was completely replaced by an amorphous basophilic material, cell debris, mononuclear cells and giant histiocytes surrounding large lipid drops, possibly reflecting coalesced material from dead adipocytes (Figure 2B). Three-dimensional reconstruction of Perilipin-1 stained scWAT from newborn mice (Figure 2C) and adipocyte size quantification confirmed that most adipocytes were smaller in the *Agpat2*^{-/-} mice (Figure 2D). In addition, adipocyte number was drastically reduced at P2.5 in *Agpat2*^{-/-} mice (Figure 2E). Three-dimensional reconstruction of Perilipin-1 stained scWAT and iBAT sections from P4.5 mice supported that the AT in *Agpat2*^{-/-} mice had abnormal adipocytes and disorganized architecture (Figure 2F). Gene expression analysis of adipocyte markers and adipogenic transcription factors was performed in AT at various times during the postnatal period. In the scWAT of wild type mice, mRNA levels of Leptin, Adiponectin, Perilipin-1, PPAR γ and *AGPAT2*, progressively increased during the first week of life (Figure 2G) as has been previously observed [22]. In contrast, the mRNA level of these genes remained either

undetectable (Leptin) or very low (Adiponectin, Perilipin-1, PPAR γ) in *Agpat2*^{-/-} scWAT (Figure 2G). In agreement with the morphological normality of BAT in newborn *Agpat2*^{-/-} mice (Figure 2B), transcript levels of Adiponectin, UCP1, CIDEA and PPAR γ were similar between *Agpat2*^{+/+} and *Agpat2*^{-/-} mice at day P0.5 (Figure 2H). However, and matching the morphological deterioration of BAT in aging *Agpat2*^{-/-} mice, the expression levels of these genes progressively decreased after birth (Figure 2H). Interestingly, AT degeneration coincides with increased lipid accumulation in the livers of *Agpat2*^{-/-} mice (Supplementary Figure 1C), suggesting that the development of the lipodystrophic phenotype triggers insulin resistance in these mice.

Transmission electron microscopy (TEM) analysis of adipocytes from anterior scWAT sections revealed a number of ultrastructural anomalies in white adipocytes of newborn *Agpat2*^{-/-} mice. Whereas *Agpat2*^{+/+} adipocytes were large, with one or two big sized LDs (Figure 3A), and had normally structured mitochondria (Figure 3C) and abundant caveolae in the plasma membrane (Figure 3C, red arrowheads); *Agpat2*^{-/-} adipocytes were smaller, had multiple LDs (Figure 3B), their mitochondria showed abnormal internal complexity (Figure 3D), and they had a markedly decreased number of caveolae (Figure 3D–E). Furthermore, *Agpat2*^{-/-} adipocytes showed abundant autophagic structures (Figure 3F–I, encircled in dashed red lines; 3J). To evaluate whether the lack of caveolae in *Agpat2*^{-/-} adipocytes is

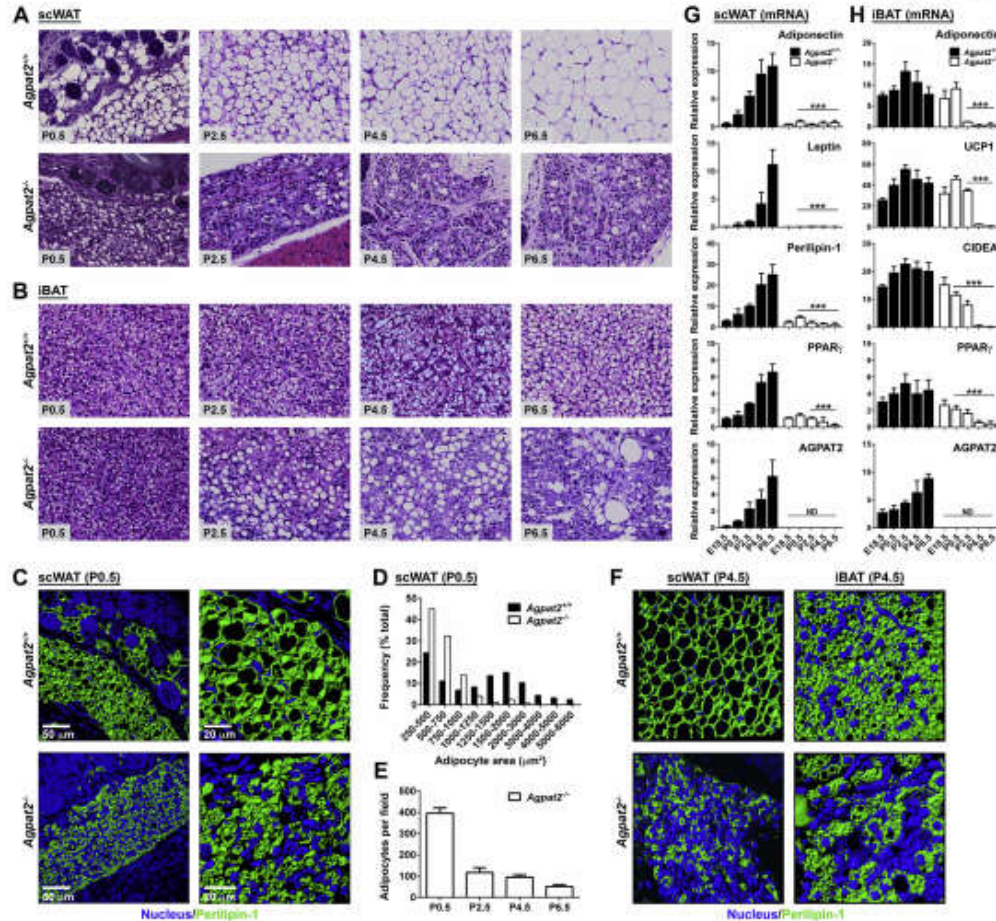


Figure 2: Postnatal adipose tissue development and growth are impaired in *Agpat2*^{-/-} mice. (A–B) Paraffin-embedded sections of anterior scWAT and IBAT from *Agpat2*^{+/+} and *Agpat2*^{-/-} mice were obtained at different days of postnatal life and stained with Hematoxylin and Eosin. Slides were photographed at 40× magnification. Images are representative of *N* > 6 per genotype and age (C, F) Three-dimensional digital reconstruction of Perilipin-1 stained (green) adipose tissue depots from *Agpat2*^{+/+} and *Agpat2*^{-/-} mice at P0.5 (C) and P4.5 (F). DAPI was used to stain nuclei (blue). (D) Histogram shows adipocyte size distribution in scWAT of *Agpat2*^{+/+} and *Agpat2*^{-/-} newborn mice (P0.5). (E) Quantitative comparison of total number of adipocyte per field in scWAT of newborn and P4.5 *Agpat2*^{-/-} mice. Adipocyte number and size were analyzed using Adiposoft software. At least 1000 adipocytes and 5–6 different areas per mouse (*N* = 4) were analyzed. (G–H) Adipose tissue mRNA markers were assessed by qPCR in scWAT and IBAT depots at different pre and postnatal time points. Graphs represent the relative abundance of each transcript normalized to 36B4 mRNA. The bars show the mean ± standard deviation (SD) of *N* = 6. ****p* < 0.001 compared to *Agpat2*^{+/+} mice at E18.5.

due to reduced levels of Caveolin-1, a major structural protein of caveolae [24]. Caveolin-1 was immunostained in the scWAT of these mice. Intriguingly, three-dimensional reconstruction of confocal images showed equivalent levels of Caveolin-1 in *Agpat2*^{+/+} and *Agpat2*^{-/-} adipocytes (Figure 3K–L). However, most *Agpat2*^{-/-} adipocytes showed abnormal distribution of Caveolin-1 (Figure 3K), possibly indicating altered trafficking or mislocalization of this protein in structures other than caveolae.

Combined, these observations suggest that both BAT and subcutaneous WAT adipocyte precursor commitment and differentiation take place normally in *Agpat2*^{-/-} fetuses and that postnatal lipodystrophic

degeneration affects both lineages equally in these mice. Even though *Agpat2*^{-/-} mice are born with near normal BAT at the histological and molecular level the scWAT has distinct morphological abnormalities.

3.2. Lack of AGPAT2 triggers postnatal adipocyte death in mice

To evaluate the mechanism of postnatal AT degeneration in *Agpat2*^{-/-} mice, cell death was assessed by TUNEL staining and TEM. TUNEL-positive cells were undetectable in AT of wild type mice at days P0.5 and P4.5 (Figure 4A, left panels). In contrast, at day P0.5, TUNEL-positive cells were present in the scWAT of *Agpat2*^{-/-} mice and were very abundant in both scWAT and BAT at day P4.5 (Figure 4A, right

Original article

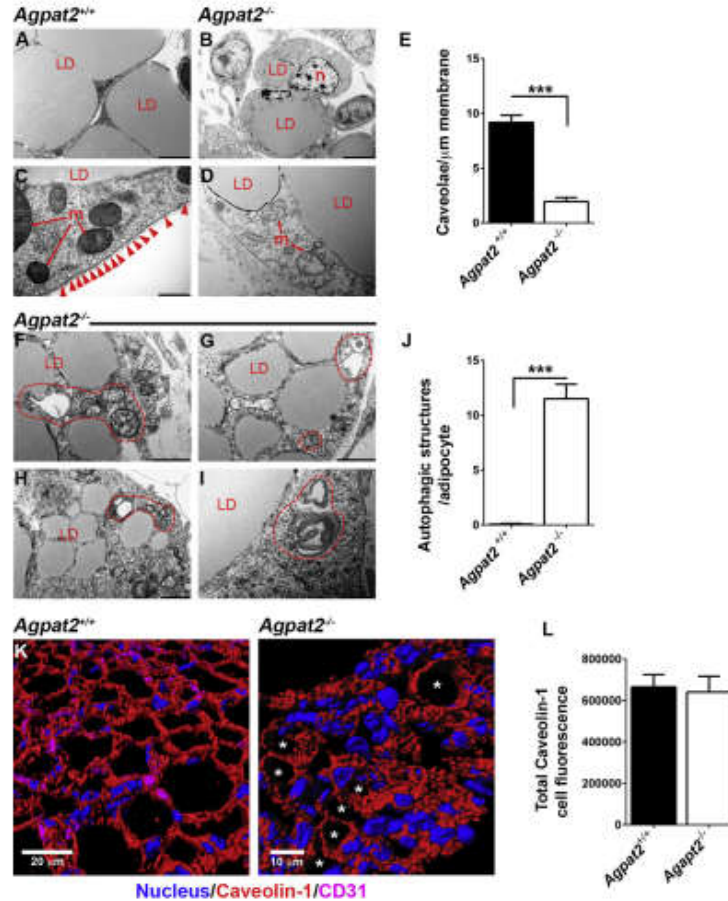


Figure 3: Transmission electron microscopy reveals ultrastructural abnormalities in scWAT from newborn *Agpat2*^{-/-} mice. (A–D) Representative images of scWAT of *Agpat2*^{+/+} and *Agpat2*^{-/-} mice. Caveolae are depicted by red arrowhead. (E) Quantification of caveolae normalized against membrane length. (F–I) scWAT of *Agpat2*^{-/-} mice show small adipocytes with numerous lipid droplets (LD), abnormal mitochondria (m), autophagic structures (enclosed by dashed red lines for clarity), and absence of plasma membrane caveolae. (J) Representative quantification of autophagic structures per adipocyte on section. For image comparative analysis and quantification, 2D adipocytes per sample were analyzed with a total of $N = 3$ samples per experimental group. (K) Representative confocal co-immunofluorescence of caveolin-1 (red) and CD31 (magenta) on scWAT of newborn mice. Asterisks indicate *Agpat2*^{-/-} adipocytes with plasma membrane-associated Caveolin-1. (L) Quantification of caveolin-1 immunofluorescence signal in adipocytes.

panels). Three-dimensional reconstruction and surface rendering of confocal data from TUNEL/Perilipin-1 double-labeled scWAT (Figure 4B, upper panel) or BAT (Figure 4B, lower panel) sections revealed that most of the TUNEL-positive nuclei belonged to adipocytes in the *Agpat2*^{-/-} mice. Moreover, pyknotic nuclei were abundant in *Agpat2*^{-/-} BAT (Figure 2B, dashed area in high magnification panel). TEM analysis revealed that the degeneration of the scWAT in *Agpat2*^{-/-} mice was also characterized by abundant apoptotic bodies of varying size (Figure 4C, red arrows), residual “free LDs” in the interstitial space (Figure 4C, yellow arrows) and neighboring phagocyte (Figure 4C, yellow arrowhead) surrounding the free lipid material extruded from dead adipocytes. Interestingly, “free LDs” have been previously

described in models of obesity-associated adipocyte death, which is characterized by morphological features of necrosis, apoptosis, and pyroptosis [25,26]. The examination of degenerating BAT also showed large areas of terminal cell disintegration with fragments of intracellular components, including abundant “free lipid” material (Figure 4C, areas outlined by red dashed lines) suggesting secondary necrosis [27].

Abundant non-adipocyte cells were detected in the AT of *Agpat2*^{-/-} mice (Figures 2B and 4C). We speculated that they corresponded to inflammatory cells infiltrating the degenerating AT of *Agpat2*^{-/-} mice. To determine the identity of these cells, the macrophage cell-surface marker MAC-2 was assessed by immunofluorescence. At day P0.5,

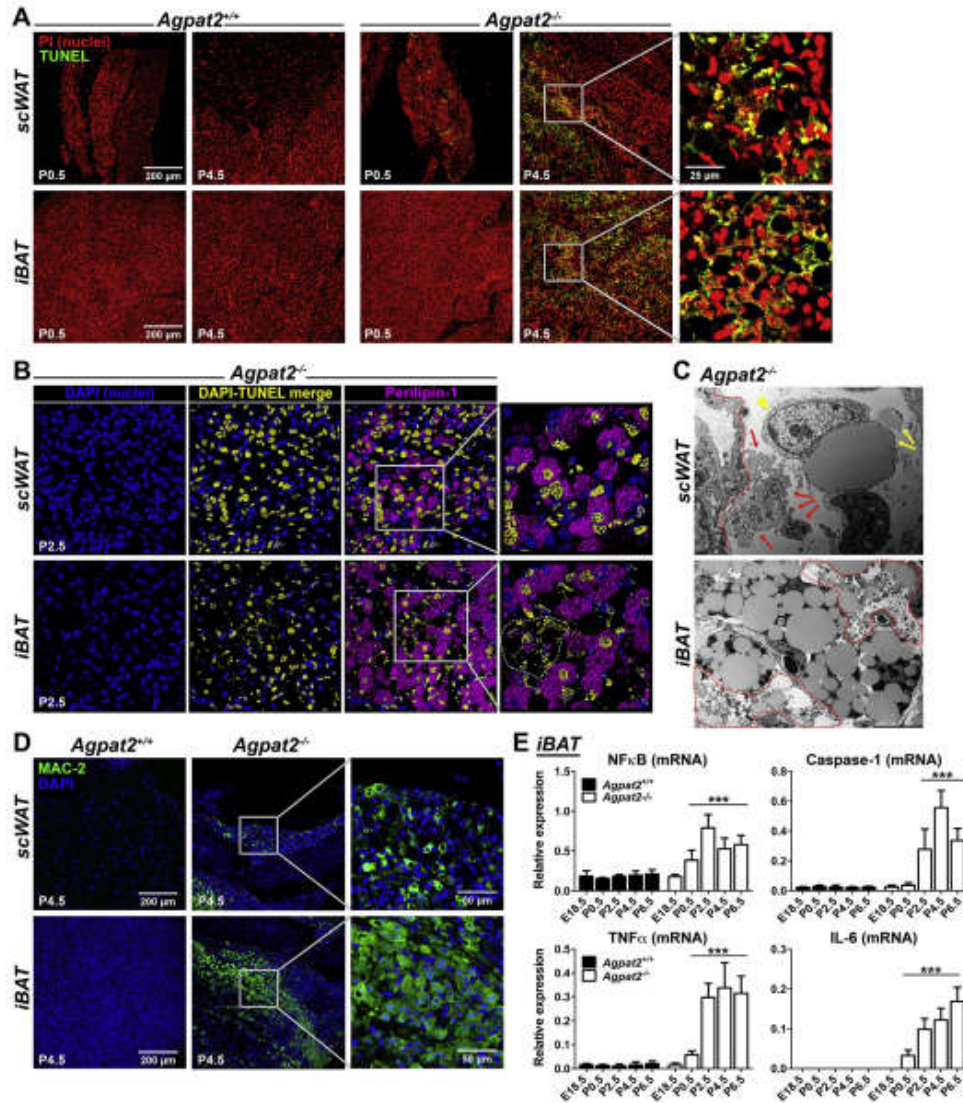


Figure 4: The loss of adipose tissue in *Agpat2*^{-/-} mice is associated with massive cell death and adipose inflammation. **(A)** Paraffin-embedded sections of scWAT and iBAT from *Agpat2*^{+/+} and *Agpat2*^{-/-} littermates were assessed by TUNEL staining. **(B)** 3D slide reconstruction and surface rendering of confocal data from TUNEL/Perilipin-1 double-labeled scWAT and iBAT from P2.5 mice. Volume-rendering in yellow color highlights TUNEL and DAPI co-localization. **(C)** TEM of degenerating adipocytes in scWAT and iBAT from *Agpat2*^{-/-} mice at P4.5. scWAT: red arrows indicate apoptotic bodies, yellow arrows indicate free lipid material (free "LDs"), red arrowhead indicates a phagocytic cell, blood vessel is outlined by a red dashed line. iBAT: red dashed areas show trace of extensive cell disintegration and leakage of intracellular components including lipid material. **(D)** Paraffin-embedded sections of scWAT and iBAT from *Agpat2*^{+/+} and *Agpat2*^{-/-} littermates were stained with anti-MAC-2 and detected by immunofluorescence. **(E)** The mRNA level of genes involved in inflammatory response were assessed by qPCR at different postnatal time points in iBAT of *Agpat2*^{+/+} and *Agpat2*^{-/-} mice. Graphs show the relative abundance of each transcript normalized to 36B4 mRNA. The bars show the means ± SD of N = 8. *** denote significant difference (p < 0.001) compared to *Agpat2*^{+/+} mice at E18.5.

Original article

MAC-2 expressing cells were undetectable in the AT of both genotypes (data not shown); however, abundant MAC-2 positive macrophages were exclusively present in AT from *Agpat2*^{-/-} mice at day P4.5, remaining undetectable in the wild type mice at that time (Figure 4D). Consistent with this observation, mRNA levels for NFκB, Caspase-1, TNFα and IL-6 were increasingly abundant in the iBAT of *Agpat2*^{-/-} mice (Figure 4E).

These observations indicate that massive adipocyte death precludes the postnatal expansion and maintenance of WAT and BAT in *Agpat2*^{-/-} newborn mice and suggest that inflammatory infiltration plays a role in the lipodystrophic phenotype of these mice.

3.3. AGPAT2 deficient MEFs have impaired adipocyte differentiation *in vitro*

To further analyze the importance of AGPAT2 for adipocyte differentiation, we evaluated the capacity of post-confluent mouse embryonic fibroblasts (MEFs) to differentiate into adipocyte-like cells *in vitro*.

After 6 days of adipogenic differentiation, nearly 50% of *Agpat2*^{+/+} MEFs accumulated neutral lipids as determined by BODIPY staining and cellularity analysis (Figure 5A–B). By contrast, only 28% of *Agpat2*^{-/-} MEFs differentiated into adipocyte-like cells (Figure 5A–B) and the total concentration of triglycerides was significantly lower in these cells (Figure 5C). The mRNA levels of key transcriptional regulators, enzymes, lipid transporters, lipid droplet (LD) associated proteins, and adipokines were also lower in adipogenically differentiated *Agpat2*^{-/-} MEFs (Figure 5D).

Perilipin-1 and Caveolin-1, both highly enriched proteins in mature adipocytes, were immunostained in MEFs after 6 days of differentiation to determine the phenotype of the lipid-laden cells. Abundant Perilipin-1 (Figure 5E) and Caveolin-1 (Figure 5F) were coating LDs and decorating the plasma membrane, respectively, in differentiated lipid-laden *Agpat2*^{+/+} MEFs. Interestingly, although lipid-laden cells were smaller in cultured *Agpat2*^{-/-} MEFs, Perilipin-1 properly coated LDs (Figure 5E). By contrast, Caveolin-1 was irregularly distributed, with a higher proportion localized in intracellular structures, possibly the Golgi complex (Figure 5F, white arrowheads). This abnormal distribution of Caveolin-1 was also present in subcutaneous adipocytes of *Agpat2*^{-/-} mice (Figure 3K).

TEM analysis of differentiated MEFs revealed ultrastructural differences between genotypes (Figure 6). Along with their characteristic large LDs, differentiated *Agpat2*^{+/+} MEFs showed abundant well-structured mitochondria (Figure 6A). In contrast, differentiated lipid-laden *Agpat2*^{-/-} MEFs had fewer mitochondria and the internal structure of these organelles was altered (Figure 6A–B). Similar to subcutaneous adipocytes of *Agpat2*^{-/-} mice (Figure 3F–I), AGPAT2 deficient MEFs had significant accumulation of autophagic structures (Figure 6A, C, yellow arrowheads; 6D). Also as observed in mice adipocytes (Figure 3C–D), caveolae were abundant in the plasma membrane of differentiated *Agpat2*^{+/+} MEFs but were virtually absent in *Agpat2*^{-/-} MEFs (Figure 6E–F). To further characterize autophagy in differentiating *Agpat2*^{-/-} MEFs, autophagy-related (ATG) proteins were assessed by immunoblotting. ATG12-ATG5 conjugate is essential for autophagosome formation [28,29] and has been shown to increase during the adipogenic differentiation in MEFs [30]. Here, we observed that ATG12-ATG5 conjugates were progressively increased as differentiation progressed in MEFs of both genotypes, but were significantly higher in *Agpat2*^{-/-} MEFs at all the time points (Supplementary Figure 2A). In contrast, levels of Beclin, which is an important regulator of vesicle nucleation during the initial steps of autophagy [28], were similar

between *Agpat2*^{+/+} and *Agpat2*^{-/-} MEFs during adipogenic differentiation (Supplementary Figure 2B).

Taken together, our results support the idea that *Agpat2*^{-/-} MEFs are able to initiate the process of adipogenic differentiation; however, they undergo a wide variety of cellular abnormalities that finally block the terminal phase of adipogenesis.

3.4. PPARγ overexpression partially rescues adipogenesis in *Agpat2*^{-/-} MEFs

The nuclear receptor PPARγ, as well as the C/EBP family of transcription factors, are critical regulators of adipogenesis [31,32]. Therefore, we assessed the expression levels of C/EBPs and PPARγ during the adipogenic differentiation of MEFs. As expected, adipogenic induction resulted in early expression of C/EBPβ and C/EBPδ, followed by upregulation of C/EBPα and PPARγ mRNA and protein levels in *Agpat2*^{+/+} MEFs (Figure 7A–B). C/EBPβ, -δ, -α, and PPARγ were also increased after adipogenic induction of *Agpat2*^{-/-} MEFs, but the expression level of these markers was significantly lower at all the time points (Figure 7A–B). In spite of these differences, differentiated lipid-laden *Agpat2*^{-/-} MEFs have similar intensity of PPARγ immunofluorescence signal than wild type differentiated lipid-laden MEFs (Figure 7C).

To test if PPARγ overexpression could rescue the capacity of *Agpat2*^{-/-} MEFs to undergo full adipogenesis *in vitro*, post-confluent MEFs were infected with a PPARγ2 encoding adenovirus 24 h before adipogenic induction (Figure 7D). As previously reported [33–36], we observed that overexpression of PPARγ2 enhanced the adipogenic potential of *Agpat2*^{+/+} MEFs in comparison with *Agpat2*^{+/+} MEFs uninfected or infected with a LacZ encoding adenovirus (data not shown). In *Agpat2*^{-/-} MEFs, PPARγ2 overexpression significantly increased the proportion of adipocyte-like cells after 6 days of differentiation (Figure 7E), as well as the total TG concentration (Figure 7F) and mRNA levels of adipocyte markers (Figure 7G) in comparison with *Agpat2*^{-/-} MEFs infected with a LacZ encoding adenovirus. Overexpression of PPARγ2 was unable to rescue the abnormal cellular morphology of differentiated *Agpat2*^{-/-} MEFs (Figure 7H). We noted that the proportion of lipid-laden *Agpat2*^{-/-} cells progressively declined during the course of the differentiation, in contrast with wild type cells that remained constant (Supplementary Figure 2B). This anomaly was not corrected by PPARγ2 overexpression (Supplementary Figure 2B), suggesting that PPARγ defects are not the main driving force for abnormal adipogenesis in AGPAT2 deficient adipocytes. To evaluate whether this decreasing number of *Agpat2*^{-/-} lipid-laden cells was the result of increased cell death, TUNEL analysis was performed in adipogenically induced MEFs cultures. Similar to our findings in postnatal adipose tissue of *Agpat2*^{-/-} mice (Figure 4A), a higher number of differentiated *Agpat2*^{-/-} MEFs was TUNEL-positive, in comparison with wild type MEFs (Supplementary Figure 2C, left panels) and PPARγ2 overexpression was unable revert the cell death of *Agpat2*^{-/-} MEFs (Supplementary Figure 2C, right panels).

3.5. Accumulation of phosphatidic acid and altered phospholipid composition in differentiated *Agpat2*^{-/-} MEFs

An altered phospholipid composition may perturb membrane remodeling, intracellular signaling, autophagy, and LD expandability during adipogenesis [37,38] and thus may be a determinant of death in AGPAT2 deficient adipocytes. Supporting this idea, it was previously reported that Caveolin-1 deficient adipocytes have abnormal phospholipid composition which is a determinant of small-sized LDs [39]. Moreover, epididymal WAT and BAT depots from adipose-specific Seipin knockout mice have accumulation of several lipid species, including

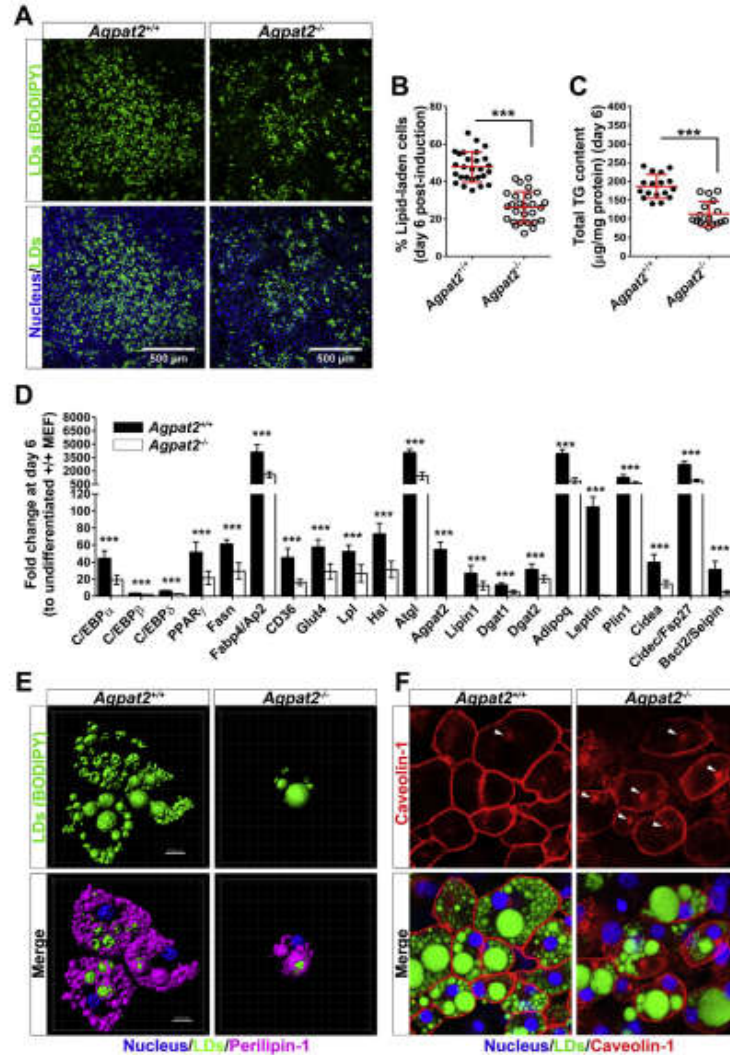


Figure 5: Adipogenic differentiation of *Agpat2*^{-/-} MEFs results in significantly fewer neutral lipid-laden cells after 6 days of differentiation. (A) Representative images ($N > 10$) from 6 days differentiated MEFs stained with the neutral lipid dye BODIPY and DAPI. (B) Graph shows the grade of adipogenic differentiation expressed as percentage of BODIPY stained cells. (C) Graph shows total cellular triglycerides quantified by an enzymatic-colorimetric method. (D) mRNA levels of adipogenic transcription factors and adipocyte related markers were quantified by qPCR. Gene expression was normalized to 36B4 mRNA levels and presented as fold-change relative to non-differentiated *Agpat2*^{+/+} MEFs. Data correspond to the means \pm SD of six independent experiments ($N > 10$). *** $p < 0.001$ and ** $p < 0.01$ denote statistically significant difference compared to differentiated *Agpat2*^{+/+} MEFs after 6 days of differentiation. (E) Three dimensional digital reconstruction of fluorescence stacks of differentiated *Agpat2*^{+/+} and *Agpat2*^{-/-} MEFs stained with BODIPY and anti-Perilipin-1 antibody. (F) Representative confocal images of Caveolin-1 (red) and lipid droplets (green) in MEFs after 6 days of adipogenic differentiation. Caveolin-1 preferentially marks the plasma membrane but also intracellular structures, possibly the Golgi complex (white arrowheads).

phospholipids, which is accompanied with cell stress and cell death of AT [40].

Since the conversion of LPA to PA by AGPATs is an intermediary step involved in glycerophospholipid biosynthesis pathway (Figure 8A) and

AGPAT2 expression is strongly elevated during adipocyte differentiation [11], we aimed to determine whether the absence of AGPAT2 generates unbalanced levels of LPA, PA and potentially other phospholipids during adipogenesis. Therefore, we quantified the abundance

Original article

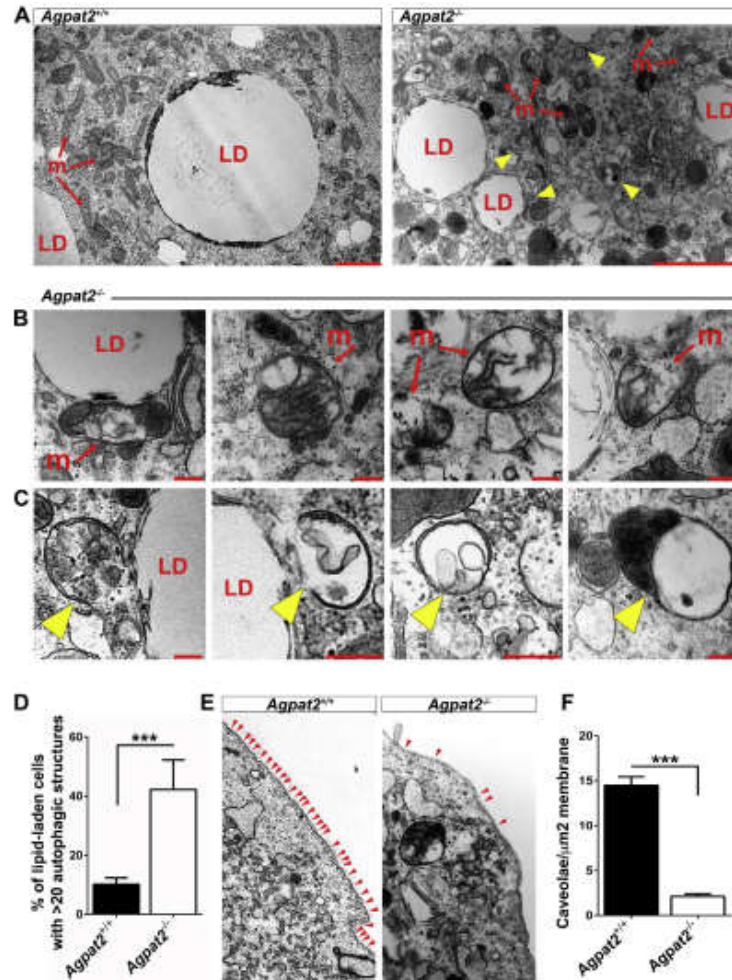


Figure 6: AGPAT2 deficiency is associated with ultrastructural abnormalities in differentiated MEFs. Transmission electron microscopy of differentiated *Agpat2*^{+/+} and *Agpat2*^{-/-} MEFs at day 6 post adipogenic induction. (A) Comparative images show lipid-laden cells from differentiated *Agpat2*^{-/-} MEFs (right panel) have aberrant mitochondria (m) and numerous autophagic structures (yellow arrowheads) in comparison with differentiated *Agpat2*^{+/+} MEFs (left panel). (B) Representative imaging of mitochondria from differentiated *Agpat2*^{-/-} MEFs. (C) Representative imaging of autophagic structures that were observed only in differentiated *Agpat2*^{-/-} MEFs. (D) Relative percentage of lipid-laden cells containing more than 20 autophagic compartments per whole cell. (E) Representative imaging of plasma membrane contrasting the differences in the density of caveolae (red arrowheads) in differentiated MEFs of both genotypes. (F) Quantification of plasma membrane-associated caveolae normalized against membrane area. For image analysis and quantification, 10 differentiated lipid-laden cells per independent sample were imaged in each experiment with a total of N = 4 samples per experimental group.

of total LPA, PA and major phospholipids in differentiated *Agpat2*^{-/-} MEFs. Mass spectrometry analysis revealed no significant differences in the LPA content between differentiated *Agpat2*^{-/-} and *Agpat2*^{+/+} MEFs. In contrast, levels of PA were ~3-fold higher in differentiated *Agpat2*^{-/-} MEFs in comparison with wild type MEFs (Figure 8B), indicating that alternative pathway(s) exist for the synthesis of PA in the absence of AGPAT2. Although the specific molecular identity of the

fatty acid moieties composing PA were not revealed by our mass spectrometry analysis, differentiated *Agpat2*^{-/-} MEFs had significantly elevated levels of 32:1, 32:0 and 34:1 PA species (Figure 8C). In addition, increased levels of phosphatidylcholine (PC) and decreased levels of phosphatidylserine (PS), phosphatidylinositol (PI) and phosphatidylglycerol (PG), were detected in differentiated *Agpat2*^{-/-} MEFs (Figure 8D). Therefore, complex changes in the phospholipid

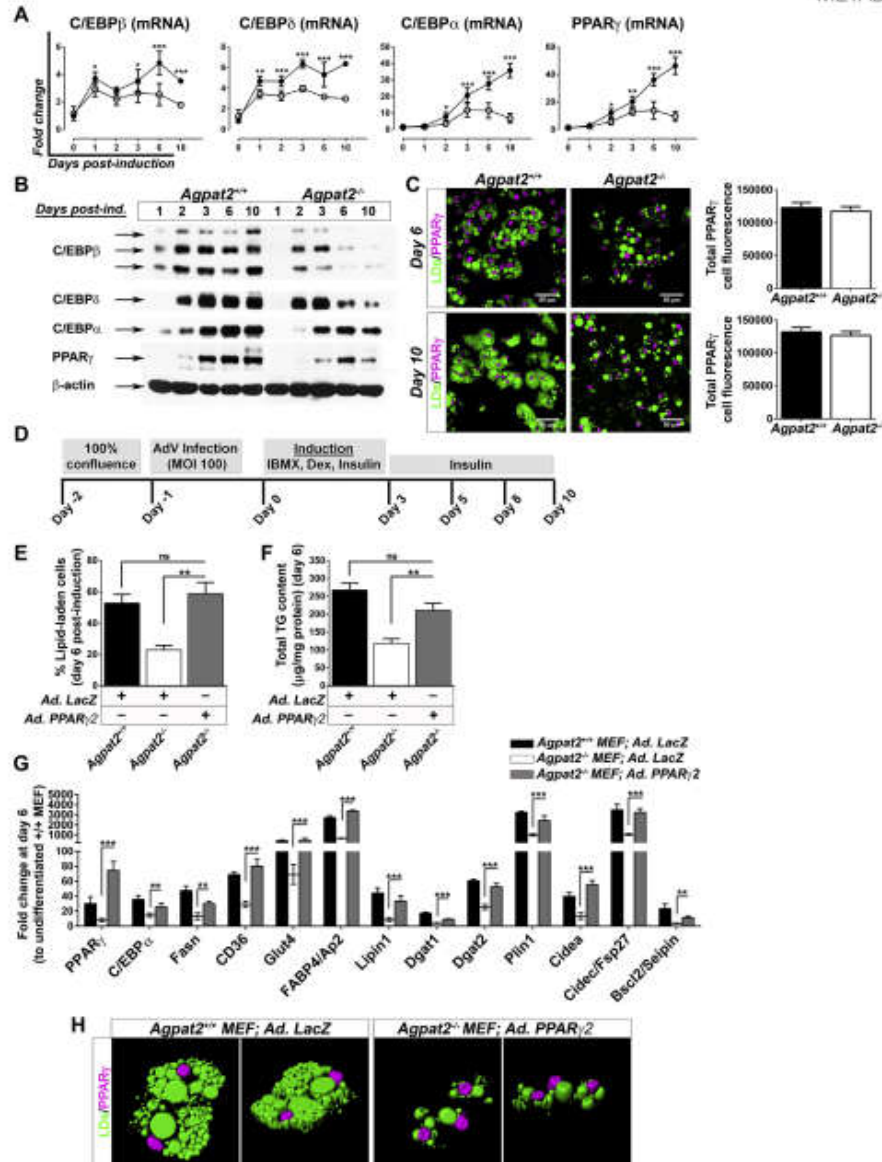


Figure 7: Overexpression of PPAR γ 2 increases the proportion of lipid laden-cells and the gene expression profile but not the morphology of differentiated *Agpat2*^{-/-} MEFs. (A) qPCR quantification of C/EBPs and PPAR γ mRNA levels at early and late stages of adipogenic differentiation. Data were normalized to 36B4 mRNA levels and expressed as relative fold changes to non-differentiated *Agpat2*^{+/+} MEFs at day 0. (B) Immunoblot analysis of whole-cell protein extracts from *Agpat2*^{+/+} and *Agpat2*^{-/-} MEFs at different days of differentiation. 50 μ g of proteins were loaded, β -actin was used as loading control. (C) Confocal immunofluorescence analysis of PPAR γ in *Agpat2*^{+/+} and *Agpat2*^{-/-} MEFs at two different stages of adipocyte differentiation. Graphs show the relative total immunofluorescence signal of nuclear PPAR γ per cell. (D) Time-line showing the adipogenic differentiation protocol used on primary cultures of *Agpat2*^{+/+} and *Agpat2*^{-/-} MEFs previously infected with recombinant adenoviruses. (E) Adipogenic differentiation expressed as percentage of BODIPY stained cells after 6 days of differentiation. (F) Total cellular triglycerides quantified by an enzymatic-colorimetric method. (G) mRNA levels of adipogenic transcription factors and adipocyte related markers were quantified by qPCR. Gene expression was normalized to 36B4 mRNA levels and presented as fold-change relative to non-differentiated *Agpat2*^{+/+} MEFs. (H) Three dimensional digital reconstruction of fluorescence stacks of differentiated *Agpat2*^{+/+} and *Agpat2*^{-/-} MEFs immunostained with anti-Perilipin-1 antibody (pink). Neutral lipids were stained with BODIPY (green). All bar graphs show mean \pm SD of three independent experiments (N > 6). *** (p < 0.001), ** (p < 0.01) and * (p < 0.05) denote significant difference compared to *Agpat2*^{+/+} MEFs.

Original article

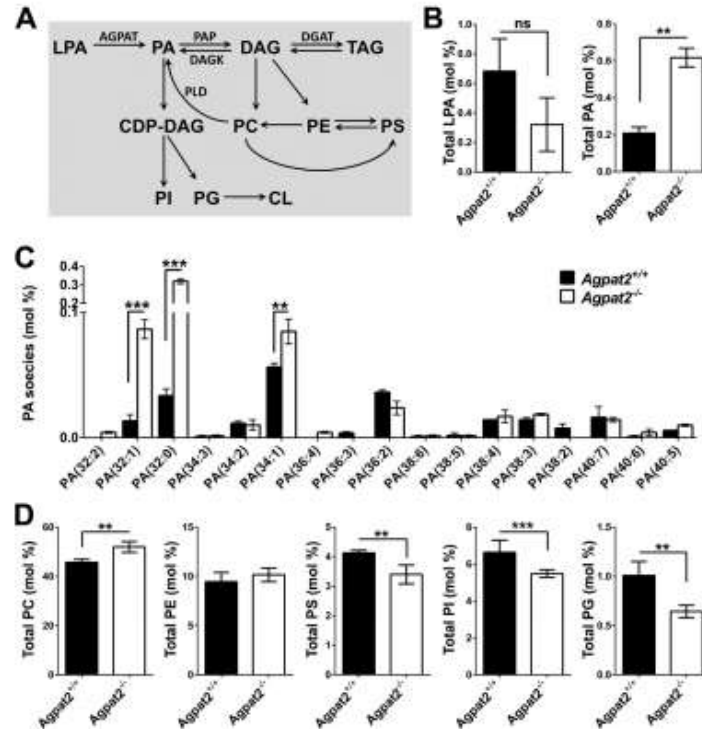


Figure 8: Phospholipid quantification in differentiated *Agpat2*^{+/+} and *Agpat2*^{-/-} MEFs. (A) Pathways for PA and phospholipid synthesis in mammals. (B–C) Electron spray ionization-mass spectrometric analysis of phospholipids in differentiated *Agpat2*^{+/+} and *Agpat2*^{-/-} MEFs. AGPAT: 1-acyl-sn-glycerol-3-phosphate acyltransferase; CL: cardiolipin; DAG: diacylglycerol; LPA: lysophosphatidic acid; PA: phosphatidic acid; PC: phosphatidylcholine; PE: phosphatidylethanolamine; PG: phosphatidylglycerol; PI: phosphatidylinositol; PS: phosphatidylserine; TAG: triacylglycerol. All bar graphs show mean \pm SD of three independent experiments ($N > 6$). *** $p < 0.001$, ** $p < 0.01$ and * $p < 0.05$ denote significant difference compared to differentiated *Agpat2*^{+/+} MEFs.

composition may disrupt not only the production of lipid mediators but also the membrane properties, lipid droplet expansion, and adipocyte survival of AGPAT2 deficient adipocytes.

4. DISCUSSION

Here we report that, in contrast to adult *Agpat2*^{-/-} mice, late fetuses and newborn *Agpat2*^{-/-} mice have near normal scWAT and iBAT with similar distribution and mass as in the wild type littermates and that lipodystrophy results from massive adipocyte death during the first week of life. At the ultrastructural level, while adipocytes in newborn *Agpat2*^{-/-} were smaller and had a marked reduction of plasma membrane caveolae, abnormally structured mitochondria and irregular LDs. In addition, enhanced accumulation of autophagic structures observed in *Agpat2*^{-/-} adipocytes suggests that alternative pathways might be responsible for the widespread adipocyte death observed in the days following birth.

Our *in vitro* studies underscore the importance of AGPAT2 during adipogenesis. It is noteworthy that *Agpat2*^{-/-} MEF cells were able to differentiate into adipocyte-like cells but in a lower proportion than

Agpat2^{+/+} MEFs. This difference was evident at early stages of adipogenesis and manifested by severely reduced abundance of C/EBPs and PPAR γ at both the mRNA and protein levels. Nonetheless, immunofluorescence analysis suggested that the levels of nuclear PPAR γ was equivalent between differentiated lipid-laden *Agpat2*^{-/-} and wild type MEFs. Treatment of *Agpat2*^{-/-} MEFs with the PPAR γ agonist, rosiglitazone, during adipogenic induction did not improve adipogenesis (data not shown); however, overexpression of PPAR γ 2 increased the proportion of *Agpat2*^{-/-} MEFs with adipocyte-like phenotype after adipogenic induction, although it did not prevent the increased death of differentiated *Agpat2*^{-/-} MEFs. Importantly, *Agpat2*^{-/-} lipid-laden MEFs also exhibit other additional hallmarks of adipogenic differentiation, including neutral lipid accumulation, presence of Perilipin-1 coated LDs and the expression of downstream adipogenic marker proteins such as aP2/FABP4 and ATGL (data not shown). Combined, these results suggest that adipogenic actions of AGPAT2 may operate upstream of PPAR γ and that PPAR γ deficiency is not a major determinant of the impaired adipogenesis of *Agpat2*^{-/-} MEFs.

In spite of these findings, we observed several ultrastructural abnormalities in differentiated *Agpat2*^{-/-} MEFs, suggesting that these cells

lack the ability to sustain the differentiation process to reach a fully mature adipocyte phenotype and eventually they die.

Interestingly, the small cellular size, the irregular localization of Caveolin-1 and the remarkable absence of caveolae in differentiated *Agpat2*^{-/-} MEFs suggest that the lipodystrophy associated with mutations in *AGPAT2*, *CAV1*, or *PTRF* genes [41–44] may be mechanistically connected. Indeed, recent studies have shown that: 1) caveolae protect adipocytes against lipotoxicity-induced autolysis [45]; 2) changes in Caveolin-1 distribution are related with the disappearance of caveolae in the plasma membrane [46]; 3) autophagosome formation is constitutively activated in Caveolin-1 deficient adipocytes and in differentiated *Cav1*^{-/-} MEFs [47]; and 4) *Cav1*^{-/-} adipocytes have increased levels of reactive species oxygen (ROS) and mitochondrial dysfunction in association with widespread adipocyte death [48,49].

Notably, excessive accumulation of autophagic structures was also present in differentiated *Agpat2*^{-/-} MEFs, in association with increased ATG12/ATG5 complex but not Beclin levels. It is possible that the extensive accumulation of autophagic structures observed in *Agpat2*^{-/-} lipid-laden cells, as well as in *Agpat2*^{-/-} adipocytes *in vivo*, result from an altered autophagic flux or failed elimination of autophagic debris in these cells. It is also possible that the intracellular dysregulation of lipid species in differentiated *Agpat2*^{-/-} MEFs plays a role on this phenomenon. Therefore, detailed studies on autophagy dynamics will be needed to determine the actual status of autophagic processes in *Agpat2*^{-/-} adipocytes and its role in the lipodystrophy of *Agpat2*^{-/-} mice [50].

We found an altered phospholipid composition in AGPAT2 deficient MEFs. At this point, we do not know whether the altered phospholipid levels are a consequence of abnormal lipid metabolism during adipogenesis of AGPAT2 deficient MEFs. Similarly, our studies do not allow us to conclude a causal role of phospholipid composition abnormalities on the adipogenic inability of *Agpat2*^{-/-} MEFs. Interestingly, increased levels of PA have been reported in other cellular models of adipogenic impairment, including OP9 and 3T3-L1 cells in which AGPAT2 [11] and Seipin [51] were knocked down, respectively. Indeed, mutations in the *Bscl2/Seipin* gene also cause CGL in humans [52] and mice [40,53,54], and *in vitro* studies with Seipin deficient cells have shown impaired adipogenesis [53,55], altered lipid metabolism [56], high levels of PA and supersized LD [57–59]. Additionally, epididymal WAT and BAT depots from adipose-specific Seipin knockout mice have increased levels of total PA, ER-stress, inflammation and cell death [40].

Interestingly, a recent study demonstrated that Seipin, AGPAT2, and Lipin-1 physically interact with each other forming a complex in the ER during adipogenesis [60]. This interaction may regulate an efficient flux of PA to specific pathways during adipogenic differentiation and also may be important for adipocyte growth. Therefore, a tentative hypothesis is that the disruption of Seipin-AGPAT2-Lipin-1 complex by the absence of one of these proteins may dysregulate other intracellular processes in which PA is implicated, including signaling, membrane trafficking and remodeling and autophagy. In support of this hypothesis, it was recently reported that increased PA levels due to Lipin-1 deficiency have deleterious effects on mitochondrial function and also impairs the autophagy flux in muscle, leading to accumulation of autophagy-related structures [61].

Although the mechanisms responsible for the elevated PA levels in AGPAT2 deficient cells remain unknown, alternative metabolic pathways must be activated to allow the synthesis of PA in these cells. In addition to the AGPAT-dependent synthesis, PA can be generated by hydrolysis of phosphatidylcholine or cardiolipin by phospholipase D

superfamily members [62–64]. PA can also be generated by phosphorylation of diacylglycerol (DAG) through the action of DAG kinases (DAGK) [65] or by the addition of a fatty acid side chain to LPA through the action of other-non AGPAT LPA acyl transferases [66,67]. A recent study did show the upregulation of *Dagk* and *Pld* in the livers of *Agpat2*^{-/-} mice [68]. Further studies will be required to biochemically dissect these pathways and to elucidate the mechanism of abnormal phospholipid composition in adipogenically differentiated *Agpat2*^{-/-} MEFs.

A limitation of our study is that we could not study the *in vivo* lipid composition of *Agpat2*^{-/-} adipocytes. This was due to our technical inability to dissect the very minute mass of scWAT in embryos and newborn mice. Ongoing strategies are aimed to generate mouse models to purify specific cell populations in *Agpat2*^{-/-} mice. These will provide new tools to assess the role of specific lipid species in the ultrastructural anomalies dependent on AGPAT2 deficiency in adipocytes and for dissecting the specific mechanisms by which adipocyte cell death causes lipodystrophy in *Agpat2*^{-/-} mice.

In summary, we show that *Agpat2*^{-/-} mice are born with AT, which undergoes a rapid degenerative process that leads to the total destruction of AT during the first week after birth. At the ultrastructural level, *Agpat2*^{-/-} adipose tissue has decreased caveolae, abnormally conformed mitochondria and LDs amid abundant autophagic structures. Adipocyte-like cells from differentiated *Agpat2*^{-/-} MEFs recapitulate the abnormal phenotype observed in scWAT of *Agpat2*^{-/-} newborn mice and have an abnormal phospholipid composition.

Based on our *in vivo* and *in vitro* findings, we propose AGPAT2 deficient adipocytes have an impaired capacity to adapt to the massive lipid availability associated with postnatal feeding, leading to cellular stress, death and inflammatory destruction of adipose tissue.

AUTHOR CONTRIBUTIONS

V.A.C. and J.D.H. designed and wrote the grant. K.M.C. designed specific aims, experiments and procedures. K.M.C. performed the experiments and data analysis under the guidance of V.A.C. and J.D.H., which also contributed with additional funding and research support. C.O.L. performed TUNEL/Perilipin-1 double-staining in tissues. Further reagents, materials, analysis tools and advice were provided by C.O.L., P.J.T., A.G. and A.A. The manuscript was written by K.M.C. and V.A.C. All authors critically read and contributed to the manuscript.

ACKNOWLEDGMENTS

The authors want to thank Dr. Philip Scherer for reviewing the manuscript and providing critical comments and suggestions, and to Dr. Ana Maria Cuervo for her advice on the analysis and interpretation of autophagy-related structures. We also want to thank Mr. John M. Shelton from UTSW for histological suggestions and discussions in processing tissue samples, Mrs. Judy Sanchez from UTSW for her invaluable technical support with the mouse colony and Kalie Tunison from UTSW for technical assistance and copyediting in the manuscripts. V.A.C. was funded by Fondecyt Grant 1141134 (Chile). K.M.C. was supported by CONICYT Doctoral Fellowship program grants 21090704, 24120971, 75120111 (Chile). J.D.H. was funded by the NIH (U.S.) grant P01 DK088761. A.G. and A.K.A. were supported by National Institutes of Health Grants DK54387 and the Southwestern Medical Foundation. Phospholipid composition analysis was performed at the Kansas Lipidomics Research Center Analytical Laboratory, supported by National Science Foundation grants EPS 0236913, MCB 0455318 and 0920663, and DBI 0521587, NIH P20RR16475, Kansas State University, the Kansas Technology Enterprise Corp., and K-IdEA Networks of Biomedical Research Excellence.

Original article

CONFLICT OF INTEREST

The authors declare no financial or commercial conflict of interest.

APPENDIX A. SUPPLEMENTARY DATA

Supplementary data related to this article can be found online at <http://dx.doi.org/10.1016/j.molmet.2016.05.004>.

REFERENCES

- [1] Garg, A., 2011. Lipodystrophies: genetic and acquired body fat disorders. *Journal of Clinical Endocrinology & Metabolism* 96:3313–3325.
- [2] Cortes, V.A., Fernandez-Gallies, M., 2015. Lipodystrophies: adipose tissue disorders with severe metabolic implications. *Journal of Physiology and Biochemistry* 71:471–478.
- [3] Agarwal, A.K., Arioglu, E., De Almeida, S., Akkoc, N., Taylor, S.I., Bowcock, A.M., et al., 2002. AGPAT2 is mutated in congenital generalized lipodystrophy linked to chromosome 9q34. *Nature Genetics* 31:21–23.
- [4] Garg, A., Fleckenstein, J.L., Peshock, R.M., Grundy, S.M., 1992. Peculiar distribution of adipose tissue in patients with congenital generalized lipodystrophy. *Journal of Clinical Endocrinology & Metabolism* 75:358–361.
- [5] Cortes, V.A., Curtis, D.E., Sukumaran, S., Shao, X., Parameswara, V., Rashid, S., et al., 2009. Molecular mechanisms of hepatic steatosis and insulin resistance in the AGPAT2-deficient mouse model of congenital generalized lipodystrophy. *Cell Metabolism* 9:165–176.
- [6] Cortes, V.A., Smalley, S.V., Goldenberg, D., Lagos, C.F., Hodgson, M.I., Santos, J.L., et al., 2014. Divergent metabolic phenotype between two sisters with congenital generalized lipodystrophy due to double AGPAT2 homozygous mutations. A clinical, genetic and in silico study. *PLoS One* 9.
- [7] Agarwal, A.K., Garg, A., 2003. Congenital generalized lipodystrophy: significance of triglyceride biosynthetic pathways. *Trends in Endocrinology and Metabolism* 14:214–221.
- [8] Eberhardt, C., Gray, P.W., Tjoefker, L.W., 1997. Human lysophosphatidic acid acyltransferase. cDNA cloning, expression, and localization to chromosome 9q34.3. *Journal of Biological Chemistry* 272:20299–20305.
- [9] Hollenback, D., Bonham, L., Law, L., Rossnagle, E., Romero, L., Carew, H., et al., 2006. Substrate specificity of lysophosphatidic acid acyltransferase beta – evidence from membrane and whole cell assays. *Journal of Lipid Research* 47:593–604.
- [10] Agarwal, A.K., Sukumaran, S., Cortes, V.A., Tunison, K., Mizuchi, D., Sanketta, S., et al., 2011. Human 1-acylglycerol-3-phosphate O-acyltransferase isoforms 1 and 2: biochemical characterization and inability to rescue hepatic steatosis in *Agpat2*(^{-/-}) gene lipodystrophic mice. *Journal of Biological Chemistry* 286:37676–37691.
- [11] Gale, S.E., Frolow, A., Han, X., Bickel, P.E., Cso, L., Bowcock, A., et al., 2006. A regulatory role for 1-acylglycerol-3-phosphate-O-acyltransferase 2 in adipocyte differentiation. *Journal of Biological Chemistry* 281:11082–11089.
- [12] Subauste, A.R., Das, A.K., Li, X., Elkot, B., Evans, C., El Azoumy, M., et al., 2012. Alterations in lipid signaling underlie lipodystrophy secondary to AGPAT2 mutations. *Diabetes* 61:2922–2931.
- [13] Devsikh, S.P., Roth, M.R., Baughman, E., Li, M., Tamura, P., Jeannotte, R., et al., 2006. Quantitative profiling of polar glycerolipid species from organs of wild-type *Arabidopsis* and a phospholipase *D* *alpha*1 knockout mutant. *Phytochemistry* 67:1907–1924.
- [14] Wetli, R., Li, W., Li, M., Sang, Y., Biesiada, H., Zhou, H.E., et al., 2002. Profiling membrane lipids in plant stress responses. Role of phospholipase *D* *alpha* in freezing-induced lipid changes in *Arabidopsis*. *Journal of Biological Chemistry* 277:31994–32002.
- [15] Galarraga, M., Campion, J., Munoz-Barrutia, A., Boque, N., Moreno, H., Martinez, J.A., et al., 2012. Adiposoft: automated software for the analysis of white adipose tissue cellularity in histological sections. *Journal of Lipid Research* 53:2791–2796.
- [16] Kanzaki, M., Pessin, J.E., 2001. Insulin-stimulated GLUT4 translocation in adipocytes is dependent upon cortical actin remodeling. *Journal of Biological Chemistry* 276:42436–42444.
- [17] Kanzaki, M., Pessin, J.E., 2002. Caveolin-associated filamentous actin (Cav-actin) defines a novel F-actin structure in adipocytes. *Journal of Biological Chemistry* 277:25867–25869.
- [18] McCloy, R.A., Rogers, S., Cordon, C.E., Larca, T., Castro, A., Burgess, A., 2014. Partial inhibition of Cdk1 in G2 phase overrides the SAC and decouples mitotic events. *Cell Cycle* 13:1400–1412.
- [19] de Jong, J.M., Larsson, O., Cannon, B., Nedergaard, J., 2015. A stringent validation of mouse adipose tissue identity markers. *American Journal of Physiology. Endocrinology and Metabolism* 308:E1085–E1105.
- [20] Sanchez-Gurmaches, J., Guertin, D.A., 2014. Adipocytes arise from multiple lineages that are heterogeneously and dynamically distributed. *Nature Communications* 5.
- [21] Cinti, S., 2012. The adipose organ at a glance. *Disease Models & Mechanisms* 5:588–594.
- [22] Birsoy, K., Berry, R., Wang, T., Ceyhan, O., Tavazoie, S., Friedman, J.M., et al., 2011. Analysis of gene networks in white adipose tissue development reveals a role for ETS2 in adipogenesis. *Development* 138:4709–4719.
- [23] Vitelli, A., Murano, I., Zingarelli, M.C., Frontini, A., Ricquier, D., Cinti, S., 2012. The adipose organ of obesity-prone C57BL/6J mice is composed of mixed white and brown adipocytes. *Journal of Lipid Research* 53:619–629.
- [24] Rothberg, K.G., Heuser, J.E., Donzell, W.C., Ying, Y.S., Glenney, J.R., Anderson, R.G., 1992. Caveolin, a protein component of caveolae membrane coats. *Cell* 68:673–682.
- [25] Cinti, S., Mitchell, G., Barbatelli, G., Murano, I., Ceresi, E., Faloia, E., et al., 2005. Adipocyte death defines macrophage localization and function in adipose tissue of obese mice and humans. *Journal of Lipid Research* 46:2347–2355.
- [26] Giordano, A., Murano, I., Mondini, E., Perugini, J., Smorlesi, A., Severi, I., et al., 2013. Obese adipocytes show ultrastructural features of stressed cells and die of pyroptosis. *Journal of Lipid Research* 54:2423–2436.
- [27] Silva, M.T., do Vale, A., dos Santos, N.M., 2008. Secondary necrosis in multicellular animals: an outcome of apoptosis with pathogenic implications. *Apoptosis* 13:463–482.
- [28] Maiuri, M.C., Zalckvar, E., Kimchi, A., Kroemer, G., 2007. Self-eating and self-killing: crosstalk between autophagy and apoptosis. *Nature Reviews Molecular Cell Biology* 8:741–752.
- [29] Walczak, M., Mariens, S., 2013. Dissecting the role of the Atg12-Atg5-Atg16 complex during autophagosome formation. *Autophagy* 9:424–425.
- [30] Baerqa, R., Zhang, Y., Chen, P.H., Goldman, S., Jin, S., 2009. Targeted deletion of autophagy-related 5 (*atg5*) impairs adipogenesis in a cellular model and in mice. *Autophagy* 5:1118–1130.
- [31] Rosen, E.D., Walkey, C.J., Puigserver, P., Spiegelman, B.M., 2000. Transcriptional regulation of adipogenesis. *Genes & Development* 14:1293–1307.
- [32] Rosen, E.D., MacDougald, D.A., 2006. Adipocyte differentiation from the inside out. *Nature Reviews Molecular Cell Biology* 7:885–896.
- [33] Jin, W., Takagi, T., Kaneshashi, S.N., Kurahashi, T., Nomura, T., Harada, J., et al., 2006. Smad3 controls BMP-dependent adipogenesis via interaction with Smad proteins. *Developmental Cell* 10:461–471.
- [34] Tontonoz, P., Hu, E.D., Spiegelman, B.M., 1994. Stimulation of adipogenesis in fibroblasts by PPAR-gamma-2, a lipid-activated transcription factor. *Cell* 79:1147–1156.
- [35] Ren, D.L., Collingwood, T.N., Rebar, E.J., Woffle, A.P., Camp, H.S., 2002. PPAR gamma knockdown by engineered transcription factors: exogenous

- PPAR gamma 2 but not PPAR gamma 1 reactivates adipogenesis. *Genes & Development* 16:27–32.
- [36] Thullier, P., Bailly, R., Sha, X.M., Clarke, S.D., 1998. Cytosolic and nuclear distribution of PPAR gamma 2 in differentiating 3T3-L1 preadipocytes. *Journal of Lipid Research* 39:2329–2338.
- [37] Eto, M., Shindou, H., Koebcke, A., Harayama, T., Yanagida, K., Shimizu, T., 2012. Lysophosphatidylcholine acyltransferase 3 is the key enzyme for incorporating arachidonic acid into glycerophospholipids during adipocyte differentiation. *International Journal of Molecular Sciences* 13:16267–16280.
- [38] Hishikawa, D., Hashidate, T., Shimizu, T., Shindou, H., 2014. Diversity and function of membrane glycerophospholipids generated by the remodeling pathway in mammalian cells. *Journal of Lipid Research* 55:799–807.
- [39] Blouin, C.M., Le Lay, S., Eberl, A., Koleler, H.C., Guenera, L.C., Klein, C., et al., 2010. Lipid droplet analysis in caveolin-deficient adipocytes: alterations in surface phospholipid composition and maturation defects. *Journal of Lipid Research* 51:945–956.
- [40] Liu, L., Jiang, Q., Wang, X., Zhang, Y., Lin, R.C., Lam, S.M., et al., 2014. Adipose-specific knockout of SEIPIN/BSC2 results in progressive lipodystrophy. *Diabetes* 63:2320–2331.
- [41] Razani, B., Combs, T.P., Wang, X.B., Frank, P.G., Park, D.S., Russell, R.G., et al., 2002. Caveolin-1-deficient mice are lean, resistant to diet-induced obesity, and show hypertriglyceridemia with adipocyte abnormalities. *Journal of Biological Chemistry* 277:8635–8647.
- [42] Liu, L., Brown, D., McKee, M., Lebrasseur, N.K., Yang, D., Albrecht, K.H., et al., 2008. Deletion of Cav1/PTRF causes global loss of caveolae, dyslipidemia, and glucose intolerance. *Cell Metabolism* 8:310–317.
- [43] Hayashi, Y.K., Matsuda, C., Ogawa, M., Goto, K., Tomimaga, K., Mitsuhashi, S., et al., 2009. Human PTRF mutations cause secondary deficiency of caveolins resulting in muscular dystrophy with generalized lipodystrophy. *Journal of Clinical Investigation* 119:2623–2633.
- [44] Kim, C.A., Desepine, M., Boutet, E., El Mourabit, H., Le Lay, S., Meier, M., et al., 2008. Association of a homozygous nonsense caveolin-1 mutation with Berardinelli-Seip congenital lipodystrophy. *Journal of Clinical Endocrinology & Metabolism* 93:1129–1134.
- [45] Meshulam, T., Breen, M.R., Liu, L., Parton, R.G., Pilch, P.F., 2011. Caveolins/caveolae protect adipocytes from fatty acid-mediated lipotoxicity. *Journal of Lipid Research* 52:1526–1532.
- [46] Briand, N., Prado, C., Mabilles, G., Lasnier, F., Le Liepvre, X., Covington, J.D., et al., 2014. Caveolin-1 expression and cavin stability regulate caveolae dynamics in adipocyte lipid store fluctuation. *Diabetes* 63:4032–4044.
- [47] Le Lay, S., Briand, N., Blouin, C.M., Chateau, D., Prado, C., Lasnier, F., et al., 2010. The lipotrophic caveolin-1 deficient mouse model reveals autophagy in mature adipocytes. *Autophagy* 6:754–763.
- [48] Bosch, M., Mari, M., Herms, A., Fernandez, A., Fajardo, A., Kressan, A., et al., 2011. Caveolin-1 deficiency causes cholesterol-dependent mitochondrial dysfunction and apoptotic susceptibility. *Current Biology* 21:681–686.
- [49] Asterholm, I.W., Mundy, D.J., Weng, J., Anderson, R.G., Scherer, P.E., 2012. Altered mitochondrial function and metabolic inflexibility associated with loss of caveolin-1. *Cell Metabolism* 15:171–185.
- [50] Klionsky, D.J., Abdelmohsen, K., Abe, A., Abedin, M.J., Abelovich, H., Acevedo Arozena, A., et al., 2016. Guidelines for the use and interpretation of assays for monitoring autophagy (3rd edition). *Autophagy* 12:1–222.
- [51] Sim, M.F., Dennis, R.J., Aubry, E.M., Ramanathan, N., Sembongi, H., Saudek, V., et al., 2012. The human lipodystrophy protein seipin is an ER membrane adaptor for the adipogenic PA phosphatase Ipin 1. *Molecular Metabolism* 2:38–46.
- [52] Magre, J., Desepine, M., Khalouf, E., Gedde-Dahl, J., T., Van Maledergem, L., Sobel, E., et al., 2001. Identification of the gene altered in Berardinelli-Seip congenital lipodystrophy on chromosome 11q13. *Nature Genetics* 28:365–370.
- [53] Chen, W., Yeheor, V.K., Chang, B.H., Li, M.V., March, K.L., Chan, L., 2009. The human lipodystrophy gene product Berardinelli-Seip congenital lipodystrophy 2/seipin plays a key role in adipocyte differentiation. *Endocrinology* 150:4552–4561.
- [54] Cui, X., Wang, Y., Tang, Y., Liu, Y., Zhao, L., Deng, J., et al., 2011. Seipin ablation in mice results in severe generalized lipodystrophy. *Human Molecular Genetics* 20:3022–3030.
- [55] Chen, W., Chang, B., Saha, P., Hartig, S.M., Li, L., Reddy, V.T., et al., 2012. Berardinelli-seip congenital lipodystrophy 2/seipin is a cell-autonomous regulator of lipolysis essential for adipocyte differentiation. *Molecular and Cellular Biology* 32:1099–1111.
- [56] Chen, W., Zhou, H., Liu, S., Phaner, C.J., Gross, B.C., Lytic, T.A., et al., 2013. Altered lipid metabolism in residual white adipose tissues of Bcl2 deficient mice. *PLoS One* 8:e62526.
- [57] Szymanski, K.M., Binns, D., Bartz, R., Grishin, N.V., Li, W.P., Agarwal, A.K., et al., 2007. The lipodystrophy protein seipin is found at endoplasmic reticulum lipid droplet junctions and is important for droplet morphology. *Proceedings of the National Academy of Sciences of the United States of America* 104:20890–20895.
- [58] Fei, W., Shui, G., Gaeta, B., Du, X., Kuenschner, L., Li, P., et al., 2008. Fld1p, a functional homologue of human seipin, regulates the size of lipid droplets in yeast. *Journal of Cell Biology* 180:473–482.
- [59] Fei, W., Shui, G., Zhang, Y., Kraemer, N., Ferguson, C., Kapterian, T.S., et al., 2011. A role for phosphatidic acid in the formation of “super-sized” lipid droplets. *PLoS Genetics* 7:e1002201.
- [60] Talukder, M.M.U., Sim, M.F.M., O’Rahilly, S., Edvardson, J.M., Rochford, J.J., 2015. Seipin oligomers can interact directly with AGPAT2 and Ipin 1, physically scaffolding critical regulators of adipogenesis. *Molecular Metabolism* 4:199–209.
- [61] Zhang, P., Verity, M.A., Reue, K., 2014. Lipin-1 regulates autophagy clearance and intersects with statin drug effects in skeletal muscle. *Cell Metabolism* 20:267–279.
- [62] Huang, H., Frohman, M.A., 2009. Lipid signaling on the mitochondrial surface. *Biochimica et Biophysica Acta* 1791:839–844.
- [63] Foster, D.A., Salkoum, D., Menon, D., Frias, M.A., 2014. Phospholipase D and the maintenance of phosphatidic acid levels for regulation of mammalian target of rapamycin (mTOR). *Journal of Biological Chemistry* 289:22583–22588.
- [64] Choi, S.Y., Huang, P., Jenkins, G.M., Chan, D.C., Schaller, J., Frohman, M.A., 2005. A common lipid links Mfn-mediated mitochondrial fusion and SNARE-regulated exocytosis. *Nature Cell Biology* 8:1255–1262.
- [65] Cai, J., Abramovici, H., Gee, S.H., Topham, M.K., 2009. Diacylglycerol kinases as sources of phosphatidic acid. *Biochimica et Biophysica Acta* 1791:942–948.
- [66] Yamashita, A., Hayashi, Y., Matsumoto, N., Nemoto-Sasaki, Y., Oka, S., Tanikawa, T., et al., 2014. Glycerophosphate/Acylglycerophosphate acyltransferases. *Biology (Basel)* 3:801–830.
- [67] Shindou, H., Hishikawa, D., Harayama, T., Yuki, K., Shimizu, T., 2009. Recent progress on acyl CoA: lysophospholipid acyltransferase research. *Journal of Lipid Research*(Suppl. 50):S46–S51.
- [68] Sankella, S., Garg, A., Horton, J.D., Agarwal, A.K., 2014. Hepatic gluconeogenesis is enhanced by phosphatidic acid which remains uninhibited by insulin in lipodystrophic *Agpat2*^{-/-} mice. *Journal of Biological Chemistry* 289:4762–4777. <http://dx.doi.org/10.1074/jbc.M113.530998> [Epub 2014 Jan 14]. PMID: 24425876.

Original Article

AGPAT2 deficiency impairs adipogenic differentiation in primary cultured preadipocytes in a non-autophagy or apoptosis dependent mechanism.

Marta Fernández-Galilea¹, Pablo Tapia¹, Kelly Cautivo¹, Eugenia Morselli²,
and Víctor A. Cortés¹

¹Department of Nutrition, Diabetes and Metabolism. Pontificia Universidad Católica de Chile. Santiago, Chile.

²Department of Physiology, Pontificia Universidad Católica de Chile. Santiago, Chile.

Correspondence: Víctor A. Cortés. Department of Nutrition, Diabetes and Metabolism. Pontificia Universidad Católica de Chile, C/. Av. Libertador Bernardo O'Higgins 340, Santiago (Chile). Tel.: (56 2) 2354 38 62. FAX: (56 2) 26338298. E-mail: vcortes@med.puc.cl.

AGPAT2, 1-acylglycerol-3-phosphate O-acyltransferase 2; BAT, brown adipose tissue; LDH, lactate dehydrogenase; ATGs, autophagy related proteins; CGL, congenital generalized lipodystrophy; C/Ebp, CCAAT-enhancer-binding proteins; Ppar, peroxisome proliferator-activated receptor; SVF, stroma-vascular fraction; FBS, Fetal bovine serum; IBMX, 3-isobutyl-1-methylxanthine; BSA, bovine serum albumin; Fsp27, Fat-specific protein 27; MEFs, mouse embryonic fibroblast.

Abstract

Aims: Mutations in 1-acylglycerol-3-phosphate O-acyltransferase 2 (AGPAT2) result in lipodystrophy, insulin resistance and diabetes. Autophagy is required for normal adipogenesis and adipose tissue development. The aim of this study was to determine whether impaired autophagy or excessive cell death underlie the adipogenic inability of *Agpat2*^{-/-} mice preadipocytes.

Methods: Preadipocytes were isolated from interscapular brown adipose tissue (BAT) of *Agpat2*^{-/-} and *Agpat2*^{+/+} newborn mice and cultured/differentiated *in vitro*. Intracellular lipids were quantified by oil red O staining. Cell death was assessed by lactate dehydrogenase (LDH) activity. Apoptosis and autophagy regulatory factors were determined at the mRNA and protein level with Real-time PCR, immunoblot and immunofluorescence.

Results: Adipogenically induced *Agpat2*^{-/-} preadipocytes had fewer lipid-loaded cells and lower levels of adipocyte markers than wild type preadipocytes. Before adipogenic differentiation, autophagy-related proteins (ATGs) ATG3, ATG5-ATG12 complex, ATG7 and LC3II were increased but autophagic flux was reduced, as suggested by increased p62 levels, in *Agpat2*^{-/-} preadipocytes. Adipogenic induction increased LDH levels in the culture media in *Agpat2*^{-/-} preadipocytes but no differences were observed in the activation of Caspase 3 or in markers of autophagic flux.

Conclusions: AGPAT2 is required for *in vitro* adipogenesis of mouse preadipocytes. Autophagy defects or apoptosis are not involved in the adipogenic failure of *Agpat2*^{-/-} preadipocytes.

Key words: AGPAT2, lipodystrophy, adipocytes, cell death, adipogenesis

Introduction

1-acylglycerol-3-phosphate O-acyltransferase 2 (AGPAT2) catalyzes the conversion of lysophosphatidic acid to phosphatidic acid by esterifying the *sn*-2 position of lysophosphatidic acid [1]. AGPAT2 is involved in the biosynthesis of glycerophospholipids and triacylglycerols and is highly expressed in the adipose tissue, pancreas and liver [2]. Nowadays, 11 human AGPAT isoforms have been described, however, only mutations in *AGPAT2* have been found in patients with congenital generalized lipodystrophy (CGL, Berardinelli-Seip syndrome) [2]. These patients develop extreme adipose tissue paucity, insulin resistance, hyperlipidemia, fatty liver and diabetes [3-5].

Resembling CGL patients, AGPAT2 deficient (*Agpat2*^{-/-}) mice have generalized lipodystrophy and develop all metabolic manifestations of insulin resistance [6]. Nonetheless, the underlying mechanisms of lipodystrophy in these mice remain unknown. It has been proposed that AGPAT2 deficiency determines inability of preadipocytes to differentiate into mature adipocytes. In fact, Subauste et al. [7] showed that muscle-derived multipotent cells from CGL patients have impaired adipogenic differentiation *in vitro* and that pioglitazone increases the levels of terminal differentiation markers C/EBP α and PPAR γ and the accumulation of lipid droplets in these cells, suggesting that AGPAT2 deficiency impairs PPAR γ activation during adipogenesis [7].

By contrast, we have found that *Agpat2*^{-/-} mice are born with normal interscapular BAT and that lipodystrophy is developed within the first week of postnatal life (Cautivo et al, unpublished data). These data suggests

ACCEPTED MANUSCRIPT

that accelerated cell death rather than insufficient preadipocytes differentiation underlies lipodystrophy in AGPAT2 deficient animals.

The differentiation process that generates mature adipocytes from fibroblast-like preadipocytes requires the development of highly specialized cellular structures such as lipid droplets, involving massive cytoplasmic remodeling. The ability of autophagy to facilitate cytoplasmic changes during adipogenesis has been reported as an essential process for adipogenesis [8]. ATG proteins are involved in autophagosome formation and autophagy progression [9]. Adipose tissue specific gene deletion of *Atg7* in mice resulted in smaller adipocytes and a severe reduction of adipose mass in comparison with wild type littermates [10]. Similar results were observed in ATG5-deficient mouse embryonic fibroblasts (MEFs) [11]. These cells showed impaired adipogenesis as indicated by failed morphological remodeling, low lipid build up and apoptotic cell death [10, 11]. Therefore, the aim of the present study was to determine whether impaired autophagy and/or excessive cell death plays a role in lipodystrophy of *Agpat2*^{-/-}. For this we characterized adipogenesis at the morphological and molecular level in primary cultured *Agpat2*^{-/-} preadipocytes and studied activation of autophagy and apoptosis pathways.

Materials and methods

Animals and primary preadipocytes generation

Agpat2^{-/-} mice were generated and genotyped as previously described [6]. Mice were housed in colony cages (3 to 4 per cage), maintained on a 12 h light/12 h dark cycle and fed a standard chow. *Agpat2*^{-/-}

ACCEPTED MANUSCRIPT

progenitors were mated in order to obtain *Agpat2^{+/+}* and *Agpat2^{-/-}* pups. At day of birth, the pups were anesthetized by isoflurane inhalation and euthanized by decapitation. Interscapular brown BAT was harvested in less than 1 min and digested with collagenase buffer (Sigma; St. Louis, MO) during 45 min. Then, blood cells were lysed by the addition of ACK buffer (Gibco, Invitrogen Corporation; Carlsbad, CA). For stroma-vascular fraction (SVF) isolation cells were centrifuged at 300 g for 5 minutes and washed 3 times with DMEM-F12 medium (Gibco) containing 10% fetal bovine serum (FBS) (Gibco) and 1% penicillin/streptomycin (Invitrogen). After that, cells were seeded for culturing and adipogenic differentiation. Animal housing, breeding, handling, surgery and euthanasia was approved by Pontificia Universidad Católica de Chile Ethics and Animal Welfare Committee, in agreement with the ethical standards of Declaration of Helsinki (1964) and its later amendments.

Adipogenic differentiation

SVF fraction was cultured in DMEM-F12 containing 17.5 mM glucose, 10% FBS (Invitrogen), and 1% penicillin and streptomycin (Gibco) and maintained in a humidified incubator at 37°C and 5% of CO₂. At confluence, cells were induced to differentiate into adipocytes by changing medium to DMEM-F12 10% FBS, 1% penicillin and streptomycin (Gibco) supplemented with dexamethasone (500 nM, Sigma), indomethacin (125 nM, Sigma), 3-isobutyl-1-methylxanthine (IBMX; 500 μM, Sigma), rosiglitazone (1 nM, Sigma), T3 (1 nM, Sigma) and insulin (20 nM, Sigma). After 2 days, this induction medium was removed and replaced with DMEM-F12 containing 10% FBS and 1% penicillin/streptomycin supplemented only with 1 nM T3 and 20 nM insulin. Medium was changed every 24 hours until day 7 post

adipogenic induction.

Oil Red O staining

After 7 days of adipogenic differentiation induction, cultured preadipocytes were fixed with 3.7% formaldehyde (Winkler; Hackensack, NJ) for 1 hour and stained with Oil Red O (Sigma) (six parts of 1% Oil Red O dye in isopropanol to 4 parts water) for 15 minutes. Stained cells were washed three times with 70% ethanol. Oil Red O staining was then evaluated by fluorescent microscopy or eluted with isopropanol for spectrophotometric quantification (Synergy HT, Biotek Instruments). Fluorescent images were analyzed with ImageJ64 (U. S. National Institutes of Health; Bethesda, MD).

Gene expression analysis by RT-PCR

Total RNA was extracted with Trizol[®] reagent (Invitrogen). RNA concentrations and purity were determined by Nanodrop spectrophotometer ND1000 (Thermo Scientific). Genomic DNA contamination in RNA samples was eliminated with Turbo DNA free kit (Ambion, Austin, TX). cDNA was generated using TaqMan[®] reverse transcription kit (Applied Biosystems; Foster City, CA). Real-time PCR was carried out using SYBR Green qPCR Reagents in a Stratagene Mx3000P thermal cycler (Stratagene, Cedar Creek TX) or Taqman[®] Assays-on-Demand and TaqMan[®] Universal Master Mix in an ABI PRISM Step One thermal cycler (Applied Biosystems). Reactions were carried out following manufacturer's instructions. Primers sequences for SYBR Green protocol (IDT Corporation; Newark, NJ) are presented in Supplemental Table I. Gene expression levels were normalized to Cyclophilin and the fold change was estimated by the $\Delta\Delta C_T$ method, as described in [12].

Western Blot analysis

Primary antibodies for Caspase 3 and Caspase 7 (total and cleaved), ATG3, ATG7, ATG5-ATG12 complex, LC3 and p62 were obtained from Cell Signaling Technology (Beverly, MA). Anti-Actin antibodies were obtained from Sigma. Secondary peroxidase-conjugated anti-mouse and anti-rabbit IgG were obtained from Thermo Scientific (Rockford, IL). For immunoblot analysis, cells were lysed in RIPA buffer (Thermo Scientific) containing Halt Protease and Phosphatase Inhibitor Cocktail (Thermo Scientific). After centrifugation proteins were collected and stored at -80°C. 50 µg of total protein were separated in 8% SDS-PAGE, transferred onto PVDF membranes (Bio-Rad), blocked, and incubated with primary and secondary antibodies. All immunoblots were visualized by SuperSignal[®] West Pico Chemiluminescent Substrate (Pierce, Rockford, IL). Immunoblot images were obtained by the C-DiGit Chemiluminescent Western Blot Scanner (Licor Biosciences; Lincoln, NE).

LDH activity analysis

Release of lactate dehydrogenase (LDH) is an indicator of membrane integrity and hence is an estimator of cell death [13]. LDH activity in the culture medium was determined using the kit LDH cytotoxicity assay kit (Cayman Chemicals; Ann Arbor, Mi) following manufacturer's indications.

LC3 immunofluorescence detection

For LC3 immunofluorescence evaluation at day 0 (before adipogenesis induction), preadipocytes were grown onto a glass coverslip. At confluence, preadipocytes were washed twice in PBS and fixed with 4% buffered

paraformaldehyde (pH 7.4) for 15 minutes at room temperature. Then, cells were permeabilized with 0.25% Triton X-100 in PBS (PBST) and blocked with 1% BSA in PBST for 30 minutes. Cells were incubated with a primary anti-LC3 antibody (Abnova; Taipei City, Taiwan) in 1% BSA in PBST for 1 hour at room temperature. Alexa fluor[®] 488 conjugated secondary anti-mouse IgG antibody (Invitrogen) was incubated for 1 hour at room temperature. Finally, coverslips were mounted onto glass slides using Fluoromont-G medium (eBioscience; San Diego, CA), which contains DAPI for nuclei staining. Stained cells were visualized with a Nikon Eclipse epifluorescent microscope (Nikon Corporation; Tokyo, Japan).

Data analysis

Data are expressed as mean with standard errors (SE). Differences were set up as statistically significant at $P < 0.05$. Multiple comparisons were analyzed by one-way ANOVA, followed by Bonferroni post hoc test. Student's t test or U-Mann Whitney was used for single comparisons as appropriate. GraphPad Prism 5.0 (Graph-Pad Software INC., San Diego, CA) was used for statistical analysis.

Results

AGPAT2 deficiency determines lower lipid accumulation and abnormal expression of adipocyte markers in adipogenically-induced preadipocytes.

In order to assess the effects of AGPAT2 deficiency on adipogenic differentiation, preadipocytes from the interscapular BAT of newborn *Agpat2*^{-/-} mice (P0.5) were cultured and adipogenically induced to differentiation *in vitro*. After 7 days of differentiation, 80% of wild type cells had large-sized lipid

droplets. By contrast, only 20% of *Agpat2*^{-/-} cells had detectable neutral lipid build up by oil red O staining (Fig. 1A). Lipid droplets were significantly fewer in differentiated lipid-loaded *Agpat2*^{-/-} cells (Fig. 1B) and, consistently, *Agpat2*^{-/-} cultures had lower total neutral lipid content (Fig. 1C).

Progression of adipogenesis was evaluated by gene expression of key adipogenic transcription factors. Two days after induction, mRNA levels of early adipogenic transcription factor CCAAT-enhancer-binding protein- δ (*C/EBP- δ*) were significantly increased in wild type cells in comparison with non-induced preadipocytes (Fig. 2A). After 3 days of differentiation, *C/EBP- δ* mRNA levels in wild type cells decreased to the levels of non-induced preadipocytes (Fig. 2A). In *Agpat2*^{-/-} preadipocytes, adipogenic induction was unexpectedly associated with a decrease of *C/EBP- δ* mRNA levels in comparison with non-induced preadipocytes, remaining significantly reduced during all times of differentiation (Fig. 2A).

At days 5 and 7 of adipogenic differentiation, nuclear receptors Peroxisome proliferator activated receptor alpha and gamma (*Ppar- α* and *Ppar- γ*) were strongly increased, at the mRNA level, in wild type cells (~8- and ~40-fold, respectively) in comparison with non-induced preadipocytes (Fig. 2A). Adipogenic induction failed to increase the mRNA levels of both nuclear receptors in *Agpat2*^{-/-} cells (Fig. 2A). Only at day 5 after induction, a small increase in *Ppar- γ* mRNA levels was observed in *Agpat2*^{-/-} cells in comparison with non-induced cells; however, this transcript remained lower than in wild type cells at the same time of differentiation.

After 3 days of adipogenic induction, mRNA levels of late adipogenic transcription factor *C/EBP- α* were increased in both wild type and *Agpat2*^{-/-}

cells; however, whereas they remained elevated in wild type cells at day 7, they fell to the level of non-induced preadipocytes in *Agpat2*^{-/-} cells (Fig. 2A).

Mature adipocytes have high levels of specific lipid droplet coating proteins. As expected, at day 2 of adipogenic differentiation the mRNA levels of Cell death-inducing DFFA-Like effector C (CideC or *Fsp27*) and *Perilipin 1* were elevated in wild type cells and reached their maximum values at day 5 of adipogenic differentiation (~3000- and ~300-fold change, respectively, in comparison with non-induced preadipocytes) (Fig. 2B). Both transcripts were significantly lower in adipogenically stimulated *Agpat2*^{-/-} cells in comparison with wild type cells, although they showed a smaller elevation in comparison with non-induced preadipocytes (Fig. 2B).

Similar findings were made for leptin and adiponectin: whereas the mRNA levels of both adipokines increased in wild type cells at day 5 of adipogenic differentiation, they remained essentially unchanged in *Agpat2*^{-/-} cells (Fig. 2C).

Cell death is not involved in the adipogenic failure of cultured AGPAT2 deficient preadipocytes.

We have previously found that *Agpat2*^{-/-} mice are born with normal mass of interscapular BAT and that this tissue rapidly degenerates during the first week of postnatal life (Cautivo et al, unpublished data). In order to evaluate whether abnormal adipogenic differentiation of cultured *Agpat2*^{-/-} preadipocytes results from increased death of differentiating cells, we quantified LDH release as an indicator of cell death. As shown in Figure 3A, LDH activity was mildly increased in the culture media of *Agpat2*^{-/-} cells only at

day 2 of differentiation, remaining unchanged before and after that time point, in comparison with wild type cells. At day 7 of differentiation, both wild type and *Agpat2*^{-/-} cells showed increased cell death in comparison with non-induced cells. Apoptosis is not associated with the release of intracellular content, including LDH. To assess apoptosis, total and cleaved caspases 3 and 7 levels were measured. Similar with LDH activity results, we found a discrete elevation of cleaved vs. total caspase 7 only at day 2 of differentiation in *Agpat2*^{-/-} cells (Fig. 3B and Suppl. Fig. 1A). No differences were detected in caspase 3 between *Agpat2*^{-/-} and wild type cells (Fig. 3C and Suppl. Fig. 1B). Combined, these data indicate that cell death is not involved in the adipogenic failure of *Agpat2*^{-/-} preadipocytes *in vitro*. Since lipodystrophy in *Agpat2*^{-/-} mice results from postnatal adipose tissue destruction, our data indicates that adipocyte death requires additional elements (cellular or humoral) that are only present *in vivo*.

Autophagic flux is impaired in undifferentiated AGPAT2 deficient preadipocytes but it is normalized after adipogenic induction.

Autophagy is involved in cell survival/death [14], in adipocyte metabolism and lipid-droplet regulation (reviewed in [15]). Concordantly, gene deletion of *Atg5* or *Atg7*, both autophagy-essential genes, determine impaired adipogenesis in cultured MEFs [10, 11] and the specific deletion of *ATG7* in adipocytes reduces the adipose mass by 80% in mice [10]. These antecedents suggest that autophagy is required for adipose tissue development. Thus we hypothesized that autophagy defects may underlie the adipogenic impairment of *Agpat2*^{-/-} preadipocytes.

ACCEPTED MANUSCRIPT

To test this hypothesis, we quantified autophagy-related proteins in differentiating *Agpat2*^{-/-} preadipocytes. We found that mRNA levels of *Atg4*, *Atg5* and *Atg7* as well as *LC3* and *p62* did not differ between undifferentiated *Agpat2*^{-/-} and wild type preadipocytes (Fig. 4A). In contrast, protein levels of ATG3, ATG5-ATG12 complex, ATG7 and the ratio LC3II/LC3I were significantly higher in undifferentiated *Agpat2*^{-/-} preadipocytes in comparison with wild type cells (Fig. 4B-E and Suppl. Fig. 2A-C), but these differences disappeared in the following days of differentiation (Fig. 4B-E and Suppl. Fig. 2A-C). Immunofluorescence analysis revealed increased LC3 puncta only in undifferentiated (Fig. 4F) but not in adipogenically induced *Agpat2*^{-/-} preadipocytes (data not shown). Autophagy flux was evaluated by quantification of p62 protein levels. Similar to the other autophagy regulators, p62 was increased only in undifferentiated *Agpat2*^{-/-} preadipocytes, but these differences disappeared after adipogenic differentiation (Fig. 4G and Suppl. Fig. 2A). Together, these data indicate that undifferentiated *Agpat2*^{-/-} preadipocytes have lower autophagic flux than wild type cells and that adipogenic differentiation normalizes autophagy in AGPAT2 deficient adipocytes.

Discussion

The present study shows that: 1) AGPAT2 is required for mouse preadipocytes to differentiate to mature adipocytes *in vitro*, and 2) AGPAT2 deficiency does not determine increased cell death nor impaired autophagic flux during adipogenesis.

ACCEPTED MANUSCRIPT

These results opposites our findings in *Agpat2^{-/-}* mice: 1) these animals are born with histologically normal adipose tissue that expresses normal abundance of mature adipocyte molecular markers (suggesting normal adipogenesis) and 2) this adipose tissue is completely lost during the first week of life (indicating accelerated cell death).

In fact, the present study shows that adipogenic induction determined lower lipid build up and failed activation of the transcriptional cascade that controls adipogenic differentiation in *Agpat2^{-/-}* preadipocytes [16]. Furthermore, *Agpat2^{-/-}* preadipocytes also failed to acquire a mature-adipocyte phenotype, manifested by a lower number of lipid droplet-containing cells, as well as, by reduced mRNA levels of lipid droplet coating proteins Fsp27 and Perilipin, and adipokines leptin and adiponectin. These results confirm previous work in adipogenic cell lines [17] and in lipodystrophy patients derived multipotent mesenchymal cells [7] showing that AGPAT2 is required for *in vitro* adipogenic differentiation.

Nonetheless, the cause of lipodystrophy in *Agpat2^{-/-}* mice, and possibly in AGPAT2 deficient patients, is not impaired adipogenesis but rather the inability to sustain adipocytes in postnatal life. The cause of this lack of concordance between *in vitro* adipogenic studies and *in vivo* pathophysiology of the disease remains to be elucidated.

Similarly, although our *in vitro* studies suggest that autophagy is not involved in the impaired adipogenic differentiation of *Agpat2^{-/-}* preadipocytes, the pathophysiologic role of autophagy in the lipodystrophy of AGPAT2 deficient mice remains unknown.

Recently, it has been reported that biallelic mutations in *PPARG* result in CGL [18], manifested by lipoatrophy, diabetes, hypertriglyceridemia and hepatomegaly. Deficiency of Seipin, (which regulates adipocyte differentiation and lipid droplet formation) also determines CGL in humans and mice as well as reduced Ppar- γ levels in adipose tissue [19]. Interestingly, Ppar- γ agonist rosiglitazone significantly improves a number of metabolic parameters in Seipin deficient mice, possibly by increasing adipogenesis and thus adipose tissue mass [19]. By contrast, we have found that forced expression of Ppar- γ and treatment with rosiglitazone does not prevent adipogenic failure of *Agpat2*^{-/-} MEFs (Cautivo et al, unpublished data), suggesting that this nuclear receptor is functionally inhibited in these cells. Subauste et al. [7] found that adipogenically induced cells from AGPAT2 deficient patients have elevated levels of cyclic phosphatidic acid and that this compound is able to prevent adipogenesis *in vitro* [7]. The implications of these findings in the pathophysiology of lipodystrophy or in the physiologic regulation of adipose tissue mass remain uncertain.

It is possible that mature adipocytes and preadipocytes are differently involved in the lipodystrophy of *Agpat2*^{-/-} mice. Whereas, mature adipocytes undergo cell death in the early days after birth, preadipocytes may contribute to lipodystrophy by their inability to differentiate to adipocytes. Nonetheless, the actual status of preadipocytes in *Agpat2*^{-/-} mice is currently unknown. It cannot be excluded that the inability of preadipocytes to differentiate in adult lipodystrophic *Agpat2*^{-/-} mice is a consequence of their increased susceptibility to cell death upon adipogenic induction.

ACCEPTED MANUSCRIPT

Autophagy is essential to preserve cellular viability during starvation [14]. In adipocytes, autophagy also contributes to lipid droplet dynamics by allowing its lysosomal degradation (reviewed in [15]). We found that undifferentiated *Agpat2*^{-/-} adipocytes have impaired basal autophagic flux as indicated by accumulation of p62, as well as increased levels of autophagy-related proteins.

Defective autophagy has been implicated in other lipodystrophy models. In fact, it has been reported that Seipin-dependent lipodystrophy associates with excessive activation of the autophagic system [20]. Moreover, in lipodystrophy syndromes associated with anti retroviral therapy, excessive amounts autophagosomes in human preadipocytes have been found, suggesting dysregulated autophagy flux [21]. Although we found impaired autophagy flux in undifferentiated *Agpat2*^{-/-} preadipocytes this was reversed by induction of adipogenic differentiation.

In conclusion, the present study shows that AGPAT2 is required for *in vitro* adipogenesis of mouse preadipocytes and that adipogenic differentiation does not induce cell death or autophagy defects in differentiating *Agpat2*^{-/-} preadipocytes.

Acknowledgements: This study was supported by Fondecyt (Regular Competition # 1141134 to V.A.C). M.F.G. was supported by Fondecyt Postdoctoral (# 3150648).

Conflict of Interests: The authors declare no conflict of interests.

References

- [1] Agarwal AK. Lysophospholipid acyltransferases: 1-acylglycerol-3-phosphate O-acyltransferases. From discovery to disease, *Curr Opin Lipidol.* 23 (2012) 290-302.
- [2] Agarwal AK, Sukumaran S, Cortes VA, Tunison K, Mizrahi D, Sankella S, et al. Human 1-acylglycerol-3-phosphate O-acyltransferase isoforms 1 and 2: biochemical characterization and inability to rescue hepatic steatosis in *Agpat2(-/-)* gene lipodystrophic mice, *J Biol Chem.* 286 (2011) 37676-91.
- [3] Garg A. Acquired and inherited lipodystrophies, *N Engl J Med.* 350 (2004) 1220-34.
- [4] Cortes VA, Smalley SV, Goldenberg D, Lagos CF, Hodgson MI, Santos JL. Divergent metabolic phenotype between two sisters with congenital generalized lipodystrophy due to double *AGPAT2* homozygous mutations. a clinical, genetic and in silico study, *PLoS One.* 9 (2014) e87173.
- [5] Cortes VA, Fernandez-Galilea M. Lipodystrophies: adipose tissue disorders with severe metabolic implications, *J Physiol Biochem.* (2015)
- [6] Cortes VA, Curtis DE, Sukumaran S, Shao X, Parameswara V, Rashid S, et al. Molecular mechanisms of hepatic steatosis and insulin resistance in the *AGPAT2*-deficient mouse model of congenital generalized lipodystrophy, *Cell Metab.* 9 (2009) 165-76.
- [7] Subauste AR, Das AK, Li X, Elliott BG, Evans C, El Azzouny M, et al. Alterations in lipid signaling underlie lipodystrophy secondary to *AGPAT2* mutations, *Diabetes.* 61 (2012) 2922-31.

- [8]Rosen ED, MacDougald OA Adipocyte differentiation from the inside out, *Nat Rev Mol Cell Biol.* 7 (2006) 885-96.
- [9]Gajewska M, Sobolewska A, Kozlowski M, Motyl T Role of autophagy in mammary gland development, *J Physiol Pharmacol.* 59 Suppl 9 (2008) 237-49.
- [10]Zhang Y, Goldman S, Baerga R, Zhao Y, Komatsu M, Jin S Adipose-specific deletion of autophagy-related gene 7 (*atg7*) in mice reveals a role in adipogenesis, *Proc Natl Acad Sci U S A.* 106 (2009) 19860-5.
- [11]Baerga R, Zhang Y, Chen PH, Goldman S, Jin S Targeted deletion of autophagy-related 5 (*atg5*) impairs adipogenesis in a cellular model and in mice, *Autophagy.* 5 (2009) 1118-30.
- [12]Perez-Matute P, Neville MJ, Tan GD, Frayn KN, Karpe F Transcriptional control of human adipose tissue blood flow, *Obesity (Silver Spring).* 17 (2009) 681-8.
- [13]Ko PS, Chan WF, Siu TH, Khoo J, Wu WC, Lam JJ Deep venous thrombosis after total hip or knee arthroplasty in a "low-risk" Chinese population, *J Arthroplasty.* 18 (2003) 174-9.
- [14]Thumm M, Egner R, Koch B, Schlumpberger M, Straub M, Veenhuis M, et al. Isolation of autophagocytosis mutants of *Saccharomyces cerevisiae*, *FEBS Lett.* 349 (1994) 275-80.
- [15]Singh R, Cuervo AM Lipophagy: connecting autophagy and lipid metabolism, *Int J Cell Biol.* 2012 (2012) 282041.
- [16]Lowell BB PPARgamma: an essential regulator of adipogenesis and modulator of fat cell function, *Cell.* 99 (1999) 239-42.

- [17]Gale SE, Frolov A, Han X, Bickel PE, Cao L, Bowcock A, et al. A regulatory role for 1-acylglycerol-3-phosphate-O-acyltransferase 2 in adipocyte differentiation, *J Biol Chem*. 281 (2006) 11082-9.
- [18]Dyment DA, Gibson WT, Huang L, Bassyouni H, Hegele RA, Innes AM Biallelic mutations at PPARG cause a congenital, generalized lipodystrophy similar to the Berardinelli-Seip syndrome, *Eur J Med Genet*. 57 (2014) 524-6.
- [19]Liu L, Jiang Q, Wang X, Zhang Y, Lin RC, Lam SM, et al. Adipose-specific knockout of SEIPIN/BSCL2 results in progressive lipodystrophy, *Diabetes*. 63 (2014) 2320-31.
- [20]Fan HD, Chen SP, Sun YX, Xu SH, Wu LJ Seipin mutation at glycosylation sites activates autophagy in transfected cells via abnormal large lipid droplets generation, *Acta Pharmacol Sin*. 36 (2015) 497-506.
- [21]Gibellini L, De Biasi S, Pinti M, Nasi M, Riccio M, Carnevale G, et al. The protease inhibitor atazanavir triggers autophagy and mitophagy in human preadipocytes, *Aids*. 26 (2012) 2017-26.

Figure legends

Fig. 1 AGPAT2 deficiency impairs lipid droplets acquisition on *in vitro* differentiated mice preadipocytes (A) Fluorescence microscopy images and absorbance measurement of Oil Red O stained *Agpat2*^{+/+} and *Agpat2*^{-/-} cells at day 7 after adipogenesis induction (B) Percentage of lipid droplet containing *Agpat2*^{+/+} and *Agpat2*^{-/-} cells at day 7 after adipogenesis induction (C) Average lipid droplets per cell in lipid droplet containing *Agpat2*^{+/+} and *Agpat2*^{-/-} cells at day 7 after adipogenesis induction. Data are expressed as mean \pm S.E. of at least 3 independent experiments. *** $P < 0.001$ vs. *Agpat2*^{+/+} cells

Fig. 2 AGPAT2 deficiency determines impaired transcriptional changes during *in vitro* adipogenesis of mice preadipocytes. (A) adipogenic transcription factors *C/EBP δ* , *C/EBP α* , *PPAR α* and *PPAR γ* (B) lipid droplet coating proteins *Fsp27* and *Perilipin* (C) adipokines *Leptin* and *Adiponectin*. Data are expressed as fold change relative to non-induced wild type preadipocytes. Values are means \pm S.E. of 4 independent experiments. * $P < 0.05$, ** $P < 0.01$ and *** $P < 0.001$ vs. respective differentiation day *Agpat2*^{+/+} cells. ^a $P < 0.05$, ^b $P < 0.01$ and ^c $P < 0.001$ vs. *Agpat2*^{-/-} undifferentiated cells (day 0). [#] $P < 0.05$, ^{##} $P < 0.01$ and ^{###} $P < 0.001$ vs. *Agpat2*^{+/+} undifferentiated cells (day 0).

Fig. 3 Effects of AGPAT2 deficiency on cell death and apoptosis during adipogenesis of *in vitro* differentiated mice preadipocytes (A) LDH activity measured in cell culture media (B) caspase 7 activation (cleaved vs. total protein content) (C) Caspase 3 activation (cleaved vs. total protein content).

ACCEPTED MANUSCRIPT

Data are expressed as mean \pm S.E. of at least 4 independent experiments. * $P < 0.005$ and ** $P < 0.01$ vs. *Agpat2*^{+/+} cells. ^a $P < 0.05$ vs. *Agpat2*^{-/-} undifferentiated cells (day 0). [#] $P < 0.05$ and ^{##} $P < 0.01$ vs. *Agpat2*^{+/+} undifferentiated cells (day 0).

Fig. 4 Effects of AGPAT2 deficiency on levels of ATGs and autophagy flux during adipogenesis of *in vitro* differentiated mice preadipocytes (A) *Atgs* and *p62* mRNA levels (differentiation day 0). (B) ATG3 protein content (C) ATG5-ATG12 complex protein content (D) ATG7 protein content (E) LC3 conversion (LC3II/LC3I ratio) (F) Immunofluorescent detection of LC3 puncta (differentiation day 0) (G) *p62* protein content. Data are expressed as mean \pm S.E. of 4 independent experiments. * $P < 0.005$ vs. respective differentiation day *Agpat2*^{+/+} cells. ^a $P < 0.005$ vs. *Agpat2*^{-/-} undifferentiated cells (day 0).

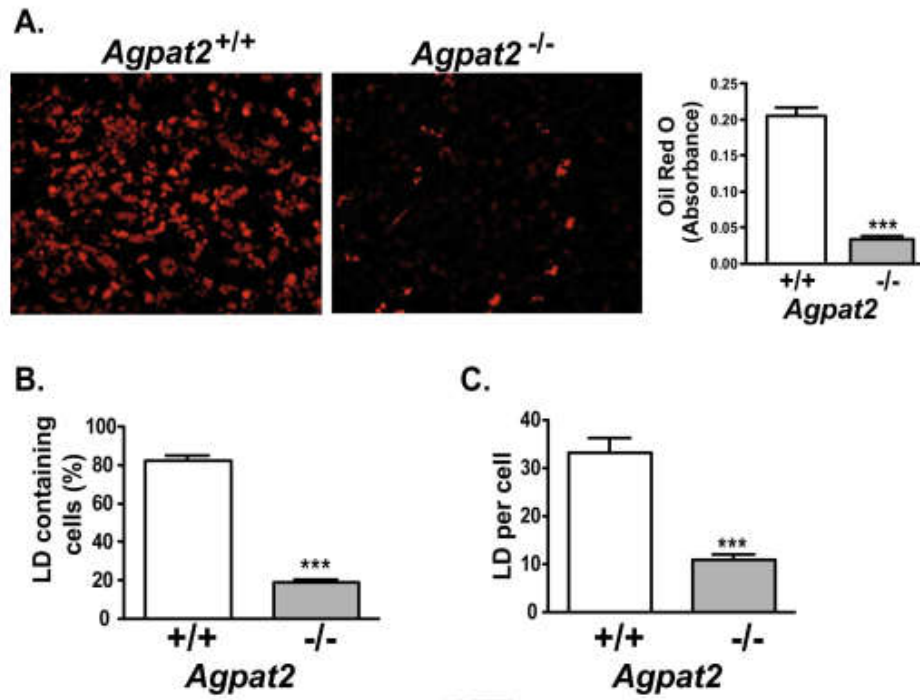
Supplemental Figure 1. Effects of AGPAT2 deficiency on apoptosis during adipogenesis of *in vitro* differentiated mouse preadipocytes. 50 μ g of whole cell protein extracts were separated and transferred as described in methods. Representative western blots of (A) Caspase 7 activation (cleaved vs. total protein content) and (B) Caspase 3 activation (cleaved vs. total protein content). N = 4 per group.

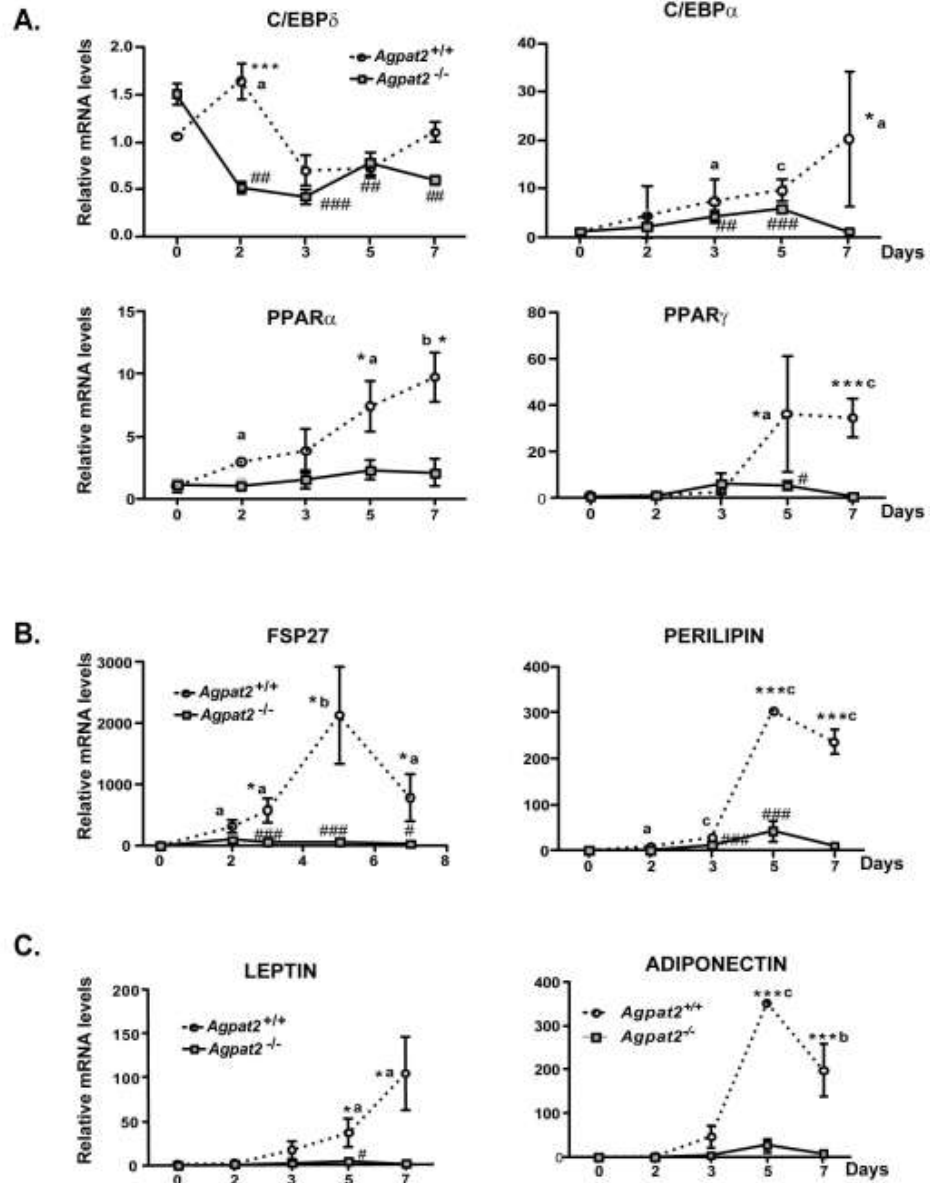
Supplemental Figure 2. Effects of AGPAT2 deficiency on levels of ATGs and autophagy flux markers during adipogenesis of *in vitro* differentiated mouse preadipocytes. 50 μ g of whole cell protein extracts were separated and transferred as described in methods. Representative western blots of (A)

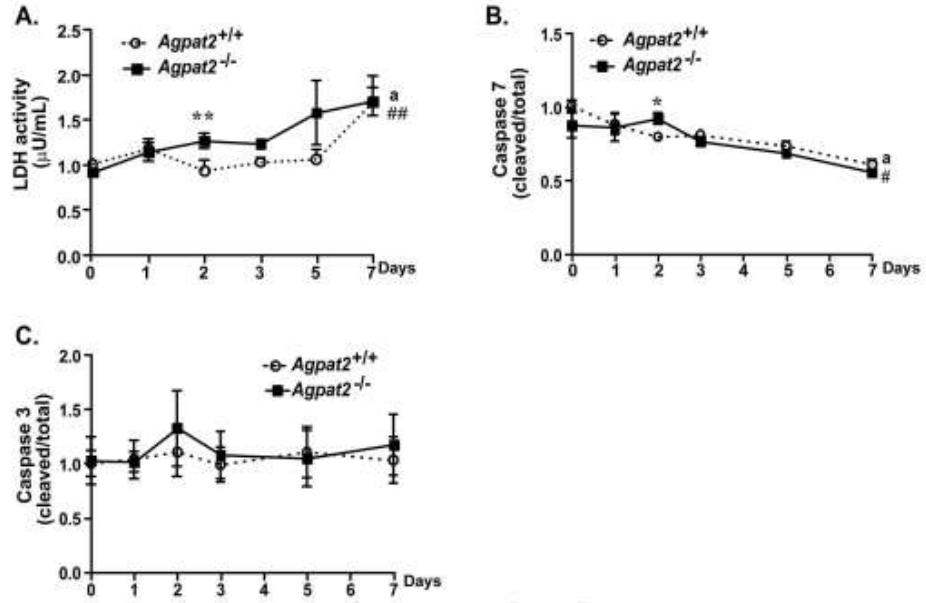
ACCEPTED MANUSCRIPT

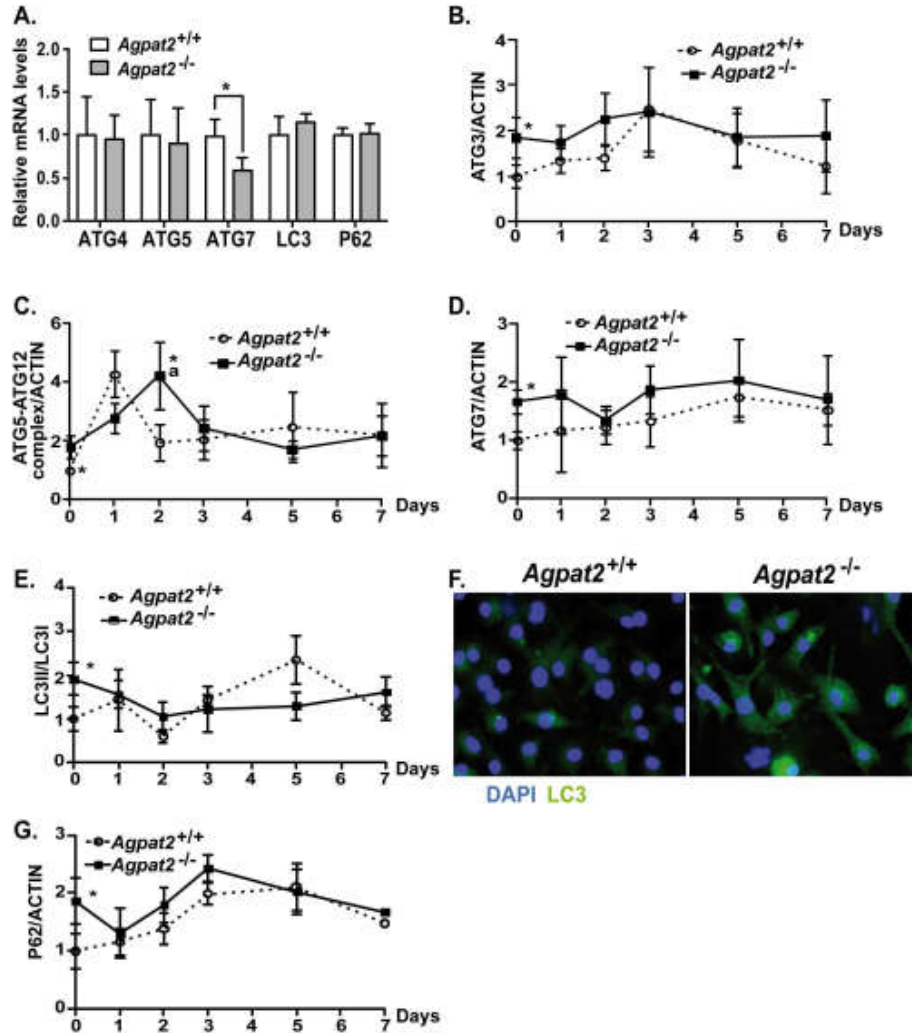
ATG3, ATG7 and p62 (B) ATG5-ATG12 and (C) LC3 conversion (LC3II/LC3I ratio). Actin was used as a loading control. N = 4 per group.

ACCEPTED MANUSCRIPT









Highlights

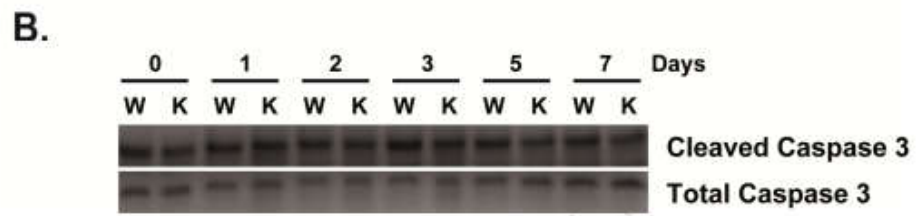
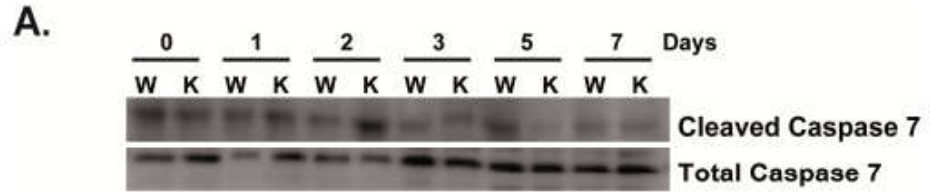
- AGPAT2 is required for *in vitro* adipogenesis of mouse preadipocytes.
- Cell death is not implicated in *Agpat2*^{-/-} preadipocytes adipogenic failure.
- Autophagy defects are present in undifferentiated *Agpat2*^{-/-} preadipocytes.
- Adipogenic induction resolves autophagy defects in *Agpat2*^{-/-} preadipocytes.

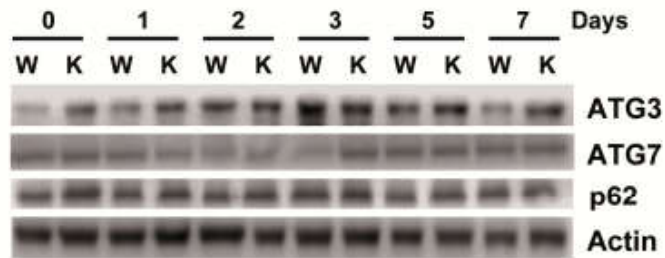
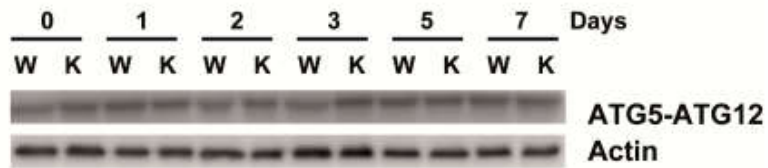
ACCEPTED MANUSCRIPT

ACCEPTED MANUSCRIPT

TABLE 1: Sequence of forward and reverse primers (5' to 3') of genes used for quantification of mRNAs by Real Time PCR.

GENE SYMBOL	NAME	FORWARD	REVERSE
C/EBP α	CCAAT enhancer binding protein alpha	GCGCAAGAGCCGAGATAAAG	CGGTCATTGTCACTGGTCAACT
C/EBP β	CCAAT enhancer binding protein beta	CGCCTTTAGACCCATGGAAG	CCCGTAGGCCAGGCAGT
C-EBP δ	CCAAT enhancer binding protein delta	GGTGGAAGAGAGCTGGGAGTCT	ACACGTTGTCCCTAGATTGAGGAA
PPAR α	Peroxisome proliferator activated receptor alpha	ACAAGGCCTCAGGGTACCA	GCCGAAAGAAGCCCTTACAG
PPAR γ	Peroxisome proliferator activated receptor gamma	CACAATGCCATCAGGTTTGG	GCTGGTCGATATCACTGGAGATC
Lep	Leptin	CTCCATCTGCTGGCCTTCTC	CATCCAGGCTCTCTGGCTTCT
AdipoQ	adiponectin	TCACGGTGTACATGAAAGATGTG	GAGAACGGCCTTGTCTTCT
Plin	perilipin (Plin), transcript variant 1	GGTGAGCGGGACCTGTGA	TTTCATAGGCATTGCACACAGA
CideC (FSP27)	Cell death-inducing DFFA-Like effector C	GCTGAACCCTGAGGACTTTATT	CTTGTAGCAGTGCAGGTCATA
Ppia	Cyclophilin	TGGAGAGCACCAAGACAGACA	TGCCGGAGTCGACAATGAT



A.**B.****C.**